AD_____

Award Number: DAMD17-99-1-9547

TITLE: Genetic and Epigenetic Mechanisms Underlying Acute and Delayed Neurodegenerative Consequences of Stress and Anticholinesterase Exposure

PRINCIPAL INVESTIGATOR: Hermona Soreq, Ph.D.

CONTRACTING ORGANIZATION: Hebrew University of Jerusalem
91904 Jerusalem, Israel

REPORT DATE: August 2002

TYPE OF REPORT: Annual

PREPARED FOR: U.S. Army Medical Research and Materiel Command
Fort Detrick, Maryland 21702-5012

REPORT DOCUMENTATION PAGE

Form Approved
OMB No. 074-0188

1. AGENCY USE ONLY (Leave blank)	2. REPORT DATE	3. REPORT TYPE AND DATES COVERED
	August 2002	Annual (15 Jul 01 - 14 Jul 02)

4. TITLE AND SUBTITLE
Genetic and Epigenetic Mechanisms Underlying Acute and Delayed Neurodegenerative Consequences of Stress and Anticholinesterase Exposure

5. FUNDING NUMBERS
DAMD17-99-1-9547

6. AUTHOR(S)
Hermona Soreq, Ph.D.

7. PERFORMING ORGANIZATION NAME(S) AND ADDRESS(ES)
Hebrew University of Jerusalem
91904 Jerusalem, Israel

E-Mail: soreq@shum.huji.ac.il

8. PERFORMING ORGANIZATION REPORT NUMBER

9. SPONSORING / MONITORING AGENCY NAME(S) AND ADDRESS(ES)
U.S. Army Medical Research and Materiel Command
Fort Detrick, Maryland 21702-5012

10. SPONSORING / MONITORING AGENCY REPORT NUMBER

11. SUPPLEMENTARY NOTES
Report contains color

12a. DISTRIBUTION / AVAILABILITY STATEMENT
Approved for Public Release; Distribution Unlimited

12b. DISTRIBUTION CODE

13. ABSTRACT *(Maximum 200 Words)*

Elevation of serum AChE-R, the stress-induced variant of acetylcholinesterase, was observed in myasthenia gravis (MG). AChE-R was manipulated in autoimmune MG of rats and in mice following the stress of forced swim or brain surgery. Also, in mice we studied the hematopoietic effects of excess AChE-R and evaluated glutamatergic neurotransmission in the hippocampus and its consequences for learning and behavioral adjustment to a circadian switch. In humans, AChE-R accumulation in the brain is accompanied by blood-brain barrier disruption, especially following occupational exposure to anti-cholinesterase insecticides. A yeast two-hybrid screen of human brain cDNA revealed binding of AChE-R to RACK1 and protein kinase CβII (PKCβ2). Transgenic mice overexpressing AChE-R display elevated PKCβ2 levels, and have physiological impairments that are reminiscent of those of patients with post-traumatic stress disorder (PTSD). Suppression of *ACHE* gene expression was induced by tetracycline-controlled antisense or ribozyme sequences in cultured cells and transgenic mice, in which the physiological consequences of such suppression are currently being characterized. Finally, molecular genetics approaches were applied to the human chromosome 7q22 *ACHE* locus: a polymorphism in the *ACHE* promoter is linked to anti-cholinesterase hypersensitivity and exaggerated stress responses, and to a previously unsuspected susceptibility to Parkinson's disease.

14. SUBJECT TERMS
neurotoxin, blood-brain barrier, conditional mutagenesis, stress response, myasthenia gravis, drug hypersensitivity, contextual fear response, post-traumatic stress disorder, Parkinson's disease

15. NUMBER OF PAGES
216

16. PRICE CODE

17. SECURITY CLASSIFICATION OF REPORT	18. SECURITY CLASSIFICATION OF THIS PAGE	19. SECURITY CLASSIFICATION OF ABSTRACT	20. LIMITATION OF ABSTRACT
Unclassified	Unclassified	Unclassified	Unlimited

NSN 7540-01-280-5500

Standard Form 298 (Rev. 2-89)
Prescribed by ANSI Std. Z39-18
298-102

Table of Contents

		page
Front cover		1
Standard form (SF) 298		2
Table of contents		3
Introduction		4
Research results		
Task 1:	The role of readthrough acetylcholinesterase in the pathophysiology of myasthenia gravis	5
	Neuronal overexpression of "readthrough" acetylcholinesterase is associated with antisense-suppressible behavioral impairments	16
Task 2:	Pyridostigmine enhances glutamatergic transmission in hippocampal CA1 neurons	32
Task 3:	AChE over-expression and its effect on hematopoiesis	40
	Development of human antibody fragments directed toward AChE-S using a semi-synthetic phage display library	42
Task 4:	Frequent blood-brain barrier disruption in the human cerebral cortex	51
Task 5:	Chronic acetylcholinesterase overexpression induces multileveled aberrations in neuromuscular physiology	61
Task 6:	Stress-induced interaction of "readthrough" acetylcholinesterase with the scaffold protein RACK1 and protein kinase CβII intensifies behavioral inhibition	71
Task 7:	Tetracycline-inducible antisense and ribozyme suppression of acetylcholinesterase gene expression in transfected cells and transgenic mice	86
Task 8:	Alternative splicing and neuritic mRNA translocation under long-term neuronal hypersensitivity	94
	Genomic dissection reveals locus response to stress for mammalian acetylcholinesterase	101
	Chromosome 7 genes, anticholinesterase hypersensitivity and their long-term consequences	110
Task 9:	statement of progress	117
Key research accomplishments		118
Reportable outcomes		119
Conclusions		122
References		123
Appendices		
Blood-brain barrier modulations . . . (Soreq et al., 2001)		
Frequent blood-brain barrier disruption . . . (Tomkins et al, 2001)		
Genomic dissection reveals . . . (Grant et al., 2001)		
Alternative splicing . . . (Meshorer et al., 2002)		
Anti-cholinesterase intensification . . . (Soreq et al. 2002)		
Antisense intervention . . . (Meshorer and Soreq, 2002)		

Introduction

The annual report of research results is arranged according to the tasks undertaken in the grant application:

task 1: characterize the sensory, cognitive and neuromotor consequences of a transgenic excess in AChE variants.

task 2: employ transgenic mouse models with up to 300-fold differences in peripheral AChE levels for demonstration of direct correlation between AChE dosage and protection from stress and chemical warfare agents and to test their responses to pyridostigmine administration.

task 3: develop RT-PCR tests in peripheral blood cells of model animals, and additional surrogate markers, for follow-up of responses and protection.

task 4: adapt such tests to use in humans following accidental exposure to agricultural anti-AChEs.

task 5: employ the transgenic mouse models to test effects of sudden changes in AChE levels at all the above sites and functions.

task 6: delineate the protein partners through which AChE exerts non-catalytic signals which lead to delayed symptoms.

task 7: develop tetracycline-inducible animal models in which AChE activity can be induced or antisense-suppressed at will.

task 8: continue the search for promoter sequence polymorphisms which lead to natural variations in human AChE levels and correlate them with responses to anti-ChEs.

task 9: expedite transgenic models for production from milk of recombinant human AChE, as a potential scavenger.

The role of readthrough acetylcholinesterase in the pathophysiology of myasthenia gravis

Summary
Alternative splicing induces, under cholinergic imbalance, overproduction of the rare "readthrough" acetylcholinesterase variant, AChE-R. We explored the pathophysiological relevance of this phenomenon in patients with myasthenia gravis (MG) and rats with experimental autoimmune MG (EAMG), both neuromuscular junction diseases with depleted acetylcholine receptors. In MG and EAMG, we detected serum AChE-R accumulation. In EAMG, we alleviated electromyographic abnormalities by nanomolar doses of EN101, an antisense oligonucleotide that selectively lowers AChE-R in blood and muscle, yet leaves unaffected the synaptic variant, AChE-S. While animals treated with placebo or conventional anticholinesterases continued to deteriorate, a 4-week daily oral administration of EN101 improved survival, neuromuscular strength and clinical status in moribund EAMG rats. The efficacy of targeting only one AChE splicing variant highlights potential advantages of mRNA-targeted therapeutics for chronic cholinergic imbalances.

Abbreviations: Ab, antibody; ACh, acetylcholine; AChE, acetylcholinesterase; AS-ON, antisense oligonucleotide; CMAP, compound muscle action potential; EAMG, experimental autoimmune myasthenia gravis; MG, myasthenia gravis; NMJ, neuromuscular junction; T-AChR, *Torpedo* acetylcholine receptor.

Introduction
Numerous impairments in nervous system functioning involve imbalances in the homeostasis of acetylcholine (ACh) and its destruction by acetylcholinesterase (AChE). Notable are Alzheimer's disease, (Coyle et al., 1983) Sjogren's syndrome, (Borda et al., 1996) acute stress responses associated with transient bursts of ACh release (Imperato et al., 1991)and myasthenia gravis (MG), in which autoantibodies to the nicotinic ACh receptor (nAChR) induce neuromuscular junction (NMJ) malfunctioning. (Vincent, 1999)

Distortions in the AChE:nAChR balance may be relevant to several human diseases, as indicated from compound mutagenesis the *ACHE* gene and the α subunit gene for nAChR. In zebrafish, such compound mutagenesis limits the severity of the impaired neuromuscular phenotype caused by *ACHE* disruption alone. (Behra et al., 2002) This calls for re-investigating conditions associated with AChE-nAChR imbalance. In the mammalian nerve and muscle, for example, imbalanced cholinergic neurotransmission induces enhanced transcription and shifted splicing options of *ACHE*, leading to overproduction and accumulation of the normally rare "readthrough" AChE-R variant. (Soreq and Seidman, 2001) In the short range, i.e. the immediate response to acute stress, elevated secretory AChE-R attenuates the initial hyperexcitation. (Kaufer et al., 1998a) However, its continued accumulation may be detrimental, as it also increases the adhesive and morphogenic non-catalytic activities of AChE, (Darboux et al., 1996; Sternfeld et al., 1998) predicting additional long-term effects under AChE-R overproduction. Such effects are likely to be variant-specific, as the synaptic AChE-S variant forms multimers that are attached to the membrane through a proline-rich membrane anchor, (Perrier et al., 2002) whereas AChE-R appears as soluble, secretory monomers. (Seidman et al., 1995) Thus, the signaling action of ACh at the receptor, its cessation by hydrolysis and the morphogenic activity of AChE may all be involved in the maintenance of neuromuscular functioning in a manner dependent on the composition of AChE variants.

MG of humans (Drachman, 1994; Vincent, 1999)and experimental autoimmune MG (EAMG) of rats (Lindstrom, 1980; Tarrab-Hazdai et al., 1975; Vincent, 1983)present valuable systems for testing this dual involvement of AChE in the pathophysiology of NMJ diseases. Loss of receptors induces severely imbalanced cholinergic neurotransmission, which causes neuromuscular weakness and accelerated, readily measurable muscle fatigue. Symptoms are transiently corrected by anticholinesterase therapy, however, the therapy is effective for only short periods and chronic imbalanced cholinergic neurotransmission persists. Based on our previous studies, (Kaufer et al., 1998a; Lev-Lehman et al., 2000) we tested the accumulation of AChE-R in MG and EAMG and employed variant-selective antisense agents to suppress AChE-R accumulation. Our findings demonstrate a role for AChE-R in EAMG pathophysiology and emphasize the added value of targeting AChE-R mRNA in neuromuscular diseases that involve a shift in pre-mRNA splicing.

Methods

Human MG patients: Serum samples from MG patients positive for anti-AChR ABs were collected according to the guidelines and with the approval of the Hebrew University's Bioethics Committee.

Materials: Unless otherwise specified, materials were purchased from Sigma Chemical Co. (St. Louis, MO).

Animals: EAMG was induced in female Lewis rats (120-150 g, Jackson Laboratory, Bar Harbor, ME), in accordance with NIH guidelines. FVB/N mice (Harlan Biotech Rehovot, Israel) and transgenic FVB/N mice that over-express AChE-R were as described. (Sternfeld et al., 2000)

Oligonucleotides: Lyophilized, HPLC-purified, GLP grade oligodeoxynucleotides (purity >90% as verified by capillary electrophoresis (Hybridon, Inc., Worchester, MA), were resuspended in sterile double distilled water (24 mg/ml), and stored at –20 °C. Their sequences were:

EN101 5'-CTGCGATATTTTCTTGTA*C*C*-3';
EN102 5'-GGGAGAGGAGGAGGAAGA*G*G*- 3' ; and
invEN102 5'-GGAGAAGGAGGAGGAGAG*G*G*-3'.

The three 3'-terminal residues (*) were substituted with oxymethyl groups at the 2' position. All of these antisense oligonucleotides (AS-ONs) are complementary to the coding sequence of the rat AChE mRNA sequence (GeneBank accession no. S50879) common to all variants, (Legay et al., 1993) and the third is inverse (inv) to it. (Grifman and Soreq, 1997)

Antibodies: Rabbit polyclonal Abs against the C-terminal sequence of AChE-R, were previously described. (Sternfeld et al., 2000) Goat polyclonal anti-nAChR (S.C.-1448) was from Santa Cruz Biotechnology (Santa Cruz, CA). Biotinylated donkey anti-rabbit Ab (Chemicon International, Temecula, CA) and biotinylated donkey anti-goat Ab (Jackson ImmunoResearch Labortories, West Grove, PA) were used as secondary Abs.

Induction of EAMG: *Torpedo* ACh receptor (T-AChR) purified from *T. californica* electroplax on neurotoxin-Sepharose resin (Boneva et al., 2000)was subcutaneously injected in the hind footpads of rats (40 μg T-AChR and 1 mg of *M. tuberculosis* H37Ra, Difco, Detroit MI, emulsified in complete Freund's adjuvant). Booster injection of the same amount was administered after 30 days. Animals that did not develop EAMG after the second injection received a third one. Animals were weighed and inspected weekly during the first

month, and daily after the booster immunization, for evaluation of muscle weakness. Their clinical status was graded as follows: (0) no weakness or fatigue, treadmill running time, 23 ± 3 min; (1) mildly decreased activity, weak grip with fatigue, weight loss >3% of body weight during a week>10 min running time on treadmill; (2) moderate weakness accompanied by weak grip, weight loss of 5-10%, 3-5 min running on treadmill; (3) moderate-severe weakness, hunched back posture at rest, head down and forelimb digit flexed, tremulous ambulation, 10% body weight loss, 1-2 min run on treadmill; and (4) severe general weakness, no audible complaint or grip, treadmill running time <1 min, weight loss >10%.

Serum analyses: Non-denaturing gel and catalytic activity measurements of AChE were as described. (Kaufer et al., 1998a) Iso-OMPA (tetraisopropylpyrophosphoramide) was used to block butyrylcholinesterase activity in serum samples ($5 \cdot 10^{-5}$ μM) and polyacrylamide gels ($5 \cdot 10^{-6}$ M).

Anti-AChR Ab determination: Sera from EAMG animals and MG patients were assayed by direct radioimmunoassay for anti-T-AChR, rat (R)-AChR or human (H)-AChR . (Boneva et al., 2000; Wirguin et al., 1994) All the EAMG rats displayed high anti-T-AChR and/or anti-R-AChR titers, with serum mean ± SEM values of 82.1 ± 16.0 nM for anti-T-AChR ABs and 19.9 ± 1.8 nM for anti-R-AChR. MG patient sera were assayed by the same radioimmunoassay using H-AChR as antigen and displayed 1 – 60 nM Ab titers.

Quantification of nAChR: AChR concentration in the gastrocnemius and tibialis muscles was determined using ^{125}I-α-bungarotoxin binding followed by precipitation in saturated ammonium sulfate as described previously. (Changeux et al., 1992)

***In situ* hybridization** was performed with fully 2'-O-methylated AChE-R- or AChE-S-specific 50-mer cRNA probes complementary to *ACHE* pseudointron 4 or exon 6, respectively. (Meshorer et al., 2002) Detection was with alkaline phosphatase and Fast Red™ substrate (Molecular Probes, Eugene, OR). DAPI (Sigma) staining served to visualize nuclei.

Immunohistochemistry was performed on 7 μm paraffin-embedded muscle sections as described elsewhere. (Mor et al., 2001) Briefly, primary Abs were diluted 1:100 and 1:30 for detecting rabbit anti-AChE-R and goat anti-AChE-R, respectively.

Drug administration: Intravenous injection and blood sampling for anti-nAChR Ab determination were via the jugular vein under anesthesia. For oral administration, a curved intubation feeding needle with a ball end (Stoelting, Wood Dale, IL) was used. Pyridostigmine (Mestinon Bromide™, Hoffmann-La Roche, Basel, Switzerland), was administered in a dose of 1 mg/Kg per treatment, the highest dose that does not cause cholinergic crisis.

Electromyography: Rats were anesthetized by *i.p.* injection of 2.5 mg/Kg pentobarbital, immobilized, and subjected to repetitive sciatic nerve stimulation at 3 Hz, using a pair of concentric needle electrodes. Baseline compound muscle action potentials (CMAPs) were recorded by electrodes placed in the gastrocnemius muscle, following a train of repetitive nerve stimulations at supramaximal intensity. Decrease (percent) in the amplitude of the fifth vs. the first muscle action potential was determined in two sets of repetitive stimulations for each animal. A reduction of 10% or more indicated neuromuscular dysfunction. (Wirguin et al., 1994) Baseline decrement in each animal was taken as 100% and changes were presented

as comparison to this value. Thus, an improvement of baseline decrement of 0.87 to 1.0 would yield a value of 113%.

Exercise training on treadmill: Animals were placed on an electrically powered treadmill (Moran et al., 1996)running at a rate of 25 m/min, a physical effort of moderate intensity, until visibly fatigued. The time the rats were able to run was recorded before and after AS-ON or pyridostigmine treatment.

Results

AChE-R in blood of human MG subjects and EAMG rats

AChE-R overproduction in MG was tested by staining for AChE activity non-denaturing polyacrylamidein gels on which had been separated sera from mice and from MG patients. The murine monomeric AChE-R variant migrates on such gels faster than the tetrameric synaptic enzyme, AChE-S. (Kaufer et al., 1998a) Serum from FVB/N mice subjected to forced swim stress (Meshorer et al., 2002)displayed higher levels than control mice of a rapidly migrating band, which was inhibitable by $5 \cdot 10^{-6}$ M BW284c51, 1,5-bis(4-allyldimethylammoniumphenyl)
pentan-3-one dibromide 284c51, an AChE-specific inhibitor, but not by the butyrylcholinesterase-specific inhibitor iso-OMPA. Sera from transgenic mice, which over-express human AChE-R, (Sternfeld et al., 2000) displayed a yet more rapidly migrating band. Fig. 1A presents these iso-OMPA-resistant activity patterns. Similarly fast-migrating AChE was observed in the sera of 10 of 19 MG patients, whereas serum from patients with an unrelated disease, e.g. hepatitis, or serum from a healthy non-stressed human showed primarily a slower-migrating AChE form. Fig. 1A further demonstrates this fast-migrating AChE variant in serum from 2 of 4 MG patients. There was no apparent correlation between the intensity of staining in the gels and anti-AChR Ab titers of the analyzed patients (an average ± SEM of 22 ± 16 nM, as compared to 1.0 nM in healthy subjects). Also, there was no correlation with total serum AChE activity, which, on average, was unchanged from levels in normal subjects. These observations suggested that the faster migrating bands represent murine and human AChE-R (mR and hR, respectively) and that AChE-R is over-represented in the blood of some MG patients. Immunoblot analysis of similar gels confirmed that in EAMG, as compared with healthy rats, there was a massive increase in serum AChE-R (rR, Fig. 1B).

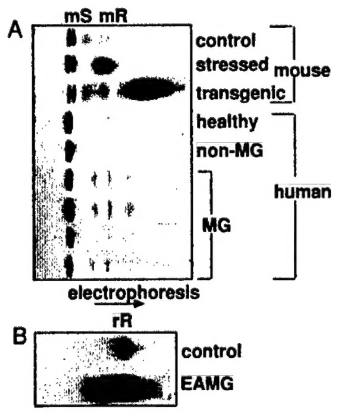

Fig. 1. A rapidly migrating AChE variant in serum of MG patients. A. AChE catalytic activity. Shown is a non-denaturing polyacrylamide gel stained for serum AChE activity in stressed, control or transgenic mice overexpressing human AChE-R and in healthy, non-MG and MG patients. Two of the MG subjects have detectable amounts of a catalytically active protein comigrating with hAChE-R. B. Immunoreactive AChE-R in EAMG rats. Shown is a non-denaturing gel tested for immunoreactive AChE-R in rat serum (rR). An EAMG rat had considerably higher level of the rapidly migrating rR variant than a control rat.

AChE-R and AChE-R mRNA accumulate in muscles of EAMG rats

Expression of alternative AChE variants (Fig. 2A) was tested in control and EAMG rats. In a quantitative immunoassay, muscle nAChR was reduced by 48 ± 7% from normal values in 10

mildly affected animals (disease grade 1-2) and by 75 ± 5% in 10 severely affected rats (grade 4) compared to controls. Immunohistochemistry with ABs to nAChR visualized this depletion in muscle sections from EAMG rats, as compared to control rats (Fig. 2B 1,2). Immunohistochemical staining with a polyclonal antiserum that selectively detects AChE-R (Sternfeld et al., 2000)revealed positive signals in some, but not all muscle fibers of control rats. Similar patterns appeared under treatment with the inert, inversely oriented oligonucleotide, invEN102 (Meshorer et al., 2002)(see Fig. 2B 3 for invEN102-treated control muscle). In EAMG rats (Fig. 2B 4), the same staining procedure showed dispersed cytoplasmic localization that is characteristic of this isoform, which is also secreted, (Soreq and Seidman, 2001) and contrasts with the membrane-associated clusters of the synaptic variant. (Rossi and Rotundo, 1993) Both the level of expression and the cellular distribution of muscle AChE-S were similar in EAMG and control, untreated or invEN102-treated rats (data not shown).

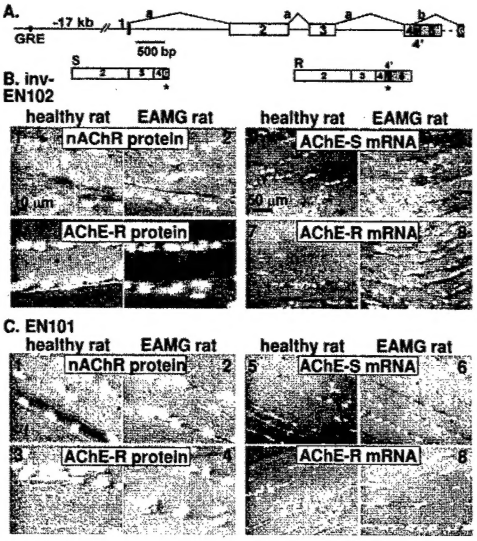

Fig. 2. Excess AChE-R expression in muscles of EAMG rats. A. AChE mRNA transcripts expressed in muscle. Shown is the stress-responding mammalian *ACHE* gene, with a functional glucocorticoid response element, GRE, in its distal enhancer, and its two muscle-expressed mRNA transcripts. Exon 6 is unique to AChE-S, whereas, pseudointron 4' is expressed only in AChE-R mRNA. Abs targeted to its C-terminal peptide served to detect the AChE-R protein, and cRNA probes to exon 6 and pseudointron 4' label the two transcripts (asterisks). B. Depleted nAChR and excess AChE-R in EAMG muscles. Paraffin-embedded sections of triceps muscle from normal or EAMG rats treated with invEN102 were similar to those of untreated rats (see text). Immunostaining (red) was with polyclonal rabbit Abs to nAChR (1,2) and AChE-R (3,4). *In situ* hybridization with probes specific for AChE-R or -S mRNAs yielded red stained RNA, with DAPI (white) used to visualize cell nuclei. AChE-R mRNA was observed in preparations from EAMG, but not control animals (5,6). AChE-S mRNA displayed punctuated expression in both control and EAMG rats (7,8). C. EN101 treatment. In EAMG rats, EN101 reduced levels of AChE-R (1,2) and AChE-R mRNA (5,6), but did not affect nAChR (3,4) or AChE-S mRNA (7,8).

Using *in situ* hybridization with variant-selective probes, we observed similarly distributed AChE-S mRNA in muscles from both untreated and invEN102-treated healthy and EAMG rats (see Fig. 2B 5,6 for invEN102 treated muscle). In contrast, normal rats displayed only weak and diffuse labeling of the AChE-R mRNA transcript, whereas pronounced punctuate labeling of AChE-R mRNA accumulations appeared in triceps muscles of EAMG rats, unaffected by invEN102 treatment (Fig. 2B 7,8). This accumulation indicated a selective over-expression of AChE-R in muscles of EAMG rats.

AChE-R and AChE-R mRNA levels in muscle respond to EN101

The soluble, secretory nature of AChE-R predicted that it would degrade ACh before it reaches the post-synaptic membrane, limiting receptor activation. To test this hypothesis, we used the EN101 AS-ON, capable of selective suppression of AChE-R production. (Galyam et al., 2001; Meshorer et al., 2002) AChE-R suppression was tested in healthy and EAMG rats

with reduced muscle nAChR levels (Fig. 2C 1,2) 24 h following a single *i.v.* injection of 250 μg/Kg EN101. Imunohistochemical staining, demonstrated that AChE-R but not AChE-S, was significantly reduced in muscles from both control and EAMG rats (Fig. 2C 3,4 and data not shown). Receptor labeling intensity remained high in healthy rats and low in EAMG animals, similarly to untreated animals and animals treated with invEN102 (compare Fig. 2B 1,2 to Fig. 2C 1,2). *In situ* hybridization indicated that AChE-S mRNA labeling was only nominally affected by EN101, suggesting that neuromuscular transmission would be maintained under this treatment (Fig. 2C 5,6). In contrast, EN101 reduced AChE-R mRNA labeling almost to the limit of detection in both control and myasthenic rats (Fig. 2C 7,8).

Suppression of AChE-R restores normal CMAP in EAMG rats

Quantification by densitometry of an immunoblot analysis confirmed the increase of serum AChE-R in EAMG and the efficacy of a single *i.v.* injection of 250 μg/Kg EN101, but not invEN102, in reducing its serum level 24 h later (Fig. 3A). To evaluate the physiological outcome of this suppression, we recorded CMAPs from the gastrocnemius muscle. EAMG rats, but never control animals, displayed a decrement in CMAP during repeated stimulation at 3 Hz. The baseline decrement, the percent difference in the heights of the fifth and the first evoked potentials, ranged from 10% to 36% (mean ± SEM = 13.0 ± 2.5%, Fig. 3B, inset) as compared to 4.0 ± 0.9% in healthy controls. Standard therapy for MG is the administration of an anti-cholinesterase, which elevates ACh levels to a threshold enabling receptor activation. Accordingly, we administered *i.p.*, neostigmine bromide (Prostigmine™, Hoffmann-La Roche, 75 μg/Kg). This rapidly and effectively corrected the CMAP decrement in EAMG rats from 87.6% of the first evoked potential in untreated animals to over 120% of this level (i.e. 105% of the first evoked potential). The effects of the cholinesterase blockade were evident starting 15 min after injection yet lasted only 2 h, after which time CMAP value, reverted to the decrement baseline (Fig 3B).

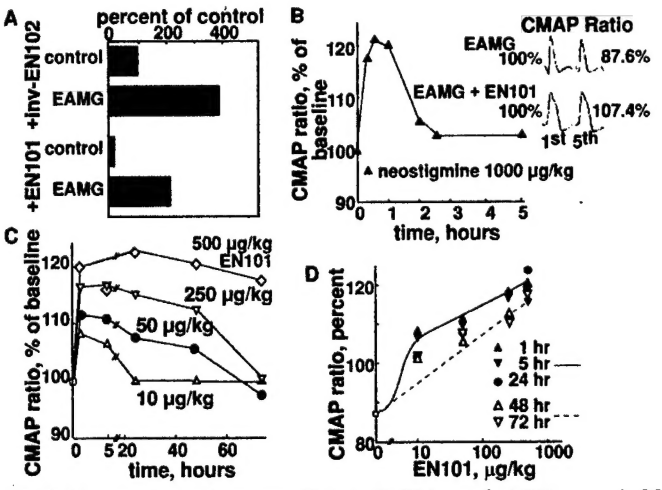

Fig. 3. Normalized EAMG muscle electrophysiology under suppression of AChE-R. A. Immunoreactive AChE-R was densitometrically determined, as in Fig. 1B, for the serum of healthy and severely affected EAMG rats, treated with EN101 or invEN102. B and C display dose- and time-dependence of treatment on average CMAP ratios, relative to baseline, at the specified times post-injection for at least 6 rats in each group. Average CMAP ratios of EAMG rats prior to and following EN101 treatment were 87 ± 2.5% and 107.4 ± 3.8% respectively (inset). B. Neostigmine. Animals were treated with a single *i.p* injection (75 μg/Kg) of the AChE inhibitor neostigmine. C. EN101 restored the decremental change for up to 72 h under 10 to 500 μg/Kg. D. Dose response. CMAP responses at each time were plotted as a function of EN101 concentration. Note that at 1 and 5 h there are clearly two effects, a steep increase dependent on a low EN101 concentration (IC_{50} < 10 μg/Kg), superimposed on a much lower-affinity effect that persists much longer.

Unlike anticholinesterases, which block all AChE variants, EN101 was shown to selectively suppress muscle AChE-R production. (Lev-Lehman et al., 2000) Therefore, retrieval of stable CMAP in EN101-teated EAMG rats may attest to the causal role of AChE-R in myasthenic neuromuscular malfunctioning. Intravenous injection of EN101 at doses ranging from 50-500 μg/Kg (2 to 20 nmol/rat) did not affect CMAP in control animals, but in EAMG rats it retrieved stable CMAP ratios within 1 h (Fig. 3B, inset, 3C and Table 1). CMAP normalization was accompanied by increased mobility, upright posture, stronger grip, and reduced tremulousness of ambulation. Both the extent and the duration of CMAP correction were dose-dependent; for example, 500 μg/Kg conferred ≥72 h rectification of CMAP up to 125% of baseline, while 50 μg/Kg was effective for only 24 h. EN102, a similarly 3' protected AS-ON targeting another sequence in AChE mRNA (AS1 in ref. (Grifman and Soreq, 1997)produced similar rectification of CMAP decrements in EAMG rats, supporting the relevance of AChE-R as a contributing element to these decrements. Comparable amounts of invEN102, did not improve muscle function, attesting to the sequence specificity of this AS-ON effect (Table 1). Dose response curves revealed that up to 5 h following an injection, EN101 produced a saturable response with IC_{50} of <10 μg/Kg. This effect appeared to be superimposed on a much longer-lasting and a much less concentration-dependent effect that showed no saturation in the range we studied (Fig. 3D), possibly reflecting altered muscle and/or neuromuscular junction properties under the stable CMAP retrieval afforded by EN101.

Table 1. Post-treatment CMAP ratios[a].

	Oral[b]					Intravenous[b]			
	Naive EN101	EAMG EN101	EAMG EN102	EAMG invEN102	EAMG pyrido-stigmine	Naive EN101	EAMG EN101	EAMG EN102	EAMG invEN102
0 h	1.01±0.01 (4)	0.84±0.03 (8)	0.82±0.02 (4)	0.78±0.06 (4)	0.90±0.01 (6)	1.00±0.00 (6)	0.87±0.01 (6)	0.85±0.06 (4)	0.89±0.02 (5)
1 h[c]	1.0±0.02 (4)	0.97±0.02 (8)	0.86±0.04 (3)	0.86±0.05 (4)	0.98±0.01 (6)	1.02±0.01 (7)	1.00±0.01 (4)	1.04±0.01 (4)	0.89±0.03 (5)
5 h	1.03±0.02 (4)	0.97±0.03 (7)	0.96±0.02 (4)	0.86±0.05 (4)	0.96±0.02 (6)	1.00±0.01 (6)	0.98±0.02 (4)	0.98±0.03 (4)	0.89±0.02 (5)
24 h	1.01±0.00 (7)	1.01±0.01 (6)	0.95±0.03 (5)	0.81±0.08 (4)	0.87±0.02 (6)	1.02±0.01 (6)	1.00±0.00 (4)	1.00±0.01 (4)	0.90±0.02 (5)

[a]CMAP ratios (5^{th} vs. 1^{st} amplitude) were determined at the noted times following treatment and the averages ± SEM are presented. Each treatment represents similarly, although not simultaneously treated rats, the numbers of which are shown in parentheses.

[b]Drug doses were 50 μg/Kg for EN101, EN102 or invEN102 and 1000 μg/Kg for pyridostigmine, for both administration routes.

[c]Note the apparently delayed effect of orally administered EN102 as compared to EN101 or pyridostigmine.

Antisense prevention of AChE-R accumulation promotes stamina in EAMG rats

Placed on a treadmill at 25 m/min, control rats ran for 23.0 ± 3.0 min and then displayed visible signs of fatigue. Starting at 5 h and for at least 24 h following administration of 250 μg/Kg EN101, EAMG rats demonstrated improved performance on the treadmill (see video clip in PNAS web site). Running time increased from 247 ± 35, 179 ± 21 and 32 ± 6 sec to 488 ± 58, 500 ± 193 and 212 ± 59 sec for animals at disease grades 2, 3 and 4, respectively

(average values for 6 to 9 animals per group.) Healthy animals, in contrast, were not significantly affected by EN101 injection.

2'-Oxymethyl protected AS-ON agents are efficient under oral administration. (Monia, 1997) The dose of 50 μg/Kg of EN101 was once-daily administered to EAMG rats via an intubation feeding needle and CMAP measured 1, 5, and 24 h later. Orally administered 50 μg/Kg EN101 and EN102 were as effective as 25 μg/Kg EN101 administered *i.v.* (Table 1 and Figs. 3 and 4), but EN102 effects appeared somewhat delayed compared to EN101. Oral pyridostigmine (1000 μg/Kg) restored CMAP for up to several hours, while invEN102 had no significant effect (Table 1).

Long-term antisense AChE-R suppression modifies the course of EAMG pathophysiology

The long-term maintenance of stable CMAP under EN101 enabled us to test whether the cholinergic imbalance contributes to the progressive physiological deterioration in EAMG. Rats were first treated with EN101 once a day for 5 days, CMAPs being determined prior to each treatment. Both the efficacy of EN101 and its capacity to reduce the inter-animal variability in CMAP values were comparable to those of pyridostigmine (Fig. 4 A,B). However, the onset of response to pyridostigmine was more rapid (Table 1), while that observed with EN101 was longer-lasting. Daily oral or *i.v.* administration of EN101 stabilized CMAPs over the entire course of treatment (Fig. 4B). In contrast, the effect of pyridostigmine wore off within several hours, causing pronounced fluctuations in muscle status (Table 1, Fig. 4).

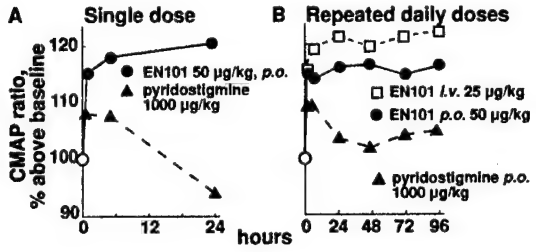

Fig. 4. Stable reversal of decremental CMAP response in EAMG rats treated orally with EN101. EAMG rats received EN101 once daily for up to 4 days by *i.v.* injection. CMAP ratios were determined in EAMG rats 1 and 5 h following the first intravenous (25 μg/Kg) or oral drug administration (50 μg/Kg) of EN101 or pyridostigmine (1000 μg/Kg), and then every 24 h, prior to the administration of the subsequent dose. A. Single dose. Orally administered pyridostigmine (n = 4) and EN101 (n = 8) relieved the decremental CMAP responses within 1 h. In contrast, no decrement was detected in rats treated with EN101. B. Repeated daily doses. Equivalent improvement is shown in muscle function following oral (50 μg/Kg, n = 8) as compared to *i.v.* (25 μg/Kg, n = 4) administration of EN101.

Five out of 6 the animals treated daily with pyridostigmine died within 5 days, while 6 out of 8 animals orally treated once daily with EN101 survived the full 5 day period. To exclude the possibility that this difference may reflect the susceptibility of EAMG rats to the repeated anesthesia and CMAP measurements, we subjected groups of moderately sick animals to 1 month of daily oral treatment with minimal interference. EAMG rats receiving daily oral doses of EN101, presented significant improvement in survival, clinical status and treadmill performance, as compared with pyridostigmine- and saline-treated animals (Fig. 5; P <0.041 for 4 weeks survival incidence, Fisher exact test, ASON vs. other treatments). One way repeated measures ANOVA yielded P <0.05 for all other measures (AS vs. other treatments at 4 weeks). In addition, rats in the saline and pyridostigmine treated groups lost 13.5 and 11 g/animal, respectively, whereas animals in the EN101-treated group gained, on average, 13 g during the treatment period.

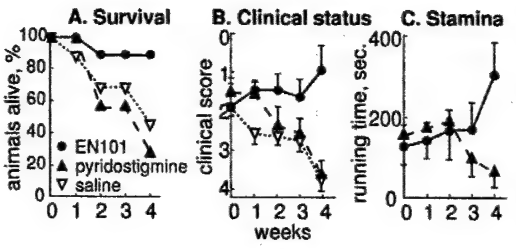

Fig. 5. Long-term EN101 treatment changes the course of EAMG. A. Survival. More animals treated once daily with EN101 (50 μg/Kg, daily, *p.o.*) survived than those treated with pyridostigmine (1000 μg/Kg) despite their similarly poor initial status. B. Clinical status. Shown are average values for the clinical status (Methods) of surviving animals from each of the treated groups. C. Stamina. Shown are average running times in sec for EN101- and pyridostigmine-treated animals. Note that before treatment, EAMG rats performed as severely sick animals (clinical status 4).

Discussion

Our observations support the notion that AChE-R plays a role in MG pathophysiology and call for evaluation of the rationale of long-term mRNA-targeted therapy for imbalanced cholinergic function at NMJs.

Cholinergic balance considerations: Neuromuscular homeostasis involves, among other elements, the balance between NMJ-bound AChE and AChR which regulates neuromuscular maintenance and functioning. (Behra et al., 2002; Ohno et al., 2000)When this balance is impaired, notably in the cases of inherited or acquired MG and EAMG or under exposure to organophosphates, (He et al., 1998) deterioration of muscle performance ensues. Fig. 6 presents a scheme of the key elements controlling the cholinergic balance in NMJs and the putative mechanism through which it may be retrieved in MG and EAMG.

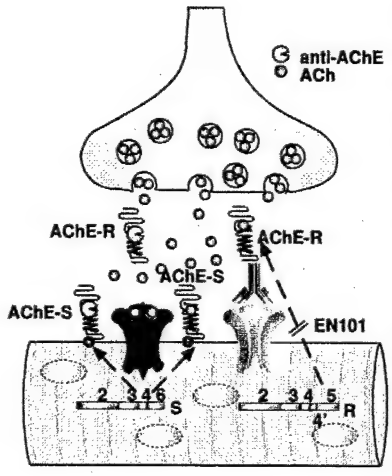

Fig. 6. Mechanistic considerations. At the neuromuscular junction, ACh released from the motoneuron terminal (top) into the synaptic cleft travels towards the muscle post-synaptic membrane (below). There, it interacts with nAChR to initiate an inward current and elicit muscle action potentials. ACh is subsequently hydrolyzed by synapse-bound AChE-S. Subsynaptic muscle nuclei (ellipses) produce, in addition to the primary AChE-S mRNA transcript, the normally rare AChE-R mRNA with its alternative 3'-end. This transcript translates into soluble, secretory AChE-R monomers. Myasthenic autoimmune Abs toward nAChR induce destruction of receptor molecules, limiting the initiation of action potentials and mimicking an ACh-deficient state. The cholinergic imbalance results in AChE-R accumulation that enhances ACh destruction, leading to muscle fatigue. Chemical anticholinesterases (indented circles) non-selectively block both AChE-S and AChE-R, which transiently increases ACh levels yet further intensifies AChE-R overproduction. In contrast, the antisense agent EN101 selectively induces AChE-R mRNA destruction, preventing AChE-R synthesis while maintaining AChE-S and sustaining normal neuromuscular transmission.

Pharmacological inhibition of AChE, a primary treatment of MG for many decades, assumed that AChE plays no role in the etiology or pathophysiology of MG; and that long-term use of AChE inhibitors does not contribute to MG or its symptoms. Anti-cholinesterase therapy, by

damping the destruction of ACh by AChE, can transiently compensate for the reduced numbers of AChRs at NMJs. (Millard and Broomfield, 1995)However, AChE-S blockade by the non-discriminative anticholinesterases induces AChE-R overproduction. (Soreq and Seidman, 2001) This would limit the duration of anticholinesterases' capacity to retrieve stable CMAP and intensify the disease-associated cholinergic imbalance.

CMAP increases occurred both under anticholinesterase treatment (for a few hours) and in EN101-treated animals (>24 h after treatment). The rapid onset of CMAP improvement under EN101 is most likely due to its easy accessibility to muscle tissue and a rapid turnover of its target mRNA. The long-lasting functioning of the AS-ON may indicate that there is no physiological change until AChE-R re-accumulates to a level at which it can cause NMJ malfunction. Under daily EN101 treatment, the steady reversal of the decremental change likely enabled sustained recovery processes, unlike the fluctuating values under conventional therapy. Interrelationships between NMJ cholinergic imbalance and stress-induced change in the cytokine balance, recently reported to affect EAMG pathophysiology, (Huang et al., 2001; Ostlie et al., 2001; Zhang et al., 1999) may explain at least part of the continuously improving clinical scores under prolonged EN101 treatment.

Drug dose and time dependence: By directing nanomolar doses of an orally delivered AS-ON drug to the long-known MG target, AChE, we achieved rapid, yet long-lasting clinical improvement, associated with stable reversal of the CMAP decrement response at 3 Hz nerve stimulation and increased muscle stamina in the treadmill test. The beneficial effect of AS-ON injection on the CMAP response began within 1 h post-treatment and lasted many more hours than the effect of anticholinesterases, likely reflecting the mechanistic differences between these two groups of drugs.

Chemical anticholinesterases stoichiometrically inhibit the large number of AChE-S molecules present in the NMJ (3000 to 5000 molecules/μm^2). (Anglister et al., 1994a) In contrast, AChE mRNA chains exist in far lower quantities than their protein products. (Rotundo, 1990) Furthermore, AChE-R mRNA is normally the least abundant of the alternative splice variants of AChE pre-mRNA. (Soreq and Seidman, 2001) In addition, AS-ON agents that target the AChE-R mRNA transcripts can operate repeatedly, i.e. one AS-ON is responsible for hydrolysis of many mRNAs. (Dove, 2002) This explains the over 100-fold difference in the molar dose of AS-ON, as compared to pyridostigmine, that is effective in relieving EAMG weakness.

Because of the intrinsic instability of the AChE-R mRNA transcript, (Chan et al., 1998) AS-ON agents targeted at the AChE mRNA sequence that is shared by all transcripts, such as EN101 or EN102, will destroy primarily the longer, less G,C-rich AChE-R mRNA. (Meshorer et al., 2002) This provides selectivity toward this normally rare transcript, while protecting most of the synaptic AChE-S variant from the antisense effect. Consequently, neuromuscular function is maintained while the disease-associated variant is efficiently prevented from being synthesized. The 3' terminal 2'-oxymethyl protection of AS-ON chains increases the hybridization affinity while minimizing toxicity, (Galyam et al., 2001) explaining its efficacy following *i.v.* as well as oral administration. In comparison, conventional anticholinesterases would non-selectively inhibit the catalytic activity of the two variants and induce a robust, multi-tissue feedback response of AChE-R over-production. (Kaufer et al., 1998a) This increases the non-catalytic activities of AChE (Behra et al., 2002)that are not necessarily blocked by anticholinesterases. (Behra et al., 2002; Soreq and Seidman, 2001) The long-term survival and improved clinical status and stamina of animals

receiving AS-ON by daily oral treatment, as compared with the poor survival of severely diseased animals under the physiologically fluctuating effects of a single daily dose of placebo or pyridostigmine, highlight these differences.

Potential relevance to other diseases: The pathogenesis of MG and EAMG is primarily related to the destructive effect of anti-AChR Abs on the NMJ. (Vincent, 1999) Neuromuscular weakness associated with cholinergic imbalance is also known in patients with congenital myasthenic syndromes, (Ohno et al., 2000) where synaptic AChE-S is the only form missing, as well as following exposure to anticholinesterases, e.g. in Gulf War veterans. (Haley et al., 1999) Other diseases with peripherally imbalanced cholinergic neurotransmission include muscle dystrophy, (Carlson, 1998) amyotrophic lateral sclerosis and post-traumatic stress disorder. (Price et al., 1993) As AS-ONs targeted to AChE mRNA provide relief of cholinergic muscle malfunction, they may be found useful for alleviating the weakness in these and other muscle malfunction syndromes.

Neuronal overexpression of "readthrough" acetylcholinesterase is associated with antisense-suppressible behavioral impairments

Summary

Molecular origin(s) of the diverse behavioral responses to anticholinesterases were explored in behaviorally impaired transgenic (Tg) FVB/N mice expressing synaptic human acetylcholinesterase (hAChE-S). Untreated hAChE-S Tg, unlike naïve FVB/N mice, presented variably intense neuronal overexpression of the alternatively spliced, stress-induced mouse "readthrough" mAChE-R mRNA. Both strains displayed similar diurnal patterns of locomotor activity that were impaired 3 days after a day-to-night switch. However, hAChE-S Tg, but not FVB/N mice responded to the circadian switch with irregular, diverse bursts of increased locomotor activity. In social recognition tests, controls displayed short-term recognition, reflected by decreased exploration of a familiar, compared to a novel juvenile conspecific as well as inverse correlation between social recognition and cortical and hippocampal AChE specific activities. In contrast, transgenics presented poor recognition, retrievable by tetrahydroaminoacridine (tacrine, 1.5 mg/Kg). Tacrine's effect was short-lived (<40 min), suggesting its effect was overcome by anticholinesterase-induced overproduction of mAChE-R. Consistent with this hypothesis, antisense oligonucleotides (2 daily intracerebroventricular injections of 25 ng) arrested mAChE-R synthesis, selectively reduced mAChE-R levels and afforded an extended (>24 hr) suppression of the abnormal social recognition pattern in transgenics. Efficacy of antisense treatment was directly correlated to AChE-R levels and the severity of the impaired phenotype, being most apparent in transgenics presenting highly abnormal pre-treatment behavior. These findings demonstrate that neuronal AChE-R overproduction is involved in various behavioral impairments and anticholinesterase responses, and point to the antisense strategy as a potential approach for re-establishing cholinergic balance.

Introduction

Social behavior is a complex phenotype, composed of the individual's general level of activity, cognitive perception and anticipation of the outcome of such behavior (Carlson, 1994). Working and storage memory and the ability to integrate information can also contribute towards social behavior, which is tightly linked to cholinergic neurotransmission. For example, the hypocholinergic features of Alzheimer's disease (AD) patients include aggressive behavior and/or avoidance of novel social challenges (Cummings and Black, 1998), as well as fears of social interactions alleviated by treatment with anticholinesterases (Giacobini, 2000). Surprisingly, anticholinesterases, e.g. tacrine (tetrahydroaminoacridine, Cognex™, Parke-Davis), donepezil (Aricept™, Pfizer), rivastigmine (Exelon™, Novartis) and galantamine (Reminyl™, Janssen), were reported to cause more pronounced improvement in more severely affected patients. To explain the molecular basis of this phenomenon, re-evaluation is needed of the linkage between cholinergic neural pathways, social behavior and acetylcholinesterase (AChE).

Both anticholinesterase exposure and stressful insults, i.e. confined swim, induce in the mammalian brain a rapid c-fos elevation that mediates muscarinic responses and subsequent *ACHE* overexpression (Kaufer et al., 1998a). A stress-associated switch in alternative splicing (Xie and McCobb., 1998; Kaufer et al., 1999) diverts AChE from the major, "synaptic" AChE-S to the normally rare "readthrough" AChE-R variant (Grisaru et al., 1999). The distinctive non-

catalytic activities of these AChE isoforms (Sternfeld et al., 2000), suggest links between AChE-R accumulation and behavioral anticholinesterase responses.

Transgenic (Tg) mice overexpressing human (h) AChE-S in brain neurons are amenable to pursuit of this linkage. These mice present , early-onset loss of learning and memory capacities (Beeri et al., 1995), progressive dendritic depletion (Beeri et al., 1997), stress-related neuropathology (Sternfeld et al., 2000), and modified anxiety responses (Erb et al., 2001). However, their social behavior and psychological stress responses have not yet been addressed.

AChE-S Tg mice constitutively overexpress AChE-R mRNA in their intestinal epithelium. When exposed to an organophosphate anticholinesterase (DFP), they fail to increase further the already overproduced AChE-R, and present extreme DFP sensitivity. Humans with inherited AChE overexpression are likewise hypersensitive to the anticholinesterase pyridostigmine (Shapira et al., 2000). Our working hypothesis postulated that at appropriate levels, AChE-R accumulation in response to stress restores normal cholinergic activity and social behavior. However, under chronic stress, acute anti-AChE treatment or exposure, or in individuals with inherited AChE excess, AChE-R increases to a limit beyond which their cholinergic system cannot further respond and impaired social behavior is a result.

To test this hypothesis, we ascertained whether (a) AChE-S Tg mice display excessive response to a mildly stressful stimulus, a switch in the day/night cycle (Suer et al., 1998), (b) examined AChE-R expression in the brain neurons of AChE-S Tg mice; and (c) studied the social recognition behavior (Thor and Holloway, 1982) of AChE-S Tg mice before and after administration of tacrine or mEN101, an antisense oligonucleotide (AS-ON) shown to selectively suppress AChE-R production (Shohami et al., 2000). Our findings demonstrate constitutive mAChE-R accumulation with inter-animal variability in brain neurons of hAChE-S Tg mice, associated with an exaggerated response to changes in circadian rhythm, and impaired social recognition, which are amenable to effective AS-ON suppression.

Materials and Methods

Animals: AChE-S Tg mice were obtained in a 100% FVB/N genotype from heterozygous breeding pairs (Beeri et al., 1995). Control, non-Tg FVB/N mice were obtained by littermate breeding. Adult, 8-20 wk old Tg and control male mice were housed 4-5/cage in a 12 hr dark/light cycle with free access to food and water. All experiments were conducted during the first half of the dark phase of a reversed 12 hr dark/light cycle, under dim illumination. Routine locomotor activity in the home cage was measured using a remote motility detector (MFU 2100, Rhema-Labortechnik, Hofheim, Germany) to quantify changes in the electromagnetic field.

Telemetric measurements: Battery operated biotelemetric transmitters (model VM-FH, Mini Mitter, Sun River, OR, USA) were implanted in the peritoneal cavity under ether anesthesia 12 days prior to the test. After implantation, mice were housed in separate cages with free access to food and water. Output was monitored by a receiver board (model RA-1010, Mini Mitter) placed under each animal's cage and fed into a peripheral processor (BCM 100) connected to a desktop computer. Locomotor activity after the dark/light shift was measured by detecting changes in signal strength as animals moved about in their cages, so that the number of pulses that were generated by the transmitter was proportional to the distance the animal moved. The cumulative

number of pulses generated over the noted periods was recorded (Yirmiya et al., 1997). Recording lasted 24 consecutive hrs, starting at 9:30 am, with the light phase of a 12:12 hr dark / light cycle beginning at 7:00 a.m. To initiate a day/night switch, the dark/light periods were reversed and recording started 72 hr after the switch and lasted 24 hr. Following intraperitoneal injection of AS-ONs (see below), recording proceeded for an additional 3 hr.

Social exploration tests: Each mouse was placed in a semicircular, transparent observation box and allowed 15 min for habituation, following which a juvenile male mouse (23-29 days old) was introduced. The time spent by the experimental mouse in social exploration consisted mainly of body and anogenital sniffing, chasing, attacking and crawling over the juvenile. Measurements covered a 4-min period, using a computerized event recorder. Each mouse underwent 2 successive social exploration sessions at the noted inter-session intervals. The first session was considered as baseline. In the second session (test), either the same or a different juvenile was introduced. Social recognition was calculated as percentage of tested out of baseline exploration time recorded for each mouse.

***In situ* hybridization and AChE activity measurements**: Animals were sacrificed by cervical dislocation, and brains were removed and dissected or fixed for *in situ* hybridization. AChE activity was measured in hippocampus, cortex and cerebellum extracts as described (Sternfeld et al., 1998). Protein determination was performed using a detergent-compatible kit (DC, Bio-Rad, München, Germany). Immunoblot detection of specific AChE isoforms was as reported (Shohami et al., 2000).

For *in situ* hybridization, 5 μm paraffin sections of brain tissue were prepared after fixation by transcardial perfusion of anaesthetized mice with 4% paraformaldehyde in PBS (pH 7.4). A 50-mer fully 2'-O-methylated 5'-biotinylated AChE-R cRNA probe was applied as described (Kaufer et al., 1998a). Following probe detection with a streptavidin-alkaline phosphatase conjugate (Amersham Pharmacia Biotech Ltd., Little Chalfont, UK) and Fast Red as the reaction substrate (Roche Diagnostics, Mannheim, Germany), micrographs of hippocampal and cortical neurons were subjected to semi-quantitative evaluation of Fast Red staining. Mean signal intensities of light micrographs (taken with a Real-14 color digital camera, CRI, Boston, MA, USA) were analyzed using Image Pro Plus (Media Cybernetics, Silver Spring, MD, USA) image analysis software. The mean intensity of Fast Red labeling was measured in CA3 hippocampal and cortical neurons and corrected for background staining in each picture.

Immunocytochemistry of glial fibrillary acidic protein (GFAP) was performed as described (Sternfeld et al., 2000). Briefly, floating, formalin-fixed, 30 μm, coronal cryostat-sections were pretreated with trypsin (type II, Sigma Chemical Co., St. Louis, MO, USA) 0.001% for 1 min. Sections were incubated overnight at 4°C with a mouse anti-glial fibrillary acidic protein (GFAP) antibody (clone GA-5, Sigma-Israel, Rehovot, Israel), diluted 1:500. Then sections were incubated overnight at 4 °C with horseradish peroxidase-labeled goat-anti-mouse antibody (Sigma-Israel), diluted 1:100. Color was developed by reaction with diaminobenzidine 0.0125%, nickel ammonium sulfate 0.05% and hydrogen peroxide (0.00125%). The development time of the DAB reaction product was controlled by stopwatch to ensure comparability between experiments. Sections were counterstained with cresyl violet.

Quantitative analysis of the hippocampal stratum lacunosum moleculare (SLM) was performed at the level of posterior 2.5 mm from bregma. Using a 40X objective, consecutive fields of the SLM were visualized with a Nikon microscope and processed using an AnalySIS image analysis system. A total of 35 astrocytes were sampled from each group (control vs. Tg). The variables that were compared were intensity of staining of the soma (arbitrary units from a range of 256 shades of gray), soma size (μm^2), and thickness of the largest process of each astrocyte at the process stem (μm). Statistical comparisons were made using Student's t-test, with 68 degrees of freedom.

Considerations for designing antisense tests: *In vivo* antisense suppression of *de novo* AChE-R synthesis was employed throughout the current study to provide a proof of concept (i.e. demonstrate the causal involvement of the secretory, soluble mAChE-R variant in the excessive locomotor activity and the impaired social recognition of Tg mice). Two types of experiments were performed: (1) intracerebroventricular (*i.c.v.*) mEN101 injection of animals subjected to longitudinal social exploration tests (up to one week post-treatment) and (2) *i.c.v.* injection followed by 1-day social exploration test, immunochemical detection and measurement of catalytic activity of brain AChE. Both of these were associated with certain inherent limitations, as is detailed below, yet each test provided evidence to support part of the explored concept.

Intracranial AS-ON injection is inherently more powerful when centrally controlled behavioral parameters are sought; limitations in this case involve the duration of tests (as the animals are all at a post-surgery state) and the requirement to control for the outcome of this surgical procedure in addition to the behavioral test itself. To avoid excessive complications, we refrained from employing double operations (and, therefore, could not use telemetric measurements, which require transmitter implantation, on *i.c.v.*-injected animals).

The experimental controls, as well, were chosen after careful consideration. Each test should involve both Tg and control animals, as well as sham treatment (injection of either saline or an irrelevant oligonucleotide) and comparison between pre- and post-treatment phenotypes. Whenever possible, animals were self-compared, requiring careful time-of-day comparisons; in other cases, groups of animals with similar pre-treatment behavior patterns were compared to each other with regard to the efficacy of the antisense treatment. Neither of these tests is conclusive by itself, however, their cumulative outcome substantially supported the possibility of employing antisense knockdown in careful behavioral tests.

Cannula implantation: Mice under sodium pentobarbital anesthesia (50 mg/Kg, *i.p.*) were placed in a stereotaxic apparatus. Skulls were exposed and a burr hole was drilled. Implantation was with a 26-gauge stainless steel guide cannula (Plastics-One Inc., Roanoke, VA, USA). The tip of the guide cannula was positioned 1 mm above the left lateral ventricle according to the following coordinates: A: -0.4 -0.66* (bl-3.8), (bl = bregma-lamda); L: 1.5; D: -2.2. The guide cannula was secured to the skull with 3 stainless-steel screws and dental cement, and was closed by a dummy cannula. Mice were housed in individual cages and allowed postoperative recovery of 10-14 days before experiments.

Preparation of AS-ON: For *i.c.v.* injection, 2'-O-methyl protected (three-3' nucleotides) oligonucleotides (5 μM) targeted against murine AChE (mEN101) or BuChE (control AS)

mRNA (Shohami et al., 2000) were combined with 13 μM of the lipophilic transfection reagent DOTAP (Roche Diagnostics) in PBS and incubated for 15 min at 37 °C prior to injection. One μl (25 ng) of this oligonucleotide solution was injected in each treatment.

***I.c.v.* administration of AS-ON**: For intracranial microinjections, solutions were administered through a 33-gauge stainless steel internal cannula (Plastic One Inc.), which was 1 mm longer than the guide cannula. A PE20 tube connected the internal cannula to a microsyringe pump (KD Scientific Instruments, Boulder, CO, USA). Solutions were administered at a constant rate during 1 min, followed by 1 min during which the internal cannula was left within the guide cannula, to avoid spillage from the guide cannula. Correct positioning of the cannula was verified following each experiment by injection of trypan blue through the cannula and testing dye distribution after removal of the brains.

Statistical analysis: The results of the *in situ* hybridization experiment were analyzed by a t-test. The results of the circadian shift (Fig. 3C) were analyzed by a three-way, repeated measures ANOVA (genotype x day (routine/reversed) x circadian phase (dark/light)). The results of the social recognition test (Fig. 4) were analyzed by a three-way, repeated measures ANOVA (genotype x stimulus animal (same or different juvenile) x intersession interval). The results of the experiment on tacrine's effect on social recognition (Fig. 5) were analyzed by a three-way ANOVA (genotype x stimulus animal (same or different juvenile) x drug (tacrine/saline)). The results of the effect of mEN101 on social recognition (Fig. 6B) were analyzed by a two-way, repeated measures ANOVA (pretreatment (short/long explorers) x time (days after injection)). The results of the specificity of mEN101 effect (Fig. 7) were analyzed by a three-way ANOVA (genotype x drug (mEN101/control AS) x time (before/after the treatment)). All ANOVAs were followed by post-hoc tests with the Fisher PLSD procedure.

Results

Transgenic mice overexpress host AChE-R: To explore the specific contribution of variant AChE mRNA transcripts towards neuronal *ACHE* gene expression, Tg mice overexpressing hAChE-S in the nervous system were tested by high resolution *in situ* hybridization using cRNA probes selective for each of the two major AChE variants. Excessive labeling was observed in hAChE-S Tg mice as compared with controls in which hybridization was performed with the AChE-S selective probe. This was consistent with the expected cumulative contribution of the overexpressed human transgene and the host mouse (m)AChE-S mRNA transcript (Beeri et al., 1995, 1997). However, hAChE-S Tg mice also displayed variably excessive labeling with the AChE-R cRNA probe, decorating mouse (m)AChE-R mRNA. Fig. 1 presents a representative micrograph of mAChE-R mRNA overexpression in the cortex and hippocampus of a Tg as compared to a control mouse. Neuronal mAChE-R mRNA overproduction in these Tg mice was heterogeneous in its extent, yet significantly higher than that in control mice. Analysis of Fast Red staining showed an increase from an average of 20 ± 3 arbitrary intensity units (± standard error of the mean, S.E.M.) in 5 control animals to 41 ± 5.5 in 6 transgenics ($t(9) = 10.27$, $P < 0.05$). This suggested an inherited predisposition to constitutive AChE-R overproduction in Tg mice. Because AChE-R overproduction is associated with psychological stress, this further called for evaluating its neuroanatomical and behavioral manifestations.

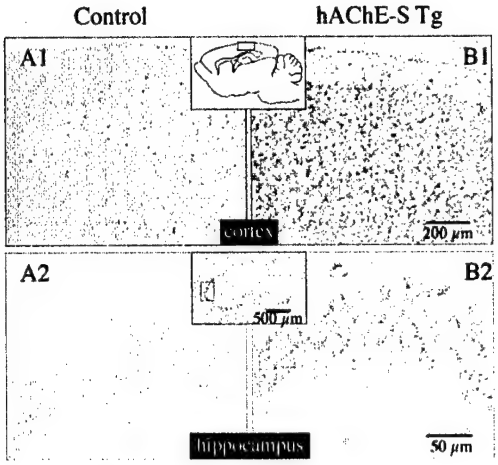

Fig. 1. Intensive neuronal AChE-R mRNA expression in Tg mice Shown are representative micrographs of *in situ* hybridization in parietal cortex (A_1, B_1) and hippocampus (A_2, B_2) using an AChE-R cRNA probe and Fast Red detection. Insets: schematic drawing (top) or low-magnification micrograph (bottom) presenting the location of higher magnification micrographs in the cortex and hippocampal CA3 region. Note the intense AChE-R expression in cortical and hippocampal neurons of Tg mice.

Hypertrophy in hippocampal astrocytes reflects elevated stress in hAChE-S Tg mice: Immunocytochemical labeling of glial fibrillary acidic protein (GFAP) was used in search of an independent parameter for evaluating the stress-prone state of hAChE-S Tg mice. Hippocampal astrocytes are known from previous studies to be sensitive to various forms of stress (Laping et al., 1994; Sirevaag et al., 1991). This property is manifest in morphological changes, increased size of cell soma and of astrocytic processes collectively called "hypertrophy" and which is accompanied by increased expression of GFAP. The hippocampal SLM is particularly enriched in astrocytes, which appeared to be hypertrophic in hAChE-S Tg mice (Fig. 2, B,D) as compared to age-matched controls (Fig. 2, A,C). Astrocytes in other regions, such as cortex appeared unchanged (Fig. 2, E,F). Fig. 2 presents this selective hippocampal change, which is generally considered to reflect the cumulative load of stressful insults in the mammalian brain and is frequently associated with impaired cognitive and behavioral properties (McEwen and Sapolsky, 1995).

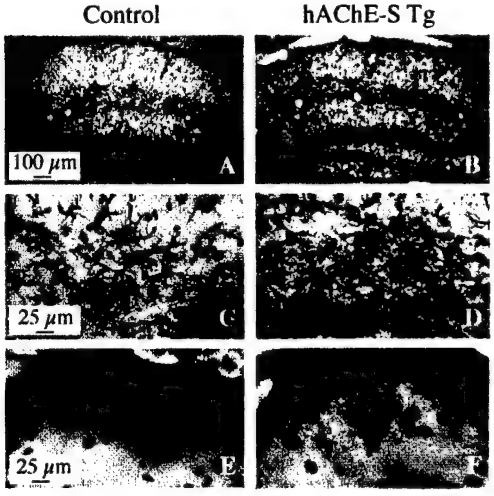

Fig. 2. Intensified GFAP staining in hypertrophic hippocampal astrocytes of hAChE-S Tg mice. Shown are light microscopy micrographs of GFAP immunocytochemical staining in the brain of control (A,C,E) and Tg (B, D, F) mice. Note the intensified cell body staining in hippocampal (A-D) but not in cortical astrocytes (E,F) and the thickened process extensions in the transgenics' astrocytes.

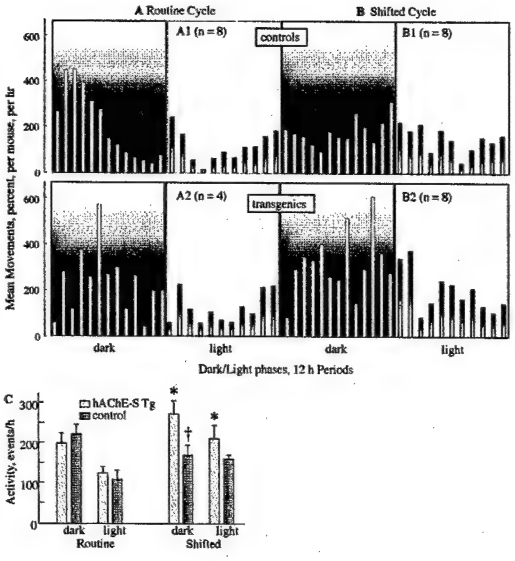

Fig. 3. Spontaneous locomotor activity of control and Tg mice under routine dark/light cycle and following cycle reversal.
Locomotor activity was detected by biotelemetric-recorded movements for 24 hr and is displayed as percent of the mean movements per mouse per hr. Shaded areas in the figure indicate the dark phases of the light/dark cycle. A, routine cycle; B, shifted cycle; C. summated activity intensification. Shown are values of locomotor activity during the dark and light phases in the daily cycle for Tg and age-matched control mice under routine and reversed cycles. *Significantly different from the corresponding group in the routine condition (P <0.05). †Significantly different from Tg mice in the dark phase of the reversed condition.

Intensity of staining of GFAP-like immunoreactivity in the astrocytic soma was significantly higher in Tg mice (176.3 ± 4.0, arbitrary units) compared to control mice (147.8 ± 3.5, t = 5.3, P <0.0001). Cross-sectional area of the astrocytic soma was significantly increased in Tg (45.9 ± 1.4 μm^2) compared to control mice (35.4 ± 1.5, t = 5.16, P < 0.0001). The stem thickness of the large astrocytic process was greater in Tg mice (1.75 ± 0.05 μm) compared to control mice (1.32 ± 0.05, t = 6.21, P <0.0001). Taken together, these data form a picture of 20-30% hypertrophy in hippocampal astrocytes of hAChE-S Tg mice, consistent with the earlier reports of stress-associated and pathology-associated astrocytic hypertrophy (Laping et al., 1994; Sirevaag et al., 1991).

AChE overexpression predisposes to hypersensitivity to changed circadian cycle: Behavioral differences between Tg and control mice were first sought by recording locomotion patterns. Under routine conditions, both genotypes displayed similar home cage activity (Fig. 3A). Their circadian rhythms included, as expected, significantly more frequent and pronounced locomotor activity during the dark phase of the circadian cycle (F(1,24) = 18.16, P <0.001) (summarized in Fig. 3C). Seventy-two hr following reversal of the light/dark phases both genotypes lost most of the circadian rhythm in their locomotor activity, as reported by others (Hillegaart and Ahlenius, 1994), but presented distinctive behavioral patterns (Fig. 3B and 3C). After the shift, hAChE-S Tg mice showed a general increase in activity, which was reflected in a significant genotype by day (routine vs. reversed) interaction (F(1,24 = 4.68, P <0.05). Post-hoc tests demonstrated in Tg mice significantly increased activity in the reversed cycle (compared with activity in the routine cycle), both during the dark and the light phases (P <0.05). In addition, activity in the dark phase of the reversed cycle, was significantly greater in Tg compared with control mice. These findings indicate that adjustment to the circadian insult was markedly impaired in Tg mice, suggesting that these mice display a genetic predisposition to abnormal responses to changes in the circadian rhythm. The transgenics' intensified activity was found to be suppressed for a short time (< 3 hr) by i.p. administration of AS-ONs targeted to the common domain shared by all AChE mRNA variants (preliminary data, data not shown).

Impaired social recognition due to AChE excess: In the social recognition paradigm, control mice could recognize a previously encountered ("same") juvenile. This is manifest as a reduction in exploration time in the second exposure of the mice to the same, but not to a different juvenile, provided that the time interval from the end of the first encounter with that juvenile to the beginning of the memory test did not exceed 15 min. As expected, this memory decayed with increased intersession interval. In contrast, Tg mice tended to explore the previously introduced juvenile longer than control mice and did not display social recognition even after a short interval of 5 min (Fig. 4). These findings were reflected by a significant statistical interaction between the genotype (control vs. Tg) and the stimulus juvenile (same/different) ($F(1,76) = 9.93$, $p<0.01$). In Tg mice, post-hoc analysis revealed significant reduction in exploration time only when Tg mice were tested immediately after the baseline (0 interval) with the same juvenile. These results are consistent with the cholinergic modulation of social recognition behavior (Winslow and Cahcho, 1995).

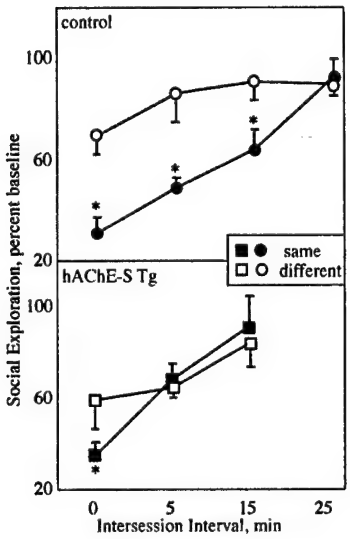

Fig. 4. Working memory deficiency in Tg mice
Shown is percent of baseline social exploration time for 8-11 wk old Tg and control male mice as a function of the intersession interval. Average baseline exploration time was 143 ± 5 and 153 ± 5 (sec ± S.E.M.) for transgenics ($n = 42$) and control mice ($n = 48$), respectively. Asterisks mark significant reductions of exploration time toward the same juvenile ($P <0.05$), as compared to a different juvenile, i.e. short-term working memory. Increased exploration time of the same juvenile with increasing intersession intervals reflects time-dependent decay in the working memory of control mice. After a 5 min interval, Tg mice displayed no reduction in exploration time toward the same juvenile, indicating that they did not remember the same mouse for even 5 min.

The reversible AChE inhibitor, tacrine, has been clinically used for blocking acetylcholine hydrolysis and extending the impaired memory of Alzheimer's disease patients (Giacobini, 2000). Therefore, we tested the capacity of tacrine (1.5 mg/Kg), injected immediately following a baseline encounter with a juvenile mouse, to improve the social recognition of Tg mice. Injected mice were tested with either the same or a different juvenile following a 10-min interval. As expected from previous reports on the beneficial effects of tacrine on social recognition in rats (Gheusi et al., 1994), injection of Tg mice with tacrine induced a significant improvement in recognition memory, with post-treatment performance similar to that displayed by untreated control mice. In contrast, Tg mice displayed no recognition of the same juvenile when injected with saline, and non-Tg control mice maintained unchanged recognition performance when injected with either tacrine or saline (Fig. 5). These findings were reflected by a significant 3-way interaction between the genotype, (control/Tg), the stimulus juvenile (same/different) and the drug (tacrine/saline) ($F(1,52) = 4.18$, $P <0.05$). In a similar experiment, in which the injections preceded the social recognition test by 40, rather than 10 min, tacrine had no effect in either Tg or control mice (data not shown). Therefore, tacrine facilitated memory consolidation when

administered during the consolidation process, but did not affect acquisition of memory when given in advance.

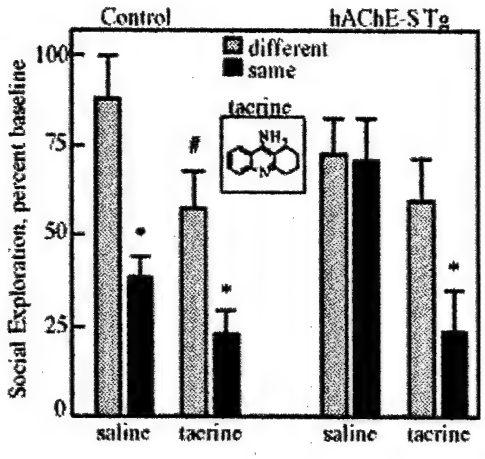

Fig. 5. Tacrine improves working memory of Tg mice.
Presented is the mean social exploration time ± S.E.M. as percentage of baseline time for 29 control and 32 Tg mice (12-15 wk. old, 7-8 mice/group) where either tacrine (1.5 mg/Kg) or saline (10 ml/Kg body weight) was administered intraperitoneally immediately following the baseline exploration period. The intersession interval was 10 min for all groups. Note the post-treatment shortening of explorative time of Tg mice, reflecting improved working memory. Asterisks mark significant reduction of exploration time toward the same juvenile ($p < 0.05$) as compared to a different juvenile. # marks a significant tacrine-induced reduction of exploration time toward the different juvenile ($P < 0.05$).

Explorative behavior is inversely correlated with brain AChE activity: Apart from its improvement of memory, tacrine suppressed the exploration behavior toward a different juvenile in control ($P < 0.05$) but not in Tg mice. Decreased locomotor activity under tacrine treatment was suggested to reflect cholinergic mediation of social exploration behavior (Shannon and Peters, 1990). To further investigate this concept, control mice were divided into 3 equal groups ($n = 10$), presenting short, intermediate or long exploration time of same juveniles. AChE activity was determined in the cortex and hippocampus of each subgroup, 24 hr following social recognition tests of the "same" juvenile (presented 10 min following first exposure). Mice with lower levels of cortical and hippocampal AChE activity spent more interaction time with the "same" juvenile than mice with high AChE activity levels (Table 1), so that their explorative behavior was inversely correlated with cortical and hippocampal AChE activity levels (correlation magnitude, r = -0.49 and 0.41, respectively). Compared to shorter explorers, longer explorer mice exhibited a 29% reduction in cortical AChE activity, corresponding to a >80% increase in social exploration time. The significance of the difference between the shorter and longer explorers was verified by ANOVA ($F(2,27) = 4.89$, $P < 0.05$) and post-hoc tests.

Table 1: Social exploration behavior and brain AChE activities.[a]

	exploration time percent of baseline	**specific AChE activity** nmol ATCh hydrolyzed/min/mg protein	
		hippocampus	**cortex**
total population	80 ± 4	87 ± 4	90 ± 5
shorter exploration time	57 ± 3	96 ± 6	104 ± 10
intermediate exploration time	78 ± 2	95 ± 6	92 ± 10
longer exploration time	104 ± 3	71 ± 7**	74 ± 8*

[a]Control FVB/N male mouse population (n = 30) (3-5 months) was divided into three equal groups (n = 10) with short, intermediate and long exploration time of the same juvenile (shown as average ± S.E.M. percent of baseline). Intersession interval was 10 min for all groups. Mice were sacrificed 24 hr after the behavior test and AChE specific activities were measured in hippocampus and cortex extracts. Asterisks mark significantly lower AChE specific activity in control long explorers as compared with short explorers (P <0.01 for hippocampus and P <0.05 for cortex; ANOVA followed by post-hoc tests with the Fisher PLSD procedure).

The lack of tacrine effect on the social recognition performance in control mice, and its improvement effect on the social recognition in transgenics, with approximately 50% excess AChE (Sternfeld et al., 2000), presented an apparent contradiction to the inverse correlation between AChE catalytic activity and social exploration. One potential explanation to this complex situation was that the inverse correlation in control mice reflected primarily the levels of the synaptic enzyme AChE-S; in contrast, the massive mAChE-R excess in the Tg brain could cause their impaired social recognition behavior. According to this working hypothesis, selective suppression of AChE-R should improve the social recognition performance. To test this hypothesis, we adopted *i.c.v.* injection of mEN101 to prevent *de novo* mAChE-R production (Shohami et al., 2000). Mice were tested in the social exploration paradigm once before (baseline) and then 1, 3 and 6 days after 2 daily injections of mEN101. Fig. 6A presents the experimental design of these tests.

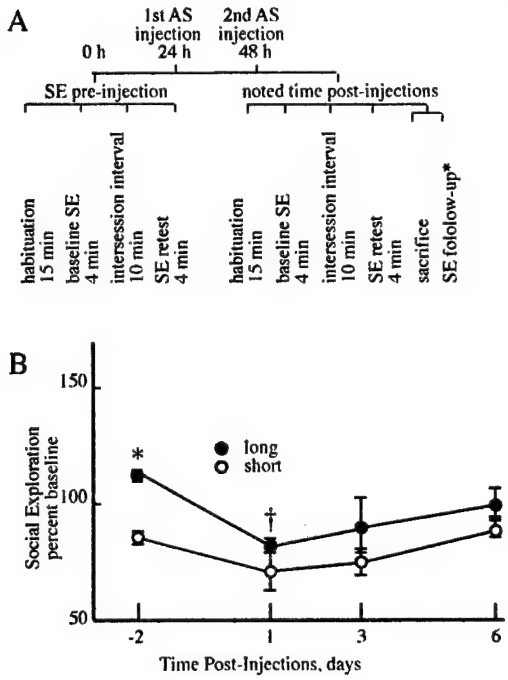

Figure 6: *I.c.v.* antisense effect on the excessive social exploration behavior of Tg mice. A. The experimental paradigm. Shown is the order of procedures and tests of the social exploration capacity in cannula-implanted mice following antisense treatment. See Materials and Methods for details. B. Long-term reversibility and correlation of treatment efficacy with the severity of pre-treatment symptoms. Shown are social exploration values, in percent of baseline performance, for cannulated hAChE-S Tg mice with short and long pre-treatment exploration of the "same" juvenile, following *i.c.v.* mEN101 treatment (n = 5 mice per group). Note that both the efficacy and the duration of the suppression effect are directly correlated to the severity of pre-treatment symptoms. *Significantly different from mice with short exploration time, at day –2 (P <0.05). †Significantly different from mice with long exploration time, at day –2 (P <0.05).

mEN101 improvement of social exploration increases in efficacy and duration in animals with severe pre-treatment impairments: Post-treatment follow-up of social exploration was performed 1, 3 and 6 days following mEN101 treatment in animals with short, medium and long pre-treatment social exploration behavior (n = 5-6/group). As expected, there was a significant

overall difference between the short and the long groups in exploration time ($F(1,24) = 10.81$, $P < 0.05$). However, post-hoc tests revealed that these groups differed significantly only during the pre-treatment day ($P < 0.05$), and not after the mEN101 treatment (Fig. 6B). Furthermore, within the long, but not the short explorers group, social exploration of the "same" juvenile was significantly reduced ($P < 0.05$) one day after the mEN101 injection, with progressive increases in social exploration time during the 5 subsequent days. Because of the pre-treatment differences, the severely impaired animals sustained a certain level of improvement even at the sixth post-treatment day (Fig. 6B) (i.e., even on this day there was no resumption of the pre-treatment difference between the short and long explorers). This experiment thus demonstrated both the efficacy and the reversibility of the antisense treatment, however with exceedingly long duration, especially in animals with severe pre-treatment impairments and in comparison to the short-term efficacy of tacrine.

Antisense AChE-R mRNA suppression selectively reduces brain AChE-R protein: Tg mice with long pre-treatment explorative behavior displayed a significant improvement in social exploration of the "same" juvenile 24 hr following the second treatment with mEN101, but not with the irrelevant control AS-ON directed against butyrylcholinesterase (Fig. 8A) ($F(1,10) = 33.95$, $P < 0.001$). Control mice with either long or short pre-treatment social exploration showed no response to either mEN101 or control AS (Fig. 7A and data not shown).

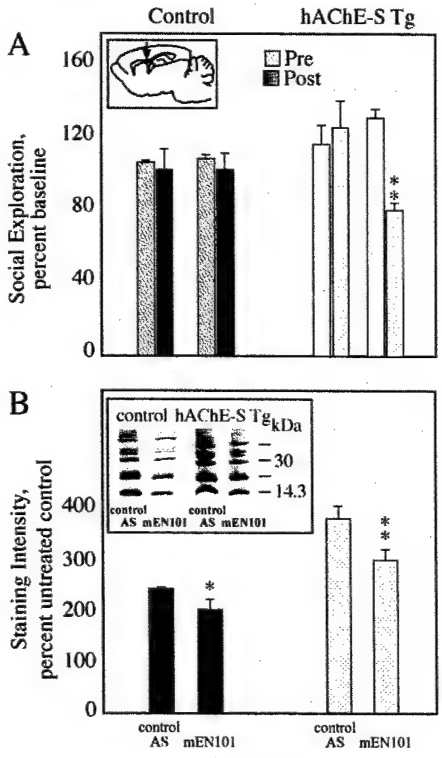

Fig. 7. mEN101 decreases brain AChE-R levels and ameliorates social recognition deficits in Tg-mice. Tg ($n = 36$) and control ($n = 22$) cannula-implanted mice, 10-20 wk old, were injected *i.c.v.* with AS-ONs targeted against AChE (mEN101) or butyrylcholinesterase (control AS) on 2 consecutive days. Social exploration of the "same" juvenile was tested 24 hr before (pre) and 24 hr after (post) injections. Mice were sacrificed immediately after the last social recognition test and brain homogenates subjected to immunodetection of AChE-R. A. Social exploration behavior. Shown are mean social exploration of the same juvenile (percent of baseline ± S.E.M.) before (pre) and 24 hr after (post) AS-ON treatment for long explorer mice (see Table 1). Asterisk marks significant reduction of social exploration time after mEN101 treatment ($P < 0.05$). Inset: Location of i.c.v. cannula in the brain (arrow). B. Immunodetected AChE-R. Mean ± S.E.M. densitometry values for immunodetected AChE-R in cortex extracts of the noted groups post-treatment. AChE-R levels in uncannulated control mice were considered 100%. Asterisks mark significant reduction of AChE-R levels in mEN101 as compared to control AS-treated mice (**:$P < 0.05$, *: $P < 0.1$). Note the significant reduction of immunodetected AChE-R and fragments thereof in cortices from both groups treated with mEN101 as compared with those treated with the control AS.

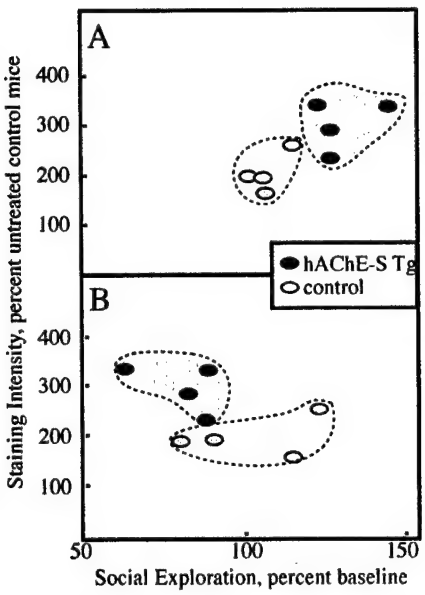

Fig. 8: Decreased AChE-R levels correlate with reduced social exploration time in Tg mice. Presented are cortical AChE-R levels (immunodetected protein, percent of levels in uncannulated controls) as a function of social exploration for each mouse before (A) and after (B) mEN101 treatment. Long-explorer mice, each represented by a dot, were sorted by their genetic backgrounds (control and Tg). Note the exclusive post-treatment shift in the clustered distribution of the Tg long explorers, with excessive mAChE-R levels, as compared with the non-shifted

Catalytic activity measurements performed 24 hr after the last AS-ON injection failed to show differences, perhaps due to the limited number of animals and the variable enzyme levels. However, immunodetected AChE-R protein levels were significantly lower in mEN101 treated mice as compared with control AS treated mice, regardless of their genotype or pre-treatment behavior pattern (Fig 7B and data not shown, $F(1,22) = 19.63$, $P < 0.001$). In contrast, densitometric analysis of immunodetected total AChE protein (detected by an antibody targeted to the N-terminus, common to both isoforms) revealed essentially unchanged signals (data not shown). In further tests for potential association, post-treatment AChE-R levels were plotted as a function of the social exploration values. Data points clustered separately before the AS-ON treatment (Fig. 8A), with both AChE-R levels and exploration times of controls clearly different from transgenics. After treatment, long explorer transgenics shifted to short exploration values (Fig. 8B). Intriguingly, the explorative behavior of long explorer controls was not affected by the treatment, indicating that the reduction in mAChE-R following mEN101 treatment affected only animals that were behaviorally impaired before the treatment. Together, these findings attest to the selectivity of the antisense treatment for treating AChE-R overexpressing animals and its sequence-specificity in reversing the AChE-R induced impairment of behavior.

Discussion

Combination of behavioral, molecular and biochemical analyses revealed multileveled contributions of cholinergic neurotransmission and *ACHE* gene expression, towards the general activity and social behavior of adult Tg mice over-expressing neuronal AChE. In addition to inherited excess of hAChE-S, these Tg mice display conspicuous yet heterogeneous overexpression of the stress-associated "readthrough" mAChE-R in their cortical and hippocampal neurons. Nevertheless, they present close to normal activity patterns under normal maintenance conditions with minimal external challenges. In contrast, their capacity to adjust to behavioral changes in response to external signals appears to be compromised, suggesting that they suffer genetic predisposition for adverse responses to stressful stimuli (McEwen and Sapolsky, 1995).

Behavioral and learning impairments of cholinergic origin: When subjected to a day/night switch, hAChE-S Tg mice respond with excessive bursts of locomotor activity, particularly during the dark phase, but also during the light phase of the post-shift diurnal cycle. In preliminary experiments, this excessive activity could be transiently suppressed by antisense oligonucleotides, which was especially encouraging in view of the progressively impaired neuromotor functioning in these mice (Andres et al, 1997). Matched controls, unlike transgenics, display, as expected, relatively suppressed locomotor activity during the post-shift dark phase (Murata et al., 1999). When confronted twice with a conspecific young mouse, hAChE-S Tg mice spend significantly longer periods than controls in the social interactions characterizing such confrontations. Similarly, in a new environment, hAChE-S Tg mice displayed increased locomotor activity as compared with controls (Erb et al., 2001). In the social recognition paradigm, they failed to remember a conspecific juvenile, even following a delay interval of only 5 min. This extends previous reports on their spatial learning and memory impairments (Beeri et al., 1995, 1997) and agrees with previous reports (Winslow and Camcho, 1995; Perio et al., 1989) on the social behavior changes associated with cholinergic impairments.
(Bluthe et al., 1990), are most likely related, as well, with impaired social interactions. In hAChE-S Tg mice, however, this phenotype may be attributed to hypocholinergic functioning due to AChE excess, as is evident from the capacity of the AChE inhibitor tacrine to retrieve their social recognition. Nevertheless, tacrine's effects appeared surprisingly short-lived, consistent with findings of others (Sekiguchi et al., 1991). In contrast, exceedingly low doses of oligonucleotides suppressing AChE-R synthesis exerted considerably longer-term improvement of the social recognition skills of Tg mice. This suggested non-catalytic activities as an alternative explanation(s) for the behavioral and cognitive impairments caused by AChE-R excess (Soreq and Seidman, 2001).

Circadian switch as a behavioral stressor: Cholinergic neurotransmission circuits are known to be subject to circadian changes (Carlson, 1994) and control the sensorimotor cortical regions regulating such activity (Fibiger, 1991). Therefore, the intensified response of hAChE-S Tg mice to the circadian switch suggested that their hypocholinergic state is the cause. The variable nature of the excessive locomotor activity in the Tg mice indicates an acquired basis for its extent and duration. A potential origin of such heterogeneity could be the variable extent of neuronal mAChE-R mRNA in the sensorimotor cortex and hippocampal neurons. Both psychological (Kaufer et al., 1998a) and physical stressors (Shohami et al., 2000) induce neuronal AChE-R overproduction. Exaggerated stress responses, such as the intense locomotor response to the mild stress of a circadian switch, can hence be expected to exacerbate the hypocholinergic state of these already compromised animals,

In social behavior tests, hAChE-S Tg mice display impaired recall processes causing poor recognition when confronted with a conspecific young mouse. Therefore AChE-R overexpression, which is also induced under stress (Kaufer et al., 1998a), may be causally involved with the reported suppression of recall processes under stress (Kramer et al., 1991) as well as with the apparent correlation between stress and hippocampal dysfunction (Liberzon et al., 1999). This suggests that excess AChE-R can simultaneously impair recall processes and induce excessive locomotion. Stress-induced effects on learning and memory processes have been reported by others (Kaneto, 1997), but were not correlated with AChE levels. Our current

findings of improvement in trangenics' exploration behavior following tacrine injection, which would be expected to augment cholinergic neurotransmission, strongly indicate that their hypocholinergic state was the cause.

Advantages and limitations of anticholinesterases: In control mice, with low AChE-R levels, tacrine did not affect the normal social recognition capacity. This suggests that suppression of AChE activity may have distinct effects under normal and stress-induced conditions. Tg mice with higher AChE levels have accommodated themselves to this state, and it may be this accommodation that renders them incapable of facing a challenge by an anticholinesterase. One option is that of a threshold AChE-R activity that would be compatible both with satisfactory memory and normal locomotion. This balance is impaired in the Tg mice and may also be disrupted under inducers of long-term AChE-R overproduction, e.g. stress or exposure to anticholinesterases (Kaufer et al., 1999). This, in turn, implies that the effect of anticholinesterases would depend on the initial levels of specific AChE variants in the treated mammal. Above the behaviorally-compatible threshold of AChE-R, anticholinesterases would exert behavioral improvement, whereas below it, their effects would be limited, which can explain their differential efficacy in patients with different severity of symptoms.

Glucocorticoid regulation of cholinergic behavioral patterns: The separation between general behavior patterns and learning paradigms as those relate to cholinergic transmission may explain why AChE transgenics, so dramatically impaired in their learning capacities, display such subtle deficiencies in their daily behavior. According to this concept, a constitutive hypocholinergic condition would be evident as a failure to learn and remember, however, its behavioral effect will be far less pronounced, unless challenged. This predisposition to drastic responses to external insults is indeed reminiscent of the reported behavior of demented patients. It had been initially attributed to their elevated cortisol levels (Weiner et al., 1997), which matches recent findings in primates (Habib et al., 2000). Indeed, cortisol upregulates *ACHE* gene expression and elevates AChE-R levels (Grisaru et al., 2001), possibly above the required threshold. In addition, both psychological stress and glucocorticoid hormones were reported to impair spatial working memory (Diamond et al., 1996; de Quervain et al., 1998), consistent with such impairments in the hAChE-S Tg mice. The intensive overexpression of mAChE-R in these mice mimics a situation in which the individual capacity for AChE-R overproduction would be tightly correlated both with the severity of the behavioral impairments induced under cholinergic hypofunction and with the capacity of anticholinesterases to affect learning and behavior properties.

Brain region specificity:
Working and storage memory and the ability to integrate information are tightly linked not only to cholinergic neurotransmission, but to other neurotransmitters as well. Several studies demonstrate that even mild environmental changes (like a day-to-night switch), are accompanied by increased dopamine and noradrenaline extracellular concentration in the prefrontal cortex, and only to a minor extent in the limbic and striatal areas (Cenci et al., 1992). This activation is very selective, since molecular studies have shown that thirty minutes of restraint increase Fos protein in dopamine neurons projecting to the cortex but not in those projecting to the n. accumbens. In this respect altered accumbens and cortical extracellular dopamine concentrations during stress are not secondary to motor activation, but instead reflect increased attention to the provocative

stimulus or attempts by the intruder to "cope" with the stimulus, and therefore are independent of a specific motor activation (Deutch et al., 1991).

The ventral hippocampus is an important neuronal "gate" which should be regarded as system modulator of the cortical response to stress. In this respect cholinergic transmission may contribute to the significance of environmental cues. When neonatal ibotenic acid lesions are produced in the ventral hippocampus, repeated intraperitoneal saline injections attenuate dopamine release in the medial prefrontal cortex, while chronic haloperidol augments dopamine release in the same area of lesioned animals compared to controls (Deutch et al., 1991). This suggests that the ventral hippocampus influences the functioning of midbrain dopamine systems during environmental and pharmacological challenges in different ways (Lipska et al, 1995).

Low dose and long duration of efficacy for antisense agents: The short duration of the behavioral and memory improvements afforded by administration of tacrine parallels the time scale reported for the induction by such inhibitors of a transcriptional activation (Kaufer et al., 1998b). Together with a shift in alternative splicing this feedback response causes secondary AChE-R accumulation facilitating the hypocholinergic condition (Coyle et al., 1983). Recent reports demonstrate AChE accumulation in the cerebrospinal fluid of anticholinesterases-treated Alzheimer's disease patients (Nordberg et al, 1999), suggesting that such feedback response occurs also in humans with cholinergic deficiencies (Coyle et all, 1983) and perhaps explaining the gradual increase in anticholinesterase dosage that is necessary to maintain their palliative value in patients.

Unlike tacrine, the temporary antisense suppression of AChE synthesis improves social recognition in Tg mice for up to 6 days. This requires exceedingly low doses (25 ng per daily treatment) of the antisense agent, about 104-fold lower in molar terms than tacrine concentrations. Active site enzyme inhibitors should be administered in stoichiometric ratios with the large numbers of their protein target molecules. Moreover, the action of such inhibitors terminates when they reach their target. In contrast, a single chemically protected antisense molecule can cause the destruction of numerous mRNA transcripts, each capable of producing dozens of protein molecules. Assuming translation rates of approximately half-hour per chain and an average half-life of several hours for each transcript, destruction of each mRNA chain would prevent the production of many protein molecules. Therefore, the cumulative efficacy of antisense agents can exceed that of protein blockers by several orders of magnitude (Seidman et al, 1999; Galyam et al., 2001). Moreover, the palliative effects of AS-ON destroying AChE-R mRNA should extend long after the AS-ON is destroyed, because AChE-R-induced adverse consequences would occur only above a certain threshold which takes time to accumulate. Therefore, the dose dependent nature of the adverse consequences of AChE-R excess makes it particularly attractive as a target for antisense therapeutics.

We have recently found that AChE-R mRNA, having a long 3' untranslated domain, is significantly more sensitive to antisense destruction than the synaptic transcript (Shohami et al., 2000; Grisaru et al., 2001). AChE-R mRNA transcripts would hence be preferentially destroyed, so that the excess of AChE-R, but not much of the synaptic enzyme, would decrease. This effect may explain the extended duration and increased efficacy of the antisense treatment in modifying behavior and learning exclusively in those mice with disturbed social recognition.

In conclusion, our study provides a tentative explanation for the behavioral impairments under imbalanced cholinergic neurotransmission, attributes much of these impairments to the stress-related effects of the AChE-R variant and suggests the development of antisense approach to selectively ameliorate these effects.
cluster of long-explorer controls.

Pyridostigmine enhances glutamatergic transmission in hippocampal CA1 neurons

Summary

Pyridostigmine, a carbamate AChE inhibitor, is routinely employed in the treatment of the autoimmune disease myasthenia gravis. Due to its positively charged ammonium group, under normal conditions pyridostigmine cannot cross the blood-brain-barrier (BBB) and penetrate the brain. However, several studies have suggested that under conditions in which the BBB is disrupted, pyridostigmine enters the brain, changes cortical excitability and leads to long-lasting alterations in gene expression. The aim of this study was to characterize the mechanisms underlying pyridostigmine-induced changes in the excitability of central neurons. Using whole cell intracellular recordings in hippocampal neurons we show that pyridostigmine decreases repetitive firing adaptation and increases the appearance of excitatory post-synaptic potentials. In voltage clamp recordings, both pyridostigmine and acetylcholine (ACh) increased the frequency but not the amplitude of excitatory post-synaptic currents. These effects were reversible upon the administration of the muscarinic receptor antagonist, atropine, and were not blocked by tetrodotoxinn (TTX). We conclude that pyridostigmine, by increasing free ACh levels, causes muscarinic dependent enhancement of excitatory transmission. This mechanism may explain central side effects previously attributed to this drug as well as the potency of AChE-inhibitors, including nerve-gas agents and organophosphate pesticides, in the initiation of cortical synchronization, epileptic discharge and excitotoxic damage.

Introduction

Pyridostigmine, a carbamate AChE inhibitor (AChE-I), is routinely employed in the treatment of the autoimmune disease myasthenia gravis (Lisak, 1999 Victor and Ropper, 2001) and is also recommended by most armies for use as a pretreatment under threat of chemical warfare because of its protective effect against organophosphate poisoning. Under routine treatment, pyridostigmine is excluded from the brain due to a positively charged ammonium group that prevents its penetration through the blood-brain-barrier (BBB). However, several reports have suggested that under acute stress pyridostigmine may penetrate the mouse brain (Esposito et al., 2001; Friedman et al., 1996; but see also Grauer et al., 2000), increase neuronal excitability and induce long-lasting alterations in gene expression (Friedman et al., 1996; Kaufer et al., 1998a).

The mechanisms underlying pyridostigmine-induced changes in neuronal excitability are not completely understood. While increased free acetylcholine (ACh) levels due to AChE inhibition may underlie depolarization as well as decreased adaptation and action potential threshold (Cole and Nicoll, 1984), other mechanisms not related to ACh have been previously reported (Mrzljak et al., 1998). Actions of ACh include both altering the conductance of specific ionic channels and modulating synaptic transmission. For example, the activation of the nicotinic α7 subunit was demonstrated to increase intracellular Ca^{2+} and to enhance glutamate release in single mossy-fibre pre-synaptic terminals (Gray et al., 1996). The electrophysiological changes secondary to activation of muscarinic receptors were studied more extensively in the CA1 region. It was suggested to decrease conductance of several K^+ channels resulting in a slow depolarization and decreased firing adaptation (Benardo et al., 1982a, 1982b; Cole and Nicoll, 1984; Madison et al., 1987; McQuiston and Madison, 1999; Segal, 1982), to enhance back propagation of action potentials along the dendritic tree (Tsubokawa and Ross, 1997) and to affect both pre- and post-synaptic processes by decreasing Ca^{2+} conductance (Gahwiler and Brown, 1987; Qian and Saggau, 1997).

In this study, based on intracellular recordings in hippocampal CA1 neurons, we propose that increased ACh levels result in alterations in intrinsic and synaptic properties that lead to enhanced neuronal excitability and explain the central side effects of pyridostigmine and its propensity to excitotoxicity.

Materials and Methods

Slice preparation:

Housing and treatment of animals were in accordance with institutional guidelines. Slices were prepared as previously reported (Fleidervish et al, 1996; Friedman et al, 1998). In short, brains of anesthetized mice were quickly removed and placed in ice-cold artificial cerebrospinal fluid (aCSF) containing (in mM): NaCl, 124; KCl, 3; $MgSO_4$, 2; NaH_2PO_4, 1.25; $NaHCO_3$, 26; D-glucose, 10; and $CaCl_2$, 2 (pH 7.4) and saturated with 95% O_2 and 5% CO_2. In order to preserve cholinergic pathways, 400 μM slices were cut in the saggital plane (Vibroslice, Campden Instruments, Loughborough, UK) because the major cholinergic input to the hippocampus originates in the anteriorly located septum. After at least 60 min of equilibration in a storage chamber, slices were transferred to a humidified holding chamber, continuously perfused with oxygenated aCSF at 32 °C (young animals) and 37 °C (adult animals).

Whole cell recordings:

Young mice (12-20 days old) of either sex were used. Whole cell recordings from cells in the CA1 pyramidal cell layer were made using the patch clamp technique (Hamill et al., 1981) as modified for blind recording in slices (Blanton et al., 1989). Patch pipettes, pulled from borosilicate glass capillaries (Hilgenberg, Germany) on a Narishige PP83 puller, had resistances of 3-5 MΩ. For voltage clamp recordings pipettes were filled with a solution consisting of (in mM): 110 CsCl, 25 CsOH, 11 EGTA, 1 $CaCl_2$, 2 $MgCl_2$, and 10N-2-hydroxyethylpiperazine- N'-2-ethansulfonic acid (HEPES). The pH (7.2) was adjusted with CsOH. Series resistance, in the range of 5-8 MΩ, was compensated by 40-85% using the built in circuitry of an Axopatch-200A (Axon Instruments, Foster City, CA) amplifier.

For current clamp recordings, pipettes were filled with a solution consisting of (in mM): 135 K-gluconate, 6 KCL, 2 $MgCl_2$, 10 HEPES. The pH (7.2) was adjusted with KOH. In some experiments extracellular stimuli of 20 μsec duration were delivered using a bipolar electrode (10 μm insulated tungsten wires, 200 μm apart) placed in the Schaffer collaterals.

Data acquisition and analysis:

Signals were filtered at 2 kHz (4-pole Bessel filter), stored on video and digitized off line at 5-10 kHz using Axotape (Axon Instruments) or WCP (J. Dempster) software. Synaptic currents were analyzed using Mini Analysis Program (Jaejin software) – demo version.

Drug application:

Drugs were applied by addition to the bathing solution or by local application as mentioned in the text. ACh and atropine (both 5 mM dissolved in aCSF) were applied by pressure microinjection (20-30 psi) from glass electrodes (tip diameter 50-100 μm) using a Picospritzer II (General Valve, Fairfield, NJ). These electrodes were positioned tangentially to, and at a distance of 100-200 μm, from the recording electrode. In some experiments pyridostigmine, atropine (1 μM each), bicuculine-mediodid (BMI, 10 μM), DL-2-amino-5-phosphonovaleric acid (AP5) or 6, 7-

dinitroquinoxaline-2, 3-dione (DNQX, 20-50 μM each) were added to the bathing solution (all drugs were purchased from Sigma).

Results

Current clamp recordings using whole cell patch configuration:

During current clamp recordings, injection of long depolarization steps evoked repetitive firing with a characteristic adaptation (Fig. 1A). Firing adaptation was reduced following the addition of pyridostigmine (10 μM) to the bathing solution similar to previous studies with the AChE inhibitor, eserine, using sharp electrodes (Madison et al, 1987). The whole cell patch configuration technique enabled us to look closely at the characteristics of spontaneous post-synaptic events. Pyridostigmine increased the frequency of spontaneous sub-threshold post-synaptic potentials (PSPs) (Fig. 1B), while it did not have any measurable effect on the passive membrane characteristics (membrane potential, input resistance around resting potential and membrane time constant) (Fig. 1A, C). These effects of pyridostigmine were reversible 30 min following the addition of atropine to the extracellular solution (Fig. 1A, B, C). While the effect of AChE-Is on firing adaptation was shown to be due to inhibition of a slow K^+ channel (Bernardo and Prince, 1982a; Madison et al., 1987), the mechanism underlying the enhanced occurrence of synaptic potentials is not known. To directly test AChE-Is effects on remotely generated excitatory synaptic currents (EPSCs), the whole cell patch configuration method was used for voltage clamp recordings.

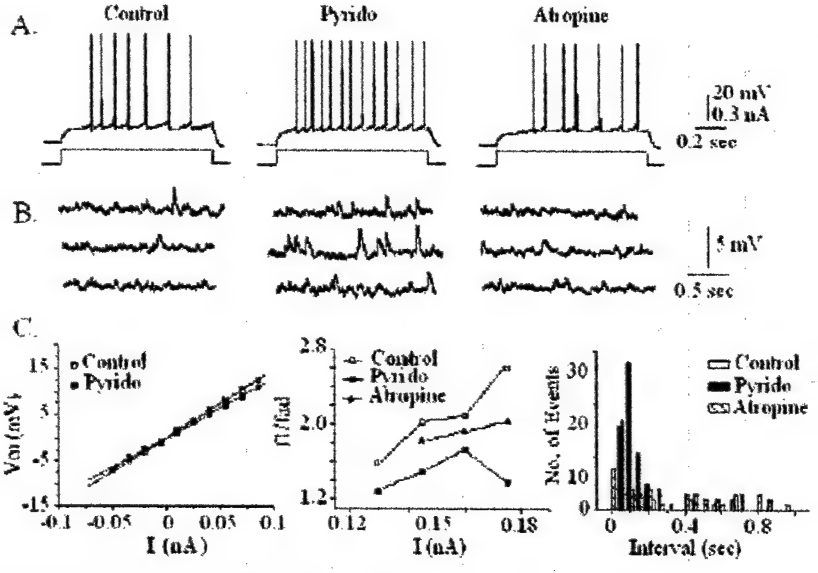

Fig. 1. Pyridostigmine enhances neuronal excitability. A. Representative current clamp recording from a CA1 pyramidal neuron. Note the decrease in firing adaptation following pyridostigmine (Pyrido, middle trace) that reversed following the addition of atropine (right). B. Three consecutive traces under control (left), pyridostigmine (middle) and atropine (right), showing increase in the appearance of spontaneous synaptic events. C. Quantitative analyses of pyridostigmine effects: Left graph: V/I curve. Averaged voltage deflection from 0.5-1 sec of sub-threshold current injection. Middle graph: Firing adaptation vs. amplitude of injected current. Firing adaptation was calculated by dividing the first interspike frequency (f1) to the adapted firing frequency (averaged frequency between 0.5-1 sec). Right graph: EPSP interval histogram in a 1-min window under the three experimental conditions.

AChE inhibitors increase EPSC frequency:

In these experiments inhibitory transmission was blocked by extracellular bicuculine monoiodit (BMI) (GABA-A receptor antagonist). Intracellular $CsCl_2$ was used to block GABA-B currents (Ling and Bernardo, 1994) as well as muscarinic-dependent K^+ channels (Coggan et al., 1994). Under these conditions, perfusion with the AChE-I, pyridostigmine (1 μM), resulted in increased EPSC frequency in 5 out of 6 recorded neurons, suggesting that the drug enhanced release of neurotransmitter vesicles. In the cell shown in Fig. 2A, under control conditions, EPSC analysis revealed 101 events during a 10 sec window (mean interval 100.6 ± 87.7 msec) as compared to 155 events 30 min following the addition of pyridostigmine (mean interval 70.9 ± 63.7, P <0.005, student t-test). The increase in frequency was not associated with significant changes in EPSC amplitude (14.4 ± 8.4 vs. 13.2 ± 8.2 pA, mean ± SDV), rise time (6.4 ± 9.9 vs. 8.4 ± 10.7 msec) or decay time (2.7 ± 4.9 vs. 2.6 ± 4.2 msec) thus indicating a pre-synaptic site of action (Fig. 2B). Since a pyridostigmine mediated increase in excitability was shown to depend upon activation of muscarinic receptors (Friedman et al., 1998; Iwasaki et al., 1988) the non-specific muscarinic antagonist, atropine, was added to the bathing solution. Following atropine perfusion, EPSC frequency decreased by >40% with no effect on amplitude, rise or decay time (n = 3, Fig. 1C).

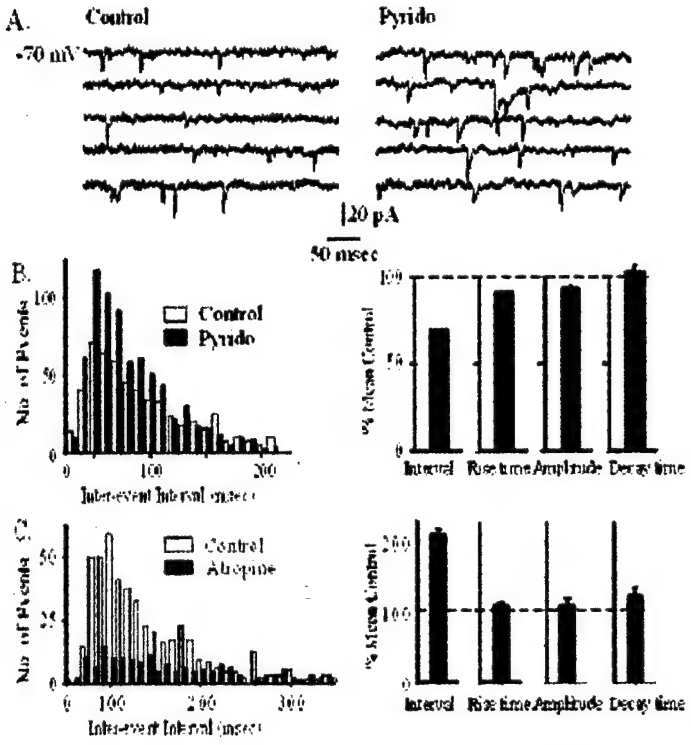

Fig. 2. Pyridostigmine increases EPSCs frequency. A. Five consecutive traces under control conditions (left) and 30 min following the addition of pyridostigmine to the bathing solution. B. Frequency histogram of 10 sec analysis of spontaneously occurring EPSCs before (open bars) and after pyridostigmine (filled bars) showing the increased appearance of events at low intervals following drug addition. On the right, averaged EPSCs characteristics following pyridostigmine in percent change related to control. C. Frequency histogram of spontaneous EPSCs (left) and averaged values of EPSCs characteristics (right) under normal aCSF and 30 min after the addition of atropine. Averaged values are given as percentage of control. EPSCs were collected and measured at holding potential of -70 mV.

ACh enhances excitatory transmission:

Next, we used drop application of ACh to explore whether AChE-Is effects were mediated through an increase in extracellular ACh concentration (see methods). In 8 out of 11 cells ACh application caused instantaneous increase in the frequency of spontaneous events that returned to baseline within 10 sec (Fig. 3A, inset). In three cells, drop application was associated with a large

inward current (>200 pA amplitude, 50-200 msec duration) followed by frequent small synaptic events occasionally riding on a slow inward current (Fig. 3A, B). In two cells, increased frequency was noted only 2-3 sec following application, presumably due to diffusion of the applied ACh. Fig. 3C summarizes detailed analysis of three cells showing the mean increase in cumulative EPSC frequency without an effect on amplitude measured during a 2 sec window following ACh application. When atropine was applied locally, 5-10 sec prior to ACh, the evoked inward current and frequent appearance of EPSCs were significantly reduced (Fig. 3D).

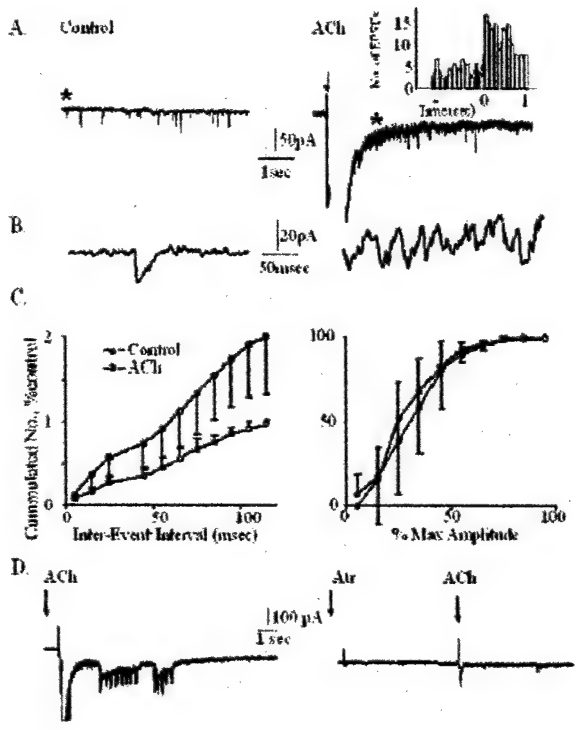

Fig. 3. ACh increases EPSCs frequency. A. Whole cell patch, voltage clamp recording from a neuron at a holding potential of –70 mV. Application of ACh induced prolonged inward current and transient increase in the frequency of spontaneous synaptic events. Inset: the bar graph shows the number of events/sec before and after ACh application (drop applied at time = 0). B. At a faster time scale, events from the asterisk showed in A. C. Cumulative frequency histogram for three cells, showing a decreased interval between EPSCs with no change in amplitude. D. Intracellular recording from a different neuron at a holding potential of -70 mV. ACh application induced inward current and small EPSCs. Prior application of atropine greatly diminished both ACh-mediated effects.

ACh enhances excitatory transmission in the presence of TTX:

Our results point to a pre-synaptic effect of ACh to enhance transmitter release. One possible explanation is that ACh increased firing in pre-synaptic axons, perhaps through a reduced K^+ conductance or direct action on Na^+ channels (Narahashi, 1996). To elucidate such mechanism, ACh was applied in the presence of TTX (10^{-6} M) in the bathing solution. TTX efficacy was assured as no action potentials were evoked when holding potential was moved to depolarizing levels (> -40 mV). Under these conditions, miniature EPSCs (mEPSCs) were recorded with an average amplitude of 7.5 ± 2.8 pA. Although the effects of ACh were less prominent under these conditions, mEPSC frequency was still significantly higher following ACh application, with no apparent change in amplitude (Fig. 4A, B). Similar increase in mEPSC frequency was measured when antagonists of either the NMDA-receptor (5-APV) or the AMPA-receptor were added to the bathing solution (data not shown).

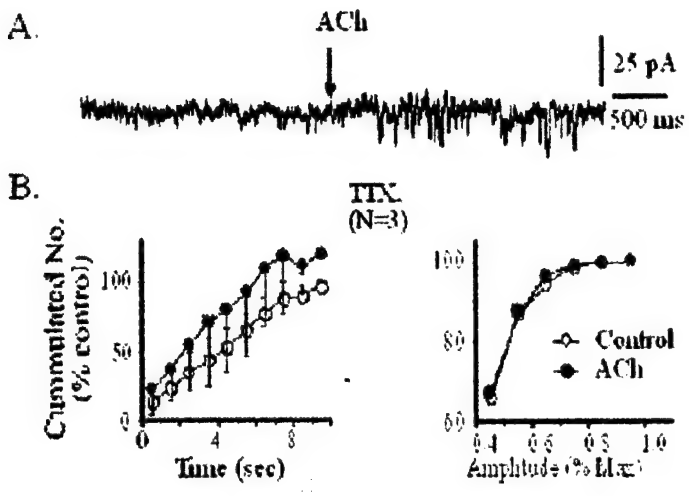

Fig. 4. ACh enhances glutamatergic transmission in the presence of TTX. A. 5 sec trace showing an increase in the appearance of miniature EPSCs following application of ACh. B. Quantitative analysis of three cells showing significant increase in the number of mEPSCs during 8 sec analysis following ACh application (left). The same analysis showed no significant change in amplitude of events (right). Cumulated numbers are presented as percentage of maximum under control conditions.

Discussion

Our results support the following conclusions regarding the effects of pyridostigmine on CA1 pyramidal neurons: (1) Pyridostigmine enhances spontaneous glutamate release. (2) These effects are mediated via increased free ACh levels and (3) ACh action is mediated through the activation of muscarinic receptors presumably located on pre-synaptic terminals.

Anatomical evidence indicates that cholinergic fibers terminating in the stratum radiatum of the CA1 area exhibit an extremely low (<10%) frequency of junctional specialization, supporting a possible role for ACh in modulating the properties of large numbers of pre- and/or post-synaptic elements (Descarries et al., 1997). Here we give evidence for a modulatory role of cholinergic afferents on excitatory transmission to CA1 cells. No detailed anatomical data exists regarding the exact location of cholinergic terminals on CA1 neurons. Yet, in the neocortex, the abundance of nonjunctional oppositions of cholinergic profiles to dendritic spines and axons (Mrzljak et al., 1995) as well as numerous muscarinic receptors in pre- and post-synaptic sites of asymmetric synapses Mrzljak et al, 1988, 1993) support the notion that paracrine ACh release plays a role in modulating excitatory transmission. While AChE inhibition is expected to increase ACh levels and affect CNS choinergic activity, other non-catalytic roles for AChE have been previously suggested. Support for this notion comes from anatomical studies in the human cerebral cortex showing that the distribution of neurons rich in AChE does not parallel cholinergic innervation (Mesulam and Geula, 1991). Moreover, Sternfeld et al. (1988) showed that in neuronal cultures AChE enhances neuritic growth and synaptic development by a mechanism unrelated to its catalytic function. These studies, together with enhanced AChE transcription following CNS exposure to pyridostigmine (Kaufer et al., 1988a) raise the possibility of non-cholinergic responses following such exposure.

Previous studies using sharp electrodes for current clamp recordings have suggested that inactivation of several slow K^+ conductances increases excitability of CA1 neurons following muscarinic activation (Bernardo and Prince, 1982a, 1982b; Cole and Nicoll, 1984; Madison et al., 1987; Segal, 1982). The introduction of the voltage clamp technique using the whole cell patch configuration allowed us to explore the effects of ACh on fast excitatory synaptic currents that emanate electrotonically distant from the soma. While increasing the occurrence of spontaneous

release may not affect somatic membrane potential because most excitatory synapses are located on the electrically isolated spine heads, the concurrent reduction of K^+ conductance along the dendritic tree will cause the cell to be more electrically compact and thus contribute to the slow EPSPs recorded in the soma following muscarinic activation (Madison et al., 1987) as well as to the boosting of action potential back propagation along the dendrites (Tsubokawa and Ross, 1997). Interestingly, Seeger and Alzheimer (2001) recently showed m2-dependent activation of an inward-rectifying K^+ current suggesting a voltage-dependent inhibition of AMPA-mediated EPSPs. Future studies are awaited to reveal the ultimate effect of muscarinic activation in relation to the precise localization of different muscarinic receptors and dependent channels. In addition, several recent studies have shown that excitatory synapses can contain NMDA receptor responses in the absence of functional AMPA receptors and are, therefore, post-synaptically silent at resting membrane potentials (Liao et al, 1995, 2001; Takumi et al., 1999). ACh-mediated enhanced glutamate release might then activate silent synapses via the rapid acquisition of AMPA receptors and may be important in synaptic plasticity and neuronal development (Liao et al., 2001). Such a mechanism could contribute to the augmented NMDA current recorded in the presence of ACh (Makram and Segal, 1990, 1992), as well as to muscarinic-dependent long-term potentiation (Auerbach and Segal, 1994; Sokolov and Kleschevnikov, 1995; Kobayashi et al., 1997) and memory formation (Perry et al., 1999). Under conditions in which ACh levels increase dramatically, such as following toxic exposure to AChE-Is (Messamore et al., 1993), the increased glutamatergic current may lead to rapid synchronization of the local network manifested as the characteristic seizure often observed after exposure to these agents. This may explain the similarities reported between organophosphates and excitatory-amino acids in inducing neuronal toxicity (Noraberg et al., 1998; Solberg and Belkin, 1997). Interestingly, ACh was reported to activate inhibitory interneurons in the CA1 region through the activation of nicotinic receptors (Alkondon et al., 1997; Jones and Yakel, 1997), abundant in interneurons but not in pyramidal cells (Sudweeks and Yakel, 2000). Concurrent activation of both excitatory and inhibitory neurotransmission was postulated to underlie ictal activity due to both GABA-A dependent dendritic depolarization as well as increased pre-synaptic excitability (Traub et al., 1996).

The mechanism underlying ACh-induced glutamate release is not known. However, a mechanism involving enhancement of release from pre-synaptic terminals is supported by our data showing no change in amplitude, rise or fall time of EPSCs following administration of either ACh, an inhibitor of the hydrolyzing enzyme or a muscarinic receptor antagonist. Our observation that ACh action was still observed following the blockade of pre-synaptic action potentials (Fig. 4) further supports a direct pre-synaptic mechanism.

Previous reports showing decrease in Ca^{2+} entry to, presumably, pre-synaptic CA3 terminals following carbachol exposure suggest that voltage dependent Ca^{2+} channels may not be involved (Qian and Saggau, 1997; Scanziani et al, 1995). In line with these data, recent experiments in isolated rat brain synaptosomes showed Ca^{2+} independent, voltage dependent direct muscarinic control on transmitter release (Ilouz et al., 1999). Future experiments should be directed to test the details of muscarinic effects on specific proteins participating in the machinery of transmitter release.

Our data implicate a functional coupling between cholinergic and glutamatergic transmission in hippocampal pyramidal cells. We have recently shown long-lasting alterations in the expression

of key cholinergic proteins in the hippocampus following acute stress or exposure to AChE-Is (Kaufer et al., 1998a; Meshorer et al., 2002). These changes in gene expression tend to reduce ACh synthesis (by down regulating choline acetyltransferase) and enhance its hydrolysis (by up-regulation of the read-through form of AChE), potentially altering the functional coupling between the two transmitter systems (Meshorer et al., 2002). Future studies should explore whether dynamic changes in cholinergic-glutamatergic coupling might occur during physiological or pathological conditions.

Our data suggest that under conditions in which the blood-brain-barrier is disrupted clinically relevant, low concentrations of pyridostigmine (Aquilonius and Hartvig, 1986) may alter cortical function. Disruption of the BBB has been reported in a wide range of clinical conditions including primary CNS pathology and systemic disease. Indeed, CNS-related side effects were occasionally reported following pyridostigmine administration in patients with myasthenia gravis (Iwasaki et al., 1988), in a soldier with low activity of the serum scavenging enzyme, butyryl-ChE (Loewenstein-Lichtenstein et al., 1995) or under stress (Shrabi et al., 1991). Further research is warranted to search for evidence of BBB disruption in patients suffering from CNS-related symptoms who are treated with pyridostigmine or other peripherally acting drugs.

AChE over-expression and its effect on hematopoiesis

FVB/N mice carrying human AChE-S cDNA under control of the promoter were constructed. Three different transgenic strains were further prepared with AChE variants under control of the minimal CMV promoter: two with different expression levels of cDNA of the AChE-R variant and the last variant that has been genetically inactivated by the insertion of a His tag into the active site, thus encoding a catalytically inactive AChE-S, AChE-Sin. Depressed white blood cell (WBC) counts were observed in the mice over-expressing high levels of AChE-S (Tg-S) and its inactive form (Tg-Sin), as compared to control, while platelet counts of the transgenic mice carrying the AChE-R form (Tg-R), were elevated significantly (Fig. 1). To evaluate the status of multipotent hematopoietic progenitors in the bone marrow of transgenic mice, we performed clonogenic progenitor assays where primary bone marrow cells are plated under conditions supporting the growth of specific hematopoietic lineages. In this assay, each colony is taken to represent a single plated progenitor or colony-forming unit (CFU). CFU-MK (megakaryocyte progenitors) and CFU-GM (granulocyte/macrophage progenitors) were significantly elevated in bone marrow from all of these AChE transgenic mouse pedigrees compared to controls ($P \leq 0.001$, Student's t test). Early mixed CFU-GEMM colonies (with the additional potential of producing mononuclear cells and erythrocytes) were also elevated in AChE transgenics, especially in line Tg-R. Interestingly, these latter differences were much less pronounced in colonies grown from mice expressing catalytically inactive AChE-S (Tg-Sin), which may be due to the differences between the cholinergic and the non-cholinergic effects of AChE excess, since AChE-Sin does not hydrolyze acetylcholine. The facilitated capacity of bone marrow progenitors from these transgenic lines to proliferate and differentiate into myeloid, megakaryocyte and adherent colonies supports the notion that AChE-R plays a role in the proliferation of hematopoietic progenitors without compromising their ability to differentiate into the various hematopoietic lineages. That the clonogenic capacity of bone marrow cells from AChE-Sin mice was reduced compared to those from other transgenics, suggests that cholinergic activities are involved.

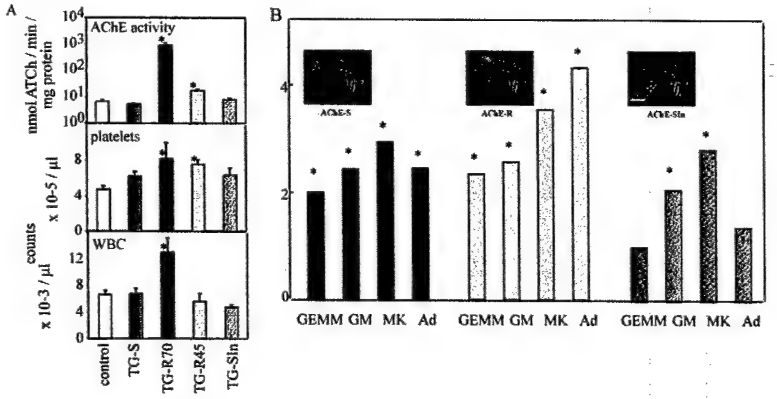

Fig. 1. Hematopoiesis in *ACHE*-transgenic mice

A. Persistent AChE-R overproduction increases platelet and WBC counts in a dose-dependent manner. Shown are intra-cardiac blood AChE levels, platelet and WBC counts determined in FVB/N mice (control, n = 22) as compared to transgenic FVB/N mice carrying the AChE-S (TG-S, n = 12), AChE-R (strains TG-R70 and TG-R45, n = 9 and = 6, respectively) or insert-inactivated AChE-S (AChE-SIn, n = 3) transgenes. Results are expressed as average ± SEM. Note that increases of 2.5- and 130-fold catalytic AChE activities in TG-R45 and TG-70R, respectively, conferred transgene-specific platelet counts increases in both these pedigrees, and that WBC counts increased only in TG-70R, suggesting a dose dependent effect. B. Enhanced clonogenic activities following 1 week in culture are pronounced for AChE-R transgenics, less prominent for AChE-S and negligible for AChE-Sin mice. Shown are fold over control values: serum activity, 7.5 nmol ATCh/min/mg protein; 4.8 x 10^5 platelets/µl; 6.6 x 10^3 WBCs/µl; 9.0 GEMM colonies; 59 GM colonies; 18.9 MK colonies; and 12.7 adherent cell foci. Sample sizes were control, n = 22; AChE-S, = 12; AChE-R, = 9; and AChE-Sin, = 3. Asterisks denote statistically significant difference from the control (P <0.01, Student's t test), for which experimental groups the standard deviations ranged up to 22% (AChE activity, platelets) of the average. Asterisks denote statistical significance (P < 0.05, ANOVA).

Development of human antibody fragments directed toward AChE-S using a semi-synthetic phage display library

Summary

Current Alzheimer's disease therapies suppress acetylcholine hydrolysis by inhibiting AChE at cholinergic synapses. However, anticholinesterases promote alternative splicing changing the composition of brain AChE variants. To study this phenomenon we developed monoclonal antibodies to AChE synaptic peptide (ASP), a synthetic peptide with the C-terminal sequence unique to the human synaptic variant AChE-S. Screening of a phage display human antibody library allowed the isolation of single-chain F_v (scF_V) antibodies that were highly specific for ASP, and displayed closely related third complementarity determining regions of the variable heavy chain domain (V_H-CDR3). BIAcore analysis demonstrated dissociation constants at the micromolar range: 1.6×10^{-6} and 2.0×10^{-6} M for ASP and the complete AChE-S protein, respectively. The anti-ASP antibodies provide a novel tool for studying the synaptic AChE-S variant, the expression of which is altered in ageing and dementia.

Abbreviations: AChE acetylcholinesterase; AChE-E erythrocytic variant; AChE-R readthrough variant; AChE-S synaptic variant; ARP acetylcholinesterase readthrough peptide; ASP acetylcholinesterase synaptic peptide; ASP C-ter acetylcholinesterase synaptic peptide C-terminal 23 amino acid residues; antiASP anti-acetylcholinesterase synaptic peptide (antibody); BSA bovine serum albumin; ELISA enzyme linked immunosorbent assay; PBS phosphate buffered saline; PCR polymerase chain reaction; RU, resonance unit; scFv single-chain fragment variable; SPR surface plasmon resonance; t.u. transforming unit; V_H-CDR3 variable heavy chain third complementarity determining region.

Introduction

Acetylcholinesterase (AChE) hydrolyzes the neurotransmitter acetylcholine at cholinergic synapses, but also exercises morphogenic activities (Soreq and Seidman, 2001). Three C-terminal variants are generated by alternative splicing of the single *ACHE* gene transcript. "Synaptic" AChE-S constitutes the principal variant protein in brain and muscle, and plays an important role in growth-regulating processes affecting neurons, independently of its catalytic activity (Sternfeld et al., 1998). "Readthrough" AChE-R is a secretory, non-synaptic form of the enzyme that is expressed in embryonic and tumor cells (Karpel et al., 1994), and is induced under psychological and chemical stressors, including therapeutic anticholinesterases (Friedman et al., 1996; Kaufer et al., 1998a). In addition, a peptide derived from the unique C-terminal sequence of AChE-R has by itself haematopoietic growth factor-like activity (Grisaru et al., 2001). "Erythrocytic" AChE-E possesses a C terminus with the potential for phosphoinositide linkage to the external membrane of red blood cells (Futerman et al., 1985).

Alzheimer's disease involves complex changes in acetylcholine-mediated neurotransmission (Coyle et al., 1983). Current therapies include inhibitors of AChE aimed at restoring the cholinergic balance (Schneider, 2001). However, increased AChE activity has been reported in the cerebrospinal fluid of Alzheimer's disease patients treated with inhibitors of the enzyme (Nordberg et al., 1999), which is consistent with AChE-R accumulation in the mouse brain under exposure to commonly used anticholinesterases (Kaufer et al., 1998a). Excess AChE accumulation may be detrimental, due to the non-catalytic structural roles of the protein. Indeed, transgenic mice over-expressing AChE-S show late-onset deterioration in cognitive (Beeri et al., 1995, 1997) and neuromotor (Andres et al., 1997) functions reminiscent of Alzheimer's disease. Moreover, accumulation of a yet undefined AChE variant

has been observed in amyloid plaques of Alzheimer's patients (Wright et al., 1993), and AChE-β-amyloid complexes were reported to be more neurotoxic than β-amyloid peptide alone (Alvarez et al., 1998). Obtaining monoclonal antibodies directed against the C-terminal region unique to each human AChE variant would be useful for research into the mechanisms by which such variants signal their morphogenic functions, as well as for studying their specific roles in the etiology and drug treatment of Alzheimer's disease. The phage antibody libraries offer an alternative way to isolate antibodies with many different specificities (Marks et al., 1991; Griffiths et al., 1993; Nissim et al., 1994; Hoogenboom et al., 1999). Selected specific antibodies, phage displayed or secreted from infected bacteria, can be readily used as reagents in immunoblotting, immunohistochemistry, flow cytometric analysis and other applications (Harrison et al., 1996). We used a library of antibodies encoded by human variable-gene segments rearranged in vitro, and displayed on the M13 bacteriophage surface as single-chain Fv (scFv) antibodies (Nissim et al., 1994). Synthetic biotinylated peptides representing the C-terminal sequence unique to human AChE-S were used as targets for selection. Three scFv antibodies were obtained which are highly specific for the AChE Synaptic Peptide (ASP) and interact with the authentic AChE-S.

Materials and methods

Preparation of biotinylated peptides

Two peptides, ASP (NH_2-DTLDEAERQWKAEFHRWSSYMVHWKNQFDHYSKQDRC SDL-COOH) and ARP (NH_2-GMQGPAGSGWEEGSGSPPGVTPLFSP-COOH), were prepared by solid phase-techniques (Atherton and Sheppard, 1989) with a 4334 peptide synthesizer (Applied Biosystems, Foster City, CA), and biotinylation was performed on the protected peptide before cleavage from the resin. The non-biotinylated ARP and ASP C-ter, the latter representing the C-terminal 23 amino acid residues of ASP, were kindly provided by Dr. M. J. Gait (MRC, UK; Grisaru et al., 2001). Peptides were purified by high-performance liquid chromatography to greater than 90% homogeneity.

Selection of phage display antibody library

We used a phage display human semi-synthetic library of >10 8 scFv antibodies (Nissim et al., 1994) for selection. An aliquot of the library (50 µl, 10^{13} t.u./ml) was two-fold diluted in PBS, 0.2% BSA (BSA-PBS) (selection buffer) containing 0.1% Tween 20, and then incubated with 4 µM biotinylated ASP for 1h at room temp. In parallel, 3 x 10^7 streptavidin-coated paramagnetic beads (Dynal, Oslo, Norway) were blocked with 1% BSA-PBS, washed with PBS and resuspended in 100 µl of selection buffer. Streptavidin beads and phage were mixed and left for 15 min on a rotating wheel at room temp. After 5 washes with selection buffer, 5 washes with PBS, 0.1% Tween 20 (PBS-T), and 5 washes with PBS, the captured phage were eluted by incubating the beads in 40 µl 4 M NaCl, 50mM Tris-HCl, pH 7.5 for 30 min at room temp; the eluates were diluted to 150 µl with water. The recovered phage particles were amplified in the *E. coli* amber suppressor strain TG1, and used in a further round of selection after rescue with the helper phage KM13 (Kristensen and Winter, 1998) followed by PEG (20% polyethylene glycol, MW 6000; 2.5 M NaCl) precipitation of the supernatant of the infected bacteria (Harrinson et al., 1996). Before the second round, streptavidin binders were depleted by preadsorption on a streptavidin-coated (10 µg/ml) tube. Selection was then repeated as above; to increase the specificity and the stringency of selection, 2 rounds of antigen binding using 2 µM ASP-biotin were performed before phage growth in bacteria ("double round").

Screening and sequencing of clones

Screening of phage binders was done as described with minor variations (Harrinson et al., 1996). Briefly, selected phage were rescued from single ampicillin-resistant colonies of

infected *E. coli* TG1 using the helper phage KM13. Bacterial supernatants containing the rescued phage were preincubated with the biotinylated ASP, at the same concentration and conditions as used for the first round of selection, and then added to a streptavidin-coated (10 μg/ml) microtiter plate to detect phage binding by ELISA. As negative controls, supernatants preincubated without the biotinylated antigen were used. The diversity of selected clones was determined by PCR amplification using as primers LMB3 (5'-CAGGAAACAGCTATGAC-3') and fd-SEQ1 (5'-GAATTTTCTGTATGAGG-3') and DNA sequencing of scFv inserts with an automated ABI377 sequencer (Applied Biosystems, Foster City, CA). Characterized monoclonal phage were used as reagents after PEG precipitation and quantification of the number of t.u. (Harrinson et al., 1996).

Induction of soluble scFvs, preparation of periplasmic fraction, and purification of antibody fragments

Once the antiASP 1 scFv antibody was selected, it was further engineered with 6 consecutive C-terminal histidine residues. To this end, a PCR amplified product encoding the scFv antibody was purified and digested with the restriction enzymes NcoI and NotI. The resultant 750 bp DNA fragment was gel-purified and ligated into the NcoI–NotI restriction sites of the phagemid vector pHEN1/pTI2 (kindly donated by Dr. I. Tomlinson, MRC, UK) encoding the His6 tail. The ligation product was introduced into the *E. coli* strain TG1 by electroporation. Transformants, picked out from ampicillin-resistant colonies, were checked for antiASP 1 scFv amino acid sequence and C-terminal histidine residues deduced after PCR amplification and DNA sequencing. AntiASP 1 phage with the His6 tail were rescued from selected TG1 transformants using the helper phage KM13, concentrated with PEG, and used to infect (non-suppressor) *E. coli* HB2151. Monoclonal His6-tagged scFvs were harvested from the periplasmic fraction of 1 l cultures of infected HB2151 bacteria induced overnight with isopropyl-D-thiogalactoside at 30°C (Harrinson et al., 1996), and purified over Ni-NTA resin following the protocol provided by the manufacturer (Qiagen). To avoid protein degradation, a protease inhibitor cocktail (Sigma Chemical Co., St. Louis, MO) was added (0.4 mg/ml) to the periplasmic fraction, and the whole protocol was carried out at 4°C. After eluting from the Ni-NTA resin with 250 mM imidazole, 300 mM NaCl, 50mM Na phosphate, pH 8.0, the purified antibody fragments were dialyzed overnight against PBS and used immediately or stored at -80°C with 10% glycerol. The purified scFvs were estimated to be >90% pure by gel electrophoresis and Coomassie staining. Protein concentration was determined with a protein assay kit (Bio-Rad, Hercules, CA).

Specificity evaluation of selected antibodies

Specificity of monoclonal phage antibodies was assessed by ELISA, essentially as described by Henderikx et al. (1998), using indirectly coated ASP. Briefly, biotinylated BSA was added to a microtiter plate at a concentration of 5 μg/ml in PBS, and incubated overnight at 4 °C. After 3 washes with PBS, streptavidin (10 μg/ml in PBS, 0.5% gelatin) and 1 μg/ml of the biotinylated antigen (ASP, or ARP as negative control) in 3% BSA-PBS were applied in consecutive steps. After coating, 10 11 t.u./ml of the indicated monoclonal phage were added to different wells. Phage binding was then detected with a 1:5,000 dilution of horseradish peroxidase/anti-M13-conjugated antibody (Amersham Pharmacia Biotech, Little Chalfont, UK). Phage and secondary antibody were diluted in 3% BSA-PBS. All incubations were for 1 h at room temp, and followed by 3 washes with 0.1% PBS-T and 3 washes with PBS. In the competition experiments, the incubation step with the phage was performed in the presence of the indicated concentrations of human recombinant AChE-S (Sigma) or ARP. For specificity analysis of the soluble antiASP 1 scFv antibody, the same ELISA protocol was carried out, but the concentration of biotinylated ASP or ARP was increased (5 μg/ml). In these experiments, the myc tag was exploited for detection of antibody fragments. This peptide tag

was originally incorporated into the expression vector of the library subjected to selection to be appended to the scFvs (Nissim et al., 1994). Purified, dialyzed scFv antibodies were added to each coated well at a concentration of 0.35 mg/ml in 3% BSA-PBS. Bound scFvs were detected by adding together 1:500 dilutions of the 9E10 antibody (Santa Cruz Biotechnology, Santa Cruz, CA), which recognizes the c-myc epitope (Munro and Pelham, 1986), and peroxidase-conjugated goat anti-mouse IgG (Jackson ImmunoResearch Laboratories, West Grove, PA) in 3% BSA-PBS. Peroxidase activity was measured with 0.1 mg/ml of 3,3',5,5'-tetramethylbenzidine containing 0.012% hydrogen peroxide in 0.1 M sodium acetate, pH 6. The reaction was stopped with 1 M H_2SO_4, and the resulting absorbance was measured at 450 nm in a microtiter plate reader (Molecular Devices, Sunnyvale, CA).

Affinity measurement using the BIAcore technology

The affinity of binding between the antiASP 1 scFv antibody and its epitope was determined using the technique of SPR (BIAcore 3000 System, Uppsala, Sweden) (Roden and Myzka, 1996). The ASP C-ter, human recombinant AChE-S (Sigma) and ARP were immobilized in the different flow cells of a CM5 sensor chip using standard amine coupling procedure (Lofas and Johnsson, 1990). To this end, the ASP C-ter peptide was dissolved to a concentration of 100 µg/ml in 10 mM acetate buffer, pH 4.5, which is below its isoelectric point, to permit preconcentration of the peptide on the biosensor matrix of the BIAcore chip via electrostatic interactions. Immobilization was carried out using a flow of 10 µl/min to obtain 1000 RU. Recombinant AChE-S was diluted to a concentration of 0.87 µM in 10 mM sodium acetate, pH 3.8, and ARP to 100 µg/ml in 10 mM glycine, pH 3.0, for direct immobilization to the chip surface of 2664 RU and 320 RU, respectively. In all cases, the same flow of 10 µl/min was used. The purified scFv antiASP 1 protein was then diluted in 10 mM HEPES, pH 7.4, 150 mM NaCl, 3 mM EDTA and 0.005% (v/v) polysorbate 20, and passed through the different flow cells on the sensor chip at 20 µl/min using concentrations ranging from 125 to 1,000 nM. To eliminate the contribution of non-specific binding, the antiASP 1 scFv antibody was passed through a blank flow cell as well. The dissociation constants were calculated using the BIAevaluation software.

Results

Selection of human phage antibodies to ASP

Two rounds of selection were performed using biotinylated ASP in solution. The conditions of the second round, in which 2 consecutive incubations with antigen were performed before phage amplification in bacteria ("double round"), were designed to enrich the population in specific binders as opposed to phage with growth advantages. A significant decrease in phage titers coming from the second double round demonstrated the stringency of these selection conditions. Whereas in the first simple round, an output phage of 7.5×10^5 t.u. was obtained for an input of 5×10^{12} t.u., only 1.5×10^2 t.u. were recovered after the second double round for the same input titer. No doubt, the preabsorption on a streptavidin-coated tube to deplete streptavidin binders also contributed to this low yield. Under these conditions, an extraordinarily high frequency (44/96, 46%) of specific anti-ASP monoclonal phage antibodies was found following 2 rounds of selection (Fig. 1). Different clones were then picked out for DNA sequencing, to determine the diversity of the selected antibodies. Three distinct specific clones to ASP were identified, namely antiASP 1, 2 and 3 (Table 1). AntiASP 1 was dominant in the population, representing 4 of the 10 sequenced clones. Moreover, the V_H-CDR3 sequences of antiASP 1 and 2 are closely related, both including the SRPS motif, attesting to the sequence specificity of their antigen-antibody interactions. Interestingly, antiASP 1, 2 and 3 were not found among the sequenced clones picked out after the first simple round (sequences not shown), indicating their low concentration in the population until

this step. Also, the percentage of anti-ASP phage antibodies was much lower in the first round (10/96, 10%) than in the second round, demonstrating efficient enrichment in specific binders owing to double selection before phage growth in bacteria. In a parallel search for ARP-specific antibodies, 2 selection attempts were performed against different concentrations (8 and 40 μM) of the biotinylated peptide. None of the selected phage antibodies were found to be specific for ARP. In protein blots using a polyclonal rabbit antibody generated against ARP (Sternfeld et al., 2000), we found that the synthetic peptide easily forms self-aggregates of high molecular weight, even in the presence of the dissociating agents sodium dodecyl sulfate and urea (data not shown). The antigenic determinants in ARP would be likely hidden inside of these aggregates, interfering with the antibody selection. ASP therefore appeared to be much more immunogenic than ARP.

Table 1. V_H-CDR3 sequences of antibody fragments selected against ASP-biotin[a].

Antibody designation	Deduced V_H-CDR3 sequence	Frequency
antiASP 1	SRPSI	4/10
antiASP 2	SRPSH	1/10
antiASP 3	GARFKE	1/10
non-specific	HRAYYS	1/10
non-specific	NSEV	1/10
non-specific	CDMHG	1/10
non-specific	REPVA	1/10

[a]The diversity of selected clones was determined by PCR amplification and DNA sequencing of scFv inserts. After 2 rounds of selection, 3 different specific anti-ASP clones were identified (antiASP 1, 2 and 3) from deduced amino acid sequences of V_H-CDR3. Moreover, the germline origin of the selected ASP-specific antibodies was determined, according to the nomenclature described in Tomlison et al. (1992). The two closely related antibody fragments, antiASP 1 and 2, use DP-24 and DP-3 germline segments, respectively; both belonging to the V_H1 family. AntiASP 3 uses DP-32 of theV_H3 family.

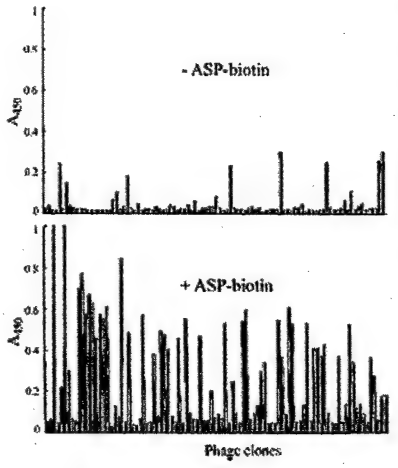

Fig. 1. Enrichment of anti-ASP phage after two rounds of selection. Shown are absorption values for culture supernatants of single bacterial clones producing selected phage antibodies. Incubation was with biotinylated ASP, followed by addition to streptavidin coated wells of a microtiter plate. Supernatants preincubated without the biotinylated antigen were used as negative controls. Binding of phage was detected via an anti-M13 peroxidase conjugate as absorption at 450 nm. Phage antibodies were considered specific when A_{450} ratios of experimental to controls exceeded 3.

Selected scFv antibodies are highly specific for ASP and do not interact with ARP

To exclude the possibility that the 3 isolated anti-ASP monoclonal phage would also interact with the distinct C-terminal peptide unique for human AChE-R, an ELISA was performed (Fig. 2). The absorbance signal was specific for all phage antibodies, since they reacted strongly with ASP, the antigen used for selection, but not with ARP. AntiASP 1 showed the

highest specific signal, as expected for the dominant clone in the population after 2 rounds of selection.

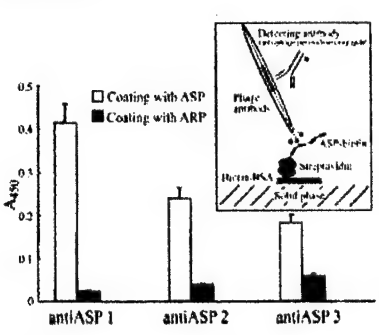

Fig. 2. Specificity analysis of monoclonal phage antibodies. An ELISA was carried out using wells indirectly coated with ASP or ARP, to check the specificity of selected antibodies. For the coating, BSA-biotin, streptavidin and the biotinylated antigen (ASP or ARP) were applied to a microtiter plate in consecutive steps, as described in Materials and Methods. After last wash, 10^{10} t.u. of phage were added to different wells. Detection of bound phage was as in Fig. 1. Values reported are average ± standard deviation from 4 independent determinations. Inset: a schematic representation of the ELISA.

The selected antiASP 1 was engineered with 6 consecutive C-terminal histidine residues, as described in Materials and Methods. AntiASP 1 phage with the embodied histidine residues were used to infect the non-suppressor HB2151 strain of *E. coli*, which was then induced to produce free scFvs (Harrison et al., 1996). The His6-tagged antibody fragments purified over a Ni-NTA resin were highly specific for ASP as judged by ELISA, and did not interact with ARP (Fig. 3). This assay thus reinforced the results obtained for the phage display antibody.

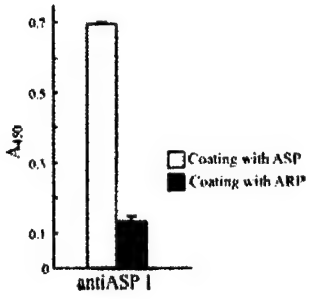

Fig. 3. Specificity analysis of soluble antiASP 1 scFv antibody. The ELISA protocol was carried out as for phage antibodies (Fig. 2), except the last detection step. Thereby, 9E10 and secondary anti-mouse peroxidase antibodies were used to detect the myc-tagged scFvs. Average ± standard deviation values are shown for three different measurements

AntiASP 1 recognizes authentic AChE-S

To test whether the antiASP 1 monoclonal phage antibody would also be selective for native AChE-S, a competitive ELISA was performed (Fig. 4). The antiASP 1 clone was chosen due to its high occurrence after the last round of selection (Table 1) and because it exhibited the strongest interaction with ASP in ELISA (Fig. 2). Phage were mixed with increasing concentrations of AChE-S or ARP, and then added to different wells of a microtiter plate coated with ASP. The AChE-S protein acted as a competitor diminishing the binding of the antiASP 1 phage to the wells, suggesting that the phage anti-body interacted specifically with soluble AChE-S. About 70% of the binding was abolished in the presence of 0.5 µM AChE-S, whereas no effect was observed in the case of soluble ARP (Fig. 4), even when an 8 µM concentration was tested (data not shown).

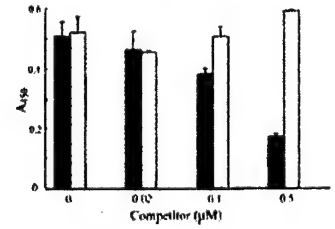

Fig. 4. AChE-S specific interaction with antiASP 1 analysed by competitive ELISA. ASP-biotin (100 ng, 19 pmol) was indirectly immobilized as in Fig. 2. AntiASP 1 phage suspension (100 µl; 10^{11} t.u./ml) was added to the ASP-coated wells in the presence of increasing concentrations of either human recombinant AChE-S (black column) or ARP (white column). Average ± standard deviation values are shown (n = 2).

AntiASP 1 binds to its antigen with micromolar affinity

The binding affinity of the soluble antiASP 1 scFv antibody was determined using SPR in the BIAcore 3000 system. A peptide with the sequence of the 23 C-terminal residues of AChE-S (ASP C-ter), human recombinant AChE-S and ARP were immobilized in the different flow cells of a CM5 sensor chip. The scFv purified antiASP 1 was passed through the flow cells at several concentrations, and the kinetic constants were determined by the evaluation software of the BIAcore version 1.2. The best fit for the binding curves was obtained using the bivalent analyte model, suggesting that the antibody fragments can partly associate to form a mixture of dimers and monomers (Nissim et al., 1994). The measured affinities of antiASP 1 show dissociation constants at the micromolar range: 1.6×10^{-6} and 2.0×10^{-6} M for ASP C-ter and AChE-S, respectively. No interaction was observed between antiASP 1 and ARP.

The ASP C-ter, unlike ARP, is rich in polar residues, which are often exposed and involved in the interactions between antibodies and antigens (Chothia and Lesk, 1987). In the V_H-CDR3 of antiASP 1, the replacement of an isoleucine with a histidine residue induces a diminution in the binding signal (Table 1 and Fig. 2, antiASP 1 versus 2). This was compatible with electrostatic repulsion, due to the high number of basic residues in ASP C-ter (2 His, 2 Lys, and 1 Arg).

Discussion

During recent years, non-classical AChE functions have been established by several research groups (Layer and Willbold, 1995; Bigbee et al., 2000; Soreq and Seidman, 2001). Cumulative information attributes some of these alternative activities to the C-terminal variants of the enzyme (Sternfeld et al., 1998, 2000). However, unequivocal evidence for this heterogeneity is still sparse. Therefore, obtaining monoclonal antibodies with the capacity to distinguish among AChE protein isoforms will be of utmost importance to study tissue and cellular distribution of each variant, and to determine whether specific functions may be assigned to specific variants. Our current findings present one step in a wider effort to develop research tools for studying the distinct properties of AChE variants. Our previous preparation of a polyclonal rabbit antibody against a glutathione transferase fusion protein with ARP (Sternfeld et al., 2000) demonstrated the very low immunogenicity of ARP, which calls for improved methods. To this end, synthetic peptides, which represent the C-terminal sequences unique to human AChE-S and AChE-R, were used as targets for selection from a phage display antibody library. This methodology offers important advantages over the classical hybridoma technology. First, phage display repertories from variable-genes rearranged in vitro enable the isolation of monoclonal antibodies with specificities that have proved difficult by animal immunization and classical technology, for example against highly conserved intracellular proteins (Nissim et al., 1994).

Second, we have assumed that the sequence homology of AChE to nervous system cell adhesion proteins, such as neurotactin, neuroligin, and gliotactin, is the basis of its morphogenic functions (Darboux et al., 1996; Grifman et al., 1998; Grisaru et al., 1999). Interaction of AChE variants with distinct protein partners would, therefore, modify cellular signaling to cause clearly different biological effects (Grisaru et al., 1999). A suitable approach to the identification of these protein partners should be to screen phage display random peptide libraries, since central to this strategy is the observation that peptides isolated by affinity selection from such libraries typically interact with biologically relevant domains of the target protein (Adey and Kay, 1997). The DNA that encodes the selected peptides can

be easily sequenced from the appropriate region in the viral genome; this enables a search of sequence homologs to identify potential AChE protein partners. Therefore, the acquired experience with phage repertoires during the selection of monoclonal antibodies will be essential to undertake the next goals of the project. Furthermore, the amino acid V_H-CDR3 sequences of antibody fragments selected from phage libraries can be readily deduced. The V_H-CDR3 is the most important region in the recognition between antigen and antibody (Chothia and Lesk, 1987), and can contribute to our understanding of the type of protein interactions in which the AChE C-termini may be involved.

A high frequency (46%) of phage carrying specific anti-ASP scFvs was found after 2 rounds of selection against the biotinylated peptide in solution (Fig. 1). The DNA sequencing of selected phage antibodies allowed identification of 3 different clones, 2 of them with closely related V_H-CDR3 (Table 1). AntiASP 1 was dominant in the population, representing the 40% of sequenced clones, and showed the strongest specific signal to ASP by ELISA (Fig. 2). Most importantly, antiASP 1 also interacted with the whole AChE-S protein as judged by competitive ELISA and BIAcore analysis (Fig. 4 and SPR results), in accordance with previous work that demonstrated the ability of antibodies selected against peptides from phage display libraries to recognize the native protein (Henderikx et al., 1998; Persic et al., 1999). The antigenic determinant for antiASP 1 is located within the C-terminal 23 amino acids of ASP, as BIAcore analysis showed interaction between the soluble scFv antibody and the ASP C-ter. By hybridoma technology, Boschetti et al. (1996) obtained monoclonal antibodies against a peptide with the sequence of the 10 C-terminal residues of AChE-S; these antibodies recognized the brain enzyme. All together, these observations demonstrate that the C-terminal sequence of ASP is an efficient and physiologically exposed immunogen, capable of interacting with antibodies also when part of the complete protein. This is an important consideration since the structural properties of ASP are not yet known. Besides surface exposure and accessibility to the large antibody molecule (Thornton et al., 1986), protein regions corresponding to antigenic peptides are thought to possess high mobility. So, based on X-ray crystallographic temperature factors, Tainer et al. (1984) showed that anti-peptide antibodies against highly mobile regions react strongly with the native protein, while anti-peptide antibodies from well-ordered regions do not. These authors suggest that molecular mobility could be an essential part not only of the antigenic recognition process but also of protein-protein recognition in general.

The core domain common to all AChE variants possesses a high degree of sequence homology with adhesion proteins but lacks the capacity to form protein interactions by itself. In contrast, their variable C-terminal chains could interact with distinct protein partners. The AChE-S variant includes an exon 6-encoded 40 residue C-terminal extension (ASP), which initiates by a putative amphipathic ring formed by the closest 16 amino acids to the core domain of the protein (Soreq and Glick, 2000). This amphipathic ring may enable the attachment of AChE-S to membranes. On the other hand, our experimental data indicate that the C-terminal 23 amino acid sequence of ASP is highly exposed and mobile, suitable for participation in protein-protein interactions when it is not involved in dimerization of AChE subunits through its cysteine residue.

In conclusion, we have selected human antibody fragments, which are highly specific for the C-terminal sequence unique to human AChE-S. The dissociation constants, calculated by SPR in BIAcore, are 1.6×10^{-6} M for the interaction between ASP C-ter and antiASP 1, and 2.0×10^{-6} M for the interaction between AChE-S and antiASP 1, within the affinity range expected

for scFv antibodies selected from phage display libraries (Marks et al., 1991; Griffiths et al., 1993; de Kruif et al., 1995). Antibodies with improved affinities can be obtained by diverse means (Marks et al., 1992; Vaughan et al., 1996; Neri et al., 1997). However, affinity maturation may not be required for in vivo biological effects or for other applications. Thereby, antiASP 1 should be useful for a quantitative assay (ELISA or immunoblot-type) for the determination of AChE-S levels in tissues and body fluids, for example during embryonic development and neurogenesis and in syndromes such as Alzheimer's disease, and for studying other processes in which AChE is involved. For these purposes, antiASP 1 can be used as either phage displayed or soluble scFvs, the latter being easy to purify through their His6-tag and detect by their myc-tag. Determination of AChE-S levels in ageing and dementia should be of particular interest.

Frequent blood-brain barrier disruption in the human cerebral cortex

Summary

The blood-brain-barrier (BBB) protects the brain from circulating xenobiotic agents. The pathophysiology, time span, spatial pattern and pathophysiological consequences of BBB disruptions are not known. Here, we report the quantification of BBB disruption by measuring enhancement levels in computerized tomography brain images. Pathological diffuse enhancement associated with elevated albumin levels in the cerebrospinal fluid (CSF) was observed in the cerebral cortex of 28 out of 43 patients, but not in controls. Four patients displayed weeks-long focal BBB impairment. In 19 other patients, BBB disruption was significantly associated with elevated blood pressure, body temperature, serum cortisol, and stress-associated CSF "readthrough" acetylcholinesterase. Multi-electrode electroencephalography revealed enhanced slow-wave activities in areas of focal BBB disruption. Thus, quantification of BBB disruption using minimally invasive procedures, demonstrated correlations with molecular, clinical, and physiological stress-associated indices. These sequelae accompany a wide range of neurological disorders, suggesting that persistent, detrimental BBB disruption is considerably more frequent than previously assumed.

Introduction

The blood-brain barrier (BBB) separates the brain's interstitial space from the blood and prevents the penetrance of circulating molecules and cells into the brain (Rubin et al, 1999; Soreq et al, 2000). Perturbations in the integrity of the BBB have been reported in both humans (Cornford and Oldendorf, 1986; Klatzo, 1983; Skoog et al, 1998; Akeson et al, 1995) and animal models (Friedman et al, 1996; Abbruscato and Davis, 1999) under numerous pathological conditions. In animal studies, BBB permeability can be quantitatively evaluated by measuring the concentration in the brain of non-permeable radioactive materials, traceable macromolecules or dyes (Friedman et al, 1996; Abbruscato and Davis, 1999). However, none of these approaches is applicable to humans due to their invasiveness and the potential risks involved. Therefore, in most human studies, BBB permeability has been estimated using brain imaging techniques (computerized tomography (CT) (Roman-Goldstein et al, 1994), magnetic resonance imaging (MRI) (Akeson et al, 1995), or single photon emission CT (SPECT) (Siegal et al, 2000)). Alternatively, altered serum constituents were searched for in the cerebrospinal fluid (CSF) (Correale et al, 1998). However, no quantitative, minimally invasive approach is as yet available for evaluating BBB integrity. Therefore, the extent of enhanced BBB permeability among different patients and to different molecules, as well as the clinical correlates that predict BBB disruption await definition. Likewise, the susceptibility of different brain sub-regions to BBB disruption and its time resolution are still unknown. Resolution of these issues would bear wide implications to many, as it may open the way both to rationalized drug delivery into the brain and to avoidance of such penetrance when undesired. To this end, we conducted a study to develop minimally invasive means for quantifying BBB integrity. Here, we report the use of brain CT image analysis for quantitative estimation of BBB integrity in patients with various Central Nervous System (CNS) disorders. Our search for clinical conditions associated with compromised BBB suggests stress responses as a possible common denominator, points to the cortex as particularly vulnerable to BBB disruption and demonstrates that such disruption may persist for at least several weeks. Focal abnormal cortical activity in areas associated with BBB disruption suggests the functional implications of such conditions. This may assist in future studies of BBB integrity in various

diseases and its implications to brain functioning as well as to the susceptibility to the penetrance of serum constituents, including drugs.

Methods

Brain CT was performed using the PICKER Helical CT-TWINS (Elscint, Haifa, Israel). Scans were taken at the standard axial slices (5mm intervals) before and ca. 1 min following the injection of the contrast agent Omnipaque (1cc/Kg body weight). "Control" brain scans were from randomly selected ambulatory patients who were referred for investigation, and were interpreted as "normal" by two radiologists. "Patients" CTs included patients who by signs and/or symptoms were suspected to suffer from CNS disorders and their brain CTs interpreted as abnormal. Eighteen patients from this group, as part of their clinical investigation, were subjected to blood analysis, lumbar tap for CSF analysis and brain CT, all within 12 hours. Intensity was measured bilaterally in Hounsfield units (Brooks, 1977) in round, 5-8mm diameter regions of interest (ROIs). ROIs included sub-cutaneous tissue of the neck, cerebellum (2 centimeters lateral from the fourth ventricle), pons (one ROI at midline), thalamus (1 centimeter lateral from the third ventricle), white matter (at the corona radiata, bilateral to the anterior horns of the lateral ventricles), and gray matter (bilateral frontal). Using an image analysis program (Adobe PhotoShop), images (pre and post contrast agent administration) were differentiated so as to reveal contrast agent enhancement. To compare between different patients, the differential image was rescaled using a colored spectrum (blue to red) between water and bone densities (0-1000 Hounsfield Units, respectively).

Magnetic Resonance Imaging (MRI) was performed using a Philips "Gyroscan" T5-NT machine (power track 1000, 0.5 telsa). Single Photon Emission CT (SPECT) scans were performed using a dual headed "Varicam" gamma camera connected to an image processing "Expert" computer (acquisition mode, format 128x128 pix. 120 images- each image at 3°). BBB penetration was measured following the administration of the permeable compound ^{99m}Tc-diethylenetriaminepentaacetic acid (Tc-DTPA). To measure blood perfusion to brain regions, patients were administered (more then 48 hours after the Tc-DTPA study) the freely permeable compound ^{99m}Tc- ethyl cysteinate dimer (Tc-ECD) as the radioactive material. Patient clinical indices were gathered from hospital records relating to the same day when scans had been performed. When more than a single value was available for a patient, an averaged value was deduced for up to 6 hours before and after time of scanning.

To detect the stress-associated readthrough variant of acetylcholinesterase (AChE-R) and its C-terminal degradation products, CSF proteins (10µl, diluted 1:10 in PBS) were separated on 4-20% polyacrylamide gels (Bio Rad laboratories, Hercules CA). Albumin was detected on these gels by Ponceau staining and its migration compared to that of commercially available albumin (Sigma Chemical Co., St. Louis, MO). Resultant immunoblot filters were incubated with rabbit antibodies elicited against a recombinant fusion protein of gluthathione S-transferase (GST) and a peptide with the sequence of the 26 C-terminal residues of AChE-R. Antibodies were preimmunoabsorbed using GST beads to ensure specificity and were proven to interact selectively with AChE-R and not with the alternative synaptic isoform AChE-S (Sternfeld et al, 2000). To detect the core AChE protein, similar blots were incubated with Chemicon anti-AChE antibodies. Detection was with peroxidase-conjugated anti-rabbit immunoglobulins and ECLTM detection (Amersham, UK).

Electroencephalogram (EEG) recordings were collected using 23 standard scalp surface electrodes (Biologic Systems Corp. Mundelein, IL, USA) according to the 10-20 standard system with additional bilateral mastoid recordings. Electrodes impedance was kept below 5 kΩ using abrasive skin prep-cream. EEG data were collected using a CEEGRAPH IV 128-channel EEG acquisition unit (Biologic Systems Corp. Mundelein, IL, USA) while the patient was resting supine with eyes closed. Artifact-free data from all electrodes were segmented into two-second epochs and a power spectrum for the entire time span was calculated for each electrode.

Results

Under normal conditions, the enhancement agent Omnipaque accumulates in peripheral tissues but does not significantly penetrate most CNS regions due to the functioning of the BBB. In search for impairments in BBB integrity, radio-opaqueness was measured (McCullough et al, 1974) before and after the injection of Omnipaque. Fig. 1 demonstrates these features in a cohort of 62 patients with normal neurological examination who were subjected to brain CT in which pathology was excluded ("controls"). Mean percent enhancement of radio-opaqueness in the soft-tissue of the neck was 25.0±33.9 (mean ± SEM). The large inter-measured variance is likely due to technical (amount of the injected agent, scanning latency) and/or physiological (e.g. venous return, cardiac output or cerebral blood flow) differences. Despite this variability, linear correlation was found between signal enhancement values in the 2 sides of the neck tissue (Fig. 1A). In contrast, brain signal enhancement measured in 9 different ROIs was significantly lower (3.4±1.8%, P<0.0001, *t*- test) and displayed a much smaller variability. No correlation was found between signal enhancement in any brain region to that of the neck tissue, demonstrating bilateral impermeability of the healthy brain to Omnipaque (Fig. 1A).

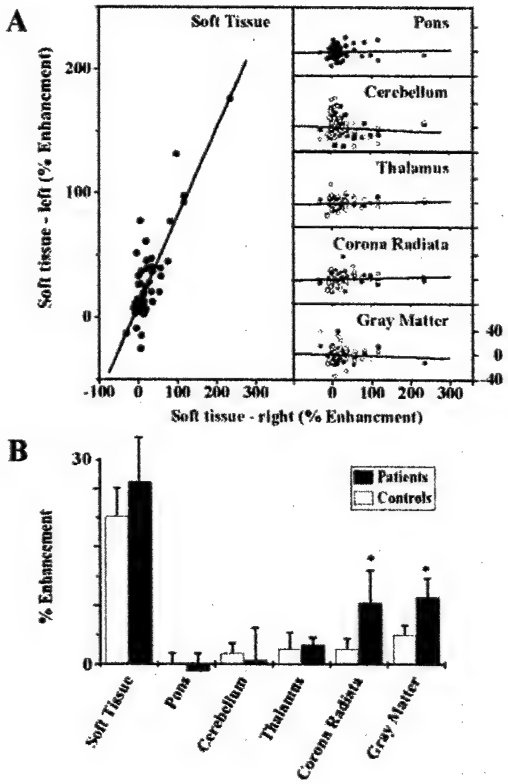

Fig. 1. CT Enhancement in controls and neurological patients

A. Control scans display impermeability to Omnipaque. All measurements were taken in Hounsfield units (HU) in 5-8 mm diameter ROIs (Methods). Readings from the left side of the neck (soft tissue) were plotted as a function of those of the right side. Note that up to 300% bilateral enhancement was measured in neck (soft tissue, left), and no penetrance into brain regions (right). B. Selective cortical susceptibility for BBB permeation in neurological patients. Shown are average enhancement values in controls (n=62, open bars) and neurological patients (n=43, filled bars). Stars note significantly higher (P<0.05, *t*-test) enhancement values in gray and white matter of the cerebral cortex (gray matter, corona radiata).

In 43 patients with neurological signs and symptoms suspected to be due to CNS abnormality ("neurological patients"), and no focal lesion was found on bCT, mean brain enhancement ranged at 5.9 to 110.2% (12.9±15.3%, mean ± SEM). This enhancement, significantly higher than that in healthy controls ($p<0.001$, *t*- test), suggests that in neurological patients penetrance may occur often, reflecting a frequent impairment of the BBB. In 26 patients (60%) average brain enhancement was greater than 2 standard deviations from the mean enhancement in the control population, reflecting significant abnormal penetrance. No significant difference was found in soft-tissue enhancement between patients and controls, excluding the possibility that differences could be attributed to the amount of injected contrast agent or variable blood flow. In most patients, the gray and white matter of the cerebral cortex were the only regions to show larger enhancement than the control population (gray matter enhancement was 8.5±13.2 and 4.5±3.2 in patients and controls, respectively, $p=0.06$, *t*-test). Interestingly, in neurological patients percent enhancement in the left cerebral cortex showed a tendency to be higher and more variable than in the right side (10.3±20.2 vs. 6.8±13.1), although this was without statistical significance.

The spatial distribution of Omnipaque penetration was also analyzed in CT scans from neurological patients with high enhancement values. Fig. 2 shows pseudocolored differential images from 4 patients with various extents and patterns of Omnipaque penetration. In normal individuals (figure 2A and data not shown), contrast material was highly concentrated and limited to venous sinuses and to brain areas that are known to lack BBB characteristics (i.e. pineal gland and neurohypophysis) (Bakay, 1976). In patients suffering from brain tumors with vasculature having abnormal BBB properties (i.e. meningiomas) (Tator and Schwartz, 1971), or following severe brain trauma, we were able to detect focal accumulation of the contrast agent in the expected location (Fig. 2B and data not shown). However, in certain cases, contrast agent accumulation was detected in brain tissue which otherwise appeared normal. For example, diffuse penetration of Omnipaque into cortical gray matter was evident in a 24 years old pregnant patient with decreased level of consciousness who suffered from hypertensive encephalopathy (Fig. 2C). An abnormal focal enhancement to a cortical gyrus in the right fronto-parietal cortex was noted in another patient, presented to the emergency room with a focal seizure in his left hand (Fig. 2D).

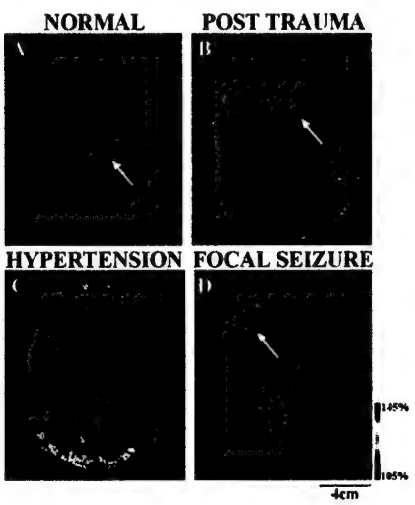

Fig. 2. Enhancement in various brain regions in patients with CNS-related disorders
Shown are pseudocoloured differential brain CT Images in which signals before Omnipaque were subtracted from those following contrast agent injection. The color code refers to the range of radio-opacity between water (no radio- opacity, dark blue) and bone (full radio- opacity, orange-red). Scale bars in all images represent 2cm. A. Ambulatory patient with a normal CT, with enhancement confined to choroid plexus (arrow). B. Focal enhancement (arrow) in an eight months old infant 1 week following head trauma. C. Diffuse enhancement in a 24 year-old pregnant woman presented with eclampsia. D. Focal enhancement (arrow) in a 56 year-old man presented with a focal seizure in his left hand.

Next, we wished to test the spatial distribution, persistence and consistency of the disrupted BBB. We therefore compared brain accumulation of 3 different contrasting agents employed in various imaging approaches. In 3 patients who were subjected to several image analyses within 1 month, focal enhancement in precisely the same site was found for Omnipaque (in a CT scan), gadolinium (under MRI analysis) or Tc-DTPA (in SPECT analysis). Fig. 3 shows a series of imaging studies demonstrating focal and persistently disrupted BBB in one of these patients 6 months following radiosurgery for arteriovenous malformation. One of the other 2 patients (images not shown) suffered from meningeal spread of tumor cells (primary CNS lymphoma) while the other from partial seizures. SPECT following administration of the brain non-penetrating compound Tc-DTPA was then compared to perfusion analysis using the freely permeable Tc-ECD (Fig. 3C). In each of these three patients, focal BBB disruption was accompanied by decreased perfusion (Figure 3C and data not shown). This ruled out enhanced perfusion as the underlying cause for contrast agent accumulation.

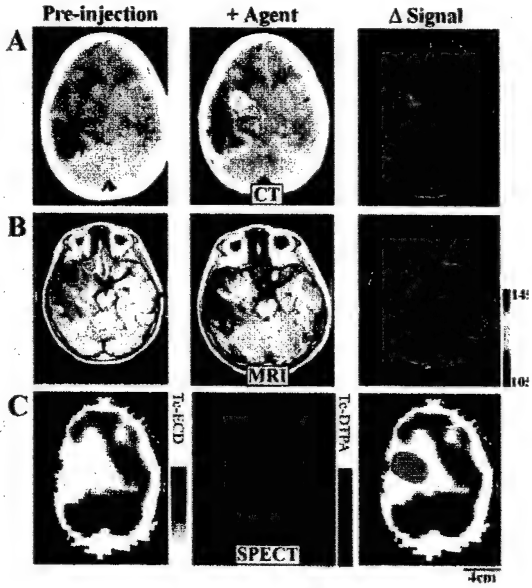

Fig. 3. BBB disruption as portrayed by CT, MRI and SPECT

Shown are axial sections from a single patient, where BBB disruption was evident by brain signal enhancement in CT (A), MRI (B) and SPECT (C) following administration of Omnipaque, gadolinium or Tc-DTPA, respectively, all within 1 month. Tc-ECD was used, 2 days after Tc-DTPA administration, for evaluating brain perfusion demonstrating that decreased perfusion (C, left) and increased brain penetrance (C, middle), overlapped (C, right).

The retrospective nature of our study offered an opportunity for non-biased exploration of clinical correlates that accompany the enhancement in CT signals due to BBB disruption. To this end, we analyzed the general clinical profiles as well as the available data on serum and CSF constituents for 19 patients who were investigated within 12 hr for various suspected neurological disorders but no focal abnormality was found in CT. These patients were classified by increasing order of signal enhancement and divided into 3 equal groups, displaying low, average and high, diffuse gray matter enhancement of contrast agent signals (Table I). Average values of patients' blood pressure, heart rate, body temperature, white blood cell and platelet counts, CSF and serum glucose and albumin as well as serum cortisol was compared between the groups. In patients from the "low penetrance" group, the averaged post-injection signal generated by the contrast agent was not significantly different from that of pre-injection (-1.8±3.8% enhancement, mean ±SEM), and was significantly lower than the >10% enhancement values calculated for the "high penetrance" group ($p=0.001$). Statistically significant differences between these two groups ($p<0.05$, Mann- Whitney test, see Table I) were also observed in body temperature, systolic and

diastolic blood pressure, total CSF protein and serum cortisol. The correlation (r^2=0.85) between enhancement values and CSF albumin concentration (Fig. 4A) further strengthens the notion that enhancement values indeed reflect quantitative estimations of the permeability of the BBB to large molecules. In all other clinical indices no significant difference was found between patients with low vs. high Omnipaque penetration (Table I). These findings suggest that inflammatory reactions in the peripheral or the central nervous system are not ultimate causes of BBB disruption (Abbott, 2000) (see discussion).

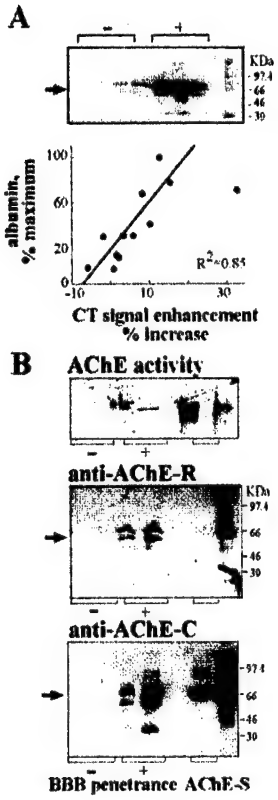

Fig. 4. BBB disruption is associated with CSF accumulation of albumin and AChE-R.

A. Albumin accumulation. Shown are albumin immunostaining following gel electrophoresis of CSF proteins (top) and correlation analysis (bottom) between CSF albumin concentrations (% of maximal level) and CT signal enhancement (% above pre-injection signal intensity). Note that albumin concentrations are linearly correlated with CT signal enhancement. B. AChE in CSF. Top: Shown is activity staining of CSF AChE following gel electrophoresis under non-denaturing conditions. Note that CSF samples with compromised (+) but not with intact (-) BBB display catalytically active AChE which co-migrates with recombinant (r) AChE-S or AChE-R produced in COS cells. Bottom: Immunoblot analyses following denaturing gel electrophoresis and incubation with antibodies selective for AChE-R (upper) or the C-terminally truncated AChE-core (lower). Note appearance of AChE-R in the same samples with AChE activity and the presence of proteolytic degradation products of the core AChE domain.

BBB disruption could not be attributed to a single CNS pathology. In one patient (#16 in Table I), high CT signal enhancement was detected, yet no obvious CNS pathology found. In other patients, diagnosed for clinical conditions assumed to induce BBB disruption, no radiological or molecular evidence was found for increased BBB permeability. For example, in patients #1 and 7 who were presented with a generalized convulsion, CT displayed none or only mild cortical enhancement and no albumin was detected in their CSF. In contrast, patients #15 and 17, both of whom also presented with a generalized convulsion, displayed high penetration. Therefore, the cumulative average of our clinical and biochemical markers suggests general stress responses rather than a specific neurological condition as the phenotype common to patients with disrupted BBB.

Several groups have previously associated stress with focal or diffused BBB disruption (Belova and Jonsson, 1982; Ben-Nathan et al, 1991; Esposito et al, 2001, Friedman et al, 1996; Sharma et al,1992), while others reported differently (Grauer et al, 2000; Sinton et al, 2000), possibly due to species, age and experimental manipulation differences, etc. Molecular biology approaches have

associated such disruption with the rapid accumulation of the "readthrough" brain AChE-R isoform (Kaufer et al, 1998a; Shohami et al, 2000). To search for this AChE isoform in patients' CSF, we used antibodies selective for the C-terminal sequence unique to AChE-R. For comparison, we employed antibodies targeted to the core domain common to all AChE isoforms (Shohami et al, 2000). Cytochemical staining of the electrophoretically separated CSF proteins was used to evaluate the capacity of CSF AChE to hydrolyze acetylthiocholine, a property common to all intact AChE isoforms (Soreq and Seidman, 2001). CSF samples from patients with compromised, but not with intact, BBB revealed conspicuous increases in catalytically active AChE (Fig. 4B). Comparative immunodetection with antibodies selective for the AChE-R variant indicated that these CSF samples included intact stress-associated AChE-R as well as degradation products from the C-terminus (Fig. 4B). Other AChE degradation products lacked the C-terminal peptide unique to AChE-R, as they reacted with antibodies targeted to the common core domain, but not to the C-terminus of AChE-R, and migrated faster than expected for the intact protein (Fig. 4B). Densitometric analysis of the immunopositive AChE-R bands displayed positive correlation with the signal enhancement levels, with an increase from an average of 29 ± 5 pixels for the low penetrance group to 58 ± 3 pixels for the high penetrance one. Further analysis will be required to test the significance of this increase in a larger group of patients.

To determine whether BBB disruption is associated with altered brain electrical activity, EEG recordings were performed on patients who showed a focal disruption in imaging studies. Fig. 5 shows the results of such correlation in a 46 year-old female patient who suffered recurrent sensory disturbances in her right hand 12 months following the complete removal of a small meningioma. While MRI ruled out tumor recurrence, SPECT-DTPA showed abnormal BBB in cortical areas adjacent to the site of surgery (Fig. 5A). Power spectrum analyses of this patient's EEG showed clear increases in abnormal slow waves (3-6 Hz). This was associated with high alpha waves (10 Hz) activity in the records collected from the C3, but not from the C4 electrode in the contra lateral hemisphere (Fig. 5B). The location of these surface wave patterns matched that of a cortical area suffering from disrupted BBB (Fig. 5B).

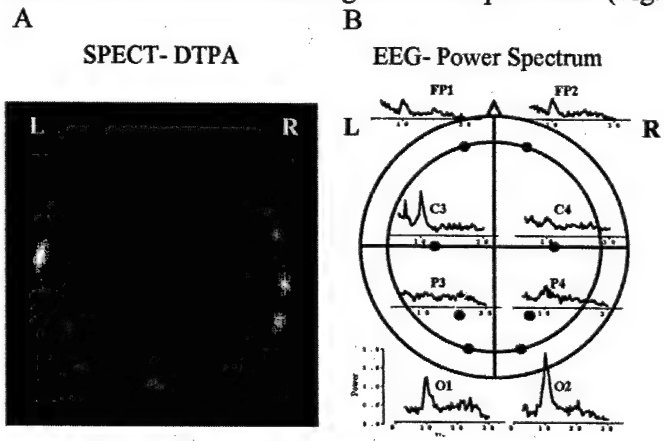

Fig. 5. EEG recordings match anatomic location of BBB disruption.
A. Axial SPECT image for the same patient performed following the administration of DTPA reveals increased signal in the left hemisphere (Arrow). B. Cortical mapping of power spectra based on 20 two-second epochs of spontaneous EEG activity (eyes closed), collected from a patient with a focal BBB disruption 12 months following surgery for the removal of a meningioma. Brain CT did not show any evidence for tumor. Spectral analyses is shown from three bilaterally matching scalp electrodes of the international 10-20 system. Left and right paired spectra are symmetrical in all electrodes with exception of the centrally located C3 and C4 electrodes, where increased slow delta and alpha frequency are shown over the left hemisphere. This area corresponds to the area of abnormal SPECT shown in A.

Discussion

In search for a minimally invasive approach for quantifying and characterizing BBB disruption in humans, we validated the use of CT brain imaging. Abnormal enhancement of brain CT signals was detected in over one-half of neurological patients but not in ambulatory patients without neurological abnormalities. CSF albumin concentrations suggest that this abnormal enhancement reflects the extent of BBB disruption. Signal enhancement was also associated with significant increases in blood pressure, serum cortisol and body temperature; in contrast, heart rate and WBC count appeared unrelated with BBB disruption. Focal BBB disruption correlated spatially with abnormal EEG, reflecting corresponding focal changes in neuronal activity, as found by EEG recordings. These colonized changes indicate the importance of an intact BBB for the maintenance of normal brain function. The significant increase in CSF AChE-R accumulation in the CSF of patients with BBB disruption further emphasizes the linkage between the cholinergic system, stress and the control over BBB permeability. Rather unexpectedly, in several patients, stable penetration patterns were observed during several weeks of clinical investigation. This suggests that BBB breakdown may persist for a long period, emphasizing the importance of the use of brain imaging for diagnosis. Recognition of BBB disruption may, in turn, call for adjustment of the treatment protocol for these patients.

The observed high incidence and persistence of BBB disruption bears both clinical and basic research implications at several levels. Regardless of the contrast agent employed, each of the brain imaging approaches yielded similar locations and apparent extent of BBB disruption. This reinforces the concept that BBB disruption may be confined to specific brain areas. The more intense general enhancement in the cerebral cortex most likely reflects a particular vulnerability of this region to BBB disruption.

The cerebral cortex microvasculature differs from other brain regions in the mechanisms controlling its blood flow (Inanami et al, 1992) as well as in its cholinergic receptors' distribution (Elhusseiny et al, 1999), and afferent innervation (Triguero et al, 1988). This further raises the possibility that the barrier function at the level of the cerebral cortex can be modulated by neuronal activity. For example, BBB permeability has been known to increase following activation of the noreadrenergic locus coeruleus (Raichle et al, 1975). Our imaging analysis supports previous reports showing BBB breakdown in epileptic patients (Cornford and Oldendorf, 1986), however, in our patients, persistent BBB disruption was observed in the absence of any evidence for active epileptic foci. While it is generally assumed that seizures induce BBB disruption it is not known how increased BBB permeability effects the physiological response of neurons. However, cortical neurons are known for their vulnerability to small changes in their extracellular environment (Lux, 1980; Schwartzkroin et al, 1998) and for their tendency to develop synchronous epileptic activity (Jefferys, 1998). This raises the possibility of consequent neuronal toxicity (Meldrum, 1993; Charriaut-Marlangue et al, 1996) in areas of persistent BBB disruption. Indeed, Kadota and colleagues (Kadota et al, 1997) reported that hippocampal neurons display excitotoxic damage following local serum infusion. Moreover, stress-induced cytokines, hormones or small molecules such as nitric oxide (van Amsterdam and Opperhuizen, 1999) may be expected to preferentially affect cortical neurons and glial cells (Sapolsky, 1996).

At the molecular level, this study adds AChE-R to albumin as a CSF-accumulated marker of BBB

disruption. Persistent stress-induced accumulation of the AChE-R protein therefore emerges as a stress response that is common to rodents and humans. The immediate source of AChE-R in human CSF can be the circulation, like albumin. Alternatively, or in addition, this secretory soluble protein may reach the CSF from stress-responding brain neurons (Shohami et al, 2000) and /or endothelial cells lining vascular brain capillaries (Flumerfelt et al, 1973). AChE-R degradation products may reflect the stress- induced increase in proteases (Chan and Mattson, 1999).

Apart from convulsions, with the highest predicted value for BBB disruption, our findings could only correlate this phenomenon with the intensity of stress responses. However, the mechanisms underlying stress-associated BBB disruption are yet to be found. Inflammatory responses (Rhodin et al, 1999), hemodynamic changes (i.e. blood pressure) (Robinson and Moody, 1980) and brain-derived modulators are all possible candidates. Individual variations in BBB disruption may also be due to its being a complex genetic trait. For example, recent findings of signal transduction in brain endothelial cells attribute rapid and long lasting changes in their functioning to the nitric oxide synthase cascade (Calingasan et al, 1998). Administration of NO-synthase inhibitors was indeed shown to reduce meningitis-associated BBB disruption in rodents (Boje, 1996). This calls for seeking potential correlation(s) between compromised BBB in patients and the NO pathway. Another example refers to the multiple drug resistance (mdr1a) gene, which encodes the drug transporting P-glycoprotein that resides in the BBB. Genomic disruption of mdr1a induces up to 10-fold increases in the uptake of dexamethasone into the mouse brain (Meijer et al, 1998). This raises the general question whether patients under massive drug treatments, in whom the mdr1a protein is fully saturated, develop transiently modulated susceptibility for BBB disruption. A yet more specific example is that of the "atypical" allele of butyrylcholinesterase (BChE) (Lowenstein-Lichtenstein et al, 1995), which increases the brain permeation of cholinesterase inhibitors due to reduced scavenging of such poisons in the circulation. Homozygous carriers of this allele may present genetic predisposition to hypersensitivity for BBB disruption under anticholinesterase exposure. Also relevant is polymorphism in a specific isoform of glutathione transferase (GSTp), which resides in endothelial cells of brain vasculature and protects the brain tissue from penetration of xenobiotics. One of the GSTp variants, with impaired substrate specificity, was found with much higher incidence in patients with Parkinson's disease, as compared to controls (Menegon et al, 1998). The common denominator to all of the genes with apparent linkage to BBB disruption (mdr1a, GSTp, BCHE and NO Synthase) is that they are all involved in scavenging processes. Acquired hypersensitivity because of previous drug or chemical exposure may hence provide a major cause of BBB disruption (Kaufer et al, 1998b). Increases in the risk for developing Parkinson's disease were indeed reported following exposure to brain-penetrable chemicals, e.g. lead from batteries (Kuhn et al, 1998), organophosphorus insecticides (Senanayake and Sanmuganathan, 1995). These acquired and inherited risks may point to the intriguing possibility that BBB disruption is causally involved with neurodegenerative diseases, so that its impaired maintenance may be relevant to both acute and delayed syndromes. While our study points to stress as an important cause underlying prolonged BBB disruption in humans, future research will elucidate the association between such disruption and stress-related excitotoxic brain damage (Sapolsky, 1996; Haley et al, 2000).

Table 1: Clinical indices of "neurological patients"[a]

	#	age	sex	diagnosis	CT-% enhancement gray matter	Hb mg/dL	platelets $x10^{-3}mm^{-3}$	WBC $10^3/mm^3$	serum glucose mg/dL	serum cortisol µg/dL	CSF glucose mg/dL	CSF protein mg/dL	heart rate min^{-1}	b.p. systole mbar	b.p. diastole mbar	core temp °C
Low	1	12	F	fever, convulsions	-6.7	12.2	172	15.3	96	16.5	75	14	125	88	50	37.0
	2	52	M	coma, staphylococcal sepsis, S/P head trauma	-6.0	8.9	414	6.8	199	14.35	101	23	87	140	72	37.2
	3	27	M	headache, investigation	-2.0	15.8	340	14	132	41.7	93	27	-	-	-	-
	4	1	M	headache	0.7	13	501	15	85	16.4	66	42	118	94.5	43	37.1
	5	93	M	vomiting	1.4	11.7	215	11.7	124	26.4	81	45	89	133	64	38.2
	6	19	F	myelopathy	2.0	13.1	406	8.8	113	15.2	61	39	104	110	54	37.0
		34		**average**	**-1.8**	**12.5**	**341.3**	**11.9**	**124.8**	**21.8**	**79.5**	**21.7**	**104.6**	**113.1**	**56.6**	**37.3**
		33.6		**SDV**	**3.8**	**2.2**	**126.2**	**3.5**	**40.3**	**10.7**	**15.4**	**12.2**	**16.9**	**22.9**	**11.5**	**0.5**
Medium	7	36	F	pneumococcal sepsis , convulsions	3.3	8.5	531	17.3	130	20.3	53	11	78	152	81	36.5
	8	59	F	fever- for investigation, S/P head trauma	4.9	9.7	938	17.3	103	17.4	48	48	90	147	102	38.0
	9	5/12	M	meningitis- proteus	5.4	13.7	88	8.2	70	-	3	95	140	-	-	34
	10	40	F	S/P, pneumococcal meningitis	5.7	11.4	285	19.7	280	35	113	48	115	134	63	37.7
	11	1	F	febrile convulsions	5.8	12.6	288	25.9	125	-	90	14	147	113	59	37.4
	12	31	M	fever for investigation	8.2	16.8	313	10.0	111	14.8	69	41	72	120	73	37.5
	13	10	M	sagittal sinus vein thrombosis	10.1	9.6	309	10.0	103	21.1	85	16	108	120	77	37.8
		25.3		**average**	**6.2**	**11.8**	**393.1**	**15.5**	**131.7**	**21.7**	**65.9**	**39.0**	**107.1**	**131.0**	**75.8**	**36.9**
		22.1		**SDV**	**2.3**	**2.9**	**272.4**	**6.4**	**68.2**	**7.3**	**35.6**	**29.5**	**29.2**	**15.9**	**15.3**	**1.4**
High	14	68	M	coma, investigation	11.0	11.9	193	12.3	137	28.5	97	41	114	166	92	37.7
	15	1	M	convulsive episode	12.6	11	449	10.4	70	25.6	85	26	137	115	57	37.4
	16	1	M	gastroenteritis – pseudomonas	15.3	7.9	669	16.1	105	27.5	-	126	148	112	55	38.3
	17		M	convulsive episode	16.7	17.3	241	10.2	393	76.2	213	64	120	143	89	37.5
	18	55	F	pneumococcal meningitis	26.4	12.3	296	20	200	92.9	62	99	103	150	72	39.2
	19	69	M	coma, investigation	33.9	10.6	497	11.4	335	20.7	184	72	112	184	88	37.6
		38.8		**average**	**19.3**	**11.8**	**390.8**	**13.4**	**206.7**	**45.2**	**128.2**	**71.3**	**122.3**	**145.0**	**75.5**	**38.0**
		34.9		**SDV**	**8.9**	**3.1**	**180.3**	**3.9**	**130.5**	**31.0**	**66.2**	**36.8**	**16.9**	**28.2**	**16.6**	**0.7**
		0.53		**p (Mann-Whitney)**	**0.001**	**0.242**	**0.35**	**0.35**	**0.155**	**0.032**	**0.123**	**0.032**	**0.123**	**0.026**	**0.041**	**0.026**

[a]Patients who were presented with "neurological signs and symptoms" but with no focal enhancing lesion in CT were evaluated. Presented in the table are the averages of all available clinical data taken on several occasions within six hours of the scan. Patients are sorted in ascending order by percent enhancement, for low, medium and high enhancement values, averages and SDV are given in bold. In all cases the most specific available diagnosis is given. "Investigation" refers to patients who were admitted with a clinical picture indicating a neurological disorder which was not identified. "Meningitis" –refers to bacterial infection (identified organism is noted). Patients #2 and 6 suffered from Head Trauma more then one month before the reported investigation. Patient #18 was more then one month following a brain surgery – for total removal of Meningioma. All convulsions were of the "general type". Percent enhancement in the cortical gray-matter is given as the average of the two cerebral hemispheres. P values between low and high (using the non-parametric Mann-Whitney test) are presented in the last row (see text).

Chronic acetylcholinesterase overexpression induces multileveled aberrations in neuromuscular physiology

Summary

Chronic overexpression of the acetylcholine-hydrolyzing enzyme acetylcholinesterase (AChE) is a notable consequence of exposure to anticholinesterase drugs or poisons. However, the physiological consequences for the resultant neuromuscular disfunction have not yet been carefully analyzed. Here, we report detailed dissection of the different components of neuromuscular function in transgenic mice previously shown to display motor fatigue and altered muscle morphology as a concequence of neuronal overexpression of AChE-S, the synaptic AChE variant. Transgenic diaphragm muscle presented exaggerated fatigue as a combined consequence of neurotransmission fading and muscle mechanical mulfunctioning. In a tetanic stimulation protocol, transgenic muscles rapidly fatigued to a larger extent than wild type muscles, either when stimulated directly or via the phrenic nerve. AChE overexpression involved aberrations of synaptic transmission with higher quantal content (measured at 0.2 mM Ca^{2+}, 2.3 mM Mg^{2+}). Furthermore, treatment with the anti- cholinesterase physostigmine revealed higher amplitude and half decay time of the transgenic quantal postsynaptic response. Our observations imply that elevated levels of neuronal AChE-S are expected to cause muscle exhaustion due to multileveled aberrations in synaptic transmission, muscle function and morphology.

Abbreviations.

AChE, acetylcholinesterase; NMJ, neuromuscular junction; TG, transgenic; WT, wild type; PSP, postsynaptic potential.

Introduction

AChE is a key enzyme in cholinergic transmission and altered activity levels of this protein are probable to disrupt the homeostasis in the synaptic cleft. Indeed, cholinergic imbalance in neuromuscular junctions (NMJ) is involved in several pathological situations, for example in congenital myasthenias (reviewed in Engel *et al.* 1999 and Ohno *et al.* 2001a), spinal muscular dystrophy (Crawford *et al.* 1996) and amyotrophic lateral sclerosis (Brown *et al.* 1995). More common is exposure to agricultural acetycholinesterase (AChE) inhibitors such as the organophosphate paraoxon. Rare, but devastating are the effects of chemical warfare agents as sarin, tabun or soman, which result, among other consequences, with muscle fibre necrosis and muscle paralysis (reviewed in Ray, D. 1998, Schwarz *et al.* 1995). The recent increase in the use of anti-cholinesterases as Alzheimer's disease drugs (Nordberg *et al.* 1999) further expands such exposure, albeit to lower, chronic doses. Previous reports demonstrated that exposure to AChE inhibitors results in the accumulation of AChE in the brain (Kaufer *et al.* 1998a) and muscle (Lev-Lehman *et al.* 2000). However, the physiological consequences of chronic AChE irregularities are yet unknown. We have therefore employed transgenic mice that chronically overexpress the synaptic variant of AChE (AChE-S) in the central nervous system. The elevated AChE activities in these mice induced multi-site dysfunctions, including cognitive deficiencies (Beeri *et al.* 1997, Cohen *et al.* 2002), intensified neuropathology markers for neurodeterioration in the brain (Sternfeld *et al.*

2000) and neuromotor impairments expressed as progressively exaggerated motor fatigue (Andres *et al.* 1997). The physiological basis of this motor dysfunction could result from central impairments or from peripheral effects. Thus, a detailed dissection of this phenotype may contribute to the understanding of the related clinical pathologies mentioned above.

Muscle fatigue may result from impaired excitation-contraction mechanisms, neurotransmission failure or a combination of both. Neurotransmission depression was reported to have an important contribution to muscle fatigue (Aldrich *et al.* 1986, Kuei *et al.* 1990, Van Lunteren & Moyer, 1996), and may result from vesicle depletion or malfunctioning of the upstream release machinery, leading to depression of release. Postsynaptically, cumulative receptor desensitisation may reduce postsynaptic potentials (PSPs). Blocking AChE activity was found to enlarge the relative fraction of neurotransmission in muscle fatigue (Panenic *et al.* 1999).

In transgenic mice overexpressing AChE-S, muscle morphology is irregular, including enlarged NMJ and abnormal ultra-structure of the synaptic clefts with either much deeper or very shallow folds (Andres *et al.* 1997). Presynaptic features were atypical as well, most prominently in higher numbers of vesicles at the transgenic presynaptic site (Andres *et al.* 1998). These changes were accompanied by altered transcription patterns in spinal cord motor neurons, for example, premature overexpression of choline acetyltransferase mRNA, or suppression of neurexin Iβ mRNA (Andres *et al.* 1997). Additionally, tongue muscles from AChE-S transgenic mice display exaggerated neurite branching and disorganized fibres (Lev-Lehman et al. 2000). Alterations in muscle fibre development and maintenance were observed in Zebra fish embryos in which the ACHE gene was replaced with a mutant enzyme with a serine^{226} substitute, which abolishes the enzymatic activity of AChE. Importantly, the phenotypes developed were mediated by nicotinic ACh receptor localization and activation (Behra *et al.* 2002).

The overall query in the present study has been to elucidate which levels, from neuronal activation to muscle contraction, are involved in the induction of motor fatigue under excess of AChE. First, we examined whether muscle properties and/or neuronal transmission are involved in the phenotype of muscle fatigue. Furthermore, we questioned whether pre- and/or post-synaptic properties are affected by excess AChE synaptic situation.

Methods

Experiments were approved by The Hebrew University's committee for animal studies and all efforts were made to minimize both the number of animals used and their suffering. AChE-S transgenic mice and age- and sex-matched FVB/N control mice were used throughout this study. Diaphragm muscles were obtained from 3- to 5-month-old mice (28-32 g). Animals were anaesthetised with ether, decapitated and the muscles were subsequently dissected. Hemi-diaphragms were isolated with the phrenic nerve and were placed in an experimental bath containing physiological salt solution with the following composition (in mM): 124 NaCl, 5 KCl, 1.3 $MgSO_4$, 1.2 NaH_2PO_4, 26 $NaHCO_3$, 10 D-

glucose and 2.4 $CaCl_2$. Muscles were perfused continuously with a salt solution, aerated with 95% O_2 - 5% CO_2 at room temperature (22–24°C) and at a rate of 2 ml min^{-1}.

Muscle fatigability measurements

The intact hemi-diaphragm was fixed at the rib side onto a sylgard coated bath. The central tendon was connected to an isometric transducer and were aligned at 45° with the experimental bath. The muscle was progressively stretched until a basal tension of 0.015 g was obtained. The output of the force transducer was digitised, stored and offline analysed. Fifteen stimulation trains separated by 10 s inter-train intervals induced nerve-evoked contractions. Each train consisted of 200 stimuli at 66 Hz, 0.1 ms duration. For direct stimulation, a group of muscle fibres was stimulated with a suction electrode placed at the far end of the rib side in order to prevent electrode movements during muscle contraction.

Cut muscle preparations

Cut muscles were prepared by cutting fibres on both sides of the main intra-muscular nerve branch. Recording of PSPs commenced after contractions were halted. Intracellular recordings were performed with microelectrodes of 20-30 MΩ resistance, filled with K-acetate (3 M) and KCl (100 mM). The nerve was stimulated with six trains of 15 stimuli at 50 Hz, 0.1 ms duration, separated by 10 s inter-train intervals. This short stimulation protocol did not create accumulating decay during subsequent trains (data not shown), therefore, averaged results are presented.

Characterization of synaptic quantal responses

Quantal size and content were measured by recordings of PSPs in low calcium, high magnesium solution (0.2 mM and 2.3 mM, respectively). Frequency of spontaneous release was measured within a 400 ms before the evoked releases. Quantal content was determined by the failure method (del Castillo & Katz, 1954) in evoked responses to over 600 stimuli per cell given at 0.5 Hz. With this sample size, and considering quantal content in the range of 0.07, the standard error was calculated to be no more than 15%. Since at this probability of release the chance for multiple quanta is ~0.002, indicating only ~3% of the evoked responses are multiple, quantal sizes of spontaneous and evoked release of each cell were merged. Rise time was measured from onset to peak amplitude, whereas decay time was measured by the time to 50% reduction of PSP amplitude. Control parameters were determined from a sample of at least 5 NMJs per diaphragm. Fresh physostigmine (10 μM, Sigma, St. Louis MI) was continuously perfused and a sample of at least 7 NMJs was taken.

Statistics

All analysed data were compared by two tailed student's paired *t* test and significant differences were determined when $P < 0.05$. Significant linear regression analysis was determined with F-test.

Results

Both nerve and muscle contribute to the phenotype of pronounced fatigue.

The first step we employed in order to examine the contribution of nerve and muscle to the fatigue phenotype was to measure muscle contraction induced by administering tetanizing stimulation either to the nerve or directly to the muscle. This approach enabled us to distinguish between the possible fatigue developed at the level of muscle excitation/contraction mechanisms and fading of neuromuscular transmission. We

subjected nerve stimulation sessions of 15 trains which induced a development of muscle fatigue within one session, as demonstrated in Fig. 1A and B for wild type (WT) and transgenic (TG) muscles, respectively. In the first few contractions of the series, there was a slow build-up of force in the course of the stimulation train; a phenomenon that was more pronounced in WT muscles. Gradually, fatigue appeared during the train itself, followed by a reduction in the initial force achieved at the subsequent contraction. With repetition, the contractions slowly attained a lower steady-state level. Although the general behaviour appeared similar, several differences between WT and TG muscles were observed in this pattern. First, the initial force achieved by WT muscles was 0.41 ± 0.06 g (mean ± SEM), significantly higher than 0.2 ± 0.02 g in TG (n = 6, in each of 4 WT and 5 TG muscles, $P < 0.05$, Fig 1C). Second, the time course of fatigue development was clearly different in the TG and WT diaphragms, in both parameters of intra- and inter-contraction fatigue. These were determined by measuring the percent reduction of the initial and final force from the maximal force obtained at the first stimulation of the session (measured, respectively, at 0.5 and 3 s from contraction onset). WT muscles decay significantly less than TG ones in the level of initial activation, reaching 49 ± 3% decrement at the last contraction, whereas TG muscles declined by 68 ± 3% ($P < 0.01$, Fig 1D). In contrast to wild-type muscles, transgenic muscles not only fatigued to a greater extent, but also failed to recover during the inter-train intervals. This phenomenon is demonstrated by the smaller difference attained between the initial and the final force in the TG contractions during the train (Fig 1D). Single exponential fit to the initial force represents a clear 1.6-fold faster fatigue time constant of TG as compared with WT muscle (52.6 s vs. 85.9 s, Fig. 1E vs. F, $P < 0.05$, F - *test*). Interestingly, the time constant of final fatigue seems to be similar in both phenotypes (45.3 s vs. 48.1 s, respectively). These results may indicate that the main difference between the TG contraction mechanism and that of the WT phenotype is a slower inter-train recovery in TG muscles.

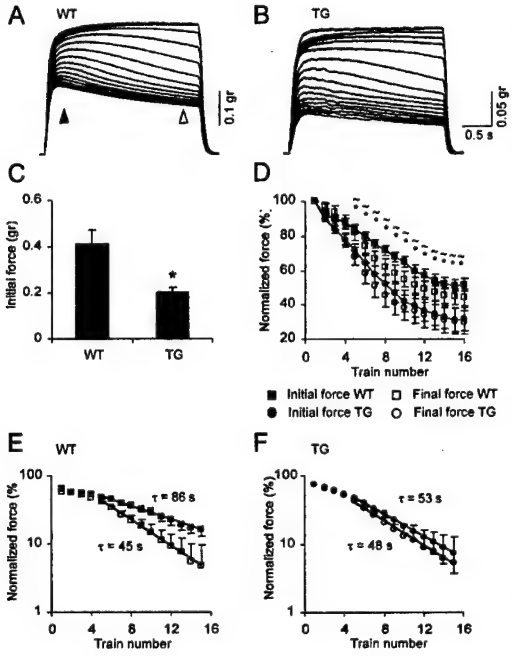

Fig. 1. Transgenic diaphragm muscle displays exaggerated contraction fatigue in tetanic nerve stimulation. (A) Nerve induced contractions in WT diaphragm muscle. Contraction sessions were composed of 15 consecutive stimulation trains of 200 stimuli at 66 Hz, with 10 s inter-train intervals. (B) Similar to A in TG diaphragm muscle. (C) Averaged initial force of 6 measurements in each of 4 WT and 5 TG diaphragms (measured at the time marked by a closed arrow in A, means ± S.E.M). * $P < 0.05$, compared with WT group, two tailed t-test. (D) Time course of initial and final forces normalized to the first contraction (final force was measured at the time marked by an opened arrow in A). * $P < 0.05$, initial forces compared with

WT values. ~ $P < 0.05$, final forces compared with WT values. (E) Semi logarithmic plot for WT initial and final forces (steady state values subtracted). Time constants derived from the slope of the line fitted by regression to the linear part were found significantly different, F-*test* $P < 0.05$. (F) Same as E for TG muscles.

The observed differences could originate either in the nerve or in the muscle. To distinguish between these possibilities, we measured the isotonic force generated by direct muscle fibers stimulation (see Methods). This approach yielded essentially similar patterns of contraction to those induced indirectly via the nerve (Fig 2A and B). However, the levels of fatigue in both inter- and intra- train stimuli were lower than those measured in indirect stimuli. In contrast to the evident recovery process in TG muscle activity induced by muscle stimulation, the recovery process in the WT muscle was very slow. Fatigue that originated from muscle excitation-contraction properties reached 25 ± 2.9% in WT and up to 40 ± 3.0% in TG muscle at the 10th contraction ($n = 6$, in each of 3 WT and 3 TG muscles, $P < 0.02$, Fig 2C). Interestingly, despite this difference in magnitude, the relative contribution of muscle mechanisms to the total fatigue is similar in TG and WT (68.9% and 70.1%, respectively, Fig 2D). To conclude, transgenic diaphragm muscle under chronic excess of AChE suffers from augmented fatigue of both neuronal and muscle origins.

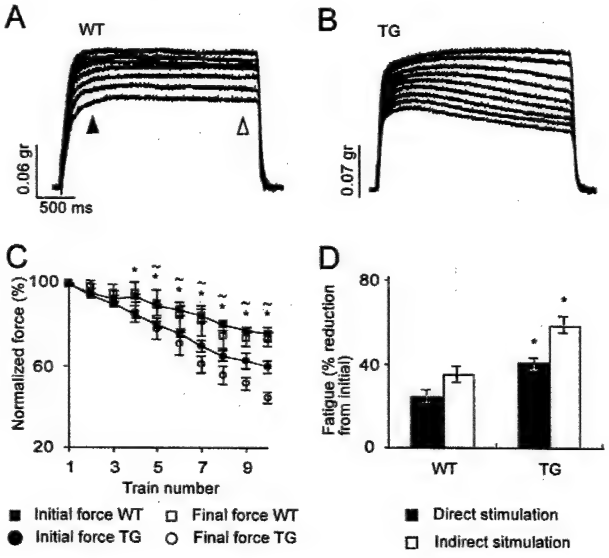

Fig. 2. Transgenic diaphragm muscle displays exaggerated contraction fatigue in tetanic direct muscle stimulation. (A) Contractions in WT diaphragm muscles induced by delivering the stimulation directly into the muscle. Contraction session was composed of 10 consecutive stimulation trains of 200 stimuli at 66 Hz, with 10 s inter-train intervals. (B) Same as A for TG muscle. (C) Time course of initial and final forces normalized to the first contraction. Values are means ± S.E.M of 6 measurements in each of 3 WT and 3 TG diaphragms. Forces were measured at the time marked by the closed and opened arrows in A. * $P < 0.05$, initial forces compared with WT values. ~ $P < 0.05$, final forces compared with WT values. (D) Summary of the muscle and nerve induced fatigue, measured at the 10th contraction in direct and indirect stimulation. Note similar ratio of muscle- and nerve- induced fatigue in the TG and WT muscles. Data is given as means ± S.E.M. * $P < 0.05$, compared with WT group, two tailed student *t*-test.

Neurotransmission failure is demonstrated directly at the synaptic level.

To characterize the physiological behaviour of neuromuscular transmission we used cut muscle preparations. As action potentials are inactivated in the cut muscle fibres (Hubbard & Wilson, 1973), it is possible to measure synaptic transmission at

physiologically high levels of release. Fig 3A presents typical trains induced in WT and TG fibers, demonstrating larger and faster decay of the PSPs in the TG fibres. No significant difference was observed in the amplitude of the first PSP in the train, suggesting no apparent effect or involvement of the elevated AChE concentrations (amplitudes were scaled in relation to the resting potentials, Fig 3B). Fig 3C shows the subsequent PSPs in the train after normalization to the first PSP, which presented an initially small facilitation followed by a gradual decrease in the amplitude within the train, which in the case of transgenic synapses declined to a lower plateau. WT fibres showed 20 ± 2.4% decrement, a significantly smaller magnitude than in transgenic synapses, demonstrating synaptic fade of 28 ± 2.5% (n = 44 and 45 cells from 9 WT and 9 TG muscles, $P < 0.03$). Synaptic fading was also faster in the transgenic NMJ than in WT, noted by a smaller time constant of the exponential part of the amplitude decay in the trains (62.7 s in WT vs. 38.4 s in TG, Fig 3D). Possibly, the lower initial force achieved by transgenic muscle contractions (Fig 1C) can be partially explained by the synaptic depression during the initial stimuli in the train, as demonstrated here.

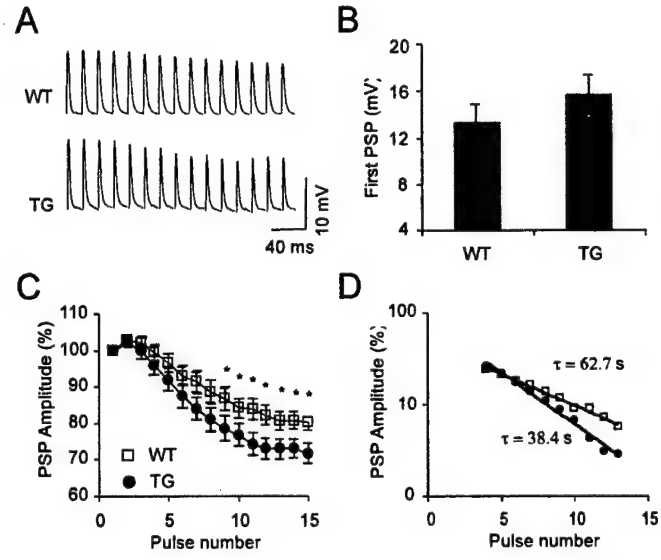

Fig. 3. TG synapses demonstrate pronounced neurotransmission depression in cut muscle preparations. (A) Examples of trains of PSPs evoked in cut muscle preparations. Trains consisted of 15 stimuli at 50 Hz with 10 s inter-train intervals. For clarity, stimulation artefacts were omitted. (B) Average amplitude (± S.E.M) of the first PSP in the train. In order to reduce PSP variability resulting from differences in membrane potentials, amplitudes were scaled to a driving force at a membrane potential of −50 mV, assuming zero as the synaptic reversal potential (Linder & Quastel, 1978). n = 44 and 45 cells from 9 WT and 9 TG muscles. (C) Time course of PSP decay during the train. PSPs are normalized to the first PSP in the train. * $P < 0.05$, compared with WT group, two tailed t-test (D) Semi logarithmic plot of PSP values (extrapolated steady state levels were subtracted). Time constants derived from the slope of the regression. $P < 0.05$ (F-*test*).

Characterization of neuromuscular transmission changes at the cellular level.

Whether AChE over-producing NMJs demonstrate different release characteristics, and if so, whether these take place at pre and/or postsynaptic sites, was tested by measuring quantal size and quantal content under conditions of low probability of release (0.2 mM Ca^{2+}, 2.3 mM Mg^{2+}). Postsynaptic quantal responses of evoked and spontaneous activity were similar in WT and TG synapses. Amplitudes were 0.98 ± 0.1 mV in WT and 1.05 ±

0.14 mV in TG (n = 75, in each of 4 WT and 5 TG muscles, $P < 0.62$, Fig 4A); rise times were 0.89 ± 0.1 ms in WT and 0.97 ± 0.1 ms in TG ($P < 0.79$, Fig 4B) and half decay times were 1.68 ± 0.22 ms in WT and 1.74 ± 0.1 ms in TG ($P < 0.88$, Fig 4C). To explore the effects of AChE's catalytic activity on these different PSP parameters, we blocked AChE with the carbamate AChE blocker, physostigmine (10 μM). Synaptic responses were recorded during 1.5 hr of physostigmine perfusion and presented quantal size increases in both amplitude and time course. Significantly larger increases in amplitude appeared in the TG animals than in WT (98% and 57% respectively, $P < 0.05$, Fig 4A), as well as in decay time (65% and 35% respectively, $P < 0.05$, Fig 4C). The rise time of both WT and TG mice increased significantly, yet to the same extent (41% and 32%, respectively, Fig 4B). Possibly, the effective concentration of physostigmine at the junctional fold was not high enough for a complete blockade of AChE, since decay time was not dramatically elevated, as expected by treatment with anti-cholinesterase (see, for example Ferry & Kelly, 1988). Yet, the larger effect of physostigmine on TG miniature PSP amplitudes is consistent with the higher levels of the catalytic activity of AChE in the TG NMJs.

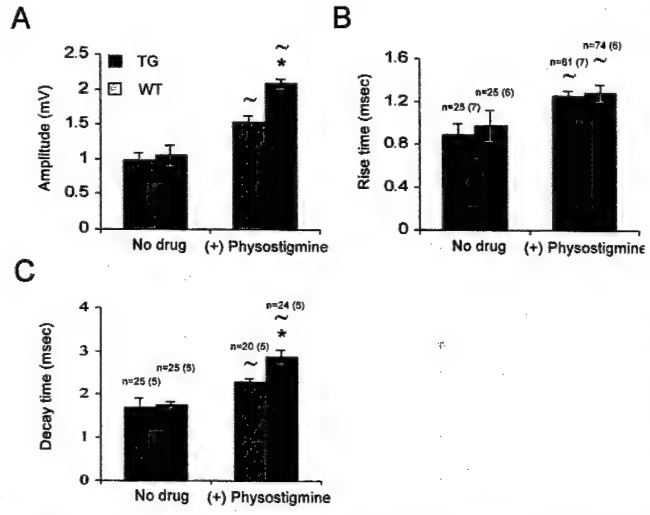

Fig. 4. TG quantal size is similar to WT responses in control conditions, but larger following physostigmine treatment. Quantal size recorded in WT and TG muscles under conditions of low probability of release (0.2 mM Ca^{2+}, 2.3 mM Mg^{2+}). Evoked and spontaneous responses were combined (see Methods). Sample of PSPs from several cells was taken in the presence of physostigmine (10 μM). (A) PSPs amplitude. (B) PSPs rise time (from onset to peak). (C) PSPs half decay time (from peak to half decay). Numbers of cells analysed are indicated above the bars, number of animals in brackets (similar numbers for A and B). Data were analyzed with unpaired two tailed t-test: * $P < 0.05$ compared with WT results, ~ $P < 0.05$, compared with no drug conditions within the same group.

Transgenic NMJs exhibit higher quantal content.

Presynaptic properties of the TG NMJ are particularly relevant since the genetic interference was limited in this TG line to the neuronal part (Beeri *et al.* 1995), therefore, excess AChE produced by the nerve terminal (Anglister *et al.* 1991) may affect the levels and/or interactions in the release machinery. Quantal content was determined by the failure method of del Castillo & Katz (1954) at lower Ca^{2+} concentration (0.2 mM Ca^{2+}, 2.3 mM Mg^{2+}). Transgenic NMJs displayed higher quantal content (0.095 ± 0.01 in TG, 0.068 ± 0.006 in WT, n = 75, in each of 4 WT and 5 TG muscles, $P < 0.05$, Fig 5A) and frequency of spontaneous release than WT ones (0.28 ± 0.015 Hz in TG and 0.15 ± 0.005

Hz in WT, $P < 0.05$, Fig 5B). Both results are in accord with possible presynaptic changes in the TG terminal that involve either increase in the average probability of release (p) and\or increase in (n) (del Castillo & Katz, 1954). Treatment with physostigmine caused a pronounced decrease in both quantal content and spontaneous release in TG synapses (21% and 27% reduction, $P < 0.05$), while changes in WT were not significant (Fig 5A and 5B, $P < 0.41$). The larger effect of physostigmine on the release probabilities of TG NMJs may reasonably present the hypo-cholinergic synaptic situation. Furthermore, the sharp effect of physostigmine better supports increase in probability of release in the TG synapse than change in the number of releasing sites.

Fig. 5. TG synapse displays higher probability of release and different susceptibility to AChE inhibition than WT. (A) Quantal content of WT and TG synapses, measured at conditions of low probability of release (0.2 mM Ca^{2+}, 2.3 mM Mg^{2+}) with and without physostigmine (10 •M). (B) Frequency of spontaneous release with and without physostigmine. Numbers of cells analysed are indicated above the bars, number of animals in brackets (similar numbers for A and B). Data were analysed with two tailed student t-test, * $P < 0.05$ comparison with WT results, ~ $P < 0.05$, comparison with no drug conditions within the same group.

Discussion

Using transgenic mice with chronic neuronal overexpression of synaptic AChE, we found that the consequences of higher levels of AChE are widespread across multiple locations in the neuromuscular system. Characterizing the transgenic muscle ex vivo, we observed an exaggerated mechanical fatigue following repetitious activation of the muscle, either directly or via the phrenic nerve. These results may explain, at least in part, the reported motor behavioural difficulties of these mice (Andres *et al.* 1997). Our results further demonstrate that the accentuated mechanical fatigue is due to a combination of alterations in both neuromuscular transmission and intrinsic muscle properties, such as excitation/contraction coupling processes. Synaptic fade was explicitly demonstrated in the cut muscle preparation, with more pronounced synaptic depression in the transgenic NMJs, while enhanced mechanical fatigue was demonstrated by repetitive direct stimulation of the diaphragm muscle. The emerging picture from our analysis is that synaptic homeostasis is altered with excess AChE. This subsequently affects release properties, yielding higher probability of release, larger quantal size and hypersensitivity to cholinergic, stress-like insults. The latter are consistent with neuronal hypersensitivity of hippocampal functioning under AChE excess (Kaufer *et al.* 1998a; Meshorer *et al.* 2002). The multiple effects on muscle function are likely to include both direct and indirect responses to the hypo-cholinergic state, and may involve components of AChE non-catalytic properties (reviewed in Soreq & Seidman, 2001).

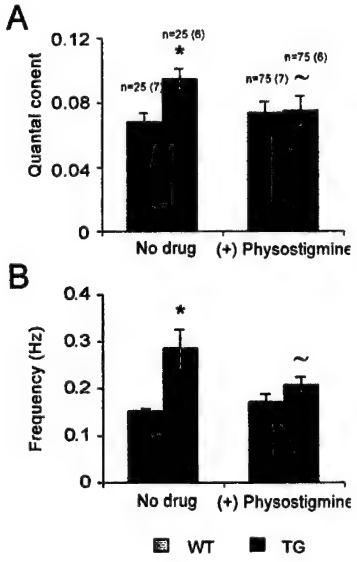

Lower tetanic force production was evident in the transgenic muscle. Total muscle force is a build-up of recruited single fibres. In the cut muscle experiments, the PSP in the transgenic fibres decays following repetitive stimulation to a lower level than in WT. Therefore, the TG muscle probably undergoes a faster reduction in the number of recruited fibres during the train, which explains, at least in part, the lower initial force production of the transgenic diaphragm. Both TG and WT muscles showed similar stereotypical changes in the contraction induced by nerve stimulation (Hill, A.V., 1970). In the nerve stimulation protocol, which combines both neurotransmission and muscle mechanics, the main difference between TG and WT muscles could be attributed to a reduction in inter-train recovery, which is reflected in a significantly smaller difference between the initial and final forces and the lower final steady state level attained by the TG muscle. The direct stimulation reveals similar time course and fatigue processes as in nerve stimulation, demonstrating an accentuated mechanic fatigue in the TG muscle. It is important to note that intra-train fatigue is low in the nerve stimulation of TG muscle, but conspicuous under the direct stimulation. Therefore, the contribution of neurotransmission fade to the fatigue processes during the train is probably underestimated in the nerve stimulation experiment. We attribute the transgenic diaphragm aberration to an impaired recovery process, and conclude that the motor fatigue phenotype involves several sites, including both neuronal and muscle elements.

AChE is known for its catalytic role in hydrolysing ACh, yet the physiological and cellular consequences of excess AChE situations in the NMJ may involve outcomes of AChE's non-catalytic, morphological properties as well (Darboux *et al.* 1996, Sternfeld *et al.* 1998, Grifman *et al.* 1998; Behra *et al.* 2002). These could account, for example, for the augmented fatigue of muscle mechanics, which does not directly relate to ACh levels.

The synaptic analysis in TG muscles revealed normal quantal responses at the postsynaptic cellular level, yet with higher quantal content in the TG neuromuscular junction. The apparent morphological atrophy of TG muscle fibres (Andres *et al.* 1997) may lead to biased sampling and therefore underestimation of release properties. AChE's content in the NMJ is contributed by both muscle and neuronal systems (Anglister *et al.* 1991). However, in the TG muscle, excess AChE originates only from the neuronal side, thus possibly elevating its concentration at presynaptic locations of the NMJs. Morphometric analysis of diaphragm endplates from AChE transgenic mice showed that they are 60% larger than WT NMJs (Andres *et al.* 1998). Theoretical models predict that a higher synaptic AChE concentration by itself will not significantly affect the quantal size (Anglister *et al.* 1994). Moreover, density calculations (Salpeter *et al.* 1978) indicate that AChE concentration in the mouse NMJ is already in excess of a critical lower limit. Consistent with these assumptions, we find a similar picture of quantal amplitudes and time courses in TG and WT NMJs. Nevertheless, blocking AChE activity revealed higher quantal amplitude in TG synapses than in WT, suggesting that in contrast to the theoretical prediction, excess enzyme in the TG synapse is effective. The higher quantal amplitude may be an outcome of larger ACh content, but could also result of high receptor number consistent with the larger TG NMJs. Therefore, we interpret the "real" amplitude as a delayed compensation response to excess AChE that retrieves the single quanta to standard sizes.

Presynaptic properties are supposedly affected by raising AChE concentration, since the faster hydrolysis of released transmitter will induce less feedback inhibition on the release system (Starke *et al.* 1989). Thus, the higher quantal content and rate of spontaneous release observed in TG endplates could result from reduction in presynaptic autoinhibition (Parnas *et al.* 2000, Slutzky *et al,* 2001), and are likely to be a direct response to the expression of the transgene. Again, this finding is consistent with morphometric evidence pointing to higher density of presynaptic vesicles at the transgenic terminal (Andres *et al.* 1998), which could by itself be responsible for the higher frequency of spontaneous release (Del Castillo & Katz, 1954). If the quantal content is affected by tonic concentration of ACh in the synaptic cleft, as suggested above, then the reduction of quantal content to WT level upon physostigmine treatment indicates that ACh level in the transgenic NMJ is lower under control conditions, and is comparable to WT synapses only under conditions of AChE blockade. Support to the lower basal level of free ACh was found in the TG brain (Erb *et al.* 2001). It thus appears that the parameters of quantal content and frequency of spontaneous release are a direct consequence of the elevated catalytic activity of AChE in the transgenic NMJ. The in-vitro synaptic situation in the TG muscle presents conditions of steady state release with higher quantal content and actual amplitude, combined with a relatively high vesicle number. Together, these probably rescue the hypo-cholinergic synaptic state under higher levels of AChE.

In conclusion, our experiments have confirmed that altered activity levels of AChE induce wide spread consequences of muscle malfunctioning beyond neuromuscular transmission. These results implicate a broad physiological spectrum to AChE related muscular pathologies.

AChE-R interaction with the scaffold protein RACK1 and protein kinase CβII intensifies stress-induced behavioral inhibition

Summary

Behavioral reactions to stress are altered in numerous psychiatric and neurodegenerative syndromes, but the corresponding molecular processes and signal transduction pathways are yet unknown. In mice, the stress-induced splice variant of acetylcholinesterase, AChE-R, interacts intraneuronally with the scaffold protein RACK1 and through it, with its target protein kinase PKCβII. Antisense suppression of AChE-R production downregulated the stress-induced brain accumulation of PKCβII and reduced conflict behavior, demonstrating physiological relevance for this interaction. Reciprocally, transgenic FVB/N mice overexpressing AChE-R displayed intensified neuronal RACK1 and PKCβII co-labeling, as well as extended conflict behavior following stressful events. Stress-associated changes in cholinergic gene expression may thus regulate neuronal PKCβII functioning, promoting fear-induced behavioral inhibition following stress.

Introduction

Behavioral reactions to traumatic events are altered from those of the general population in several psychiatric disorders, e.g. post-traumatic stress disorder (PTSD, Newport and Nemeroff, 2000) depression (Duman et al., 1999) and Alzheimer's disease (Cummings and Back, 1998). Disease-associated changes often intensify "freezing" or "fear-induced behavioral inhibition" characterized by suppression of behavior, as opposed to excitatory "flight" behavior (Gray, 2000). Impaired resolution of the conflict among these potential responses to stress thus yields an imbalanced response, however, the mechanisms underlying these changes are yet unknown. Stress responses involve several neural pathways (Herman and Cullinan, 1997) and endocrine systems (Tronche et al., 1999). For example, the cholinergic pathway from the medial septum to the hippocampus suppresses escape reactions in favor of freezing or hiding reactions (Giovannini et al., 2001). In the hippocampus, stress responses induce initial cholinergic excitation followed by feedback inhibition of neural activity (Kaufer et al., 1998a). This suggests involvement of cholinergic elements in the conflict among competing behavioral responses to stressful events.

Of the key cholinergic elements, acetylcholinesterase (AChE) possesses both catalytic and neuronal plasticity activities (Behra et al., 2002). In mice, stress-induced alternative splicing facilitates overproduction of the normally rare AChE-R variant, associated with weeks-long neuronal hypersensitivity (Meshorer et al., 2002). Transgenic mice overexpressing intraneuronal AChE-R (TgR), display reduced levels of stress-associated neuropathologies (Sternfeld et al., 2000), suggesting that this enzyme is functionally effective. In humans, behaviorally effective anticholinesterase therapies induce AChE-R accumulation in the cerebrospinal fluid of Alzheimer's disease patients (Darreh-Shori et al., 2002). In extracellular sites, AChE-R reduces the stress-induced acetylcholine levels (Kaufer et al., 1998a). However, AChE-R also accumulates in neuronal cell bodies, where acetylcholine hydrolysis is unlikely. Since the core domain, common to all of the AChE variants is sufficient for acetylcholine hydrolysis (Duval et al., 1992), the C-terminal domain unique to AChE-R emerged as an attractive candidate for intracellular protein-protein interactions transducing stress-induced signals.

Signal transduction pathways involve specific subtypes of protein kinase C (PKC, Coussens et al., 1986). These are activated under physiological (Feng et al., 2001), biochemical (Paola et

al., 2000) and cellular stresses (McNamara et al., 1999). PKC activity enhances peak NMDA-evoked currents, compatible with the weeks-long enhancement of glutamatergic activity following stress (Meshorer et al., 2002). In addition, however PKC phosphorylation of the C-terminal peptide of the NR1 subunit of the NMDA receptor depresses steady-state NMDA-evoked currents though a Ca^{+2}- dependent, Src-signaling independent pathway (Lu et al., 2000). Together, these effects predict complex PKC-dependent changes in glutamatergic neurotransmission and related behavioral phenotypes under stress. In particular, PKCβII, an alternative splicing product of the PKCβ gene (Ono et al., 1987), is intimately associated with oxidative (Paola et al., 2000) and ischemic stresses (Cardell and Wieloch, 1993) and is essential for fear conditioning (Weeber et al., 2000).

Exposure to phorbol ester or dopamine β_2 agonists activates PKCβII, promoting its subcellular movement in complex with the shuttling protein RACK1 (Ron et al., 1999). RACK1 belongs to the family of WD proteins, which can simultaneously bind different partners to various regions in their multi-blade rings (Smith et al., 1999). For example, RACK1 interacts with β-integrin (Liliental and Chang, 1998), cAMP phosphodiesterase (Yarwood et al., 1999), phospholipase C-γ1 (Disatnik et al., 1994), src kinase (Chang et al., 2001) or the β-adrenergic receptor (Rodriguez et al., 1999). Some reports indicate RACK1 deficits in the brain of Alzheimer's disease patients (Battaini et al., 1999), where phosphorylation impairments are a distinct feature of the disease phenotype. However, the ubiquitous nature of RACK1, makes it unlikely to be the primary inducer of PKCβII-mediated stress related cascades.

Using a yeast 2-hybrid screen (Chien et al., 1991) we discovered that AChE-R forms tight, co-immunoprecipitable triple complexes with RACK1 and PKCβII, and facilitates stress-induced, antisense-suppressible PKCβII accumulation associated with prolonged conflict behavior patterns. Our findings suggest that the formation of neuronal AChE-R/RACK1/ PKCβII complexes tilts the balance of stress-induced behavior towards intensifying behavioral inhibition.

Materials and methods

Vectors. The "bait" plasmid pGBK-ARP51 included a *EcoRI/HpaI* fragment of human AChE-R cDNA (nt 1796-1865 of hAChE, accession number M55040, followed by nt 1-111 from the genomic hAChE I4-E5 domain (accession S71129, stop codon in position 86)) cloned into the EcoR1/SmaI sites of pGBK-T7 (Clontech, Palo Alto, CA). PGARP is PGBK-ARP51 cloned into the Bsp120I/XbaI sites of pEGFP-C2 (Clontech).

Two hybrid screening. Yeast AH109 cells (Clontech) were transformed with the pGBK-ARP51 plasmid (Yeastmaker transformation system, Clontech), including the DNA-binding domain (BD) (amino acids 1-147) of the yeast GAL4 transcriptional activator, then with 10-25 μg of an amplified human fetal brain cDNA library cloned into the GAL4 activation domain AD vector (Chien et al., 1991). Screening covered 240,000 independent clones.

Cell cultures and transfection experiments. Transient transfections of PC12 or COS cells with AChE-R encoding plasmid (Sternfeld et al., 2000) and Lipofectamine Plus (Life Technologies, Paisley, UK) were followed by lysis 24 h later in 0.1 M phosphate buffer, pH 7.4, 1% Triton X-100, and complete mini protease inhibitor cocktail (Roche, Mannheim, Germany). Clear supernatants were prepared by centrifugation (12,000 x g, 4° C, 30 min).

Coimmunoprecipitation. Cell supernatants (200 μL, 1.5 mg protein/mL) were diluted 1:5 in 50 mM Tris-HCl, pH 7.4, 150 mM NaCl, 1 mM EDTA, 0.25% gelatin, protease inhibitors cocktail (Roche), 0.05% Triton X-100 for overnight rotation at 4° C with goat polyclonal

antibodies (cat. no. SC-6431, Santa Cruz Biotechnology, Santa Cruz, CA) targeted to the N-terminal domain of hAChE (10 µL, 200 µg/ mL). Mixtures with protein G MicroBeads (Miltenyi Biotec, Auburn, CA, 75 µL, 1 hr) were loaded on MACS columns (Miltenyi Biotec), washed (3x 200 µL of TBS 0.1M tris pH 7.4, 1.7 M NaCl, 0.05% Tween-20) and eluted with gel loading buffer (50 mM tris pH = 6.8, 100 mM DTT, 2% SDS, 0.1% bromophenol blue, 10% glycerol). Eluates were separated by denaturing SDS-PAGE (Bio-Rad, Hercules, CA), blocked (1 hr, 3% non fat dried milk, 2% BSA, 0.2% Tween-20 in TBS) and blotted. Immunodetection was with rabbit anti-N-terminus AChE antibodies (cat. no. N-19, Santa Cruz), 1:500; mouse-anti-PKCβII (P8083, Sigma, St. Louis, MO), dilution 1:8000, or mouse monoclonal antibody against RACK1 (R20620, Transduction Laboratories, San Diego, CA), dilution 1:2500. Second antibodies were horseradish-peroxidase-conjugated goat anti-rabbit IgG or goat anti mouse (1:10,000, Jackson Laboratories, Bar Harbor, ME). Chemiluminescent detection was with the ECL kit (Amersham Life Sciences, Uppsala, Sweden) as instructed.

Recombinant RACK1 preparation. A plasmid overexpressing RACK1 fused to the maltose binding protein (MBP-RACK1) in *E. coli* pDEM31, a derivative of pMAL-c2 (New England Biolabs, Beverly, MA) (Rodriguez et al., 1999), was a gift from Dr. Daria Mochly-Rosen, Stanford. Following purification on an amylose affinity column (New England Biolabs), the 36 kDa RACK1 protein was released by proteolysis with factor Xa (New England Biolabs).

Overlay assay. Recombinant RACK1 was electrophoretically separated, blotted to nitrocellulose membranes and incubated in a blocking solution (1 hr, 3% non fat dried milk, 2% BSA, 0.2% Tween-20 in TBS). PC12 cell supernatants (1:20 dilution, 2 mg/mL protein, in 50 mM Tris-HCl, pH 7.5, 0.2 M NaCl, 0.1% BSA, 0.1% polyethylene glycol (PEG), 12 mM β-mercaptoethanol, protease inhibitors cocktail (Roche), in a final concentration of 0.05% Triton X-100) were added for 1 hr at room temp. Following 3 brief washes, three 5 min washes in 0.05% Tween-20 in TBS and fixation with 4% paraformaldehyde (30 min, 4° C), bound AChE was detected using sc-6431 antibodies (Santa Cruz Biotechnology, dilution 1:500).

Laboratory Animal Experiments were approved by the Hebrew University Committee for Animal Experimentation. Male FVB/N and TgR mice, 6-8 weeks old, naive or injected with saline (0.2 ml, 0.9%, intraperitoneal) to induce mild psychological stress, were deeply anesthetized with pental (pentobarbitone sodium, CTS Chemical industries, Petach Tikva, Israel, 100 mg/Kg) and sacrificed 6 or 24 hr post-injection. For neuroanatomy analyses, anesthetized mice were transcardially perfused with 4% (v/v) paraformaldehyde and processed as in Sternfeld et al (2000). Brain homogenates were prepared from non-transfused mice in 0.01 M Na-phosphate buffer, pH 7.4/1% Triton X-100 (9:1 volumes), incubated on ice (1 hr), and centrifuged (14,000 rpm, 45 min in an Eppendorf model 5417R centrifuge); supernatants were kept at –20° C until use.

Cholinesterase activity assays were as described (Kaufer et al., 1998a). BW284C51 (1×10^{-5} M) was used to suppress AChE activity in butyrylcholinesterase assays, and iso-OMPA (1×10^{-5} M) was used to suppress butyrylcholinesterase activity in AChE assays.

PKC activity measurements involved two distinct peptide substrates and were performed essentially as instructed in the corresponding kits (PKC assay kit, Upstate Biotechnology, Lake Placid, NY; PepTag®, Promega, Madison, WI). Reported PKC activity assays were confirmed in both methods.

Immunohistochemical analyses were essentially as previously described using rabbit anti-ARP (Sternfeld et al., 2000)1:100, rabbit anti PKCβII (Cat. No. sc-210, Santa Cruz) 1:100, rabbit anti PKCβII (Sigma) 1:250 and mouse anti RACK1 (Cat. No. R20620, Transduction Labratories) 1:200. Sections were incubated with the primary antibody, then with biotin-

conjugated donkey anti- rabbit antibody (Cat No. AP132B, Chemicon, Temecula, CA, 1 hr, room temp., overnight at 2-8° C). RACK1 staining was further preceded by trypsin type II treatment (Sigma), 1 μg/mL with $CaCl_2$ 0.001%, 0.001% soybean trypsin inhibitor (Sigma), 2 min, room temp. Detection was with horseradish peroxidase-conjugated goat anti-mouse antibody (1:100 dilution, Sigma), followed by incubation in 0.0125% diaminobenzidine, 0.05% nickel ammonium sulfate, and 0.00018% hydrogen peroxide. Anti-RACK1 pre-incubation with 10 μM RACK1 (1 hr, room temp) totally eliminated anti-RACK1 staining, demonstrating specificity.

EPM tests were conducted under dim illumination (Trullas and Skolnick, 1993). Overall motor activity was estimated by total number of arm entries. Time spent in open arms and the fraction of entries into open arms out of total arm entries reflected the conflict between exploration tendency and the innate tendency to hide possible anxiety (Bolivar et al., 2001). Time spent at the center of the EPM, where mice stop before making a choice of arm entry provided a measure of conflict behavior. Both reduced choice of open arms and increased time spent at the choice point were interpreted as increased fear-induced behavioral inhibition. 2 months old, TgR and FVB/N females were placed in individual tilt-bin boxes (30 min), injected intraperitonealy with saline (0.9%, 0.1 mL) or oligonucleotides (Meshorer et al., 2002), kept in the tilt bin box for another 30 min and returned to their home cages during the dark phase of the light:dark cycle (10:00-11:00 am). Twenty-four hr later, mice were put again in the tilt-bin boxes for 30 min and then tested and videotaped for 5 min in the EPM. Control uninjected naive mice were similarly placed in the box for 30 min, and then EPM tested.

Emergence into an open field. A 9 x 10 x 11 cm tilt bin box (Arnon Caine, IL) was placed in the center of a black painted plywood 100 x 100 cm open field with 50 cm walls. A 32 x 14 cm stainless steel cage top (Techinplast, Milano, Italy) leaning on this box formed a platform reaching 5.5 cm above the open field floor. Latencies were measured for exit from the tilt-bin box to the platform and for descending from the platform to the open field floor.

Statistical analyses: Two-factor analysis of variance subjected to post-hoc analyses involved transgenic overexpression (TgR vs. FVB/N) and stress (saline injection vs. no injection).

Results

In spite of its secretory nature, AChE-R accumulates within the cell body and processes of hippocampal neurons (Fig. 1A). We used the Gal4 two-hybrid system to search for its intracellular partner(s).

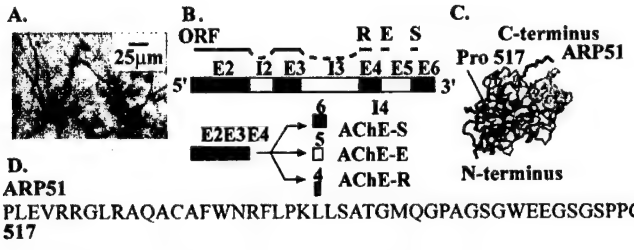

Fig. 1. The ARP51 C-terminal sequence of AChE.

A. CA1 hippocampal neurons from TgR mice stained for human (h) AChE-R. B. Schematic diagram of the human *ACHE* gene (E = exon, I = intron, ORF = open reading frame) with its synaptic (AChE-S), erythrocyte (AChE-E), and "readthrough" (AChE-R) mRNA 3' alternative splicing products, giving rise to protein variants with different C-termini. C. 3D simulated structure of mouse AChE (http://www.rcsb.org/pdb/index.html, accession No. 1C2B). Residues 1-517 but not the C-terminal 51 residues (ARP51) are required for acetylcholine hydrolysis. D. The ARP51 sequence. The residues in black are unique to the human AChE-R variant.

Two-hybrid screening for protein partners of AChE-R. As "bait", we used the human AChE-R readthrough peptide ARP51, composed of the C-terminal 51-amino acid residues of AChE-R, 25 of which are tightly conserved in evolution (Fig. 1B-D and Esther database: http://www.ensam.inra.fr/cgi-bin/ace/index).

Several potential partner proteins from human fetal brain enabled survival of yeast clones expressing the ARP51 peptide. Of these, only the WD protein RACK1 appeared in six cDNA fragments of different lengths (Fig. 2A and sequence data not shown). ARP51/ RACK1 expressing yeast cells displayed comparable β-galactosidase activity to that induced by p53 – T antigen interaction (dissociation constant 2 x 10^8 M^{-1}; Kuhn et al., 1999, Fig. 2B, inset). RACK1 is homologous to the propeller part of the G protein β_2 subunit, a prototypic member of the WD domain family (Smith et al., 1999). The sequence domain which conferred binding to ARP51 in the two-hybrid system included large parts of blades 5 and 6 out of the 7 domains in the wheel-like propeller structure of the RACK1 protein. The binding site to PKCβII on blade 6 of RACK1 (Rodriguez et al., 1999, Fig. 2A,C) but not the PKCβII binding site on blade 3 emerges as apparently masked under ARP51 interaction.

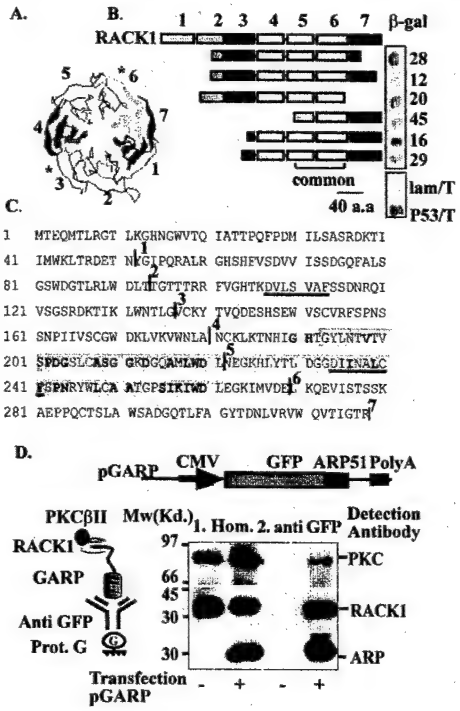

Fig. 2. Two-hybrid positive RACK1 clones.
A. Schematic structure of the G protein β subunit (http://pdb.ccdc.cam.ac.uk/pdb/, accession no. 1gp2). Highlighted are the concentric antiparalell 4 strands in the numbered blades of WD proteins (Smith et al., 1999, RACK1 sequence Blast identity 26%, similarity 44%; accession no. AAH04186). Stars note PKCβII binding sites in RACK1. B. Schematic alignment of RACK1 clones. Scaled drawings of the 7 WD domains (boxes numbered above) in RACK1 (top, accession no. P25388) and the six viable RACK1 clones of human fetal brain origin, in the two-hybrid screen. The yellow WD domains 5 and 6 common sequence included in all clones is underlined. ARP51-RACK1 interactions in representative colonies is shown by β-gal staining (blue spots). Positive and negative controls were p53-T-antigen (p53/T) and lamin C-T antigen (lam/T) interactions in yeast. C. Human RACK1 amino acid sequence. Highlighted in yellow is the common sequence, with residues which fit the WD consensus (Smith et al., 1999) marked in red. Repeat boundaries (1-7) are numbered, and the PKCβII binding peptides underlined (red). D. ARP51 promotes AChE-R/ RACK1/ PKCβII triple complex formation in transfected COS cells. Top scheme: the pGARP CMV-based, GFP fusion protein with ARP51. Side drawing presents the experimental design. Homogenates: immunolabeled RACK1, PKCβII and ARP51 in non-transfected (-) or GARP transfected (+) COS cell homogenates. Anti-GFP: Immunoprecipitation with anti-GFP antibodies of PKCβII, GARP and RACK1 in transfected but not in non-transfected COS cells.

ARP51 promotes triple complex formation with RACK1 and PKCβII. None of the β-gal inducing RACK1 clones included WD domain 1 (Fig. 2A,B), suggesting that this domain

might interfere with ARP51- RACK1 interactions. To address this question, we fused green fluorescent protein (GFP) with ARP51 under the CMV promoter (pGARP, Fig. 2D). In transfected COS cells, both anti-ARP and anti-GFP antibodies detected GARP expression. Moreover, anti-GFP antibodies immunoprecipitated GARP, full length RACK1 and PKCβII from homogenates of GARP-transfected but not non-transfected COS cells (Fig. 2D), demonstrating this triple complex formation in live cells.

RACK1-hAChE-R interaction in live cells. Anti-RACK1 antibodies failed to precipitate GARP or PKCβII, perhaps reflecting interference of the antigenic RACK1 epitope with ARP51 interaction. To test for RACK1 interaction with full-length AChE-R, we therefore used an *in vitro* overlay. A fusion between maltose-binding protein (MBP) and RACK1, expressed in *E. coli*, was purified by affinity chromatography to maltose. Site-specific factor Xa protease released RACK1 (Fig 3A). In protein blots, anti-RACK1 antibodies labeled the fusion protein, proteolytically-released RACK1 and fragments thereof, but not MBP (Fig 3B). Similar membranes were overlaid with a homogenate obtained from rat phaeochromocytoma (PC12) cells transfected with a plasmid encoding AChE-R (Sternfeld et al., 2000). Antibodies to the N-terminus of human AChE detected in the overlaid membrane, but not a control one, specific binding of AChE to the intact RACK1 protein but not its degradation products or MBP (Fig. 3C, D).

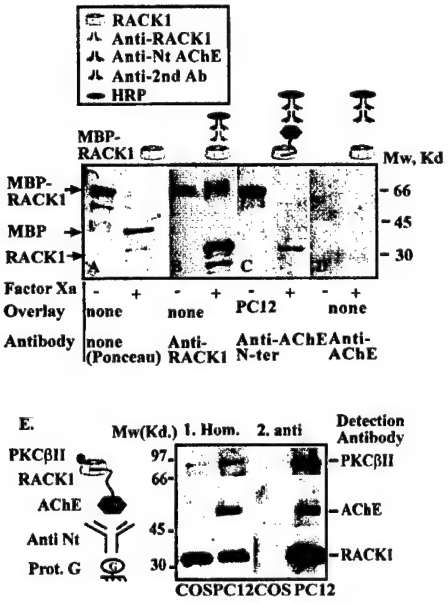

Fig. 3. Triple AChE-R /RACK1/ PKCβII complexes in cultured PC12 cells.
A.The MBP-RACK1 complex is cleavable. Ponceau S staining of purified RACK1 fused to bacterial maltose binding protein (MBP-RACK1) or the 36 kDa RACK1 protein released by factor Xa proteolysis (+). Maltose binding protein (MBP) served as an internal control. B. RACK1 immunolabeling. Horseradish peroxidase (HRP) immunolabeled RACK1 and its MBP complex and degradation products. C. RACK1-AChE-R complexes. Overlay incubation with a PC12 cell homogenate overproducing recombinant hAChE-R, then with an antibody to the AChE N-terminus, labels full-length RACK1, but not its degradation product. D. AChE-R requirement for complex formation. Membranes that were not overlaid previously with the AChE-R overproducing cell homogenate show no label with anti- AChE antibody. E. RACK1 and PKCβII Co-immunoprecipitate with anti-AChE antibodies. Drawing shows the experimental design. 1. Homogenates (Hom): Immunodetected PKCβII and RACK1 but not AChE, appear in homogenates of COS cells. PC12 cell homogenates display PKCβII, RACK1 and AChE. 2. Anti-AChE N ter: Dissolved immunoprecipitates with antibodies to the N-terminus of AChE display all 3 partner proteins in PC12 cells but no signals in COS cells. Note intensified PKCβII and RACK1 signals as compared with those observed in homogenates.

To find out if AChE-R interacts with RACK1 to form triple complexes with PKCβII within live cells, we used COS and PC12 cells. Both express RACK1 and PKCβII, whereas only PC12 cells express AChE-R. Neither anti-RACK1 nor anti-PKCβII antibodies were capable of co-precipitating triple complexes. However, antibodies targeted to the N-terminus of AChE co-immunoprecipitated both PKCβII and RACK1 from the soluble fraction of PC12 cell

homogenates but not the control COS cells. This supported the notion of tight AChE-R/ RACK1/ PKCβII linkage in PC12 cells (Fig. 3E1,2).

AChE-R /RACK1/PKCβII co-expression in brain neurons. In the brain of both naive FVB/N and C57B6J mice, immunoreactive RACK1 appeared in the cytoplasm and closely proximal processes of pyramidal neurons, in layers 3 and 5 of the frontal and parietal cortex, in both superficial and deep layers of the piriform cortex, and in regions CA1-3 of the hippocampus. Subsets of these neurons also over-express AChE-R under confined swim stress (Kaufer et al., 1998a; Meshorer et al., 2002). Diffuse staining with anti-PKCβII antibodies was observed in sub-regions of layers 5, 6 in the cortex, in the stratum oriens and stratum radiatum layers of the hippocampus CA1 field, in the striatum matrix, in the substantia nigra pars reticulata and in axonal bundles including the nigro-striatal tract. In addition, dense PKCβII clusters appeared in neuronal perikarya and axonal stems of the upper layers of the parietal, temporal and piriform cortices, dorsal striatum, the fear-conditioning associated basolateral amygdala (Blair et al., 2001), hippocampal CA1 and lateral septum (data not shown).

Co-accumulation of antisense-suppressible AChE-R and PKCβII in stress-responding brain regions. In the brain of naive mice, catalytic AChE activities ranged from 0.8 ± 0.03 nmol substrate hydrolyzed per μg protein per min (average ± standard error of the mean, SEM) in the anterior cingulate cortex to 1.00 ± 0.04 in the parietal cortex. We then measured AChE activities 6 hr following intraperitoneal saline injection, which activates similar stress-responding brain regions to those activated by immobilization, footshock or forced swim stresses (Ryabinin et al., 1999). EN101, 2'-oxymethylated antisense oligonucleotide inducing selective destruction of neuronal AChE-R mRNA (Meshorer et al., 2002) served to study the physiological significance of AChE-R/RACK1/PKCβII interactions. 2'-oxymethylation of oligonucleotides promotes their brain penetrance (Tavitian et al., 1998). Yet, EN101 is well tolerated, with no detrimental effect on behavior. It reduces the brain levels of AChE-R but not the AChE-S protein under conditions where an irrelevant oligonucleotide targeted towards the homologous butyrylcholinesterase gene has no effect. Also, peripherally administrated EN101 successfully suppresses stress-induced locomotor impairments (Cohen et al., 2002). When injected intraperitoneally, EN101 could therefore be expected to suppress the stress-induced accumulation of neuronal AChE-R (Fig. 4A).

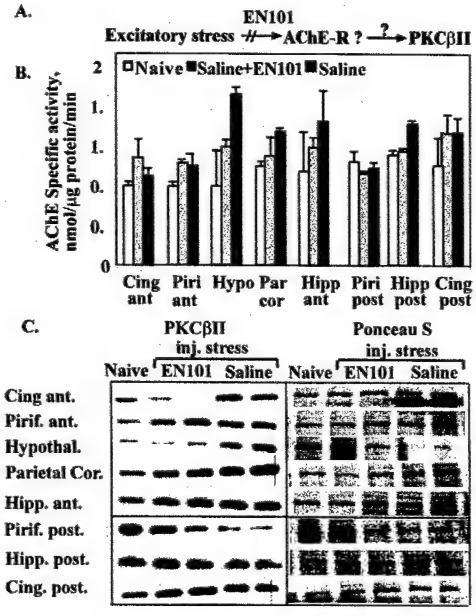

Fig. 4. AChE-directed antisense oligonucleotide suppresses stress-induced PKCβII and AChE-R accumulation.

A. The experimental outline. Mild injection stress may cause AChE-R and PKCβII accumulation. If inter-related, they should both be suppressible by EN101, an antisense oligonucleotide that induces AChE-R mRNA destruction. B. Stress-induced increases in AChE enzyme activity. Average AChE specific activities ± standard error of the mean (SEM) in brain regions from FVB/N naive mice or mice sacrificed 6 h after intraperitoneal saline injection. 500 μg/kg EN101 (a 20-mer 2`-O-methyl protected antisense oligonucleotide) was injected 1 hr prior to saline injection. One of 3 experiments. C.

EN101-suppressible PKCβII accumulation. Immunolabeling intensities of PKCβII (left) and Ponceau S protein staining (right) in brain region homogenates from individual mice treated as detailed under B. Top box: Stress-induced accumulation ($p<0.003$ as compared to naive, Student's t test) of PKCβII in the cingulate anterior cortex (Cing ant.), Piriform anterior cortex (Piri ant.), Hypothalamus (Hypothal.), Parietal cortex (Parietal cor.) and anterior hippocampus (Hipp ant.), and EN101-induced prevention of such increases. Bottom box: Less responsive brain regions(P=0.9): posterior piriform (Piri post) and cingulate cortex (Cing post) and posterior hippocamus (Hipp. Post).

In our mice, injection stress induced significant ($P < 0.01$) yet antisense-suppressible ($P < 0.05$) increases in AChE hydrolytic activity in several stress-responding regions (e.g. over 2-fold injection-induced increases in hypothalamic AChE activity, half of which was prevented under EN101, Fig 4B). EN101 did not prevent the parallel increases in butyrylcholinesterase activities in these brain regions (by up to 50%, $P < 0.05$), attesting to the specificity of its effects. Other regions, e.g. posterior piriform cortex, showed neither increase nor EN101 effects (Fig. 4B).

Injection-induced and EN101 preventable increases were also observed in PKCβII in the parietal, anterior cingulate and piriform cortices, hypothalamus and anterior hippocampus (Fig. 4C, top). In yet other areas, e.g. the posterior piriform cortex, injection stress reduced PKCβII levels, and these decreases as well appeared more limited under EN101. In other regions, e.g. the posterior cingulate cortex, PKCβII increases appeared refractory to EN101, excluding causal correlations between AChE-R and PKCβII increases in such regions (Fig. 4C, bottom).

Transgenic AChE-R overexpression intensifies neuronal PKCβII clusters. Hippocampal homogenates and sections from TgR mice (Sternfeld et al., 2000) served to test whether chronic AChE-R overproduction modulates the levels, properties and/or neuronal localization of RACK1 and PKCβII. Enzymatic PKC activities were elevated in hippocampal homogenates from these mice, as compared to the parent FVB/N strain (Fig. 5A, left). This was accompanied by increases in immunopositive neuronal AChE-R and RACK1 and a faster migrating PKCβII band, only faintly detected in the FVB/N hippocampus (Fig. 5B, right).

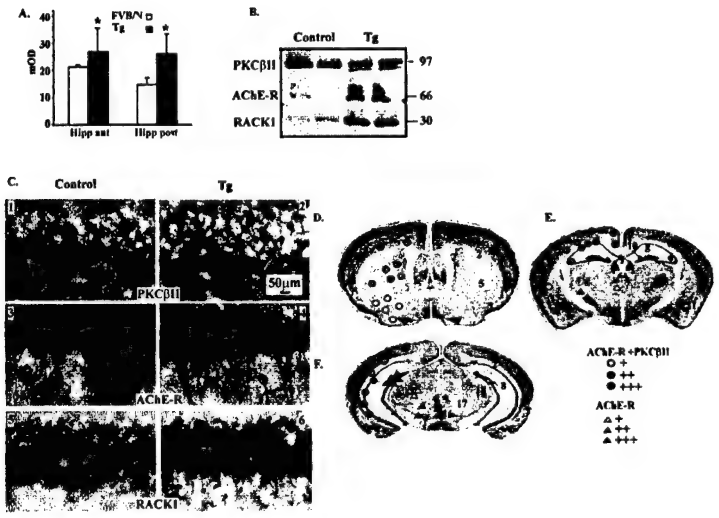

Fig. 5. Transgenic AChE-R overexpression intensifies neuronal RACK1 and PKCβII labeling in hippocampal CA1 neurons. A. Increased PKC activity in TgR mice. PKC activity in pooled anterior or posterior hippocampal homogenates from 2 TgR and 2 FVB/N mice. Asterisks note statistically significant differences (Student's t test, $P < 0.03$) for all tested samples. B. RACK1 and PKCβII elevation in TgR mice. Immunoblot signals for

PKCβII, AChE-R and RACK1 following gel electrophoresis of clear hippocampal homogenates from 2 individual FVB/N controls and 2 sex and age-matched TgR mice (Tg). Representative results from 5 reproducible experiments. C. Intensified neuronal labeling. Hippocampal CA1 immuohistochemistry analyses from representative control and TgR mice stained with the noted antibodies. D-F. Partial overlaps in neuronal AChE-R accumulation and PKCβII distributions. Shown in selected brain sections (posterior to Bregma 0.0-0.2 mm, 1.5-1.7 mm and 2.9-3.1mm, respectively) are the areas where AChE-R accumulation (triangles) or PKCβII co-labeling in AChE-R accumulating neurons (circles) were detected. Staining intensity was low (wWhite, for co-staining, or gray for AChE-R alone,+), medium (orange or pale blue,++) or high (red or dark blue,+++), for: 1, cortex upper layers; 2, cingulate anterior cortex, 3; cingulate posterior cortex, 4; cortex lower layers; 5, sStriatum; 6, lateral septum; 7, pPiriform cortex; 8, hippocampus CA1; 9, hippocampus CA3; 10, hippocampus dentate gyrus; 11, basolateral amygdala; 12, central amygdala; 13, lateral hypothalamus; 14, ventromedial hypothalamus; 15, ventral lateral thalamus; 16, Edinger-Westphal nucleus; 17, red nucleus; 18, pre-tectal area.

Immunohistochemical analysis demonstrated wide brain region distribution for RACK1 and AChE-R in the TgR brain (Fig. 5C and data not shown). Punctiform PKCβII staining (Fig. 5C1-4) appeared in the cell bodies and proximal processes of a specific subset of CA1 neurons. Both in FVB/N and TgR mice, AChE-R overexpression in hippocampal neurons was accompanied by positively labeled cells with morphology reminiscent of microglia (Fig. 5C 3, 4). In TgR mice, intensified RACK1 labeling of perikaria and closely proximal neurites of CA1 pyramidal neurons was also observed (Fig. 5C 5, 6).

Diffuse and punctiform PKCβII staining displayed essentially similar distribution in TgR mice and in the FVB/N strain. Yet, punctiform PKCβII staining was intensified within several stress-responding brain areas in some, but not all of the AChE-R accumulating neurons in TgR mice. These included neurons in upper cortical layers, hippocampal CA1 and CA3, lateral septum, and basolateral amygdala. AChE-R accumulating neurons in the lateral and ventro-medial hypothalamus, central nucleus of the amygdala, the hippocampal dentate gyrus, ventro-lateral thalamus, and Edinger-Westphal nucleus of TgR mice showed no PKCβII punctiform staining (Fig. 5D-F and data not shown). In other brain regions of TgR mice (globus pallidus, substantia nigra, superior culliculus, medial septum and diagonal band), AChE-R accumulating neurons were rare with little or no PKCβII punctation (Fig. 5 D-F).

TgR mice display prolonged conflict behavior following mild stress. In the elevated plus maze (EPM, Fig. 6A), female rodents display greater tendency then males to escape (Steenbergen et al., 1990). Thus, females provided a better baseline for studying conflict behavior. Female mice were placed in a holding box for 30 min, received an intraperitoneal injection of 0.1 ml saline, and were kept there for another 30 min, to create a contextual link. General locomotor activity and open arm exploration were tested in the EPM 24 hr following injection. At the center square of the EPM, mice engaged in approach-avoidance conflict behavior, which was also measured (Fernandez Espejo, 1997).

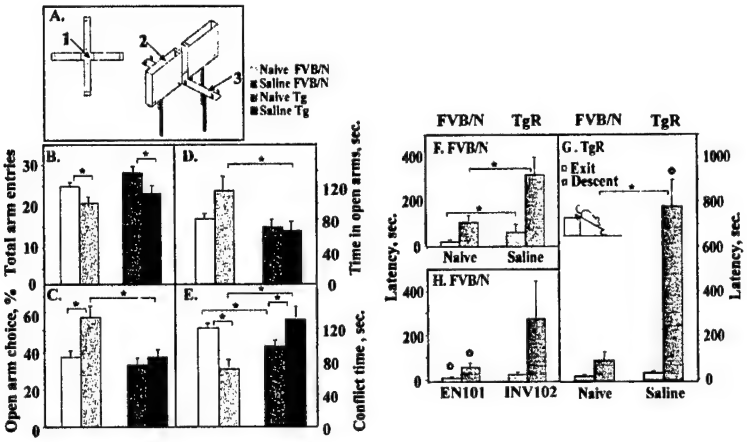

Fig. 6. TgR mice display delayed reaction to mild stress.

A. EPM choices. Scheme (adapted from Columbus Instruments http://www.colinst.com/maze-el.html), demonstrates three choices: 1. conflict (remain at the center space); 2. shelter (hide in sheltered arms) and 3. escape (into open arms). B. Locomotor activities in mildly stressed FVB/N and TgR mice. Total arm entry numbers for naive and pre-stressed FVB/N and TgR mice (ten 2-4 month old females per group) ± SEM. Asterisks note statistically significant differences between marked columns. C. Pre-stressed FVB/N, but not TgR mice escape into open arms. Percent open arm choices ± SEM by the above mouse groups during 5 min. D. Pre-stressed FVB/N, but not TgR mice spend more time in open arms. Total times spent in open arms in sec for the different groups ± SEM. E. Increased conflict time in pre-stressed TgR, but not FVB/N mice. Times spent in sec by each group in the maze's center. F. Post-stress exit and descent latencies into an open field. Latency times (sec) of exit from a box following contextual habituation time, and descent over a tilted cage cover into an open field (N= 6 naive and 6 saline-injected FVB/N mice). G. Extended descent latency in TgR mice. Experiment was as in 6F. Asterisks and stars note significant differences from naive, or saline injected FVB/N mice, respectively. Inset: scheme of the emergence test. H. Antisense suppression of post-stress latency. Exit and descent latencies for FVB/N mice 24h post-injection with EN101 or the inverse INV102 oligonucleotides (Methods). Note that the antisense, but not the inverse sequence suppressed the injection-induced extended latency. Stars note significant differences from saline-injected mice (6F).

Saline injection, but not congenital AChE-R overexpression, reduced general motor activity of both TgR and FVB/N mice in analysis of variance [ANOVA] and post-hoc Newman Keuls tests ([$F(1,30) = 5.84$, $P < 0.02$], Fig. 6B). In FVB/N but not in TgR mice, saline injection further increased open arm exploration compared to no injection controls ($P < 0.002$). Compatible with disrupted risk assessment by prior stress (Quartermain et al., 1996), injection also increased open arm preference in FVB/N, more than in TgR mice (Fig. 6D, $p<0.002$). Percent open arm entries revealed main effects for both transgenic overexpression [$F(1,30) = 10.80$,[$P < 0.03$] and saline injection [$F(1,30) = 10.70$, $P < 0.03$], as well as significant interaction of transgenic overexpression with saline injection [$F(1,30) = 4.80$, $P < 0.04$].

Saline injection decreased the conflict behavior time in FVB/N mice ($P < 0.005$), but increased it in TgR mice ($P < 0.03$, Fig. 6E). Therefore, saline-injected TgR mice spent considerably longer time at the EPM center than saline injected FVB/N mice ($p<0.0008$). Analysis of conflict behavior time thus revealed clear interaction of transgenic overexpression and saline injection [$F(1,30) = 18.52$, $P < 0.002$], possibly reflecting opposite effects in these groups.

Delayed emergence into an open field: Latencies were measured for exit from a sheltered box to a higher platform and then for descent from this platform to an unfamiliar, and

therefore threatening open field floor. Conflict was manifested in repeated episodes of approach to the edge of the platform and retreat back to the box. Saline injection increased latencies to exit and to descend from the platform to the open field floor (Fig. 6F). Saline exerted main effect on exit latency [$F(1,33) = 7.74$; $P < 0.001$], but had no interaction with AChE-R overexpression. TgR mice displayed yet longer exit and descent latencies. Within a 25 min limit, all FVB/N mice descended but 2 of the 12 TgR mice did not descend at all to the open field floor.

Saline injection induced a significant main effect on exit latency [$F(1,33) = 11.36$, $P < 0.002$] and descent latency [$F(1,34) = 51.8$, $P < 0.0001$; Fig 6F]. Transgenic overexpression did not affect exit latency, but increased descent latency following saline injection [$F(1,34)= 7.03$, $p<0.02$; Fig. 6G]. Significant interaction of transgenic overexpression and injection stress [$F(1,34) = 4.69$, $P < 0.04$] revealed greater descent latency in saline-injected TgR mice compared to saline-injected FVB/N mice ($P < 0.005$). Thus, TgR mice displayed increased conflict behavior following a stressful event, both in the EPM and in the emergence into an open field test.

To test whether the delayed descent time in stressed FVB/N mice was due to AChE-R accumulation, injected saline was replaced with the antisense oligonucleotide EN101, attenuating AChE-R accumulation, or with the inversely oriented oligonucleotide INV102 (Meshorer et al., 2002) as negative control. In the emergence test 24 h later, we observed antisense suppression of exit latency (a significant main effect, [$F(3,26) = 3.35$, $P < 0.04$]) compared to saline treatment ($P < 0.03$, Fig. 6H compared to F). EN101 further suppressed descent latency [$F(3,26) = 2.91$, $P < 0.05$] compared to saline treatment ($p<0.04$, Fig. 6H compared to F). In contrast, INV102-injected FVB/N mice behaved similarly to saline-injected ones, demonstrating sequence specificity for the EN101 effect (Fig. 6H). Thus, the extended fear response in FVB/N mice depended on AChE-R overproduction, which (in the limbic system) we have found to be a pre-requisite for PKCβII accumulation.

Discussion

Our search for stress-induced neuronal signal transduction revealed that AChE-R overproduction tilts the balance of post-stress conflict behavior away from the excitatory tendency to escape toward inhibitory freezing behavior. The 2 hybrid screen findings further attribute this modified behavior pattern to the intracellular formation of triple complexes of AChE-R/RACK1/PKCβII. While much in this hypothesis awaits further exploration, it points to RACK1 as a novel component in the molecular cascade controlling physiological stress responses and provides a putative explanation to the long-known behavioral effects of neuroactive agents that modulate cholinergic neurotransmission.

Intracellular accumulation of the stress-induced AChE-R variant: The immunocytochemically observed intracellular localization of AChE-R, an essential pre-requisite for AChE's interaction with RACK1 and PKCβII, was rather unexpected because to the existence of a signal peptide in the nascent AChE-R polypeptide and the generally extracellular occurence of this protein (Soreq and Seidman, 2001). However, recent reports describe proteins that release nascent polypeptides destined for secretion from the rough endoplasmic reticulum into the cytoplasm (Ye et al., 2001). Although several of these proteins were targeted for ubiquitin-dependent processing, this suggests that the signal peptide by itself does not ensure immutable secretion of proteins that contain it, and calls for studying the

possibility that, similarly to alternative splicing, the intracellular compartmentalization of secretory proteins is altered under stress.

Robust response to very mild signals: We have previously shown robust, long-lasting accumulation of AChE-R following acute stress, e.g. head injury, anticholinesterase exposure or forced swim (Meshorer et al., 2002; Soreq and Seidman, 2001). That the same phenomenon also occurs after a single intraperitoneal saline injection and that it affects the fine tuning of conflict behavior came as a second surprise. Conflict behavior is known to depend, to a large extent, on previous experiences, e.g. traumatic events (Martijena et al., 1997), combined with inherited factors (Bolivar et al., 2001). Our findings demonstrate that a relatively mild stressful event against an uneventful background (animal colony routine), is sufficient to activate a cascade of signal transduction similar to that induced by intense stress. This may be relevant to PTSD phenomena, in which the severity of the stress was found less important than the victim's perception of threat to survival (Newport and Nemeroff, 2000).

Behavioral antisense effects: The *in vivo* effectiveness in the brain of peripherally administered EN101 antisense agent was a third surprise, although we have recently shown that EN101 reduces AChE-R mRNA and AChE-R protein levels in the brain and suppresses stress-induced locomotor impairments (Cohen et al., 2002). To suppress AChE-R-induced contextual fear responses following injection stress, at least part of the injected EN101 should first penetrate the blood-brain barrier. 2'-oxymethyl protection of EN101 promotes such penetrance: minor, but detectable levels of peripherally administered 2'-oxymethyl protected oligonucleotides were observed by imaging techniques in the brain of Rhesus monkeys (Tavitian et al., 1998). Once in the brain, EN101 should induce sufficient destruction of AChE-R mRNA to reduce AChE-R amounts below the threshold level inducing contextual fear responses. Based on a molecular weight of $6x10^3$ and an estimated 30 µl free extracellular volume for the murine brain, 10 ng (0.1% of the injected 10 µg/mouse) yields 50 pM. This is within the maximal range for inducing AChE-R mRNA destruction, yet low enough to avoid non- specific up-regulation of *ACHE* gene expression (Galyam *et al.*, 2001).

AChE-R/RACK1/PKCβII complexes as modulators of conflict behavior: In TgR mice, which present increased PKC activity and modified neural distribution of PKCβII, contextual fear responses exceeded those of their parent strain FVB/N. Antisense prevention of AChE-R accumulation following stress attenuated PKCβII increases and rescued a normal behavior pattern in FVB/N mice, in agreement with the deficits in both cued and contextual fear conditioning in PKCβII knockout mice (Weeber et al., 2000).

That mild injection stress induced modest increases in AChE-R and promoted escape behavior in FVB/N females is compatible with the female-characteristic preference for escape in conflict situations that follow a stressful event (Steenbergen et al., 1990). In TgR females, the chronic excess of AChE-R, RACK1 and PKCβII, attributes to AChE-R interactions, a behavioral inhibitory effect that likely reflects combined contribution of strain and sex-specific properties (Ohno et al., 2001; Trullas and Skolnick, 1993). That the extended emergence latency of FVB/N mice was attenuated by antisense suppression of AChE-R production, and that transgenic mice displayed yet longer latency to emerge compared to mice from their parent strain, FVB/N, supports this interpretation.

Two lines of evidence thus demonstrate association between intraneuronal AChE-R and conflict behavior. First, transgenic mice overexpressing AChE-R present extended conflict

behavior, both in the EPM and in the exit-emergence test; second, EN101 but not a negative control agent, suppressed this accumulation, preserving a normal emergence behavior in injected FVB/N mice. The mild stress employed and the "prophylactic" treatment mode likely contributed to this behavioral response.

The RACK1 scaffold protein performs multiple shuttling functions. The RACK1 region supporting AChE-R interaction consists of ca. 30% of the RACK1 perimeter, including two antiparallel four strand "blades" with many conserved WD domain residues.

Conformational changes in RACK1 likely expose it to the binding of other proteins. RACK1/AChE-R interactions and PKC activators, which modulate RACK1/PKCβII interactions (Rodriguez et al., 1999), would therefore compete with other RACK1 associations, changing the subcellular balance between the different RACK1-containing complexes under stress.

Our findings that AChE-R interacts with RACK1 and PKCβII, increases their neuronal levels and modifies their intracellular locations provide a feasible mechanism for the AChE-R effect on conflict behavior. This is consistent with the role of acetylcholine as a modulator of various stimulus-associated neurotransmission pathways (Changeux and Dehaene, 2000). For example, RACK1/PKCβII interactions suppress the phosphorylation of the NR2B subunit of the excitatory NMDA receptor (Yaka et al., 2002), which may interfere with the excitatory serotonergic control over the inhibitory GABAergic input toward behavioral responses (Feng et al., 2001).

Punctiform PKCβII labeling highlights neural circuits modulating stress responses. In the deep cortical layers, stratum oriens and stratum radiatum of CA1 hippocampal neurons, PKCβII may transduce signals across synapses between axons coming from outside the region. In the nigro-striatal tract, PKCβII is distributed along the entire axon of some neurons. In neuronal cell bodies, its punctiform staining, only partially overlaps RACK1 and AChE-R labeling patterns, suggesting relevance of each of these three proteins to both distinct and common functions.

Mapping AChE-R-filled neurons with both punctiform PKCβII and RACK1 labeling unraveled neuronal pathways associated with inhibitory behavior (Herman and Cullinan, 1997). These were located, as expected, in the stress-responsive cortical upper layers (Feng et al., 2001; Hamner et al., 1999), hippocampal CA1 region (Gould and Tanapat, 1999), lateral septum and basolateral amygdala (Amorapanth et al., 2000; Garcia et al., 1999). The amygdala, considered excitatory under fear and anxiety, also includes stress-inhibitory neurons (Killcross et al., 1997). These presumably suppress the stress-excitatory basolateral amygdala neurons; therefore, their intensified labeling is consistent with the limited stress-related neuropathology hallmarks in the brain of TgR mice.

Based on the above arguments, the dissociation between RACK1 and PKCβII under ethanol exposure (Ron et al., 2000) may contribute to the anti-conflict and dis-inhibitory effects of alcohol (Lapin, 1993). Also, AChE-R and/or PKCβII accumulation may be relevant for impairments in other processes where fear conditioning is intimately involved, and in which PKCβII plays a major role, e.g. panic attacks (Battaglia, 2002), post-traumatic stress disorder (Newport and Nemeroff, 2000) or post-stroke phenomena.

AChE-R-filled neurons also appeared in cell populations devoid of PKCβII punctiform staining. This suggests that AChE-R is involved, in addition, in physiological mechanisms other than those that engage PKCβII. Likewise, PKCβII–positive neurons which are not AChE-R-enriched may participate in physiological mechanisms that depend on other, AChE-R-independent PKCβII activities.

Combinatorial aspects of stress-induced proteins. PKCβII and RACK1 are readily available in many neurons. However, their previously unrecognized mobilization into densely packed clusters under stress, compatible with the known intracellular mobility of PKCβII localization, may rapidly change their function.

PKCβII/AChE-R-filled neurons, likely belong to neural circuitries with particular combinations of transcription and splicing factors, the functioning of which depend on intracellular PKCβII-mediated signal transduction. AChE-R/RACK1/PKCβII complex formation may therefore affect the neuronal distribution of PKCβII in brain development (Gallicano et al., 1997), aging (Battaini et al., 1999) and neurodegeneration (McNamara et al., 1999), all of which involve considerable modulation in AChE-R levels. AChE-R is further present in other RACK1/PKCβII producing tissues, including epithelial, muscle and germ cells (reviewed by Soreq and Seidman, 2001) where its capacity to induce PKCβII-mediated changes should be examined. In hematopoietic progenitor cells, for example, AChE-R exerts myeloid proliferative and growth factor activities, compatible with the role of PKCβII in myeloid differentiation (Kaneki et al., 1999).

The signaling cascades involving AChE-R/RACK1/PKCβII complexes may well be just one thread in a complex network of many pathways transducing stress responses. Also, each of the components of these triple complexes represents one of several options. Thus, AChE-R is one out of three AChE isoforms, each with its own C-terminal peptide and possibly different interactions. Likewise, other PKC isoforms and splice variants may interact with different shuttling proteins, exerting distinct effects on the complex physiological phenomena that follow traumatic experiences. Finally, RACK1 operates as a shuttle among many other proteins. Further screening efforts should shed more light on the potential participants in this interaction.

Further implications: Of particular interest are the implications of our findings for drug responses and exposure to chemicals that modulate cholinergic neurotransmission. In essence, any agent that induces an increase in acetylcholine levels should promote the feedback response leading to AChE-R mRNA accumulation and dendritic translocation (Kaufer et al., 1998a; Meshorer et al., 2002). Such agents include insecticide, e.g. chlorpyrifos Sanchez-Amate et al., 2001), and therapeutic anticholinesterases, e.g. all of the currently approved Alzheimer's disease drugs. Recent studies demonstrate that numerous antidepressants inhibit human AChE, e.g. fluoxine, sertraline and amitriptyline (Muller et al., 2002), and that various antipsychotic drugs induce ACh release, e.g. chloropromazine, clozapine, haloperidol, risperidone and ziprisidone (Ichikawa et al., 2002). It is thus tempting to speculate that at least some of the physiological effectiveness (Duman et al., 1999), therapeutic value and/or attraction to the caretaker of these agents is due to their capacity to shift the conflict behavior balance from the excitatory flight pattern to the inhibitory freeze-like behavior. In a reciprocal extension of this concept, it would be intriguing to test whether patients with PTSD, with reported tendency toward exaggerated inhibitory behavior (Newport and Nemeroff, 2000),

display higher blood AChE-R levels than those observed in individuals who successfully recover from similarly acute traumatic experiences.

In conclusion, the intracellular interaction of the stress-induced AChE-R variant with RACK1 and PKCβII adds a new dimension to our understanding of the interrelationship between cholinergic gene expression and the complex phenotype of conflict behavior.

Tetracycline-inducible antisense and ribozyme suppression of acetylcholinesterase gene expression in transfected cells and transgenic mice

Summary
Tetracycline-inducible constructs for endogenous expression of an antisense and a ribozyme targeted to exon 6 of the AChE mRNA transcript were transiently or stably expressed in PC12 cells. Over 80% inhibition of AChE expression was obtained in the stably transfected cell lines, indicating leakiness of the tetracycline control. However, additional tetracycline-dependent modulation of these levels, which rose to 50% inhibition of *ACHE* expression in the stably transfected PC12 cells, sufficed to induce impaired NGF-dependent neuronal differentiation. The tetracycline-controlled antisense sequence was further used to create mice with tetracycline-dependent suppression of AChE-R synthesis. Due to the leakiness of the control, these mice display constitutively reduced AChE activities in cortex (but not hippocampus). However, administration of doxycycline further reduces their cortical AChE activity. Moreover, exposure of these mice to bacterial lipopolysaccharide did not lead to increases in plasma AChE-R, unlike in the parental strain, in which such accumulation was clearly evident. Our study has developed *in vitro* and *in vivo* model systems in which the cellular and physiological effects of the stress-induced increases in AChE-R are amenable to experimentation.

Introduction.
Two reciprocal approaches to studying gene function in mammalian cells include over-expression of transfected genes and targeted genomic disruption of the relevant gene. The genomic disruption approach to loss-of-function carries the obvious limitation that it is irreversible. This is particularly problematic with regard to neuronal proteins, considering that terminal differentiation is involved. In order to study the molecular basis of both normal and pathological changes occurring in differentiated neurons, cultured cell models can offer controlled, reversible down-regulation of important neuronal genes. The principal substitute for appropriate neuronal models until now has been pharmacological manipulation of neurotransmitter receptors and ion channels with a growing arsenal of agonists and antagonists. Unfortunately, central nervous system drugs display complex pharmacokinetics, are notoriously non-specific, and often cannot distinguish between specific receptor subtypes or isoforms. The use of antisense oligonucleotides (AS-ONs) and ribozymes (RZs) targeted to specific mRNAs offers a promising approach to overcoming the problem of specificity in the nervous system (reviewed by Soreq and Seidman, 2000). In a novel extension of the AS-ON/RZ approach, we utilized inducible gene expression protocol, the tetracycline-dependent Tet-On approach (Gossen et al., 1995; Schultze et al., 1996), for controlled delivery of AS-ON/RZ RNA targeted against AChE mRNA in mammalian neurons.

Previously, we had found domains on the AChE mRNA that are particularly vulnerable to AS-ON (Grifman et al., 1998) or the RZ degradation *in vitro* (Birikh et al., 1997). In this study we investigated endogenously expressed inducible RZeand AS-ON targeted to these sites on AChE mRNA in cultured cells and in transgenic mice.

Results
Design of an exogenously expressed ribozyme targeted to the synaptic isoform of AChE (AChE-S)
Previously we found several sites on AChE mRNA which are efficiently cleaved by RZs *in vitro*. We attempted to check whether these sites would be efficient targets for RZs *in vivo* as well. We

chose the target site situated in exon 6 of AChE mRNA, which was most efficiently cleaved *in vitro*. Besides, it would provide a specific cleavage of the synaptic isoform mRNA, as two other splice variants contain exon 5, which has a polyadenylation site (Fig. 1A,B). We chose to use endogenously expressed RZ to avoid delivery problems and produce a stable long-lasting inhibition of the target gene. In contrast to the synthetic RZs studied *in vitro*, the endogenous RZ must be imbedded in a longer RNA molecule, however the length of the annealing arms remained, as previously, 7 nt each. Flanking 3' and 5' regions encoded by the expression vector are necessary for the efficient expression and stability of the RNA. Besides, we introduced an additional element into this structure: a stretch of RNA complementary to a part of the 5'-flanking region to form a stem holding the catalytic domain in a loop (Fig. 1C). This approach was suggested previously by others (Lieber and Strauss, 1995) to prevent integration of the RZ into unfavorable secondary structures.

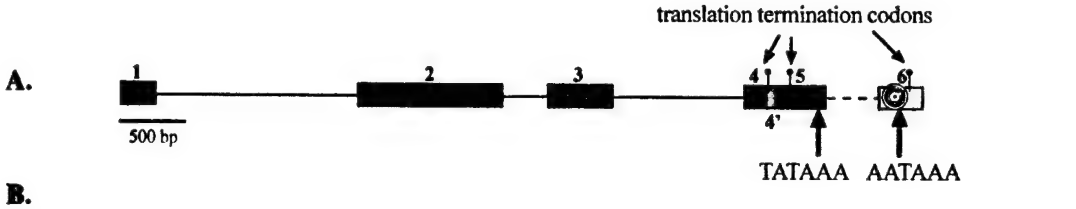

B.

```
Human 1858 cccaaattgctcagcgccaccgacacgctcgacgaggcggagcgccagtggaaggccgag 1917
Rat   1702 cccaaattgctcagcgccaccgatac                                   1761
      568   P  K  L  L  S  A  T  D  T  L  D  E  A  E  R  Q  W  K  A  E

Human 1918 ttccaccgctggagctcctacatggtgcactggaagaaccagttcgaccactacagcaag 1977
Rat   1762                                                            1821
      588   F  H  R  W  S  S  Y  M  V  H  W  K  N  Q  F  D  H  Y  S  K

Human 1978 caggatcgctgctcagacctgtgaccccggcgggacccccatgtcct-ccgctccgcccg 2036
Rat   1822 ctcagacctgtgacccccttgggga-ccccaggtcctgccgccctgcccg            1880
      608   Q  E  R  C  S  D  L  ^^^
```

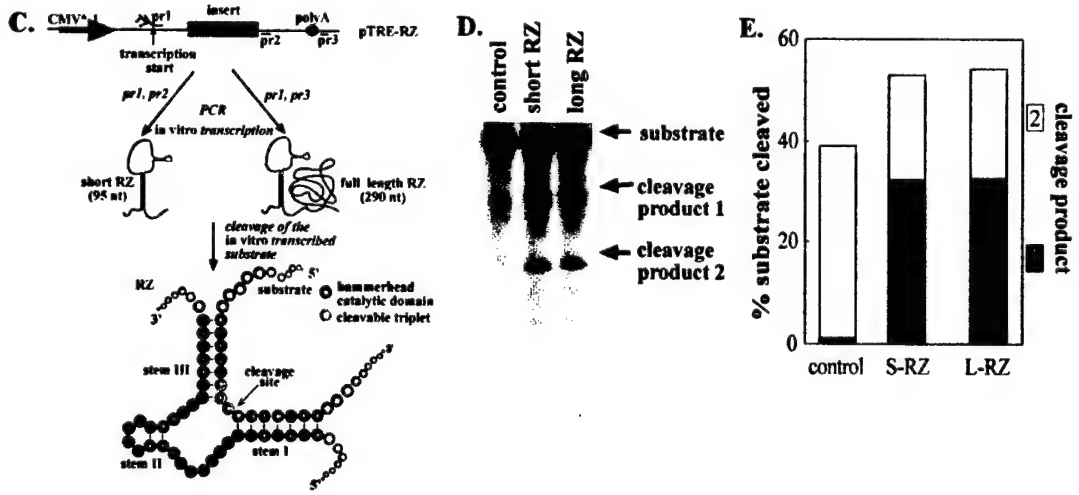

Fig. 1. Strategy. A. Schematic presentation of AChE mRNA splicing isoforms with the target site for the RZ and AS-ON indicated as concentric circles. B. Aligned sequences of the target region from human and rat AChE-S mRNA. Note that the RZ binding site (indicated in yellow) is fully conserved between these species. The murine AS-ON sequence has only two mismatches with rat mRNA on the span of a 100 nt (red). C. Experimental paradigm of testing of the interference of the vector encoded 3'-flanking sequence of the RZ with its activity *in vitro*. D. Autoradiograph of the RZ cleavage reactions. E. Comparison of cleavage efficiencies of the short and long RZs.

In vitro *cleavage of the AChE transcript by the long chain ribozyme.*
In the overall structure of the RZ transcript, the catalytic core embraced in the stem-loop structure is followed by an extended 3' fragment that was suspected of interfering with the correct folding of the RZ. In order to explore this possibility we compared *in vitro* catalytic activity of the full length RZ transcript and its shortened version devoid of the 3' region. For this experiment we generated two PCR fragments with T7 promoter introduced in the upstream primer. These fragments served as a template for *in vitro* transcription to generate the truncated - 95 nt RZ and the full length 290 nt RZ. A 150-nt fragment of AChE mRNA generated by *in vitro* transcription was used as a substrate in this experiment. No difference was observed in cleavage efficiency of the two RZs (Fig. 1D,E), indicating that the 3'-flanking region does not interfere with the RZ activity.

Transient transfection of Tet-On CHO cells with the ribozyme and antisense expressing constructs.
A synthetic 51 bp duplex coding for the catalytic domain and for one strand of the holding stem was cloned into pTRE plasmid (Clontech) behind the minimal CMV promoter which can be activated in the presence of doxycycline by the rtTA protein activator constitutively expressed from a different plasmid (Tet-On system).

We first checked the RZ activity in COS cells, in a transient transfection assay. In parallel we conducted the same experiments with a long chain antisense RNA (100 nt) targeted to the same region of AChE (Fig. 1B), which was successfully used previously to inhibit *ACHE* expression in PC12 cells (Grifman et al., 1998). We recloned this AS-ON construct into the same vector (pTRE) as the RZ. In this experiment we used CHO-Tet-Off cell line (Clontech), which is stably transfected with a pTet-off plasmid. AChE was found not to be expressed in these cells. We co-transfected each of the RZs (or AS-ON or empty vehicle) with the AChE-S cDNA expression construct (Sternfeld et al., 1998) at a ratio of 1:10. AChE activity was determined three days after transfection (Fig. 2). In the induced state (in the absence of doxycycline, as is required in the case of the Tet-Off system) both RZs and the AS-ON showed about 50% inhibition of the AChE activity. In the non-induced state (doxycycline, 10 μg/ml) the AS-ON still inhibited the AChE expression to the same extent, probably due to leakiness of the system. The empty vehicle had no effect on AChE activity in these cells.

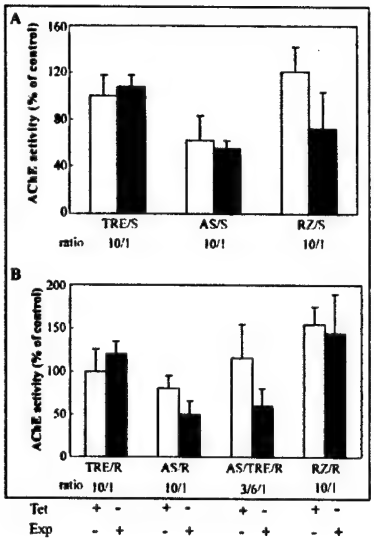

Fig. 2. Ribozyme- and antisense-dependent inhibition of the recombinant AChE expression in CHO cells. *ACHE* gene expression was assessed in CHO-Tet-Off cells under transient transfection conditions. Ratios of the substrate encoding plasmid pCMV-E6 (E6) and the RZ (RZ)/ antisense/vehicle (RZ/AS) (TRE) encoding plasmid was 1/10.

Stably transfected cell lines expressing ribozyme and antisense agents under Tet-On control

Our next task was to establish cell lines of neuronal origin with inducible inhibition of AChE expression. We purchased the PC12-Tet-ON cell line from Clontech (the rat neuroendocrine phaeochromocytoma (PC12) cells stably transfected with a pTet-On plasmid). This cell line was stably transfected with the above AS and RZ expressing constructs. In order to find colonies most responsive to doxycycline, 50 colonies from each transfection were trypsinized and divided into 3 wells of equal cell density. One of the wells was for the stock culture, and the other two for further AChE activity measurements. In one of the "activity" wells, cells were grown in the presence of doxycycline (induced state). After four days, AChE activity was measured, and several cell lines with higher differences between the induced and non-induced state were selected for more thorough investigation. From these cell lines we selected two of the RZ and two of the AS-ON lines showing about 50% lower AChE level in the induced state as compared to the noninduced. However, when compared to the non-transfected PC12-TetON cells, the overall AChE level was greatly reduced, indicating that the RZ/AS expression control was leaky. Interestingly, the overall inhibition of AChE expression by the RZ was even greater, than that by the AS-ON.

To test which isoforms of the AChE protein were suppressed, homogenates prepared from the AS expressing cell lines were western-blotted with antibodies targeted to the core of the AChE, AChE-C, which detects all isoforms, or to the C-ternimal peptide of the stress-associated isoform AChE-R, unique for this isoform. As expected, the overall amount of protein was reduced. AChE-R immunolabeling was up-regulated in the transfected cells (Fig. 3B), probably due to a feedback response. This suggests selective suppression of the AChE-S mRNA transcript.

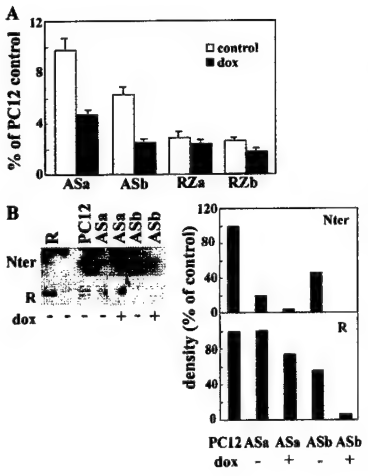

Fig. 3A. Conditional expression A. RZ- and AS-ON-mediated inhibition of endogenous AChE expression. Inhibition was observed in PC12-Tet-on cell lines stably transfected with AS-ON/RZ constructs. Two independent cell lines for each construct are shown. The AChE activity is depicted as percent of the control PC12-Tet-on activity. Note that significant doxycycline-induced inhibition is observed in addition to basal doxycycline independent inhibition, apparently due to the leakiness of the AS transcription. B. Conditional suppression of distinct AChE variants. Immunoblot analysis of the homogenates of PC12-Tet-On cell lines stably transfected with the AS-ON constructs. Cell lines were grown in the presence of doxycycline (+ dox) or in the absence (- dox), equal amounts of total cellular protein was loaded in each well. The top panel represents immunoblotting with isofrm-nonspecific antibody (AChE-Nter), and the bottom panel represents the reaction with stress-isoform-specific antibody (AChE-R). Note that total amount of the immune-positive AChE protein is reduced in AS-expressing cell lines.

NGF-induced neurite outgrowth in PC12 cells is highly sensitive to the reduced AChE level.
It has been previously reported that 80% inhibition of *ACHE* gene expression abolishes the NGF-induced outgrowth of neuronal processes (Grifman et al., 1998). NGF-induced neuronal differentiation was therefore tested in the AS and RZ expressing cell lines. The AS cell line characterized by AChE level (under tetracycline treatment) of 50% of untreated cells presented largely impaired processes outgrowth, although the morphology of the non-differentiated cells remained typical for PC12 cells (Fig. 4). In contrast, RZ cell lines (over 80% inhibition) exhibited fibroblast like shape of the cells, compatible with the report of Grifman et.al (1998), and failed to send neurites upon NGF treatment, indicating that this process is highly dependent on AChE levels.

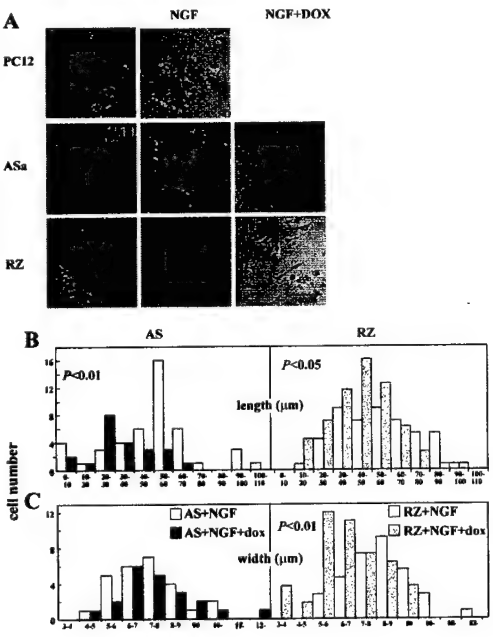

Fig. 4. NGF-induced differentiation of parent and AS/RZ cell lines. A. Three days after NGF treatment, transfected cell lines extended abnormally-shaped processes in response to NGF. Lower panels: population analysis. AS expression primarily reduced NGF-induced process elongation (B, $P < 0.01$) but did not change process width (B). In contrast, RZ expression reduced process length (B, $P < 0.05$) and decreased process width (C, $P < 0.01$).

Conditional in vivo *suppression of AChE-R overproduction under stress of an endotoxin.*
Binary transgenic mice were created that express the Tet-On or the AS-*ACHE* agents. Mating of homozygous mice from the two lines created animals expressing both transgenes. Mice of the parent FVB/N strain served as controls. Animals were offered doxycycline in their dirinking water (2 mg/ml) for 6 consecutive days and were then injected with 50 µg/Kg *E. coli* lipopolysaccharide (LPS) to induce endotoxic stress. Plama samples removed 24 hr post-treatment were subjected to non-denaturing polyacrylamide gel electrophoresis and blotting onto nylon membranes. Parallel membranes were subjected to immunolabeling with anti-AChE-R antibodies or to cytochemical staining of AChE activity (Fig. 5). Plasma samples from AChE-R transgenic mice with constitutive AChE-R overexpression served as controls.

Mice of the parent strain, but not AS-Tet-On mice, presented massive increases of rapidly migrating immunopositive AChE-R in response to LPS injection (Fig. 5A). Activity staining showed non-suppressed increases in enzyme migrating as AChE-E dimers, which appeared in both control and AS-Tet-On mice. This suggested that the tetracycline controlled AS-ON was selectively effective against AChE-R overproduction under stress.

Conditional AChE suppression is effective in multiple organs.
The tissue specificity of AS-Tet-On expression was tested in biochemical assays. Plasma samples displayed significant (Student's t test, $P < 0.05$) suppression of AChE activities following doxycycline treatment of Tet-AS mice, as compared to similarly treated mice of the parent strain (Fig. 5A). Intestinal homogenates presented lower AChE activity, even in untreated Tet-AS mice, as compared to controls (which were insensitive to doxycycline treatment, data not shown). Doxycycline treatment, further, reduced intestinal enzyme activity, suggesting both leakiness and tetracycline sensitivity of the suppression activity (Fig. 5B). A similar pattern was observed in cortical homogenates, with yet higher significance (Fig. 5C). In contrast, there was no apparent change in hippocampal homogenates (Fig. 5D).

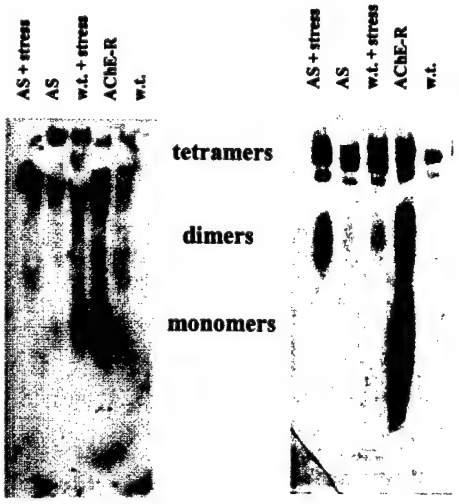

Fig. 5. Native PAGE of transgenic and w.t. mice with and without induction of endotoxic stress.
A. Immunolabeling with anti-AChE-R antibody. B. cytochemical staining for AChE activity (left to right) Tet-On/AS mouse after doxycycline administration and endotoxic stress induction (AS stress), Tet-On/AS mouse after doxyclycine administration without stress induction (AS), wild type CB6 mouse after endotoxic stress induction (w.t. + stress), mouse from a separate transgenic line which over-expresses AChE-R (AChE-R), control; – wild type mouse that was not stressed (w.t.).

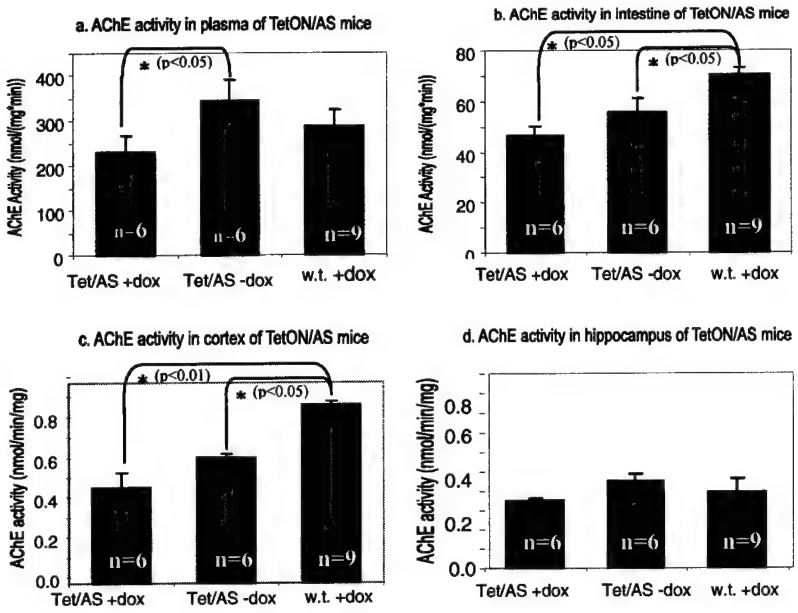

Fig. 6. AChE activity in dissected samples of cortex (a), plasma (b), intestine (c) cortex, and (d) hippocampus from compound transgenic TetON/AS mice who underwent activation of the AS-ON gene by doxycycline administration (Tet/AS+dox), compound TetON/AS mice that were not administered doxycycline (Tet/AS-dox), and control mice that were administered doxycycline (w.t.+dox).

Discussion

We attempted to create *in vitro* and *in vivo* model systems in PC12 cells and transgenic mice with inducible inhibition of expression of specific AChE isoforms. For this purpose we combined AS-ON or RZ mediated gene inhibition approach with an inducible tetracycline-controlled promoter system.

In the original form of this system (Tet-Off), the tet-repressor (rT) was genetically coupled to the HSV-VP16 transcription activating domain and placed under the control of a constitutive basal promoter to generate the tet-controlled transactivator protein (tTA). In the absence of tetracycline, this protein would bind to the minimal CMV promoter provided with the tet operator sequence and activate target gene expression. The expression level of the target gene in this system could be modulated within orders of magnitude by the varying of the tetracycline concentration (Gossen and Bujard, 1992). The obvious drawback of this system is that on the animal model one must continue to feed the animals with the antibiotic to have the gene of interest remain silent. A new generation of the tetracycline controlled systems, which we used in our study is based on a mutant "reverse" tTA (rtTA), whose activation of transcription is dependent on the presence, rather than the absence, of tetracycline ("Tet-On" system). In this system the expression level of the target gene in the presence of a tetracycline derivative doxycycline (1 μg/ml) was reported to be induced to a level of up to 1000-fold over the background (Gossen et al., 1995).

There have been reports on using RZs expressed in a tetracycline controlled system (Wirth et al., 2002; Thybusch-Bernhardt et al. 2001; Thomas et al., 2001; and others). All but one of them used the Tet-Off system and reached 40-70% inhibition of the target gene in the RZ-induced state. At the same time the background inhibition, where tested, was reasonably low. However, in the paper by Thomas and coauthors, where the Tet-On system was used, a very substantial leakiness was observed. In our study two independent stably transfected cell lines showed more than 80% inhibition in the induced state and only a slightly lower inhibition in the noninduced state,

indicating that this RZ efficiently operates even at low expression levels. It also highlights the fact that basal leakiness of the system is especially critical in the case of the RZ or AS-ON expression, because on the one hand they might efficiently work at very low concentrations, on the other hand once the concentration is well above the K_m it reaches the saturation it terms of activity. Add to this the feedback response, which was reported for AChE expression inhibition, and the RZ might work even more efficiently at lower concentrations, then at high.

The above considerations might explain the seemingly contradictory results obtained with the transient and stable transfection. Under transient transfection conditions, where the expression level of the RZ and AS-ON should be higher, the percent inhibition is lower. This might well be, because the RZ level reached the saturation, whereas it must cleave a much higher level of the AChE mRNA. Thus, we developed an endogenously expressed RZ, which can efficiently inhibit AChE expression even at low concentrations. However, modulation of its activity using tetracycline-controlled expression system proved to be difficult, apparently due to the catalytic nature of the RZ, complex expression control of the AChE gene and leakiness of the Tet-On system.

The physiological effectiveness of the AS and RZ agents was tested by measuring the length and width of PC12-indkuced neurite outgrowth. The AS sequence predictably suppressed neurite lengthening, but the RZ agent suppressed both length and width, compatible with its enhanced effectiveness. *In vivo*, the AS but not RZ agent appeared effective. Constitutive suppression levels were observed in the brain and intestine, and prevention of plasma AChE-R accumulation under endotoxin stress suggested conditional efficacy of the transgenic system. Future studies will address the effects of this AChE-R accumulation on mammalian multi-tissue responses to various stresses.

Alternative splicing and neuritic mRNA translocation under long-term neuronal hypersensitivity

Summary
To explore neuronal mechanisms underlying long-term consequences of stress, we studied stress-induced changes in the neuritic translocation of acetylcholinesterase (AChE) splice variants. Under normal conditions, we found the synaptic AChE-S mRNA and protein in neurites. Corticosterone, anticholinesterases, and forced swim, each facilitated a rapid (minutes), yet long-lasting (weeks), shift from AChE-S to the normally rare AChE-R mRNA, promoted AChE-R mRNA translocation into neurites, and induced enzyme secretion. Weeks after stress, electrophysiological measurements in hippocampus slices displayed apparently normal evoked synaptic responses but extreme hypersensitivity to both anticholinesterases and atropine. Our findings suggest that neuronal hypersensitivity under stress involves neuritic replacement of AChE-S with AChE-R.

Introduction
To explore neuronal mechanisms underlying long-term consequences of stress, we studied stress-induced changes in the neuritic translocation of acetylcholinesterase (AChE) splice variants. Under normal conditions, we found the synaptic AChE-S mRNA and protein in neurites. Corticosterone, anticholinesterases, and forced swim, each facilitated a rapid (minutes), yet long-lasting (weeks), shift from AChE-S to the normally rare AChE-R mRNA, promoted AChE-R mRNA translocation into neurites, and induced enzyme secretion. Weeks after stress, electrophysiological measurements in hippocampus slices displayed apparently normal evoked synaptic responses but extreme hypersensitivity to both anticholinesterases and atropine. Our findings suggest that neuronal hypersensitivity under stress involves neuritic replacement of AChE-S with AChE-R.

Traumatic stress is often followed by long-term pathological changes (McEwen, 1999; Sapolsky t al., 2000). In humans, extreme cases of such changes are clinically recognized as posttraumatic stress disorder (PTSD) (Mezey and Robbins, 2001). Although the immediate response to acute stressful insults has been extensively studied, the molecular mechanisms leading to the long-term neuronal hypersensitivity that is characteristic of PTSD are yet unknown. Stimulus-induced changes in alternative splicing have recently emerged as a major mechanism of neuronal adaptation to stress, contributing to the versatility and complexity of the expression patterns of the human genome (McCormick et al., 2000; Xie and McCobb, 1998; Daoud et al., 1999). Another stimulus-induced post-transcriptional process is dendritic mRNA translocation, which has been described for several transcripts (Davis et al., 1987; Foster and Brown, 1996; Steward et al., 1998; Kang and Schuman, 1996; Bailey et al, 1996; Stweard and Schuman, 2001). Because psychological, physical, and chemical stressors all cause neuronal activation and hyperexcitation, dendritic translocation of specific target mRNAs may follow.

Results
Acetylcholinesterase (AChE) modulations provide an appropriate case study for exploring long-term stress effects. Chemical, psychological, and physical stresses all shift splicing from the primary mRNA product that encodes the synaptic membrane AChE-S multimeric protein to the normally rare "readthrough" AChE-R transcript, which yields soluble monomers (Soreq and Seidman, 2001). We thus examined neuronal distributions of the two splice variants, which have characteristic 3' regions (Fig. 1A). A comprehensive search of the NCBI GenBank

and EST databases revealed several AChE-S mRNAs but only a single AChE-R mRNA of rodent brain origin (GenBank accession number X70141), attesting to the scarcity and/or instability of neuronal AChE-R mRNA under normal conditions. To study changes in gene expression at the subcellular level, we used double-label fluorescence *in situ* hybridization (FISH) of specific AChE mRNA splice variants and confocal microscope image analysis.

FISH detection efficiencies likely depend on probe sequences, but subcellular distributions can be reliably compared for single transcripts in different cells and conditions. Cultured PC12 cells (Galyam et al., 2001), primary cultures of mouse cerebellar neurons (Schramm et al., 1990), and pyramidal neurons in paraffin-embedded sections of the prefrontal cortex (Kaufer et al., 1998a) all displayed a larger fraction of AChE-S mRNA transcripts in neuronal processes than of AChE-R mRNA (Fig. 1, B through D). Also, both cell types displayed nuclear localization of AChE-R but not of AChE-S mRNA (Fig. 1, B and C). To test whether labeling properties prejudiced this conclusion, we reversed the fluorophores on the two probes (Fig. 1, B and C). In paraffin-embedded brain sections from naïve mice, cortical pyramidal neurons presented dispersed AChE-S mRNA throughout the processes, while AChE-R mRNA was localized to the cell body. In addition, the perikaryal cytoplasm exhibited punctated concentrations of AChE-R mRNA alternating with double-labeled regions, whereas neurites had AChE-S mRNA with foci of both transcripts (Fig. 1D). The neurite contents of cultured PC12 cells and developing cerebellar neurons, also known to express ample AChE (Soreq et al., 1984), and of prefrontal cortex neurons *in vivo* were 22 ± 3, 28 ± 4 and $28 \pm 7\%$, respectively, for AChE-S mRNA but only 10 ± 2, 7 ± 2 and $11 \pm 6\%$ for AChE-R mRNA ($P < 0.05$, two-tailed Student's *t*-test). AChE-S mRNA, thus, preferentially localized in neurites (except under stress, see Fig. 1E, below).

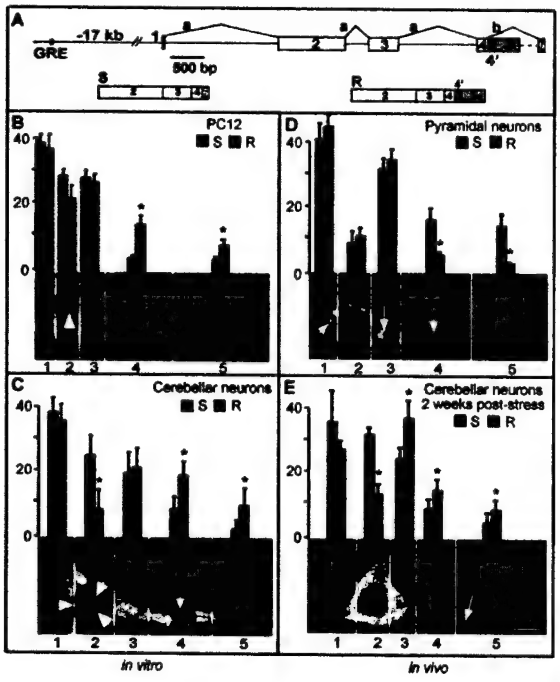

Fig. 1. Variant-specific subcellular distribution of AChE mRNAs. (A) Alternative splicing. Shown are the distal enhancer glucocorticoid response element (GRE) and the mouse *ACHE* gene (top), as well as AChE-S mRNA (S) and AChE-R mRNA (R). Linkage of exons 2, 3, and 4 is common to both variants (a). The R transcript includes at its 3' terminus pseudointron 4 (green) and exon 5; option b yields the S transcript by connecting exon 4 to 6 (red). (B through E). Localization of the S and R transcripts *in vitro* and *in vivo*. Shown are percentages ± SD of FISH signals for the S and R transcripts (each totaling 100%) in three parts of the perikaryon and two neurite areas of 10 PC12 cells (B), cultured primary cerebellar neurons (C), pyramidal neurons from a paraffin-embedded slice of the prefrontal cortex (D), and cerebellar neurons from an embedded brain slice of a mouse that had been stressed for four consecutive days (2[a] 4 min forced swim), and sacrificed 2 weeks later (E). In control mice (D), the fraction of AChE-R mRNA in segments 4+5 was $9 \pm 2\%$ in both cortical and cerebellar neurons; for poststress mice, it was $24 \pm 7\%$ (E) ($P < 0.05$). Note nuclear labeling of the R transcript in

cultured cerebellar neurons (arrowheads) and the punctated pattern of transcript accumulation in vivo [arrows in (D) and (E)]. Asterisks indicate columns with significant differences between AChE-S and AChE-R mRNAs ($P < 0.05$).

The human *ACHE* gene includes a glucocorticoid response element (GRE) about 17 kb upstream from the transcription initiation site (Fig. 1A). In humans, a deletion adjacent to the GRE causes constitutive overexpression and anti-AChE hypersensitivity (Shapira et al., 2000), which suggests a physiologically significant role for glucocorticoids in regulating both neuronal *ACHE* gene expression and anticholinesterase hypersensitivity. We therefore compared PC12 cells treated for 6 hours with corticosterone (10 μM, 0.1% ethanol) to control cells (0.1% ethanol). Twenty-four hours after treatment, catalytic activity against acetylthiocholine rose by 25 ± 14% ($P < 0.05$) in PC12 cells. Corticosterone, further, increased by 30 to 50% the levels of both splice variants within 24 hours ($P < 0.05$) (Fig. 2, A through H). However, the AChE-S mRNA-labeled area remained essentially unchanged under control conditions (distance from nuclear border to limit of mRNA labeling = 37 ± 13 μm) or corticosterone (34 ± 13 μm). In contrast, AChE-R mRNA labeling extended a smaller distance from the nucleus, 25 ± 9 μm under control conditions, increasing to 33 ± 17 μm under corticosterone ($P < 0.05$).

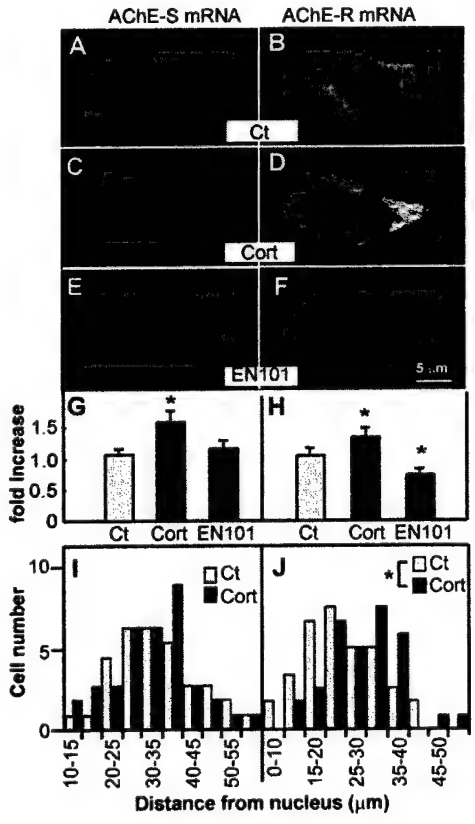

Fig. 2. Corticosterone induction and antisense suppression of AChE mRNA in PC12 cells. Shown are confocal micrographs (A through F), average labeling intensities (G and H) and distributions of distances from the nucleus to the cell border (I and J) of the S (red) and R (green) transcripts in PC12 cells ($n = 40$) under control conditions [(A) and (B)], or after 3 hours in 10 μM corticosterone [(C) and (D)] or 1.5 nM EN101 [(E) and (F)]. Asterisks indicate columns with significant differences from controls ($P < 0.05$). Panels (I) and (J) present the numbers of cells that contain AChE-S or AChE-R mRNA versus their maximum distance from the nucleus.

Three-hour incubation of PC12 cells with 1.5 nM EN101, an antisense oligonucleotide that induces preferential degradation of AChE-R mRNA (Galyam et al., 2001), affected the selective, yet limited, suppression of AChE-R mRNA (30 ± 8%, $P < 0.05$), but left unchanged AChE-S mRNA levels (Fig. 2, E through H). An inversely oriented sequence, INV101, affected neither the AChE-R mRNA level nor its distribution in PC12 cells, attesting to the sequence specificity of the antisense effect. The labeled area remained unchanged either with

AChE-S or AChE-R cRNA probes, following EN101 treatment, suggesting full EN101 accessibility to the cell body (Fig. 2, I and J).

To test whether EN101 is effective similarly in neurites and perikaryal subcellular sites, we employed cerebellar neurons in primary culture. DIG labeling of AChE-S mRNA was not affected differently by EN101 and INV101, in either cell body or neurites. In contrast, EN101 reduced AChE-R mRNA labeling in the cell body of cerebellar neurons in culture, down to almost 50% of its level in INV101-treated controls (Fig. 3). This suppression was completely restricted to the perikaryon, with no difference observed for neuritic AChE-R mRNA in antisense-treated cerebellar neurons.

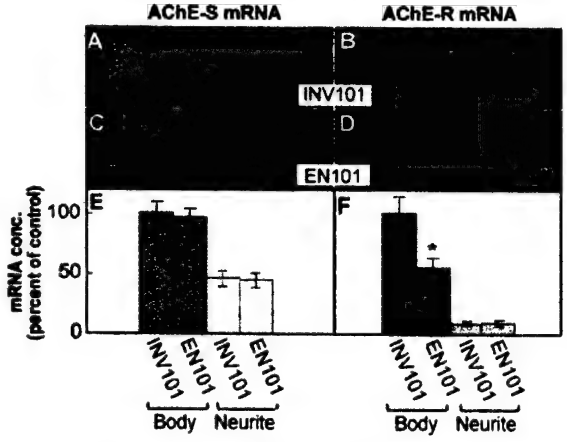

Fig. 3. Antisense suppression in cerebellar neurons is limited to perikaryal AChE-R mRNA. Fluorescence *in situ* hybridization using 50-mer 5′-biotinylated cRNA probes specific for AChE-S (**A** and **C**) and AChE-R (**B** and **D**) mRNAs, was performed on cerebellar cultured neurons. Cells were treated for 3 hours with an antisense oligonucleotide (EN101, 5′-CTGCAATATTTTCTTGCACC-3′, 2 nM) targeted against exon 2 of AChE. The inversely-oriented oligonucleotide, INV101, was used as control. Detection was carried out using Cy2 (green) or Cy3 (red) streptavidin conjugates. Shown are representative compound confocal micrographs (A through D) and average labeling intensities (E and F) for 10 cells in each group. INV101-treated cell body of was taken to be 100%. AChE-S mRNA was not affected by EN101 administration in the cell body or neurites. AChE-R mRNA was markedly reduced in the cell body, and not affected in the neurites. The asterisk indicates statistically significant difference from the control ($P < 0.05$, 2-tailed Student's t-test).

Cytochemical staining of catalytically active AChE (Kaufer et al., 1998a) revealed intensified AChE activity in the cell bodies of corticosterone-treated cultured cerebellar neurons (Fig. 4, A and C). This suggested that the overexpressed AChE mRNA transcripts were translated to yield active enzyme. Immunocytochemical staining with an antibody targeted against recombinant AChE-S presented apparently similar staining patterns in neurites of control and corticosterone-treated cultured cerebellar neurons (Fig. 4, B and D). This indicated that neurites under stress secrete the hormone-induced soluble AChE-R, with no increase in the synaptic membrane-associated AChE-S.

We used FISH detection of the intracellular AChE-R mRNA transcript to assess the expression levels of this variant in vivo. Dorsal hippocampus neurons of naïve FVB/N mice express extremely low levels of AChE-R mRNA under normal conditions (Fig. 4E). Two days following the stress of surgical implantation of a microdialysis cannula (Erb et al., 2001), the range of neurite labeling increased from 2.0 ± 0.3 to 5.1 ± 1.0 μm from the nucleus (Fig. 4G, $P < 0.0005$). Injection through the cannula of the AChE inhibitor neostigmine (125 nmol) resulted in a more extensive translocation of AChE-R mRNA within 25 min (to 8.5 ± 1.2 μm from the nucleus, Fig. 4I). In neurites of untreated hypersensitive AChE-S transgenic mice, AChE-R mRNA reached greater distances from the nucleus (9 ± 1 μm) than those of their

strain-matched controls (Fig. 4F, $P < 0.0005$). Sham injection failed to further increase transport (10 ± 1 μm, Fig. 4H), but AChE-R mRNA reached dendrite distances of 15 ± 2 μm under neostigmine (Fig. 4J), significantly longer than either similarly treated nontransgenic animals, or sham injected transgenics (in both cases $P < 0.0005$; Fig. 4, K and L).

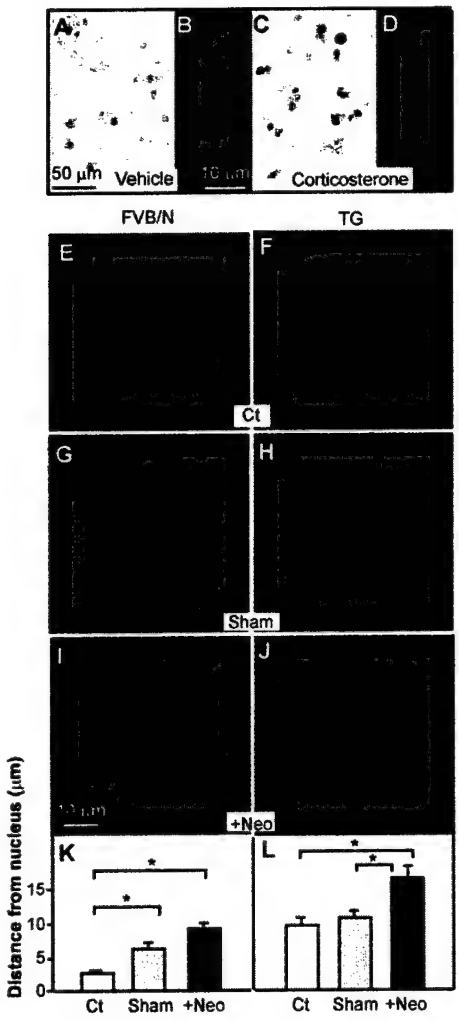

Fig. 4. Increased AChE-R expression and dendritic translocation under hormone, genetic background, sham injection, and chemical stressors. (A through D) Shown are primary cerebellar neurons stained for AChE activity under vehicle treatment [(A), 0.1% ethanol] or corticosterone [(C), 10 μM, 6 hours]. (B) and (D) Higher magnification immunocytochemical AChE-S labeling. (E through J) Confocal field images of hippocampal CA1 neurons from normal FVB/N mice [(E), (G), and (I)] and transgenic animals overexpressing human AChE [(F), (H), and (J)], under control conditions [(E) and (F)], 2 days following cannula implantation and perfusion with artificial cerebrospinal fluid [(G) and (H)], or following injection through this probe of 125 nmol neostigmine [(I) and (J)]. (K and L) Neuritic translocation of detectable AChE-R mRNA labeling (in μm from nucleus) for 30 neurons from at least two animals in each group. Significant differences from noted values are starred ($P < 0.0005$).

Reported rates of mRNA dendrite transport range from 10 to 20 $\mu m \cdot hour^{-1}$ (Davis et al., 1990) to 300 to 360 $\mu m \cdot hour^{-1}$ (Wallace et al., 1998). In our study, assuming a constant rate, AChE-R mRNA traveled a minimum of 8 ± 5 $\mu m \cdot hour^{-1}$ in anticholinesterase-treated FVB/N mice, which increased to 14 ± 7 $\mu m \cdot hour^{-1}$ in similarly treated hAChE-S transgenic mice ($P < 0.0005$). This rate is consistent with the lower range estimate. The stability of AChE-R mRNA in the face of an antisense agent predicted long-lasting poststress neuritic presence of this transcript in vivo. To test this, we subjected FVB/N mice to 4 consecutive days of forced swim (two 4-min sessions per day). In naïve mice, cerebellar granule neuron processes were loaded with $28 \pm 12\%$ of the cellular AChE-S mRNA but only $9 \pm 2\%$ of the AChE-R mRNA content (Fig. 1C). Two weeks post-stress, a considerably larger fraction ($24 \pm 7\%$) of the stress-increased amount of AChE-R mRNA translocated into neurites and displayed patches of concentrated AChE-R mRNA in both the cell bodies and processes (Fig. 1E). Thus, both the absolute levels and the neurite fraction of AChE-R mRNA increased considerably.

In nontransgenic mice, hippocampal AChE-R mRNA is generally limited to the granular layer (Kaufer et al., 1998a). AChE-R mRNA levels remained considerably higher than baseline 4 weeks after 4 consecutive days of forced swim or 3-day exposure to very low diisopropylfluorophosphonate (DFP) levels (0.1 $mg \cdot kg^{-1} \cdot day^{-1}$, i.p., $LD_{50} = 2.5\ mg \cdot kg^{-1}$). Prestressed or preexposed animals presented high-intensity labeling in the hippocampus CA1 region, dentate gyrus, and dendrite layer (Fig. 5, A through F), predicting modified composition of neuritic AChE variants either after stress or low-level exposure to an anticholinesterase.

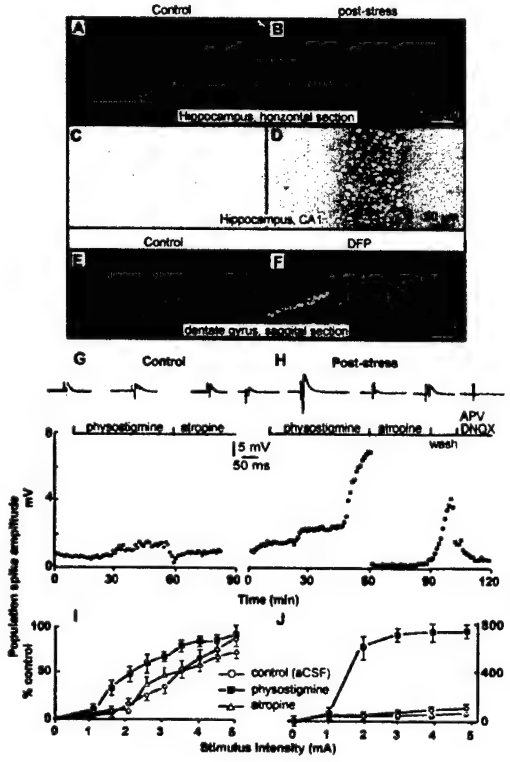

Fig. 5. Hypersensitivity in hippocampal slices under long-lasting overexpression of AChE-R mRNA. (A through F) Neuronal overexpression. Shown is a comparison of hippocampal slices from control mice to those stressed 1 month earlier by forced swim [(A) to (D), Fast Red colorimetry] or exposure to DFP [0.1 mg kg^{-1}, three consecutive daily injections, (E) and (F), ELF fluorimetry]. (G through J) Cholinergic hypersensitivity. Shown are extracellular recordings (average ± SD) on the CA1 areas of two to four hippocampus slices from each of three mice, in response to stratum oriens stimulation of slices from controls [(G) and (I)] or 1 month following consecutive daily stress sessions [(H) and (J)]. Above treatment descriptions are shown representative voltage traces. Stimulations (20 s each) were delivered using a bipolar electrode (10 μm insulated tungsten wires, 200 μm apart) placed in the Schaffer collaterals. Applied drug concentrations were: physostigmine, 10 μM; atropine, 10 μM; APV, 50 μM; DNQX, 20 μM

Released neuronal acetylcholine binds to both pre- and postsynaptic receptors and is assumed to serve as a modulatory neurotransmitter and set the response level of the neuronal network to incoming stimuli (Gray et al., 1996). This involves electrophysiological mechanisms that are only partly understood, but depend on synaptic hydrolysis of acetylcholine by AChE-S. To test whether the supplementation of neuritic AChE-S with AChE-R compromises the capacity to confront intensified cholinergic stimuli, we stimulated the CA2/CA3 region of the stratum oriens, a region rich in cholinergic fibers, and recorded population field potentials (pfps), which sum the responses of a large number of neurons, in the cell body layer of the CA1 region (Kaufer et al., 1998a). Recording in hippocampus slices (Friedman et al., 1998) was performed 1 month after exposure to stress or in slices from naïve animals. The anticholinesterase physostigmine induced an increase (42 ± 15%, $P < 0.05$) in the amplitude of the evoked population spike response of naïve mice (Fig. 5, G and I). This response was 70% reversible following the addition of atropine to the bathing solution, indicating major action through muscarinic receptors. In nonstimulated slices from animals tested 1 month following 4 days of repeated stress, the mean pfp amplitude was similar to that of nonstimulated controls. However, exposure of slices from stressed mice to physostigmine resulted in a 12-fold larger increase over baseline in stimulation-evoked population spike

amplitudes than that observed in nonstressed animals. Atropine administration reversibly blocked this response by more than 90%, much more effectively than its capacity to block field potentials in the control brain (Fig. 5H versus 4G). The stronger responses to both stimulators and antagonists following stress spanned the entire range of stimulus intensity (Fig. 5, I and J), similar to the hypersensitivity patterns seen in humans as PTSD. As in control mice, the evoked pfp was blocked by the NMDA and AMPA antagonists, aminophosphonopentanoic acid (APV) and dinitroquinoxalinedione (DNQX), respectively, attesting to the glutamatergic, i.e., excitatory, nature of the hypersensitized synapses. Neuronal hypersensitivity has long been known to follow stressful experiences (Antelman et al., 1980), but the mechanisms leading to it remained unknown. Our current findings suggest a role for stimulus-induced AChE-R overexpression and neuritic translocation in this phenomenon.

Discussion

Translocation into neuronal processes presumably depends on *cis*-acting elements and/or secondary structures, primarily within the 3' untranslated region (Wallace et al., 1998; Blichenberg et al., 1999). AChE-R mRNA includes no known neurite-targeting motif; its transport into dendrites may thus be associated with its unique 3' sequence, or with the stress-induced accumulation of many more nascent AChE-R mRNA transcripts. The normally short half-life of AChE-R mRNA, ~4 hours (Chan et al., 1998), also appears to be modified following stress. AChE-R mRNA includes a long U-rich element in the 3'-UTR (positions 13,020 through 13,007 in GenBank accession number AF312033), which may contribute to mRNA destabilization through the binding of *trans*-acting proteins (Guhaniyogi and Brewer, 2001). Although the importance of this element to the stability of AChE-R mRNA remains to be tested, the differential resistance of neurite AChE-R mRNA to antisense oligonucleotide-mediated degradation may reflect low nuclease levels in neurites, especially of ribonuclease H, which targets DNA-RNA hybrids. AChE mRNA had been shown to be stabilized during neuronal differentiation (Luo et al., 1999); our observations suggest that this may be due, at least partially, to AChE-R transcripts being sequestered in neurites.

The weeks-long hypersensitivity of prestressed hippocampus to anticholinesterases attributes a role to the hippocampus in the cholinergic component of post-stress sensitization. The recorded field potentials were sensitive to both cholinergic and glutamatergic antagonists, suggesting a long-term change in the interactions between these two transmitter systems. Cholinergic-glutamatergic interactions have been associated with higher brain functions such as long-term potentiation, memory, and behavior (Aigner et al., 1995), all of which are affected by stress. The hypersensitization may also reflect an involvement of neuritic AChE-R in plasticity, due to its capacity to affect cell-cell and cell-matrix interactions (Soreq and Seidman, 2001).

In conclusion, we find that the stress-induced increases in cholinergic neurotransmission (Imperato et al., 1991) promote a long-term replacement of synaptic membrane AChE-S protein by its soluble AChE-R counterpart. The long-term hypersensitization to repeated stimuli shown by cholinergic brain tracts may be due to this substitution.

Genomic dissection reveals locus response to stress for mammalian acetylcholinesterase

Summary
The mammalian acetylcholinesterase *(ACH*E) locus was investigated using computational predictive methods and experiments of reverse transcription polymerase chain reaction (RT-PCR). Computational analysis identified two genes downstream to *ACH*E, an inversely oriented arsenite resistance gene homologue *(ARS*), and a novel previously unidentified gene *(PIX*), co-oriented with *ACH*E. Experimental evidence shows coregulation of murine *ACHE* and *ARS* following confined swim, indicating coordinated locus response to stress, that is possibly mediated by altered cholinergic neurotransmission.

Introduction
Chromosomal abnormalities involving the *ACHE* locus harboring the gene that codes for the acetylcholine hydrolyzing enzyme, acetylcholinesterase (AChE), are associated with much human pathology. Some of these abnormalities are attributed to chromosomal aberrations involving band 7q22, harboring the human (h)*ACHE* locus (e.g., *hACHE* gene amplification in ovarian carcinoma (Zakut *et al.*, 1990)) and to frequent breakage in various types of leukemias (Johnson and Cotter, 1997). Others appear to involve changes in AChE expression. Increased AChE levels were reported in glioma tumors, as compared with benign astrocytes (Razon *et al.*, 1984), whereas reduced AChE levels were observed in lymphomas (Lampert and Van Noorden, 1996). While it is possible that the noncatalytic proliferative capacities of AChE (reviewed by Soreq and Seidman, 2001) are causally involved in these pathologies, the molecular mechanism(s) underlying such processes are not yet known.

In the central nervous system, abnormally high AChE expression was shown in transgenic mouse models to be associated with long-term structural and functional impairments (Andres *et al.*, 1997; Beeri *et al.*, 1995; Erb *et al.*, 2001; Sternfeld *et al.*, 2000). This suggests long lasting, delayed consequences of AChE accumulation that are most likely associated both with its catalytic and noncatalytic activities. Both psychological stress and exposure to anti-AChEs, such as Alzheimer's disease drugs (reviewed by Soreq and Glick, 1999), induce similarly efficient AChE overproduction (Friedman *et al.*, 1996; Kaufer *et al.*, 1998a; Shapira *et al.*, 2000), demonstrating that this long-lasting impairment is physiologically relevant. Moreover, long-term exposure to organophosphate anti-AChE insecticides increases the risk for non-Hodgkin's lymphomas (Brown *et al.*, 1990), possibly hinting at locus involvement under such environmental exposure as well.

The intricate regulation of the *ACHE* gene in conjunction with the apparent instability of the *ACHE* locus raise interesting questions with regard to the general control over transcription from this locus. Several loci are known where transcriptional activation spans more than one gene, for example, the β-globin locus, which contains a developmentally regulated "switch" in the form of locus control regions (LCRs). These are cis-acting DNA segments that are needed for activation of an entire locus or gene cluster (Hardison *et al.*, 1997). Another such locus, with yet uncharacterized regulation but probably with some degree of coordination in its transcription, is the cholinergic locus. This locus comprises two genes, encoding the vesicular acetylcholine transporter (vAChT) and the choline acetyltransferase gene (ChAT), the former located within an intron of the latter (Eiden, 1998; Mallet *et al.*, 1998). A coordinately regulated locus implies that conditions that activate one gene would also induce expression of adjacent genes in the locus. In the context of the *ACHE* locus, one would expect such candidate genes to be activated during embryonic development (Grisaru *et al.*, 1999; Layer, 1996; Massoulie *et al.*, 1998), under psychological stress in cholinergic neurons

(Kaufer *et al*., 1999) and hematopoietic cells alike (Grisaru *et al*., 2001), and in both brain and intestinal epithelium under exposure to anti-AChEs (Shapira *et al*., 2000). Because neighboring gene(s) may have other biological roles, such activation can have far-reaching implications on additional, yet undefined physiological processes.

To investigate the *ACHE* locus, one should: (a) identify neighboring genes on this locus; (b) characterize the tissue expression profiles of such genes as compared to that of the *ACHE* gene; and (c) test for selective changes in their expression levels under conditions where *ACHE* gene expression is modulated. A later phase, dependent on knowledge of the biological role(s) of the neighboring genes, would enable prediction of the physiological outcome of changes in their expression levels.

On the basis of these arguments, we initiated a search for structural features in the *ACHE* locus that may be responsible for genomic instability. We further tested the expression from this locus; for evaluating the possible consequences of such expression, we combined molecular genetic approaches with searches of genomic databases to explore genes residing on the *hACHE* locus. These analyses identified *hARS*, a gene overexpressed in Chinese hamster cells when those become resistant to the toxin arsenite, and *hPIX*, a cysteine protease homologous gene located between *ARS* and *ACH*E. Here, we report both *hARS* and *hPIX* exon/intron structure and tissue-specific expression patterns, and demonstrate *ARS* co-induction with *ACHE* in the mouse brain under psychological stress. We further discuss these results in relation to arsenite resistance as well as to AChE responses to anti-AChEs.

Methods

Sequence Analyses

Searches for open reading frames (ORFs) in the *hACHE* locus, percentage GC content, repetitive sequences in the *ACHE* upstream sequence, and expression sequence tags (ESTs) derived from this locus were performed using the programs RepeatMasker2 and BLAST. Analysis of putative protein products was performed using the following programs: PSORT (cellular localization prediction), PSSM (protein folding prediction), and Expasy ProtScale (hydrophobicity plots).

cDNA Clones

Deposited cDNAclones were obtained from Genetic Research (Huntsville, AL, U.S.A.), distributors for the IMAGE Consortium and the National Human Genome Research Institute/NIH.

Sequencing of cDNA Clones

DNA sequencing was performed by chromosome walking using an ABI377 automated sequencer (Applied Biosystems Pharmacia, Foster City, CA).

Reverse Transcription PCR (RT-PCR)

Primers were designed using the OLIGO primer design program. Primers for PCR amplification were as follows: for homologous murine *mARS* 50 –AGGTCCCGATATTCC-ACAAT-30 (C) and 50 -CTCTGCCTGAGATCAAGCCA-30 (-); for homologous murine *mPIX* 50 -GTTGCGATGGACTGGATGAC-30 (C) and 50 –CCTCTACACAGCCGATC-CAG-30 (-); for homologous murine actin *mACT* 50 –GAAACAACATACAATTCCATCAT-G AAGTGTGAC-30 (C) and 50 -GGAGCGATAATCTTGATCTTCATGGTGCT-30 (-); primers complementary to exon 2 of murine (m)*ACHE* which is common to all AChE isoforms, as well as kinetic follow-up of PCR products accumulation were as described (Friedman *et al*., 1996).

Animal Experiments

Animal experiments were performed as described elsewhere (Kaufer *et al*., 1998a; Shapira *et al*., 2000). All experiments were approved by the committee for Animal Experimentation at the Institute of Life Sciences.

Potential Molecular Basis for Genomic Instability at the hACHE Locus

RepeatMasker2 analysis of the *hACHE*locus indicates an extremely high prevalence of Alu repeats, nonviral retrotransposons which are part of the family of short interspersed elements (SINEs; Fig. 1(A)).

Thirty-nine of these repeats were identified along 22 kb of *ACHE* upstream sequence. This is a higher density of SINEs than that reported for the hypoxanthine phosphoribosyl transferase gene locus *(HPRT*), considered to be rich in Alu repeats, which contains 49 such repeats in 57 kb (Renwick *et al*., 1997). The presence of so many Alu repeats in a relatively small region is compatible with both a long history of transposition events and unequal crossing-over in this region. In accordance with this hypothesis, the upstream region was found to be markedly lower in its GC content than the *ACHE* gene itself. Taken together, these data provide a possible basis for the instability of the *ACHE* locus.

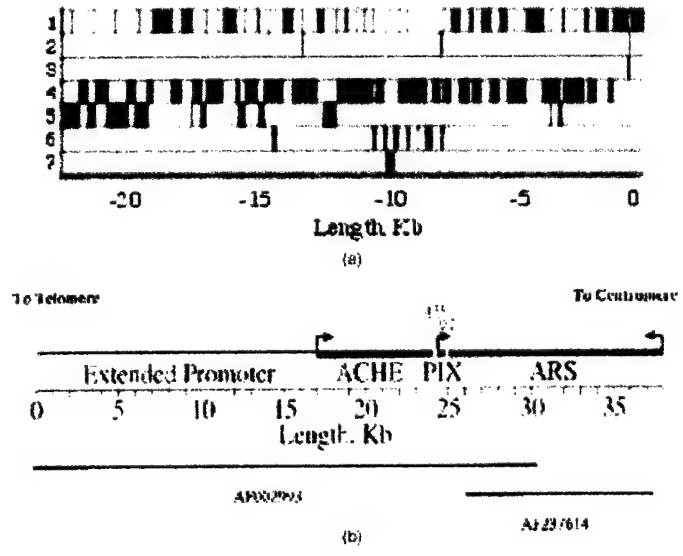

Fig. 1. The mammalian *ACHE* locus. (A) Sequence characteristics in the *ACHE* extended promoter. Presented is a down-to-scale analysis of the *hACHE* extended promoter (22.5 kb), with the transcription start site being at position 0. 1: Repeatless regions, variable repeat elements; 2: Simple sequence DNA; 3: Low complexity sequence; 4: Short interspersed nucleotide elements (SINEs), most of which are Alu repeats; 5: LTRs; 6: Retroviral long interspersed nucleotide elements (LINES); 7: SRP classed SINEs. (B). Map of the Human ACHE Locus. Shown is a drawn to scale physical map of the human acetylcholinesterase locus containing the extended promoter, ACHE, PIX, and ARS. Note the close proximity of the three genes at this locus.

ARS and PIX Identified Downstream to ACHE

One kilobase downstream from *ACHE* we identified a gene that showed conspicuous homology to the Chinese hamster (ch)*ARS2* cDNA, the expression of which is induced in cell cultures resistant to arsenite poisoning (Wang and Rossman, 1993). Briefly, the chARS gene was isolated from a subtraction cDNA library prepared from a cell line of lung origin that was treated with subtoxic concentrations of arsenite and then selected by exposure to very high, normally toxic concentrations of this poison (Wang and Rossman, 1993). c*hARS2* was shown to confer arsenite resistance on cultured cells, demonstrating its functional relevance (Rossman and Wang, 1999). The human gene was named, accordingly, *hAR*S. Further analysis of expressed sequence tag (EST) alignments to the *ACHE* region identified another gene called Potentially Induced eXon or *hPIX*, completely contained within the kilobase of sequence between *hACHE* and *hAR*S.The 7 kb long *hACHE* gene is hence followed by the much shorter 800 bp *hPIX* gene, located only 350 bp downstream in the same orientation as *hACH*E. One hundred base pairs downstream from *hPIX* lies the 13 kb long *hARS* gene,

inversely orientated to both *hPIX* and *hACHE* (Fig. 1B). Genomic PCR amplification of mouse DNA, using primers from the 30 domains of *ARS* and the inversely oriented *ACHE* genes, resulted in the production of a 1.6 kb fragment, confirming similar proximity for these genes in the mouse and human genomes.

Table I. Expression From the 7q22 Locus as Reflected in the EST Database

Tissue origin of EST	Expressed gene *hARS*	Expressed gene *hPIX*	Expressed gene *hACHE*
Brain	++[a]	++[a]	++
B cells	++		(+)[b,c]
Breast	++		
Retina	++		++
Heart	++		+
Colon	++		++
Kidney	++	(+)[b]	++
Skeletal muscle			++
Skin–melanotic melanoma		+	
Placenta	++		
Germ cell tumors			++
Fetal liver and spleen	++		++
Pituitary gland	+		
Fetal lung	+	(+)[b]	++
Cervix	+		
Ovary	+	+	
Uterus	+		
Testis	+		(+)[b]
Prostate	+		
Bone marrow	+		(+)[b]
Bone	+		(+)[b]
Thymus	+		(+)[b]
T cells	+		
Pineal gland			+
Omentum			+
Fibroblasts	+		

group present *ACHE* or *PIX* expression. *c* Very low expression.

Table I. Expression from the 7q22 locus as reflected in the EST database

Note. Shown is a summary of Blasts output obtained by a search against the dbEST, with the AF002993 cosmid as a query sequence and restricting the search to human sequences. Designated are the tissue origins of the different ESTs. *a* Highly-represented tissues (with >3 ESTs of the respective tissue origins). *b* In parentheses are tissues where RT-PCR experiments from our

To discover which tissues express *hACHE*,*hARS*, and *hPIX*, we searched the dbEST. ESTs originating from both *hACHE* and *hARS* mRNA transcripts were found in many different tissues, including both adult (brain, intestine, skeletal muscle, colon, and kidney) and fetal tissues (liver and spleen, lung and heart) (Table I). *hARS* mRNA was considerably more abundant than the other two transcripts; in addition, a variety of alternatively spliced *hARS* mRNA sequences were found in all of the above tissues as well as in B cells, breast tissue, placenta, pituitary gland, fetal lung, cervix, thymus, T cells, and fibroblasts. In contrast, dbEST data reflecting *hPIX* expression were limited to very few tissue types, mostly tumors (brain glioblastoma, skin melanoma, and ovarian carcinoma). RT-PCR of total RNA extracts showed a wider mouse tissue distribution than that indicated by the dbEST. The *mPIX* transcripts were detected in cortex and kidney, with lower level expression in lung, and no transcripts were detected in pancreas (Table I).

In silico comparison of *hARS* ESTs from cDNA libraries of various tissue origins was used to outline its alternative splicing patterns in various tissues (Fig. 2). On the basis of a dbEST Blast search, three brain cDNA clones were ordered (accession numbers R87621, AA077557, and R90838; Genetic Research, Huntsville, AL, U.S.A.) and were fully sequenced to derive the human brain mRNA sequence. Comparison to the cosmid sequence revealed that the 5'-end of the cDNA extended beyond AF002993. Therefore, an adjacent cosmid clone (AF237614, gratefully received from Lap-Chee Tsui, Toronto) containing a partially overlapping insert was sequenced by primer walking. This extended the gene sequence by adding ca. 3 kb to its 50-end (data not shown). The resultant brain *hARS* gene-product shows a 76% identity to the rodent *ARS* gene-product (U41500) as well as 46% homology to a recently deposited *Drosophila* genomic sequence (AAF57281). A comparison of the brain

cDNA sequence with the sequence of a cloned human brain cDNA recently deposited in GenBank (AL096723) identified several differences between the two sequences.

hARS

The AL096723 sequence contained a longer 50-end, and therefore a more up-stream translation start site for the putative protein product. It also included an insert at its 30-end, resulting in an alternative C-terminus for its putative protein product (Fig. 3). These differences may point to the existence of more than one brain mRNA variant for the *hARS* gene. However, the absolute majority of ESTs including the 30 insert in both brain and other tissues points at the sequence lacking it as an exception. The putative translation product of the composite brain *hARS* cDNA sequence is a hydrophilic 791 amino acid protein, which contains a bipartite nuclear localization signal (NLS), KKEDSEKEAKKSSKKRN. This type of NLS was first identified in *Xenopus* nucleoplasmin (Robbins *et al.*, 1991), and has the signature pattern of 2 basic residues, a 10 residue spacer, and another basic region consisting of at least 3 basic residues out of 5 residues (Fig. 3). On the basis of this, the prediction made by the PSORT program, is a 56%chance of this protein being nuclear. Arsenite extrusion by various transporters, or modification by methylases or by glutathione S-transferase (reviewed in Rosen, 1995), predicts the existence of transmembrane domains or homologies to the already known arsenite resistance proteins, respectively. However, the PSORT program could not identify in *hARS* putative transmembrane domains; a hydropathy plot supported the absence of such domains (Fig. 4(A)). *hARS* further lacks resemblance to any known protein or common protein motif, including other arsenite resistance proteins.

hPIX

The identification of *hPIX* from ESTs showed that *hPIX* contains a short TATA-less promoter region, a 50 untranslated region (UTR), and a 30 UTR.The open reading frame for *hPIX* shows a predicted peptide of 227 amino acids encoded by a single exon. Predicted *hPIX* is a soluble, hydrophilic protein of 24.2 kD in weight (Fig. 4(B)). The nucleotide and peptide sequences share homologous sequences in mouse and rat. Murine (m)*PIX*, like *hPIX* is located directly downstream to *mACHE* and encodes a generally neutral (Fig. 4(B)) polypeptide of similar size and composition (*mPIX* is 217aa). Protein homology searches reveal homologous protein sequences in a multitude of organisms *(Drosophila melanogaste*r, *Caenorhabditis elegans*, *Arabidopsis thalania*, *Staphylococcus xylosus*, and *Schizosaccharomyces pombe*) including an additional human peptide sequence, raising the possibility of a conserved family of PIX-like proteins in humans and other organisms. In several organisms (e.g., *Caenorhabditis elegans*), the *PIX* homologous region is linked to an additional protein domain, creating a much longer polypeptide, possibly indicating domain integration producing novel functional members in the *PIX*-like family. Protein sequence analysis indicates that the PIX family of peptides share a low level of sequence homology (36%) with cysteine protease-like enzymes. However, *hPIX* includes within the *hPIX* family homologous regions only two of the three amino acid residues that are required to compose the Cys-His-Asn catalytic triad, and lacks several other highly conserved residues characteristic of cysteine proteases. Homology between *PIX* family members is confined to several small regions, encompassing the cysteine protease catalytic domain and supporting secondary structures. In those PIX family members that are much longer than others, the *hPIX*-like domain, with homology to other family members, is restricted to the last 200 residues. These are preceded by 400 residues which appear to fold into a separate domain, and have an as yet unknown role.

Analysis of the folding properties (PSSM fold recognition server) and composition of the *hPIX* peptide is, at this phase, only indicative. *hPIX* can fold, with a PSSM fold accuracy value of 83%, into a papain-like cysteine protease fold family. Cysteine proteases are notably involved in many normal cellular processes, as well as several pathological phenomena, for example, neuronal apoptosis following spinal cord injury (Ray *et al*., 2001). This family of papain-like cysteine proteases is extensive and includes members with low overt homology to one another, but with two putative residues in distinct conserved sequences separated by a substantial nonconserved region (Fig. 5).

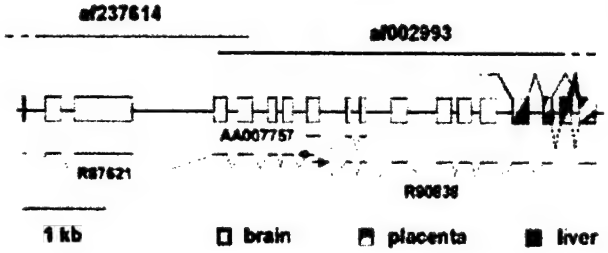

Fig. 2. Alternative splicing in hARS mRNA. Depicted is the drawn-to-scale exon–intron structure of brain hARS cDNA, as derived from the sequenced brain clones. Intronic sequences are shown as thin lines, brain exons as open boxes, and 3-alternative splicing patterns as dashed or full connecting lines, with the alternative exons shaded according to the tissue sources of dbEST clones from which they were derived. The 30 liver alternative splicing pattern is shown as a thick line and a dashed line represents yet missing information referring to the liver splicing pattern in upstream exons. Below this scheme are depicted the brain cDNA clones used to derive this information with the corresponding accession numbers of the original ESTs. As above, thin connecting lines represent spliced sequences that are not found in these cDNA sequences. Note that the 50-30 orientation in this figure is opposite to that of Figs. 1 and 2.

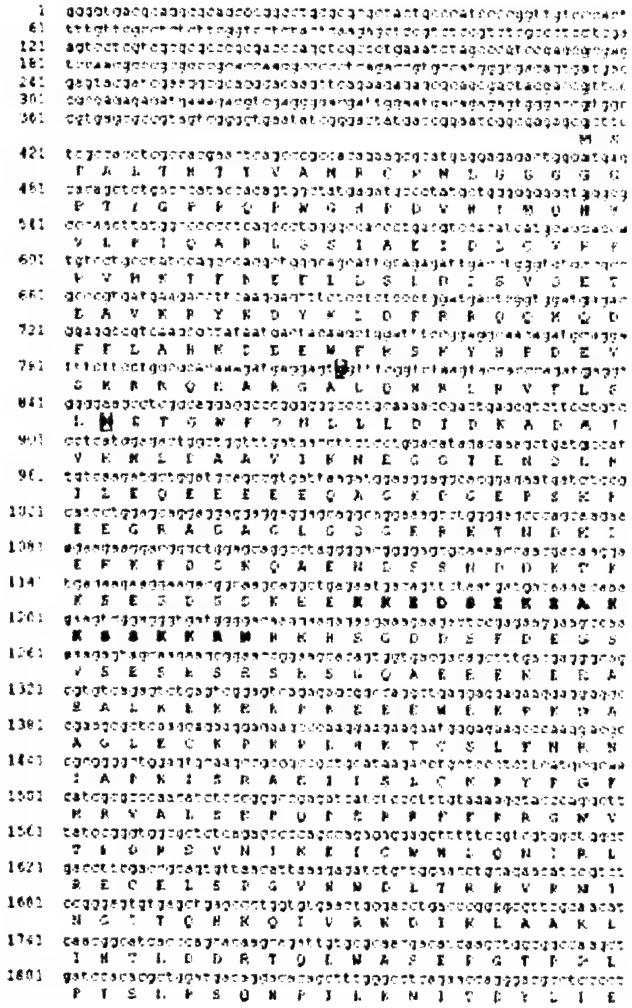

Fig. 3. Brain hARS cDNA sequence and its translation product. Shown is the sequence of the brain cDNA clone (accession number AL096723) and its translation product aligned with the respective codons. Boxed letters indicate the first nucleotide and first methionine of the sequence we obtained from the 3 assembled brain cDNA clones and its translation product, respectively. Bold nucleotides represent an insert existing in AL096723 and most other ESTs compared with our sequence, causing a putative alternative C-terminus. Bold amino acids designate a bipartite nuclear localization signal existing in both predicted proteins. Underlined sequences designate the location of the PCR primers used for quantitative RT-PCR.

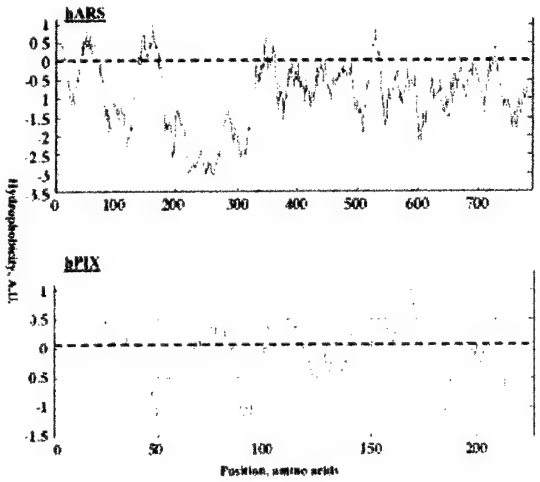

Fig. 4. Hydropathy plot of the hARS (upper) and hPIX (lower) brain gene-products prepared in the Expasy ProtScale web site according to the Kyte and Doolittle algorithm; window size used for analysis was 19 residues. Hydrophobic segments have values above zero in the Y-axis; Areas of the protein with values that are greater than or equal to C 1:8 are possibly in a transmembrane domain. Note that most of the hARS protein is highly hydrophilic, except its N-terminus which is slightly hydrophobic, while hPIX is also mostly hydrophilic.

Fig. 5. Human PIX mRNA sequence and its translation product. Shown is the sequence of a brain EST and its translation product aligned with the respective codons. Boxed letters indicate the first codon and first methionine of the brain EST and its translation product, respectively. Underlined residues represent conserved PIX-family motifs. The cysteine and histidine residues at the predicted positions of the conserved Pix-family motifs that are possible members of the Cys-His-Asn cysteine protease catalytic triad are boxed.

Coregulation of *mACHE* and *mARS*

*ACHE*is known to be transcriptionally activated under exposure to anti-AChEs, and arsentie is known to be a quasi-irreversible AChE inhibitor (Shapira *et al.*, 1998; Wilson and Silman, 1977), thought to bind to AChE in the vicinity of the active site.

A novel possibility therefore emerged which postulated a general locus control, with AChE serving as a sensor for different stressors, including arsenite. To be subject to joint regulation, the mammalian *ARS* and *ACHE* genes should display coexpression patterns in different tissues and experimental conditions. Their colocalization in the human genome could facilitate such regulation through locus control. The partial overlap in tissue distribution of mRNA transcripts of *hARS* and *hACHE* (Table I), together with their close genomic proximity in both man and mouse, supported the possibility of coordinated transcriptional regulation of this entire chromosomal domain. To test whether this is also the case under experimental modulations of transcription, we compared the levels of mAChE and mARS mRNA in the brain of control mice to those in mice subjected to the forced-swim protocol causing psychological stress (Friedman *et al.*, 1996). ARS specific primers that were employed for RT-PCR were complementary to sequences flanking the region differing between the two inferred brain cDNAs (Fig. 2(B)). The size of the PCR product (ca. 320 bp) demonstrated that the transcript containing this amplified sequence is, at least in the mouse brain, the major variant obtained from the *ARS* gene. Stressed mice displayed, as expected, increased AChE mRNA levels in their brain (Kaufer *et al.*, 1998a; Shapira *et al.*, 2000).

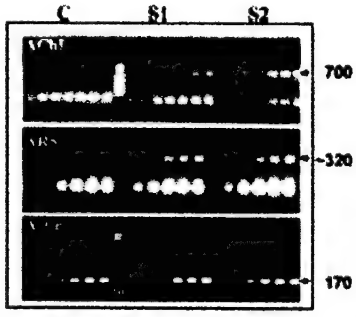

Fig. 6. Psychological stress increases both AChE and ARS mRNA levels in the mouse medulla. Shown is one out of three reproducible experiments presenting a semiquantitative kinetic follow-up of RT-PCR evaluation, with amplified DNA samples removed at every cycle. Arrow-labeled are AChE, ARS, and actin cDNA products in extracts prepared from the brain stem (medulla) region of either a control mouse (C) or two different mice subjected to psychological stress (S) (Kaufer *et al.*, 1998a). Densitometry of the fluorescent signals presented 8-fold stress-related increases for the AChE transcripts. Fourfold increases were detected for ARS products in brains of stressed as compared to control mice. Actin products showed no difference associated with stress, demonstrating specificity of the AChE and ARS increases.

The medulla region from these mice displayed massive co-induction in the brain of *ARS* and AChE mRNA2 h post-stress, while maintaining unchanged actin mRNA levels (Fig. 6). This supported the notion of a stress-associated regulation of gene expression in the *ACHE* locus.

Discussion

The human *ACHE* gene, located on the long arm of chromosome seven, extends into a long upstream region void of genes. This sequence contains a very high number of repetitive elements, which may contribute to the inherent instability of this genomic region. Together, these repetitive upstream sequences constitute a region rich in highly complex and diverse regulatory sequence motifs. These can potentially modulate the expression, not only of the *ACHE* gene, but also of the wider *ACHE* locus. Our current analysis shows that the human *ACHE* gene is less isolated at its downstream end, where two newly characterized genes, *hARS* and *hPIX*, are situated extremely close to *hACHE*. The *ACHE* and *ARS* genes have potentially related functional characteristics that permit consideration of several complex interregulatory mechanisms for the entire region, especially with regards to chemical exposure and stress. Likewise, the evolutionary conservation of *PIX* homologues is likely indicative of a common basic function of this gene. Cysteine proteases are known to be

induced under various stressful insults, for example, under exposure to the dopaminergic neurotoxin, MPP(C), which induces cell death in substantia nigra neurons (Choi *et al.*, 2001). While the *PIX* protein product may not be catalytically active, its conserved folding pattern suggests that it may interact with the protein targets of cysteine proteases. The very short distance, and same orientation of *hACHE* and *hPIX*, and their murine counterparts, suggest concerted regulation of this gene as well.

It is not clear yet whether *PIX* may be independently regulated by its own very short promoter, or if its induction exclusively depends on ACHE being transcribed. Also, the absence of existing sequences of previously characterized proteins with significant homology to *hPIX* is of considerable disadvantage in the process of deducing a role for this gene through reliable comparative homology. In contrast, *hARS* shares homology with several proteins with a previously characterized role in arsenite resistance.

Overexpression of the Chinese hamster *ARS* protein appears to be not merely coincidental with arsenite resistance, but is rather able to confer such a resistance in transfected cells (Rossman and Wang, 1999). However, ARS contains no known protein domains or motifs; therefore, it is very unlikely that the *hARS* protein confers arsenite resistance through any of the known mechanisms. Moreover, arsenite extrusion by various transporters, or modification by methylases or by glutathione S-transferase (reviewed in Rosen, 1995), predicts the existence of transmembrane domains, even in cases where there are no homologies to the already known arsenite resistance proteins. That no such domains were found in *hARS* suggests that it is actively involved in conferring arsenite resistance through a new, yet unknown mechanism(s).

The notion of *ARS* being coregulated with *ACHE* is supported by our experimental results. *AChE* inhibitors would cause an increase in acetylcholine levels, enhancing cholinergic gene expression in a manner similar to that occurring under psychological stress. That both arsenite and better known anti-AChEs induce transcriptional activation of the *ACHE* locus, together with arsenite being an AChE inhibitor, suggests a role for AChE as a sensor of arsenite, which can cause a protective multigenic transcriptional response. That brain *mARS* expression also increases under stress suggests that acetylcholine is the cause, as it is for *ACHE* gene expression, and raises the question whether the ARS protein product also exerts function(s) associated with mammalian stress responses. While it is still unclear whether *hARS* function requires and/or induces alterations in *ACHE* gene expression, an interesting link is that arsenite exposure, like anti-AChEs exposure, increases the risk for tumorogenesis (Lee *et al.*, 1988). It thus appears that transcriptional overactivation of the *ACHE* locus often leads to changes in cell proliferation, albeit not necessarily in the same tissues. A general locus response to stress, where *ACHE*, *PIX*, and *ARS* are regulated as a single unit is an intriguing possibility.

Chromosome 7 genes, anticholinesterase hypersensitivity and their long-term consequences: review and preliminary findings

Exposure, even sub-acute, to xenobiotics may induce a toxic response of the intestine, the immune system, muscle or brain, and alter metabolic activities to the extent that longevity is affected, all depending on the genotype of the patient, type of exposure, and level of the toxin's penetrance.

Anti-cholinesterase examples of such xenobiotics are carbamates and organophosphates (OPs) that block AChE and BuChE , but also other gene products, and which are known to induce the risk for several diseases, thus shortening life-expectancy. Specific examples of affected enzymes are 'atypical' BuChE, which bears the D70G mutation that confers acute sensitivity to anti-cholinesterases (Neville et al, 1990; Lowenstein et al., 1995), and *PON1*, the gene for paraoxonase, which hydrolyzes OPs and is subject to complex polymorphism (Costa et al., 1999). The upstream promoter of the *ACHE* gene includes two mutations, which confer over-production and hypersensitivity to anti-ChEs (Shapira et al., 2000; Fig. 1).

Fig. 1: The *ACHE* promoter and coding region:

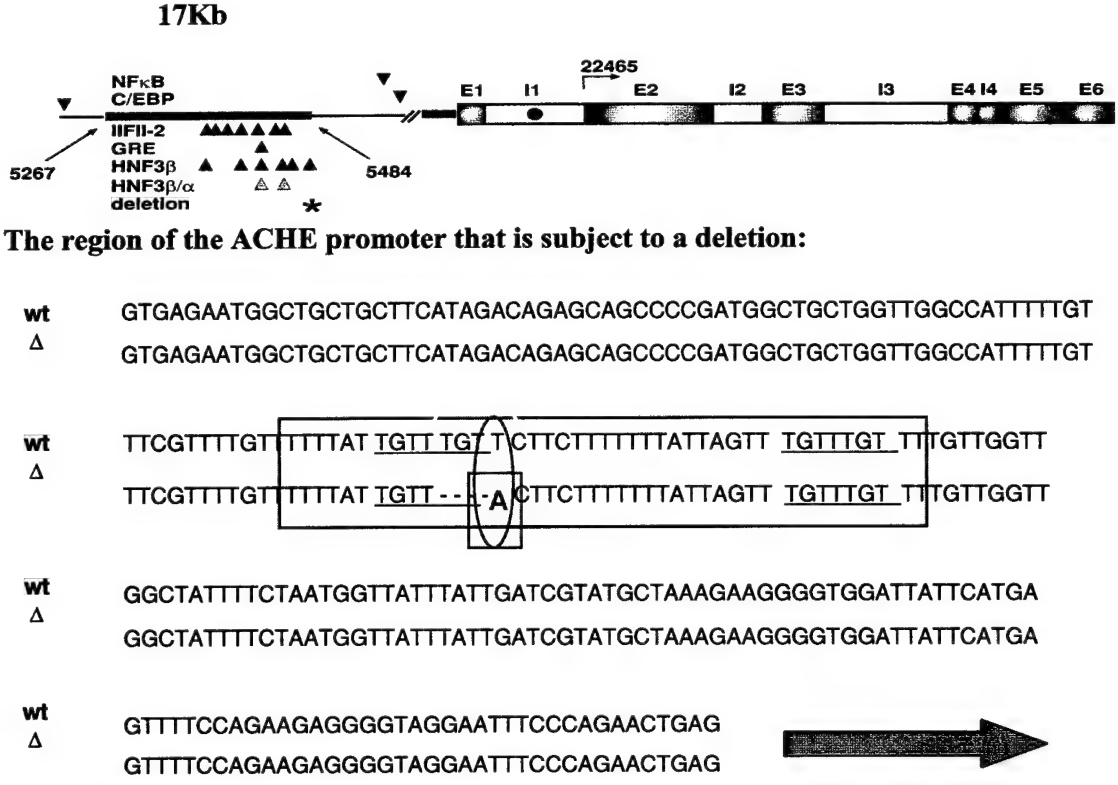

The region of the ACHE promoter that is subject to a deletion:

Fig. 1. Selecting domains prone to effective polymorphism in the h*ACHE* upstream region. Above: Density of consensus motifs. Shown are cumulative numbers of consensus motifs in 500 bp regions along the af002993 cosmid reverse DNA sequence. Arrow above represents the *ACHE* transcription start site (nt. 22465 in the cosmid sequence. Consensus binding sites for transcription factors in region I. Presented (wedges) are approximate positions within region I of binding sites for the transcription factors designated on the left. Sites with complete consensus sequences as well as the GRE half-palindromic site, TGTTCT, were located using FindPatterns of the GCG software package and the MatInspector program.

Black wedges represent consensus sequences known to bind either HNF3α or HNF3β; asterisk designates the mutated binding site. First and last nucleotides of region I as well as the transcription start site are marked. Below: Region I sequence. Presented is the normal region I sequence (wt; the T/A substitution is circled) aligned with the mutant sequence allele carrying the 4-bp deletion (Δ); nucleotide 1 is 5267 in the af002993 cosmid reverse sequence. The two HNF3 consensus binding sites are underlined.

Carriers of the *ACHE* promoter deletion express higher blood cell AChE levels and higher AChE activity (twice normal) in immortalized lymphocytes. Transgenic human AChE-over-expressing mice suffer hypersensititivity to both carbamate and OP inhibitors and survive for a shorter time after injection of a lethal dose of diisopropylfluorophosphonate (DFP) than mice of the parent strain. Unlike normal mice, they are unable to induce AChE-R over-production following exposure, which contributes to their hypersensitivity (Shapira et al., 2000)

***ACHE* haplotypes:**

The different polymorphisms in the *ACHE* locus together form a haplotype with internal linkage that confers a common heritage. H332N (Asn for His) is the serological marker of the Yt^b blood group. P446 is a silent mutation (Fig. 2).

Fig. 2. The incidence of the deletion mutation is ten-fold higher in Israeli than in the American populations. Shown are the A*CHE* haplotype (right) and the incidence of the promoter deletion in Israelis and Americans (Shapira et al., 2001).

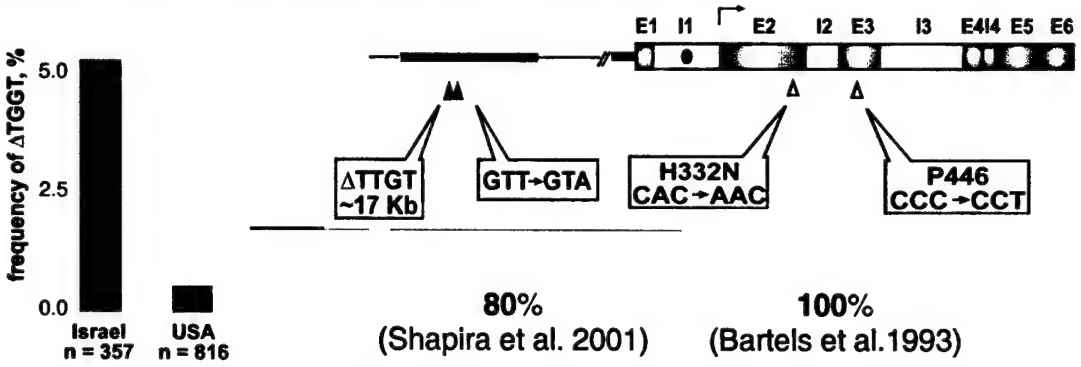

The incidence of the promoter polymorphism was tested in several groups of Israelis, healthy and unhealthy. The latter group included women with pregnancy complications as well as older patients following stroke or with Parkinson's disease (PD; Fig. 3).

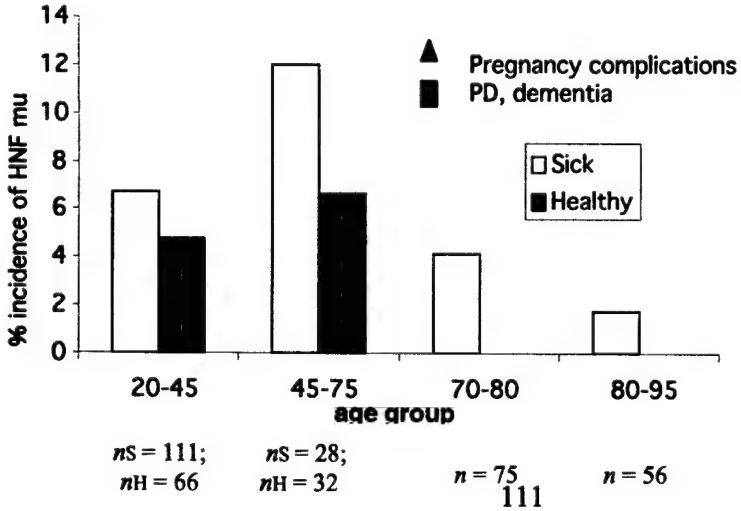

Fig. 3. The *ACHE* promoter polymorphism in various age groups and health conditions

Within the Israeli group, between the ages 20 and 75, sick individuals (with pregnancy complications, Parkinson's disease or dementia) displayed somewhat higher incidence of the deletion. In addition, its incidence in aged individuals (> 80 years) was considerably lower than the average. Because of the small sample sizes, the frequency of the mutation in some of the groups must be considered a preliminary finding.

At least 3 genes are known to induce increased risk for PD. These are *PARK*1, *PARK2* and *GST* (Gasser, 2000). Exposure to xenobiotics acts as a direct cause of PD in sporadic cases (also see Kaufer & Soreq, 1999). The relationship between the two causes is yet unknown. However, there is a clear cholinergic link to PD:

1. Over one-third of PD patients suffer cholinergic deficiencies (Soreq and Zakut, 1993).
2. Exposure to anti-AChEs, which causes AChE over-expression, is known to increase the risk for PD (Furlong et al., 1998).
3. Therefore, we explored the possibility that the activating polymorphism is also associated with increased risk for PD.
4. There does seem to be a trend to that effect, which is increased patients who had been exposed to agricultural insecticides (Fig. 4) .

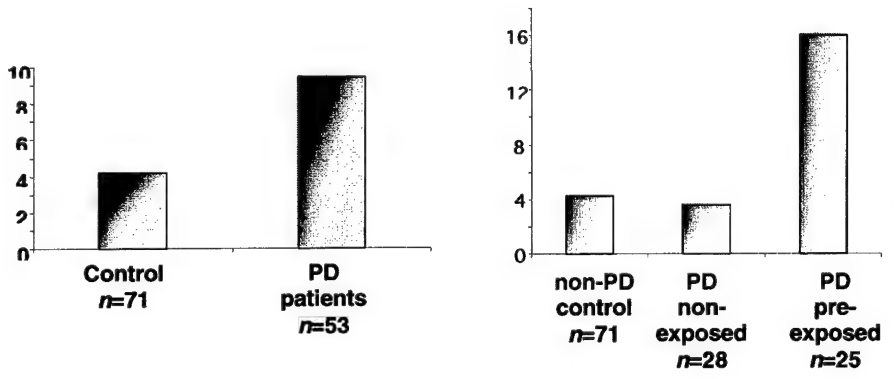

Fig. 4. Percent frequency of HNF mutation Shown is recent analysis of the incidence of *ACHE* mutations in Parkinson's disease patients, and in particular in PD patients who were exposed to agricultural insecticides.

Paraoxonase 1 and Parkinson's disease

Paraoxonase 1 (PON1) acts in the blood stream to hydrolyze various toxins which escape hepatic detoxification. There are two known polymorphisms to the *PON1* gene: an arginine to glutamine interchange at position 191 (Arg-Gln 191), and methionine to leucine at position 54 (Leu-Met 54).These polymorphisms have an influence on the ability of PON1 to hydrolyze toxins, and may intensify the effects of pollutants, organophosphates and other environmental chemicals in PD development.

In a study by Akhmedova et al. (2001) to determine the PD association of the Leu-Met 54 polymorphism, 117 unrelated idiopathic PD patients were chosen, and blood samples were obtained. Using PCR methods the DNA was amplified. The polymorphism creates a new cleavage site for the restriction enzyme *Nco*I, so that when incubated with it, the products could be separated by electrophoresis in a 10% polyacrylamide gel, stained with ethidium bromide and visualized under UV light. In this way the presence of the polymorphism within the alleles was detected. When compared to the distribution of the polymorphism in the

general population, it was found that PD patients presented more with the Leu-Met 54 polymorphism when compared to controls (P <0.003).

Therefore, an association exists between the appearance of the Leu-Met 54 polymorphism and an increased risk of PD. The change in the activity of the enzyme, following the polymorphism, does not ensure that one will contract the disease, it merely indicates a higher sensitivity towards various chemicals and toxins which might bring upon the disorder.

To conclude, it can be deduced that PD appears in a variety of forms, from the early onset disease with no presence of Lewy bodies, to the "classic" late onset manifestation. The occurrence of the disorder is influenced by many factors, some are environmental, as the exposure to various chemicals (MPTP, neuroleptic drugs, organophosphates, and such), rural living (which might also be connected to an increase in exposure to such compounds) or occupation. Genetic predisposition also plays a role in the appearance of Parkinson's disease. Some families in which the disease was found to be transmitted from one generation to the other showed specific point mutations which could be associated with the disease. In others, the connection between the genetic changes and the disorder was less obvious and apparently influenced by a combination of genetic and environmental factors, while still other genetic mutations, such as that in the *PON1* gene, only act to increase the risk of obtaining the disorder due to exposure to environmental conditions. All these factors, together, show us that the appearance of PD is influenced by many factors. In some cases the genetic/familial ones predominate, while in others they only act to increase the risk of contracting the disease, thereby possibly elucidating also the occurrence of sporadic PD.

PON1

This choromosome 7 gene, mutation of which is a risk factor associated with PD, can be characterized as follows:

- The gene product, *PON1*, is an aryldialkylphosphatase, a.k.a. paraoxonase
- It hydrolyzes soman, sarin, paraoxon, diazinon and other OP substrates.
- PON1 is a glycoprotein associated with a subset of HDL molecules.
- Its gene family includes 2 or more genes of unknown natural function
- It is produced in and secreted by the liver and exists in many tissues, particularly liver, kidney, small intestine and serum.

Fig 5. The PD susceptibility locus on chromosome 7- Spamming the region of $9_{21.3}$ - 9_{22} on the long arm of Chr. 7, this locus includes the *PON*, *ACHE*, ARS and PIX genes (Grant et al., 2001).

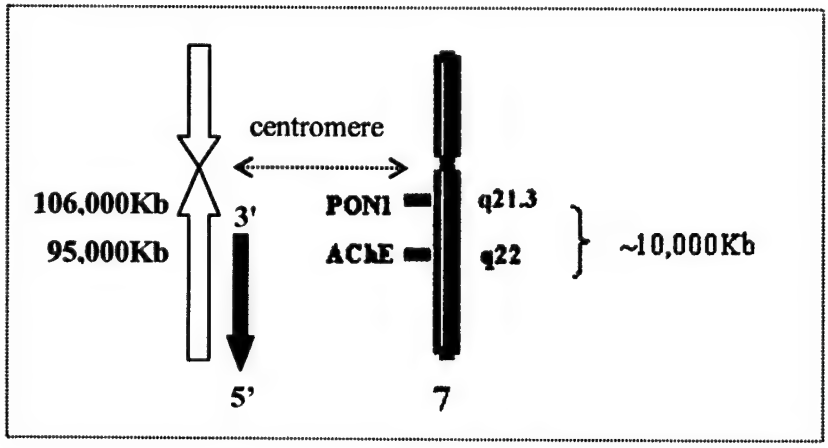

The *PON1* gene maps to chromosome 7q21.34, 10,000 Kb downstream from *ACHE*.

PON1 detoxifies OPs by hydrolyzing them; it also prevents lipodoxidation in LDL and HDL (Mackness et al., 1998).

PON1 serum levels may vary by up to 40-fold from one individual to another; 2 coding region polymorphisms and 5 promoter polymorphisms are known.

Fig. 6. *PON1* polymorphisms

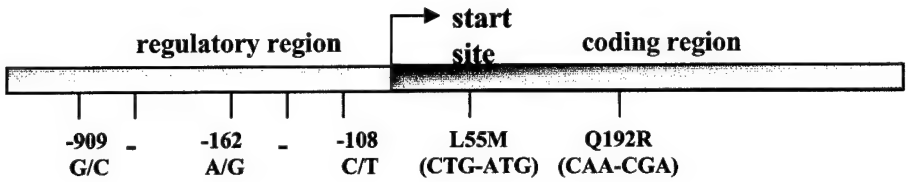

The 55L allele is linked to the 192R allele.

The PON1 192R alloenzmye is more active with these OPs than is the R alloenzyme:

paraoxon
methylparaoxon
chlorothion EPN oxon
Armin

Whereas the 192Q variant affords the carrier better protection against these OPs:

Diazoxon
Sarin
Soman

And both alloenzymes hydrolyze these substrates equally well:

phenyl acetate
chlorpyrifos oxon
naphthyl acetate-2

The polymorphisms at 192 affect mRNA and protein levels, but not biochemical properties. The M variant is associated with low serum levels, and thus affords low protection.

Promoter polymorphisms

-108 C/T This is the most effective polymorphism. It occurs at a putative SP1 binding site. The C variant is more active an enzyme than is the T variant.

-909 G/C This variant has no major effect on gene expression, except when it is linked to other polymorphisms.

-162 A/G The A variant promotes higher activities than the G variant. It is a suspected NF1 binding site.

PON1 status is defined as the combination of genotype and phenotype at this locus. It is affected by a high fat diet, exposure to xenobiotics, all of which reduce PON1 expression, regardless of the genotype.

The PON1 alleles show different distributions in specific ethnic groups. No study has yet been performed in Israel.

Chinese/Japanese	Caucasian	polymorphism
		-909:
Ł	žł	G
Ł	žł	C
		-162
žł–ž	žł	A
žł ž	žł	G
		-108
0.48	0.50	C
0.52	0.50	T
		55
0.94	0.64	L
0.06	0.36	M
		192
0.40	0.73	Q
0.60	0.27	R

Evolutionary considerations
Species with low PON1 activities display higher OP sensitivities (Costa et al., 1987). Knockout mice (PON1 -/-) are 5- to 10-fold more sensitive to the anti-ChEs diazoxon and chlorpyrifos oxon (Furlong et al, 1998) than is the wildtype. PON1 192R carriers have a higher risk for coronary heart disease.

PON1 polymorphisms and the Gulf War syndrome.
In a study of Gulf War veterans, the R allele appeared more frequently in those affected by GWS and those unaffected (Haley et al., 1999). PON1 192Q carriers display lower PON1 serum activities in sick, as compared to healthy, veterans.

connection between PD and PON1	ethnic group
no link	Caucasian (Taylor et al., 2000)
no link	Chinese (Wang et al., 2000)
Higher PON1 192R incidence in PD patients. R homozygotes show 1.6 ratio of increased risk.[a]	Japanese (Kondo et al., 1998)
Higher PON1 55M incidence in PD patients, with 2.19 odds ratio. Yet higher PON1 55M incidence in PD patients, with 2.19 odds ratio. Yet higher PON1 55M in PD patients with <51% early onset. Odds ratio, 5.15. Yet higher risk for those homozygous for the 192Q allele.	Russian (Akhmedova et al, 2001)

[a]The risk ratio is the frequency of PD among the population under study compared to the frequency in a control population.

Preliminary findings in Israel: genotyped PD patients reveal a single haplotype which apparently spans over 10,000 Kb and includes both *PON1* and *ACHE* polymoprhisms

Table 1. Apparent linkage between *ACHE* and *PON1* polymorphisms in agriculturally exposed PD patients.

patient no.	haplotype 55 – 192 – Δ – Yt – P446	Information medical history, sex, country of birth
35	L/M – Q/R – het – A/B - het	OP exposure, M, 58, Argentina
40	L/M – Q/R – het – A/B - hom	OP exposure, M, 78, Russia
41	L/M – Q/R – het – A/B - het	OP exposure, M, 65, Russia
46	L/M – Q/R – het – A/B - het	OP exposure, M, 58, Argentina
1027	L/M – Q/R – het – A/B - het	OP exposure, M, 70, Morocco
1007	M/M – Q/Q – het – A/B - het	OP exposure, M, 42

Note that in spite of the different ethnic origins, there is a common genotype that spans both the ACHE and PON1loci in all PD patients.

Fig 7. The *PON1-ACHE* polymorphism pattern

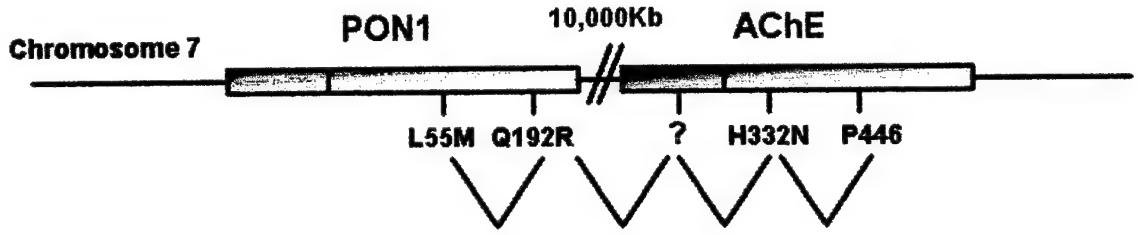

Implications

- Risk-associated variants in *PON1* and *ACHE* may be genetically linked.
- Both genes have variants that induce PD risk; therefore, combined inheritance may induce yet larger risk. This should be tested on a larger population
- The *ACHE*- and *PON1*-related risks were each studied in different populations, but the combined contirbution was not yet studied.
- Immortalized lympohocytes from mutaion carriers may prove excellent systems for exploration of the disease-causing mechanisms.

Task 9.

Discussions are in progress with Nexia Biotechnologies, Inc. (Montreal, PQ) for the isolation of recombinant human AChE from the milk of transgenic goats. Meanwhile, the further characterization of the human enzymes from the milk of transgenic mice is in progress.

Key accomplishments

- Establishment of a role for AChE-R in the pathophysiology of myasthenia gravis and in muscle fatigue.
- Demonstration that neuronal overexpression of AChE-R is associated with antisense-suppressible behavioral impairments.
- Discovery of hypersensitivity to cholinergic agonists and antagonists under conditions of persistent overexpression of AChE- R.
- Substantiation of the effect of AChE over-expression on hematopoiesis
- Demonstration of frequent blood-brain barrier disruption in the human cerebral cortex.
- Development of transfected cell and mouse models for inducible antisense and ribozyme suppression of *ACHE* gene expression.
- Discovery that stress-induced interaction of AChE-R with the scaffold protein RACK1 and protein kinase CβII intensifies behavioral inhibition.
- Finding that patterns of neuritic mRNA translocation are altered under conditions of long-term neuronal hypersensitivity.
- Mapping of the area surrounding the *ACHE* locus and screening for the chromosome 7 genes, which are associated with the locus response and anticholinesterase hypersensitivity.

Reportable outcomes

The following are new articles that have appeared or will shortly appear in peer-reviewed journals:

Grant AD, Shapira M, Soreq H (2001) Genomic dissection reveals locus response to stress for mammalian acetylcholinesterase. *Cell Mol Neurobiol* 21: 783-797.

Tomkins O, Kaufer D, Korn A, Shelef I, Golan H, Reichenhal E, Soreq H, Friedman A (2001) Frequent blood-brain barrier disruption in the human cerebral cortex. *Cell Mol Neurobiol* 21: 675-691.

Meshorer E, Erb C, Gazit R, Pavlovsky L, Kaufer D, Friedman A, Glick D, Ben-Arie N, Soreq H (2002) Alternative splicing and neuritic mRNA translocation under long-term neuronal hypersensitivity. *Science* 295: 508-512.

Cohen O, Erb C, Ginzberg D, Pollak Y, Seidman S, Shoham S, Yirmiya R, Soreq H (in press) Neuronal overexpression of "readthrough" acetylcholinesterase is associated with antisense-suppressible behavioral impairments. *Mol. Psychiatry.*

Pavlovsky L, Browne RO and Friedman A (in press) Pyridostigmine enhances glutamatergic transmission in hippocampal CA1 neurons. *Exp Neurol.*

The following are conference reports and review articles that have appeared or will shortly appear:

Soreq H, Kaufer D, Friedman A, Glick D (2001) Blood-brain barrier modulations and low-level exposure to xenobiotics. In Somani SM, Romano JA (eds), *Chemical Warfare Agents: Low Level Toxicity*, CRC Press, Boca Raton, FL, pp. 121-144.

Meshorer E, Soreq H (2002) Antisense intervention with cholinergic impairment associated with neurodegenerative disease. In: Mizuno Y, Fisher A, Hanin I (eds), *Mapping the Progress of Alzheimer's and Parkinson' Disease*, Kluwer Academic/Plenum Publishers, New York, pp. 45-48.

Soreq H, Meshorer E, Cohen O, Yirmiya R, Ginzberg D, Glick D (in press) The molecular neurobiology of acetylcholinesterase variants. In: Giacobini E (ed) *Cholinergic Mechanisms*, Martin Dunitz, London.

Aviv E, Shelef I, Golan H, Korn A, Tomkins O, Pavlovsky L, Friedman A (in press) Blood-brain barrier disruption is associated with abnormal cortical theta rhythm generation: the potential involvement of acetylcholinesterase. In: Giacobini E (ed) *Cholinergic Mechanisms*, Martin Dunitz, London.

Meshorer E, Soreq H (in press) Pre-mRNA splicing modulations in senescence, *Aging Cell.*

Shoham S, Kovalev, E, Sklan E, Soreq H (in press) Readthrough acetylcholinesterase and cholinergic neurotransmission.. In: Giacobini E (ed) *Cholinergic Mechanisms*, Martin Dunitz, London.

Evron, T, Soreq H (in press) Transgenic manipuiltions of neuromuscular junction maintenance. In: Giacobini E (ed) *Cholinergic Mechanisms*, Martin Dunitz, London.

Sklan EH, Birikh KR, Soreq H (in press) Two-hybrid approach to the intracellular function(s) of readthrough acetylcholinesterase. In: Giacobini E (ed) *Cholinergic Mechanisms*, Martin Dunitz, London.

Degrees granted:

Dan Girsaru MD, received a PhD (Biological Chemistry) from Tel-Aviv University (June 2002)

Employment opportunities resulting from work on this grant:

Dan Grisaru, MD, PhD, was appointed head of the Gyneco-Oncology Unit at Sourasky Medical Center (Tel-Aviv).

Awards:

Honorary professorship to H.S. by Universidad Maimónides, Buenos Aires (August 2001)

Haselkorn Fellowship for studies toward the MSc degree from the Hebrew University Institute of Life Sciences to Liat Ben-Moyal (January 2002)

Fellowship for doctoral studies from the Hebrew University Faculty of Sciences to Inbal Mor (October 2000)

Fellowshipfor doctoral studies from the Israel Interdisciplinary Center for Neural Computation to Eran Meshorer (July 2002)

American Physicians Fellowship for Medicine in Israel to A.F. (2002)

Funding applied for based on work suported by this grant:

By Prof. Soreq, to the European Union, as part of a consortium under the direction of Prof. S. Stamm of the University of Erlangen Nurenberg (Germany) to create an alternative RNA splicing database as a tool in the diagnosis of human diseases.

By Prof. Soreq, to the Israel Science Foundation for studies on "Molecular mechanisms mediating long-term nervous system stress responses".

Collaborations initiated:

By Prof. Soreq, with Prof. W.S. Brimijoin of the Mayo Clinic Dept. of Pharmacology, on the action of acetylcholinesterase in promoting β-amyloid plaques in the cerebral cortex.

By Prof. Soreq, with Prof. Mariella De Biasi of the Baylor College of Medicine Division of Neuroscience, on stress-assoicated impoairments of cholinergic balance.

Training of personnel:

Ningshang Wang, PhD, a post-doctoral fellow from the laboratory of Prof. Mariella De Biasi, Division of Neurosciences, Baylor College of Medicine, Houston TX, spent two months in the laboratory of Prof. Soreq to learn *in situ* hybridization techniques.

Tatiana Vander, MD, a neurologist from Soroka Hospital (Beersheva), is continuing to receive training at Hebrew University to enable the Beersheva group, under Dr. Friedman, perform AChE enzyme and protein concentration assays and determine genomic polymorphisms.

Orie Browne, a candidate for a MD and a PhD in physiology from Dr. Friedman's laboratory in Beersheva participated in the annual workshop offered by Prof. Soreq in Jerusalem, "From transgene to organism: new techniques in molecular cell biology" in February 2002.

Sam Fletcher, a candidate for a MSc in plant biology from the laboratory of Tsafrir Mor at the Arizona State University, Tempe AZ, also participated in the workshop, "From transgene to organism: new techniques in molecular cell biology".

Rebecca Eizak, a candidate for a MSc in biochemistry and molecular biology from the laboratory of Prof. Esther Sabban at the New York Medical College, Valhalla NY, spent the summer of 2002 in Prof. Soreq's laboratory learning molecular cell biology techniques.

Major lectures:

by H. Soreq:

American Society of Neurochemistry, Miami Beach, FL (June 2001)

Universidad de Buenos Aires (August 2001)

International Society of Developmental Neuroscience, Sidney, Australia (February 2002)

VIIth International Geneva/Springfield Symposium on Advances in Alzheimer Therapy, Geneva, Switzerland (April 2002)

US Ministry of Defense (DARPA meeting), Lexington, KY (April 2002)

XIth International Symposium on Cholinergic Mechanisms, St. Moritz, Switzerland (May 2002)

Bioscience 2002 Medical Defense Review, Hunt Valley MD (June 2002)

by A. Friedman:

Johannes Muller Institute for Physiology, Humboldt University, Berlin (2001)

XIth International Symposium on Cholinergic Mechanisms, St. Moritz, Switzerland (May 2002)

Conclusions

By combining various conceptual and experimental approaches, we have found that the *ACHE* gene and the adjacent sequences on the long arm of human chromosome 7 are subject to a universal pattern of response to a variety of stresses (report under task 8). Both in humans and in experimental animals we observed stress-induced activation of transcription and diversion of the alternative splicing of AChE mRNA transcripts, so that instead of the major "synaptic" AChE-S mRNA, this gene produces the normally rare "readthrough" AChE-R mRNA variant. This also changes the AChE protein profile to yield a soluble monomer, instead of synapse-associated tetramers. At the short term, production of AChE-R above the levels needed to maintain normal neurotransmission can be useful for the scavenging of chemical warfare agents. This improved anti-AChE protection possibly explains the prophylactic action of pyridostigmine, which raises AChE-R levels. The increased level of AChE can also prevent epileptic seizures due to synchronous hyperexcitation of too many neurons. However, under long-term or chronic overexpression, this same protein appears to be associated with multiple pathologies:

(1) It causes extracellular impairment of cholinergic balance, which induces muscle fatigue, which can be prevented by antisense destruction of AChE-R mRNA. (reports under tasks 1 and 5);
(2) It may disrupt synaptic interactions because of the sequence and structural homologies between AChE and neuroligins (Soreq and Seidman). This disruption may be associated with cognitive deterioration (report under task 1);
(3) It leads to extrasynaptic functioning of AChE-R, due to its mRNA being translocated into neurites under stress (report under task 8). This can cause glutamatergic hypexcitation and neuronal hypersensitivity;
(4) Intracellular accumulation of AChE-R can induce stress signal transduction that elevates contextual fear responses (reported under task 6);

The above features (fatigue, cognitive and behavioral impairments, hyperexcitation and hypersensitivity, and contextual fear responses) are all features of post-traumatic stress disorder (PTSD), suggesting that there may be a link between chronic AChE-R overproduction and PTSD.

References

Abbott NJ ¸2000˘ Inflammatory mediators and modulation of blood-brain barrier permeability. Cell Mol Neurobiol 20:131-147.

Abbruscato TJ, Davis TP ¸1999˘ Protein expression of brain endothelial cell E-cadherin after hypoxia/aglycemia: influence of astrocyte contact. Brain Res 842: 277-286.

Adey NB, Kay BK (1997) Isolation of peptides from phage-displayed random peptide libraries that interact with the talin-binding domain of vinculin. Biochem J 324: 523–528.

Aigner TG (1995) Pharmacology of memory: cholinergic-glutamatergic interactions. Curr Opin Neurobiol 5: 155-160.

Akeson P, Larsson EM, Kristoffersen DT, Jonsson E, Holtas S ¸1995˘ Brain metastases-comparison of gadodiamide injection-enhanced MR imaging at standard and high dose, contrast-enhanced CT and non-contrast-enhanced MR imaging. Acta Radiol 36: 300-306.

Akhmedova SN, Yakimovsky AK, Schwartz EI. (2001) Paraoxonase 1 Met--Leu 54 polymorphism is associated with Parkinson's disease. J Neurol Sci184:179-182.

Aldrich TK, Shander A, Chaudry I, Nagshima H (1986) Fatigue of isolated rat diaphragm: role of impaired neuromuscular transmission. J Appl Physiol 61: 1077-1083.

Alkondon M, Pereira EF, Barbosa CT, Albuquerque EX (1997) Neuronal nicotinic acetylcholine receptor activation modulates gamma- aminobutyric acid release from CA1 neurons of rat hippocampal slices. J Pharmacol Exp Ther 283:1396-1411.

Alvarez A, Alarcon R, Opazo C, Campos EO, Munoz FJ, Calderon FH, Dajas F, Gentry MK, Doctor BP, De Mello FG, Inestrosa NC (1998) Stable complexes involving acetylcholinesterase and amyloid-peptide change the biochemical properties of the enzyme and increase the neurotoxicity of Alzheimer's fibrils. J Neurosci 18: 3213–3223.

Aminoff MJ (2001) Parkinson's disease and other extrapyramidal disorders. In: Braunwald E, Fauci AS, Kasper DL,Hauser SL, Longo DL, Jamson JL (eds) *Harrison's Principles of Internal medicine*. MacGraw Hill, pp. 2399-2406.

Amorapanth P, LeDoux JE, Nader (2000) Different lateral amygdala outputs mediate reactions and actions elicited by a fear-arousing stimulus. Nat Neurosci 3: 74-79.

Andres C, Beeri R, Friedman A, Lev-Lehman E, Henis S, Timberg R, Shani M, Soreq H (1997) Acetylcholinesterase-transgenic mice display embryonic modulations in spinal cord choline acetyltransferase and neurexin Iβ gene expression followed by late-onset neuromotor deterioration. Proc Natl Acad Sci USA 94: 8173-8178.

Andres C, Seidman S, Beeri R, Timberg R, Soreq H. (1998) Transgenic acetylcholinesterase induces enlargement of murine neuromuscular junctions but leaves spinal cord synapses intact. Neurochem Internatl 32: 449-456.

Anglister L (1991) Acetylcholinesterase from the motor nerve terminal accumulates on the synaptic basal lamina of the myofiber. J Cell Biol 115: 755-764.

Anglister L, Haesaert B, McMahan UJ (1994a) Globular and asymmetric acetylcholinesterase in the synaptic basal lamina of skeletal muscle. J Cell Biol 125: 183-196.

Anglister L, Stiles, JR, Salpeter MM (1994b) Acetylcholinesterase density and turnover number at frog neuromuscular junctions, with modeling of their role in synaptic function. Neuron 12: 783-794.

Antelman SM, Eichler AJ, Black CA, Kocan D (1980) Interchangeability of stress and amphetamine in sensitization. Science 207: 329-331.

Aquilonius SM, Hartvig P (1986) Clinical pharmacokinetics of cholinesterase inhibitors. Clin Pharmacokinet 11:236-249.

Atherton E, Sheppard RC (1989) *Solid phase peptide synthesis: a practical approach*. IRL Press, Oxford.

Auerbach JM, Segal M (1994) A novel cholinergic induction of long-term potentiation in rat hippocampus. J Neurophysiol 72: 2034-2040.

Bailey CH, Bartsch D, Kandel ER (1996) Toward a molecular definition of long-term memory storage. Proc Natl Acad Sci USA 93: 13445-13452.

Bakay L (1976) Blood-brain barrier and its alteration in pathological states. In Vinken PJ, Bruyn GW (eds.), *Handbook of Clinical Neurology* Elsevier/North-Holland Biomedical Press, Amsterdam, vol. 28. p. 370.

Bartels CF, Zelinski T, Lockridge O (1993) Mutation at codon 322 in the human acetylcholinesterase (ACHE) gene accounts for YT blood group polymorphism. J Hum Genet 52: 928-936.

Battaglia M (2002) Beyond the usual suspects: a cholinergic route for panic attacks. Molecular Psychiatry 7: 239-246.

Battaini F, Pascale A, Lucchi L, Pasinetti GM, Govoni S (1999) Protein kinase C anchoring deficit in postmortem brains of Alzheimer's disease patients. Exp Neurol 159: 559-564.

Beeri R, Andres C, Lev-Lehman E, Timberg R, Huberman T, Hani M, Soreq H (1995) Transgenic expression of human acetylcholinesterase induces progressive cognitive deterioration in mice. Curr Biol 5: 1063-1071.

Beeri R, Le Novere N, Mervis R, Huberman T, Grauer E, Changeux J-P, Soreq H (1997) Enhanced hemicholinium binding and attenuated dendrite branching in cognitively impaired acetylcholinesterase-transgenic mice. J Neurochem 69: 2441-2451.

Behra M, Cousin X, Bertrand C, Vonesch JL, Biellmann D, Chatonnet A, Strahle U (2002) Acetylcholinesterase is required for neuronal and muscular development in the zebrafish embryo. Nat Neurosci 5: 111-118.

Belova I, Jonsson G (1982) Blood-brain barrier permeability and immobilization stress. Acta Physiol Scand 116: 21-29.

Benardo LS, Prince A (1982a) Cholinergic excitation of mammalian hippocampal pyramidal cells. Brain Res 249: 315-331.

Benardo LS, Prince DA (1982b) Ionic mechanisms of cholinergic excitation in mammalian hippocampal pyramidal cells. Brain Res 249: 333-344.

Ben-Nathan D, Lustig S, Danenberg HD (1991) Stress-induced neuroinvasiveness of a neurovirulent noninvasive Sindbis virus in cold or isolation subjected mice. Life Sci 48: 1493-1500.

Bigbee JW, Sharma KV, Chan EL, Bogler O (2000) Evidence for the direct role of acetylcholinesterase in neurite outgrowth in primary dorsal root ganglion neurons. Brain Res 861: 354–362.

Birikh KR, Berlin YA, Soreq H, Eckstein F (1997) Probing accessible sites for ribozymes on human acetylcholinesterase RNA. RNA 3: 429-437.

Blair HT, Schafe GE, Bauer EP, Rodrigues SM, LeDoux JE (2001) Synaptic plasticity in the lateral amygdala: a cellular hypothesis of fear conditioning. Learn Mem 8: 229-242.

Blanton MG, Lo Turco JJ, Kriegstein AR(1989) Whole cell recording from neurons in slices of reptili an and mammalian cerebral cortex. J Neurosci Methods 30: 203-210.

Blichenberg A, Schwanke B, Rehbein M, Garner CC, Richter D, Kindler S (1999) Identification of a cis-acting dendritic targeting element in MAP2 mRNAs. J Neurosci 19: 8818-8829.

Bluthe RM, Schoenen J, Dantzer R (1990) Androgen-dependent vasopressinergic neurons are involved in social recognition in rats. Brain Res 519: 150-157.

Boje KM (1996) Inhibition of nitric oxide synthase attenuates blood-brain barrier disruption during experimental meningitis. Brain Res 720: 75-83.

Bolivar VJ, Pooler O, Flaherty L (2001) Inbred strain variation in contextual and cued fear conditioning behavior. Mamm Genome, 12: 651-656.

Boneva N, Brenner T, Argov Z (2000) Gabapentin may be hazardous in myasthenia gravis. Muscle Nerve 23: 1204-1208.

Borda E, Camusso JJ, Perez Leiros C, Bacman S, Hubscher O, Arana R, Sterin-Borda L (1996) Circulating antibodies against neonatal cardiac muscarinic acetylcholine receptor in patients with Sjogren's syndrome. Mol Cell Biochem 163-164: 335-341.

Boschetti N, Brodbeck U, Jensen SP, Koch C, Norgaard-Pedersen B (1996) Monoclonal antibodies against a C-terminal peptide of human brain acetylcholinesterase distinguish between erythrocyte and brain acetylcholinesterases. Clin Chem 42: 19–23.

Brooks RA ¸1977˘ A quantitative theory of the Hounsfield unit and its application to dual energy scanning. J Comput Assist Tomogr 1: 487-493.

Brown G Jr (1995) Amyotrophic lateral sclerosis: recent insight from genetics and transgenic mice. Cell 80: 687-692.

Brown LM, Blair A, Gibson R, Everett G., Cantor KP, Schuman LM, Burmeister LF, Van Lier SF, Dick F (1990) Pesticide exposure and other agricultural risk factors for leukemia among man in Iowa and Minnesota. Cancer Res 50: 6585–6591.

Cabib S, Puglisi-Allegra S. Stress (1996) depression and the mesolimbic dopamine system. Psychopharmacology (Berl) 128: 331-342.

Calingasan NY, Park LC, Calo LL, Trifiletti RR, Gandy SE, Gibson GE (1998˘ Induction of nitric oxide synthase and microglial responses precede selective cell death induced by chronic impairment of oxidative metabolism. Am J Pathol 153: 599-610.

Cardell M, Wieloch T (1993) Time course of the translocation and inhibition of protein kinase C during complete cerebral ischemia in the rat. J Neurochem 61: 1308-1314.

Carlson NR (1994) *Physiology of Behavior*, Allyn and Bacon, Needham Heights, MA.

Carlson CG (1998) The dystrophinopathies: an alternative to the structural hypothesis. Neurobiol Dis 5: 3-15.

Cenci MA, Kalen P, Mandel RJ, Bjorklund A (1992) Regional differences in the regulation of dopamine and noradrenaline release in medial frontal cortex, nucleus accumbens and caudate-putamen: a microdialysis study in the rat. Brain Res 581: 217-228.

Chan RY, Adatia FA, Krupa AM, Jasmin BJ (1998) Increased expression of acetylcholinesterase T and R transcripts during hematopoietic differentiation is accompanied by parallel elevations in the levels of their respective molecular forms. J Biol Chem 273: 9727-9733.

Chan SL, Mattson MP ¸1999˘ Caspase and calpain substrates: roles in synaptic plasticity and cell death. J Neurosci Res 58: 167-190.

Chang B, Chiang M, Cartwright CA (2001) The interaction of Src and RACK1 is enhanced by activation of protein kinase C and tyrosine phosphorylation of RACK1. J Biol Chem 276: 20346-20356.

Changeux JP, Dehaene S (2000) Hierarchical neuronal modeling of cognitive functions: from synaptic transmission to the Tower of London. Int J Psychophysiol 35: 179-187.

Changeux J-P, Galzi JL, Devillers-Thiery A, Bertrand D (1992) The functional architecture of the acetylcholine nicotinic receptor explored by affinity labelling and site-directed mutagenesis. Q Rev Biophys 25: 395-432.

Charriaut-Marlangue C, Aggoun-Zouaoui D, Represa A, Ben-Ari Y ¸1996˘ Apoptotic features of selective neuronal death in ischemia, epilepsy and gp 120 toxicity. Trends Neurosci 19: 109-114.

Chien CT, Bartel PL, Sternglanz R, Fields S (1991) The two-hybrid system: a method to identify and clone genes for proteins that interact with a protein of interest. Proc Natl Acad Sci USA 88: 9578-9582.

Choi WS, Lee EH, Chung CW, Jung YK, Jin BK, Kim SU, Oh TH, Saido TC, Oh YJ (2001) Cleavage of Bax is mediated by caspase-dependent or -independent calpain activation in dopaminergic neuronal cells: protective role of Bcl-2. J Neurochem 77: 1531–1541.

Chothia C, Lesk AM (1987) Canonical structures for the hypervariable regions of immunoglobulins. J Mol Biol 196: 901–917.

Coggan JS, Purnyn SL, Knoper SR, Kreulen DL. 1994. Muscarinic inhibition of two potassium currents in guinea-pig prevertebral neurons: differentiation by extracellular cesium. Neuroscience 59:349-361.

Cohen O, Erb C, Ginzberg D, Pollak Y, Sohami S, Seidman S, Soreq H, Yirmiya R (in press) Overexpression of "readthrough" acetylcholinesterase is associated with antisense suppressible behavioral impairments. Mol Psychiatry.

Cole AE, Nicoll RA (1984). Characterization of a slow cholinergic post-synaptic potential recorded in vitro from rat hippocampal pyramidal cells. J Physiol 352: 173-188.

Cornford EM, Oldendorf WH ,1986' Epilepsy and the blood-brain barrier. Adv Neurol 44: 787-812.

Correale J, Rabinowicz AL, Heck CN, Smith TD, Loskota WJ, DeGiorgio CM (1998) Status epilepticus increases CSF levels of neuron-specific enolase and alters the blood-brain barrier. Neurology 50: 1388-1391.

Costa LG, Richter RJ, Murphy, SD, Omenn GS, Motulsky AG, Furlong CE. (1987) Species differences in serum paraoxonase correlate with sensitivity to paraoxon toxicity. In: Costa LG, Galli CL, Murphy SD, eds. *Toxocology of pesticides: experimental, clinical and regulatory perspectives*.Springer-Verlag, Heidelberg, 263-266.

Costa LG, Li WF, Richter RJ, Shih DM, Lusis A, Furlong CE (1999) The role of paraoxonase (PON1) in the detoxication of organophosphates and its human polymorphism. Chem Biol Interact 1999 May 14;119-120:429-438.

Coussens L, Parker,PJ, Rhee L, Yang-Feng TL, Chen E, Waterfield MD, Francke U, Ullrich A (1986) Multiple, distinct forms of bovine and human protein kinase C suggest diversity in cellular signaling pathways. Science 233: 859-866.

Coyle JT, Price DL, DeLong MR. (1983) Alzheimer's disease: a disorder of cortical cholinergic innervation. Science 219: 1184-1190.

Crawford TO, Pardo CA (1996) The neurobiology of childhood spinal muscular atrophy. Neurobiol Dis 3: 97-110.

Cummings JL, Back C (1998) The cholinergic hypothesis of neuropsychiatric symptoms in Alzheimer's disease. Am J Geriatr Psychiatry 6: S64-78.

Daoud R, Da Penha Berzaghi M, Siedler F, Hubener M, Stamm S (1999) Activity-dependent regulation of alternative splicing patterns in the rat brain. Eur J Neurosci 11: 788-802.

Darboux I, Barthalay Y, Piovant M, Hipeau Jacquotte R (1996) The structure-function relationships in Drosophila neurotactin show that cholinesterasic domains may have adhesive properties. EMBO J 15: 4835-4843.

Darreh-Shori T, Almkvist O, Guan Z, Garlined A, Strandberg B, Svensson A-L, Soreq H, Hellstrom-Lindahl E, Nordberg A (in press) Susteined cholinesterase inhibition in Alzheimer's disease patients receiving rivastigmine for 12 mounths. Neurology.

Davis L, Banker GA, Steward O (1987) Selective dendritic transport of RNA in hippocampal neurons in culture. Nature 330: 477-479.

Davis L, Burger B, Banker GA, Steward O (1990) Dendritic transport: quantitative analysis of the time course of somatodendritic transport of recently synthesized RNA J Neurosci 10: 3056-3068. (1990)

de Kruif J, Boel E, Logtenberg T (1995) Selection and application of human single chain Fv antibody fragments from a semi-synthetic phage antibody display library with designed CDR3 regions. J Mol Biol 248: 97–105.

de Quervain DJ, Roozendaal B, McGaugh JL (1998) Stress and glucocorticoids impair retrieval of long-term spatial memory. Nature 394: 787-790.

Del Castillo J, Katz B (1954) Quantal components of the endplate potential. J Physiol 124: 560-573.

Descarries L, Gisiger V, Steriade M. (1997) Diffuse transmission by acetylcholine in the CNS. Prog Neurobiol 53: 603-625.

Deutch AY, Lee MC, Gillham MH, Cameron DA, Goldstein M, Iadarola MJ (1991) Stress selectively increases fos protein in dopamine neurons innervating the prefrontal cortex. Cereb Cortex 1: 273-292

Diamond DM, Fleshner M, Ingersoll N, Rose G (1996). Psychological stress impairs spatial working memory: relevance to electrophysiological studies of hippocampal function. Behav Neurosci 110: 661-672.

Disatnik MH, Hernandez-Sotomayor SM, Jones G, Carpenter G, Mochly-Rosen D (1994) Phospholipase C-gamma 1 binding to intracellular receptors for activated protein kinase C. Proc Natl Acad Sci USA 91: 559-563.

Dove A (2002) Antisense and sensibility. Nat Biotechnol 20, 121-124.

Drachman DB (1994) Myasthenia gravis. N Engl J Med 330: 1797-1810.

Duman RS, Malberg J, Nakagawa S, D'Sa C (2000) Neuronal plasticity and survival in mood disorders. Biol Psychiatry 48: 732-739.

Duval N, Massoulie J, Bon S (1992) H and T subunits of acetylcholinesterase from Torpedo, expressed in COS cells, generate all types of globular forms. J Cell Biol 118: 641-653.

Eiden LE (1998) The cholinergic gene locus. J Neurochem 70: 2227–2240.

Elhusseiny A, Cohen Z, Olivier A, Stanimirovic DB, Hamel E. ˛1999˘ Functional acetylcholine muscarinic receptor subtypes in human brain microcirculation: identification and cellular localization. J Cereb Blood Flow Metab 19: 794-802.

Engel AG, Ohno K, Sine SM (1999) *Myastenia Gravis and Myastenic Disorders*. Oxford University Press, pp. 251-297.

Erb C, Troost J, Kopf S, Schmitt U, Löffelholz K, Soreq H, Klein J (2001) Compensatory mechanisms enhance hippocampal acetylcholine release in transgenic mice expressing human acetylcholinesterase J Neurochem 77: 638-646.

Esposito P, Gheorghe D, Kandere K, Pang X, Connolly R, Jacobson S, Theoharides TC (2001) Acute stress increases permeability of the blood–brain-barrier through activation of brain mast cells. Brain Res 888: 117-127.

Feng J, Cai X, Zhao J, Yan Z (2001) Serotonin receptors modulate GABA(A) receptor channels through activation of anchored protein kinase C in prefrontal cortical neurons. J Neurosci 21, 6502-6511.

Fernandez Espejo E (1997) Structure of the mouse behaviour on the elevated plus-maze test of anxiety. Behav Brain Res 86: 105-112.

Ferry CB, Kelly SS (1988) The nature of the presynaptic effects of (+)-tubocurarine at the mouse neuromuscular junction. J Physiol 403: 425-437.

Fibiger HC. Damsma G, Day JC (1991) Behavioral pharmacology and biochemistry of central cholinergic neurotransmission. Adv Exp Med Biol 295: 399-414.

Fleidervish IA, Friedman A, Gutnick M.J. (1996). Slow inactivation of Na+ current and slow cumulative spike adaptation in mouse and guinea-pig neocortical neurones in slices. J Physiol 493: 83-97.

Flumerfelt BA, Lewis PR, Gwyn DG ˛1973˘ Cholinesterase activity of capillaries in the rat brain. A light and electron microscopic study. Histochem J 5: 67-77.

Foster JA, Brown IR (1996) Intracellular localization of heat shock mRNAs (hsc70 and hsp70) to neural cell bodies and processes in the control and hyperthermic rabbit brain. J Neurosci Res 46: 652-665.

Friedman A, Kaufer D , Shemer J, Hendler I, Soreq H, Tur-Kaspa I (1996) Pyridostigmine brain penetration under stress enhances neuronal excitability and induces early immediate transcriptional response. Nat Med 2: 1382-1385.

Friedman A, Kaufer D, Pavlovsky L, Soreq H (1998) Cholinergic excitation induces activity-dependent electrophysiological and transcriptional responses in hippocampal slices.J Physiol Paris 92: 329-335.

Furlong CE, Li WF, Costa LG, Richter RJ, Shih DM, Lusis AJ. (1998) Genetically determined susceptibility to organophosphorus insecticides and nerve agents: developing a mouse model. Neurotoxicol 19: 645-650.

Futerman AH, Low MG, Michaelson DM, Silman I (1985) Solubilization of membrane-bound acetylcholinesterase by a phosphatidylinositol-specific phospholipase C. J Neurochem 45: 1487–1494.

Gahwiler BH, Brown DA (1987) Muscarine affects calcium-currents in rat hippocampal pyramidal cells in vitro. Neurosci Lett 76: 301-306.

Gallicano GI, Yousef MC, Capco DG (1997) PKC--a pivotal regulator of early development. Bioassays 19: 29-36.

Galyam N, Grisaru D, Grifman M, Melamed-Book N, Eckstein F, Seidman S, Eldor A, Soreq H (2001) Complex host cell responses to antisense suppression of ACHE gene expression. Antisense Nucleic Acid Drug Dev 11: 51-57.

Garcia R, Vouimba RM, Baudry M, Thompson RF (1999) The amygdala modulates prefrontal cortex activity relative to conditioned fear. Nature 402: 294-296.

Gasser T (2000) Autosomal-dominantly inherited forms of Parkinson's disease. J Neural Transm Suppl 58:31-40.

Gheusi G, Bluthe RM, Goodall G, Dantzer R (1994) Ethological study of the effects of tetrahydroaminoacridine (THA) on social recognition in rats. Psychopharmacology (Berl) 114: 644-650.

Giacobini E (2000) Present and future of Alzheimer therapy. J Neural Transm Suppl 59: 231-242.

Giovannini MG, Rakovska A, Benton RS, Pazzagli M, Bianchi L, Pepeu G (2001) Effects of novelty and habituation on acetylcholine, GABA, and glutamate release from the frontal cortex and hippocampus of freely moving rats. Neuroscience 106: 43-53.

Gossen M, Bujard H (1992) Tight control of gene expression in mammalian cells by tetracycline-responsive promoters. Proc Natl Acad Sci USA 89: 5547-5551.

Gossen M, Freundlieb S, Bender G, Muller G, Hillen W, Bujard H (1995) Transcriptional activation by tetracyclines in mammalian cells. Science 268: 1766-1769.

Gould E, Tanapat P (1999) Stress and hippocampal neurogenesis. Biol Psychiatry 46: 1472-1479.

Grauer E, Alkalai D, Kapon J, Cohen G, Raveh (2000) Stress does not enable pyridostigmine to inhibit brain cholinesterase after parenteral administration. Toxicol Appl Pharmacol 164: 301-304.

Gray JA (2000) *The Neuropsycology of Anxiety: an Inquiry into the Functions of the Septo-hippocampal System.* Oxford University Press, Oxford.

Gray R, Rajan AS, Radcliffe KA, Yakehiro M, Dani JA (1996). Hippocampal synaptic transmission enhanced by low concentrations of nicotine. Nature 383: 713-716.

Griffiths AD, Malmqvist M, Marks JD, Bye JM, Embleton MJ, McCafferty J, Baier M, Holliger KP, Gorick BD, Hughes-Jones NC, Hoogenboom HR, Winter G (1993) Human anti-self antibodies with high specificity from phage display libraries. EMBO J 12: 725-734.

Grifman M, Soreq H. (1997) Differentiation intensifies the susceptibility of pheochromocytoma cells to antisense oligodeoxynucleotide-dependent suppression of acetylcholinesterase activity. Antisense Nucleic Acid Drug Dev 7: 351-359.

Grifman M, Galyam N, Seidman S, Soreq H (1998) Functional redundancy of acetylcholine-esterase and neuroligin in mammalian neuritogenesis. Proc Natl Acad Sci USA. 95: 13935-13940.

Grisaru D, Sternfeld M, Eldor A, Glick D, Soreq H. (1999) Structural roles of acetylcholinesterase variants in biology and pathology. Eur J Biochem 264: 672-686.

Grisaru D, Deutsch V, Shapira M, Pick M, Sternfeld M, Melamed-Book N, Kaufer D, Galyam N, Gait MJ, Owen D, Lessing JB, Eldor A, Soreq H (2001) ARP, a peptide derived from the stress-associated acetylcholinesterase variant, has hematopoietic growth promoting activities. Mol Med 7: 93-105.

Guhaniyogi J, Brewer G (2001) Regulation of mRNA stability in mammalian cells. Gene 265: 11-23.

Habib KE, Weld KP, Rice KC, Pushkas J, Champoux M, Listwak S, Webster EL, Atkinson AJ, Schulkin J, Contoreggi C, Chrousos GP, McCann SM, Suomi SJ, Higley JD, Gold PW (2000) Oral administration of a corticotropin-releasing hormone receptor antagonist significantly attenuates behavioral, neuroendocrine, and autonomic responses to stress in primates. Proc Natl Acad Sci USA 97: 6079-6084.

Haley RW, Billecke S, La Du BN (1999) Association of low PON1 type Q (type A) arylesterase activity with neurologic symptom complexes in Gulf War veterans. Toxicol Appl Pharmacol 157: 227-233.

Haley RW, Marshall WW, McDonald GG, Daugherty MA, Petty F, Fleckenstein JL (2000) Brain abnormalities in Gulf War syndrome: evaluation with 1H MR spectroscopy. Radiology 215: 807-817.

Hamill P, Marty A, Neher E, Sakmann B, Sigworth FJ (1981) Improved patch-clamp techniques for high-resolution current recording from cells and cell-free membrane patches. Pflugers Arch 391:85-100.

Hamner MB, Lorberbaum JP, George MS (1999) Potential role of the anterior cingulate cortex in PTSD: review and hypothesis. Depress Anxiety 9: 1-14.

Hardison R, Slightom JL, Gumucio DL, Goodman M, Stojanovic N, Miller W (1997) Locus control regions of mammalian beta-globin gene clusters: combining phylogenetic analyses and experimental results to gain functional insights. Gene 205: 73–94.

Harrinson JL, Williams SC, Winter G, Nissim A (1996) Screening of phage antibody libraries. Meth Enzymol 267: 83–109.

He F, Xu H, Qin F, Xu L, Huang J, He X (1998) Intermediate myasthenia syndrome following acute organophosphates poisoning--an analysis of 21 cases. Hum Exp Toxicol 17: 40-45.

Henderikx P, Kandilogiannaki M, Petrarca C, von Mensdorff-Pouilly S, Hilgers JHM, Krambovitis E, Arends J, Hoogenboom HR (1998) Human single-chain Fv anti-bodies to MUC1 core peptide selected from phage display libraries recognize unique epitopes and predominantly bind adenocarcinoma. Cancer Res 58: 4324–4332.

Herman JP, Cullinan WE (1997) Neurocircuitry of stress: central control of the hypothalamo-pituitary- adrenocortical axis. Trends Neurosci 20: 78-84.

Hill AV (!970) The development and duration of the active state in stimulated muscle, as revealed by an applied stretch. *First and last experiments in muscle mechanics.* Cambridge University Press, p. 62-75.

Hillegaart V, Ahlenius S (1994) Time course for synchronization of spontaneous locomotor activity in the rat following reversal of the daylight (12:12 h) cycle. Physiol Behav 55: 73-75.

Holmes C, Jones SA, Budd TC, Greenfield SA (1997) Non-cholinergic, trophic action of recombinant acetylcholinesterase on mid-brain dopaminergic neurons. Journal of Neuroscience Res 49: 207-218.

Hoogenboom HR, Lutgerink JT, Pelsers MM, Rousch MJ, Coote J, van Neer N, De Bruine A, Van Nieuwenhoven FA, Glatz JF, Arends JW (1999) Selection-dominant and nonaccessible epitopes on cell-surface receptors revealed by cell-panning with a large phage antibody library. Eur J Biochem 260: 774–784.

Hu GY, Hvalby O, Walaas SI, Albert KA, Skjeflo P, Andersen P, Greengard P (1987) Protein kinase C injection into hippocampal pyramidal cells elicits features of long term potentiation. Nature 328: 426-429.

Huang D, Shi FD, Giscombe R, Zhou Y, Ljunggren HG, Lefvert AK (2001) Disruption of the IL-1beta gene diminishes acetylcholine receptor- induced immune responses in a murine model of myasthenia gravis. Eur J Immunol 31: 225-232.

Hubbard JI, Wilson DF (1973) Neuromuscular transmission in a mammalian preparation in the absence of blocking drugs and the effect of D-tubocurarine. J Physiol 228: 307-325.

Ichikawa J, Dai J, O'Laughlin I, Fowle, W, Meltzer H (2002) Atypical, but not typical, antipsychotic drugs increase cortical acetylcholine release without an effect in the nucleus accumbens or striatum. Neuropsychopharmacol 26: 325-339.

Ilouz N, Branski L, Parnis J, Parnas H, Linial M (1999) Depolarization affects the binding properties of muscarinic acetylcholine receptors and their interaction with proteins of the exocytic apparatus. J Biol Chem 274: 29519-29528.

Imperato A, Puglisi-Allegra S, Casolini P, Angelucci L (1991) Changes in brain dopamine and acetylcholine release during and following stress are independent of the pituitary-adrenocortical axis.Brain Res 538: 111-117.

Inanami O, Ohno K, Sato A (1992). Responses of regional cerebral blood flow to intravenous administration of thyrotropin releasing hormone in aged rats. Neurosci Lett 143: 151-154.

Iwasaki Y, Wakata N, Kinoshita M (1988) Parkinsonism induced by pyridostigmine. Acta Neurol Scand 78: 236.

Jefferys JG (1998) Mechanisms and experimental models of seizure generation. Curr Opin Neurol 11: 123-127.

Johnson E, Cotter FE (1997). Monosomy 7 and 7q associated with myeloid malignancy. Blood Rev 11: 46–55.

Jones S, Yakel JL (1997) Functional nicotinic ACh receptors on interneurones in the rat hippocampus. J Physiol 504: 603-610.

Kadota E, Nonaka K, Karasuno M, Nishi K, Teramura K, Hashimoto S (1997) Neurotoxicity of serum components, comparison between CA1 and striatum. Acta Neurochir Suppl Wien 70: 141-143.

Kaneki M, Kharbanda S, Pandey P, Yoshida K, Takekawa M, Liou J, Stone R, Kufe D (1999) Functional role for protein kinase Cbeta as a regulator of stress-activated protein kinase activation and monocytic differentiation of myeloid leukemia cells. Mol Cell Biol 19: 461-470.

Kaneto H. (1997) Learning/memory processes under stress conditions. Behav Brain Res 83: 71-74.

Kang H, Schuman EM (1996) A requirement for local protein synthesis in neurotrophin-induced hippocampal synaptic plasticity. Science 273: 1402-1406..

Karpel R, Ben Aziz-Aloya R, Sternfeld M, Ehrlich G, Ginzberg D, Tarroni P, Clementi F, Zakut H, Soreq H (1994) Expression of three alternative acetylcholinesterase messenger RNAs in human tumor cell lines of different tissue origins. Exp Cell Res 210: 268–277.

Kaufer D, Friedman A, Seidman S, Soreq H (1998a) Acute stress facilitates long-lasting changes in cholinergic gene expression. Nature 393: 308-309.

Kaufer D, Friedman A, Seidman S, Soreq H (1998b) Anticholinesterases induce multigenic transcriptional feedback response suppressing cholinergic neurotransmission. Chem-Biol Interact 119: 349-360.

Kaufer D, Soreq H. (1999) Tracking cholinergic pathways from psychological and chemical stressors to variable neurodeterioration paradigms. Curr Opin Neurol 12:739-743.

Killcross S, Robbins TW, Everitt BJ (1997) Different types of fear-conditioned behaviour mediated by separate nuclei within amygdala. Nature 388: 377-380.

Kitada T, Asakawa S, Hattori N, Matsumine H, Yamamura Y, Minoshima S (1998) Mutations in the parkin gene cause autosomal recessive juvenile parkinsonism. Nature 392: 605-608.

Klatzo I (1983) Disturbances of the blood-brain barrier in cerebrovascular disorders. Acta Neuropathol Suppl Berl 8: 81-8.

Kobayashi M, Ohno M, Shibata S, Yamamoto T, Watanabe S (1997) Concurrent blockade of beta-adrenergic and muscarinic receptors suppresses synergistically long-term potentiation of population spikes in the rat hippocampal CA1 region. Brain Res 777: 242-246.

Kondo I, Yamamoto M. (1998) Genetic polymorphism of paraoxonase 1 (PON1) and susceptibility to Parkinson's disease. Brain Res 806:271-273.

Kramer TH, Buckhout R, Fox P, Widman E, et-al. (1991) Effects of stress on recall. Appl Cog Psychol 5: 483-488.

Kristensen P, Winter G (1998) Proteolytic selection for protein folding using filamentous bacteriophages. Fold Des 3: 321–328.

Kuei JH, Shadmehr R, Sieck GC (1990) Relative contribution of neurotransmission failure to diaphragm fatigue.J App Physiol 68: 174-180.

Kuhn W, Winkel R, Woitalla D, Meves S, Przuntek H, Muller T (1998) High prevalence of parkinsonism after occupational exposure to lead-sulfate batteries. Neurology 50: 1885-1886.

Kuhn C, Muller F, Melle C, Nasheuer HP, Janus F, Deppert W, Grosse F (1999) Surface plasmon resonance measurements reveal stable complex formation between p53 and DNA polymerase alpha. Oncogene 18: 769-774.

Lampert IA, Van Noorden S (1996) Acetylcholinesterase is expressed in the follicular dendritic cells of germinal centres: Differences between normal and neoplastic follicles. J Pathol 180: 169–174.

Lapin IP (1993) Anxiogenic effect of phenylethylamine and amphetamine in the elevated plus-maze in mice and its attenuation by ethanol. Pharmacol Biochem Behav 44: 241-243.

Laping NJ, Nichols NR, Day JR, Johnson SA, Finch CE (1994) Transcriptional control of glial fibrillary acidic protein and glutamine synthetase in vivo shows opposite responses to corticosterone in the hippocampus. Endocrinology 135: 1928-1933.

Layer PG (1996) Non-classical actions of cholinesterases: Role in cellular differentiation, tumorigenesis and Alzheimer's disease. Neurochem Int 28: 491–495.

Layer PG, Willbold E (1995) Novel functions of cholinesterases in development, physiology and disease. Prog Histochem Cytochem 29: 1–94.

Lee TC, Tanaka N, Lamb PW, Gilmer TM, Barrett JC (1988) Induction of gene amplification by arsenic. Science 241: 79–81.

Legay C, Bon S, Vernier P, Coussen F, Massoulie J (1993) Cloning and expression of a rat acetylcholinesterase subunit: generation of multiple molecular forms and complementarity with a Torpedo collagenic subunit. J Neurochem 60: 337-346.

Lev-Lehman E, Evron T, Broide RS, Meshorer E, Ariel I, Seidman S, Soreq H (2000) Synaptogenesis and myopathy under acetylcholinesterase overexpression. J Mol Neurosci 14: 93-105.

Liao D, Hessler NA, Malinow R (1995). Activation of postsynaptically silent synapses during pairing-induced LTP in CA1 region of hippocampal slice. Nature 375: 400-404.

Liao D, Scannevin RH, Huganir R (2001). Activation of silent synapses by rapid activity-dependent synaptic recruitment of AMPA receptors. J Neurosci 21: 6008-6017.

Liberzon I, Lopez JF, Flagel SB, Vazquez DM, Young EA (1999) Differential regulation of hippocampal glucocorticoid receptors mRNA and fast feedback: relevance to post-traumatic stress disorder. J Neuroendocrinol 11: 11-17.

Lieber A, Strauss M. (1995) Selection of efficient cleavage cites in target RNAs by using a ribozyme expression library. Mol Cell Biol 15: 540-551.

Liliental J, Chang DD (1998) Rack1, a receptor for activated protein kinase C, interacts with integrin beta subunit. J Biol Chem 273: 2379-2383.

Linder TM, Quastel DM.J (1978) A voltage clamp study of the permeability change induced by quanta of transmitter at the mouse end-plate. J Physiol 281: 535-556.

Lindstrom J (1980). Experimental autoimmune myasthenia gravis. J Neurol Neurosurg Psychiatry 43: 568-576.

Ling DS, Benardo LS (1994) Properties of isolated GABAB-mediated inhibitory postsynaptic currents in hippocampal pyramidal cells. Neuroscience 63: 937-944.

Lipska BK, Chrapusta SJ, Egan MF, Weinberger DR (1995) Neonatal excitotoxic ventral hippocampal damage alters dopamine response to mild repeated stress and to chronic haloperidol. Synapse 20: 125-130.

Lisak RP (1999) Myasthenia Gravis. Curr Treat Opin Neurol 1: 239-250.

Loewenstein-Lichtenstein Y, Schwarz M, Glick D, Norgaard-Pedersen B, Zakut H, Soreq H (1995) Genetic predisposition to adverse consequences of anti-cholinesterases in 'atypical' BCHE carriers. Nat Med 1: 1082-1085.

Lofas S, Johnsson B (1990) A novel hydrogel matrix on gold surfaces in surface plasmon resonance sensors for fast and efficient covalent immobilization of ligands. J Chem Soc Chem Commun 21: 1526–1528.

Lu WY, Jackson MF, Bai D, Orser BA, MacDonald JF (2000) In CA1 pyramidal neurons of the hippocampus protein kinase C regulates calcium-dependent inactivation of NMDA receptors. J Neurosci 20: 4452-4461.

Lucking CB, Durr A, Bonifati V, Vaughan J, De Michele G, Gasser T, Harhangi BS, Meco G, Denefle P, Wood NW, Agid Y, Brice A (2000) Association between early-onset Parkinson's disease and mutations in parkin gene. N Engl J Med 342: 1560-1567.

Luo ZD, Wang Y, Werlen G, Camp S, Chien KR, Taylor P (1999) Calcineurin Enhances Acetylcholinesterase mRNA stability during C2-C12 muscle cell differentiation. Mol Pharmacol 56: 886-894.

Lux HD (1980) Ionic conditions and membrane behavior. Adv Neurol 27: 63-83.

Mackness B, Durrington PN, Mackness MI (1998) Human serum paraoxonase. Gen Pharmac. 31: 329-336.

Madison DV, Lancaster B, Nicoll RA (1987) Voltage clamp analysis of cholinergic action in the hippocampus. J Neurosci 7: 733-741.

Mallet J, Houhou L, Pajak F, Oda Y, Cervini R, Bejanin S, Berrard S (1998) The cholinergic locus: ChAT and VAChT genes. J Physiol Paris 92: 145–147.

Markram H, Segal M (1990) Acetylcholine potentiates responses to N-methyl-D-aspartate in the rat hippocampus. Neurosci Lett 113: 62-65.

Markram H, Segal M (1992). The inositol 1,4,5-trisphosphate pathway mediates cholinergic potentiation of rat hippocampal neuronal responses to NMDA. J Physiol 447: 513-533.

Marks JD, Hoogenboom HR, Bonnert TP, McCafferty J, Griffiths AD, Winter G (1991) By-passing immunization. Human antibodies from V-gene libraries displayed on phage. J Mol Biol 222: 581–597.

Marks JD, Griffiths AD, Malmqvist M, Clackson TP, Bye JM, Winter G (1992) By-passing immunization: building high affinity human antibodies by chain shuffling. Biotechnology 10: 779–783.

Martijena ID, Calvo N, Volosin M, Molina VA (1997) Prior exposure to a brief restraint session facilitates the occurrence of fear in response to a conflict situation: behavioral and neurochemical correlates. Brain Res 752: 136-142.

Massoulie J, Anselmet A, Bon S, Krejci E, Legay C, Morel N, Simon S (1998) Acetylcholinesterase: C-terminal domains, molecular froms and functional localization. J Physiol Paris 92: 183–190.

McCormick JA, Lyons V, Jacobson MD, Noble J, Diorio J, Nyirenda M, Weaver S, Ester W, Yau JLW, Meaney MJ, Seckl JR, Chapman KE (2000) 5'-Heterogeneity of glucocorticoid receptor messenger RNA is tissue specific. Mol Endocrinol 14: 506-517.

McCullough EC, Baker HL Jr, Houser OW, Reese DF (1974) An evaluation of the quantitative and radiation features of a scanning x-ray transverse axial tomograph: the EMI scanner. Radiology 111: 709-715.

McEwen BS (1999) Stress and hippocampal plasticity. Annu Rev Neurosci 22: 122-105.

McEwen BS, Sapolsky RM (1995) Stress and cognitive function. Curr Opin Neurobiol 5: 205-216.

McNamara RK, Wees EA, Lenox RH (1999) Differential subcellular redistribution of protein kinase C isozymes in the rat hippocampus induced by kainic acid. J Neurochem 72: 1735-1743.

McQuiston AR, Madison DV (1999). Muscarinic receptor activity has multiple effects on the resting membrane potentials of CA1 hippocampal interneurons. J Neurosci 19: 5693-5702.

Meijer OC, de Lange EC, Breimer DD, de Boer AG, Workel JO, de Kloet ER (1998) Penetration of dexamethasone into brain glucocorticoid targets is enhanced in mdr1A P-glycoprotein knockout mice. Endocrinology 139: 1789-1793.

Meldrum BS (1993) Excitotoxicity and selective neuronal loss in epilepsy. Brain Pathol 3: 405-412.

Menegon A, Board PG, Blackburn AC, Mellick GD, Le Couteur DG (1998) Parkinson's disease, pesticides, and glutathione transferase polymorphisms. Lancet 352: 1344-1346.

Meshorer E, Erb C, Gazit R, Pavlovsky L, Kaufer D, Friedman A, Glick D, Ben-Arie N, Soreq H (2002) Alternative splicing and neuritic mRNA translocation under long-term neuronal hypersensitivity. Science 295: 508-512.

Messamore E, Warpman U, Ogane N, Giacobini E (1993). Cholinesterase inhibitor effects on extracellular acetylcholine in rat cortex. Neuropharmacol 32: 745-750.

Mesulam MM, Geula C (1991) Acetylcholinesterase-rich neurons of the human cerebral cortex: cytoarchitectonic and ontogenetic patterns of distribution. J Comp Neurol 306: 193-220.

Mezey G, Robbins I (2001) There but for the grace . . . Brit Med J 323: 56.

Millard CB, Broomfield CA (1995) Anticholinesterases: medical applications of neurochemical principles. J Neurochem 64: 1909-1918.

Monia BP (1997) First- and second-generation antisense oligonucleotide inhibitors targeted agains human c-raf kinase. Ciba Found Symp 209: 107-119.

Mor I, Grisaru D, Titelbaum L, Evron T, Richler C, Wahrman J, Sternfeld M, Yogev L, Meiri N, Seidman S, Soreq H (2001) Modified testicular expression of stress-associated "readthrough" acetylcholiensterase predicts male infertility. FASEB J 15: 2039-2041.

Moran D, Shapiro Y, Meiri U, Laor A, Epstein Y, Horowitz M (1996). Exercise in the heat: Individual impacts of heat acclimation and exercise training on cardiovascular performance. J Therm Biol 21: 171-181.

Moretto A (1998) Experimental and clinical toxicology of anticholinesterase agents. Toxicol Lett 102-103: 509-513.

Mrzljak L, Levey AI, Goldman-Rakic PS (1993) Association of m1 and m2 muscarinic receptor proteins with asymmetric synapses in the primate cerebral cortex: morphological evidence for cholinergic modulation of excitatory neurotransmission. Proc Natl Acad Sci USA 90: 5194-5198.

Mrzljak L, Pappy M, Leranth C, Goldman-Rakic PS (1995) Cholinergic synaptic circuitry in the macaque prefrontal cortex. J Comp Neurol 357: 603-617.

Mrzljak L, Levey AI, Goldman-Rakic PS (1998) Localization of the m2 muscarinic acetylcholine receptor protein and mRNA in cortical neurons of the normal and cholinergically deafferented rhesus monkey. J Comp Neurol 390: 112-132.

Muller TC, Rocha JB, Morsch VM, Neis RT, Schetinger MR (2002) Antidepressants inhibit human acetylcholinesterase and butyrylcholinesterase activity. Biochim Biophys Acta 1587: 92-98.

Munro S, Pelham HR (1986) An Hsp70-like protein in the ER: identity with the 78 kd glucose-regulated protein and immunoglobulin heavy chain binding protein. Cell 46: 291–300.

Murata J, Matsukawa K, Shimizu J, Matsumoto M, Wada T, Ninomiya I (1999) Effects of mental stress on cardiac and motor rhythms. J Auton Nerv Syst 75: 32-37.

Narahashi T (1996). Neuronal ion channels as the target sites of insecticides. Pharmacol Toxicol 79: 1-14.

Neri D, Carnemolla B, Nissim A, Leprini A, Querze G, Balza E, Pini A, Tarli L, Halin C, Neri P, Zardi L, Winter G (1997) Targeting by affinity-matured recombinant anti-body fragments of an angiogenesis associated fibronectin isoform. Nat Biotechnol 15: 1271–1275.

Neville LF, Gnatt A, Padan R, Seidman S, Soreq H (1990) Anionic site interactions in human butyrylcholinesterase disrupted by two single point mutations. J Biol Chem 265: 20735-20738.

Newport DJ, Nemeroff CB (2000) Neurobiology of posttraumatic stress disorder. Curr Opin Neurobiol 10: 211-218.

Nissim A, Hoogenboom HR, Tomlinson IM, Flynn G, Midgley C, Lane D, Winter G (1994) Antibody fragments from a "single pot" phage display library as immuno-chemical reagents. EMBO J 13: 692–698.

Noraberg J, Gramsbergen JBP, Fonnum F, Zimmer J (1998) Trimethyltin (TMT) neurotoxicity in organotypic rat hippocampal slice cultures. Brain Res 783: 305-315.

Nordberg A, Hellstrom-Lindahl E, Almkvist O, Meurling L (1999) Activity of acetylcholinesterase in CSF increases in Alzheimer's patients after treatment with tacrine. Alzheimer's Reports 2: 347-352.

Ohno K, Engel AG, Brengman J M, Shen XM, Heidenreich F, Vincent A, Milone M, Tan E, Demirci M, Walsh P, Nakano S, Akiguchi I (2000) The spectrum of mutations causing end-plate acetylcholinesterase deficiency. Ann Neurol 47: 162-170.

Ohno M, Frankland PW, Chen AP, Costa RM, Silva AJ (2001) Inducible, pharmacogenetic approaches to the study of learning and memory. Nat Neurosci 4: 1238-1243.

Ono Y, Kikkawa U, Ogita K, Fujii T, Kurokawa T, Asaoka Y, Sekiguchi K, Ase K, Igarashi, K, Nishizuka Y (1987) Expression and properties of two types of protein kinase C: alternative splicing from a single gene. Science 236: 1116-1120.

Ostlie NS, Karachunski PI, Wang W, Monfardini C, Kronenberg M, Conti-Fine BM (2001) Transgenic expression of IL-10 in T cells facilitates development of experimental myasthenia gravis. J Immunol 166: 4853-4862.

Panenic R, Gisiger V, Gardiner PF (1999) Fatigability of rat hindlimb muscles after acute irreversible acetylcholinesterase inhibition. J Appl Physiol 87: 1455–1462.

Paola D, Domenicotti C, Nitti M, Vitali A, Borghi R, Cottalasso D, Zaccheo D, Odetti P, Strocchi P, Marinari UM, Tabaton M, Pronzato MA (2000) Oxidative stress induces increase in intracellular amyloid beta-protein production and selective activation of betaI and betaII PKCs in NT2 cells. Biochem Biophys Res Commun 268: 642-646.

Parnas H, Segal L, Dudel J, Parnas I (2000) Autoreceptors, membrane potential and regulation of transmitter release. Trends Neurosci 23: 60-68.

Perio A, Terranova JP, Worms P, Bluthe RM, Dantzer R, Biziere K (1989) Specific modulation of social memory in rats by cholinomimetic and nootropic drugs, by benzodiazepine inverse agonists, but not by psychostimulants. Psychopharmacology 97: 262-268.

Seidman S, Eckstein F, Grifman M, Soreq H (1999) Antisense technologies have a future fighting neurodegenerative diseases. Antisense Nucleic Acid Drug Dev 9: 333-340.

Perrier AL, Massoulie J, Krejci E (2002) PRiMA: the membrane anchor of acetylcholinesterase in the brain. Neuron 33: 275-285.

Perry E, Walker M, Grace J, Perry R (1999) Acetylcholine in mind: a neurotransmitter correlate of consciousness? Trends Neurosci 22: 273-280.

Persic L, Horn IR, Rybak S, Cattaneo A, Hoogenboom HR, Bradbury A (1999) Single-chain variable fragments selected on the 57–76 p21Ras neutralising epitope from phage antibody libraries recognise the parental protein. FEBS Lett 443: 112–116.

Price DL, Koliatsos VE, Clatterbuck RC (1993) Cholinergic systems: human diseases, animal models, and prospects for therapy. Prog Brain Res 98: 51-60.

Qian J, Saggau P (1997) Presynaptic inhibition of synaptic transmission in the rat hippocampus by activation of muscarinic receptors: involvement of presynaptic calcium influx. Br J Pharmacol 122: 511-519.

Quartermain D, Stone EA Charbonneau G (1996) Acute stress disrupts risk assessment behavior in mice. Physiol Behav 59: 937-940.

Raichle ME, Hartman BK, Eichling JO, Sharpe LG (1975) Central noradrenergic regulation of cerebral blood flow and vascular permeability. Proc Natl Acad Sci USA 72: 3726-3730.

Ray D (1998) *Organophosphorus esters: An evluation of chronic neurotoxic effects*. IEH Publication.

Ray SK, Matzelle DD, Wilford GG, Hogan EL, Banik NL (2001) Cell death in spinal cord injury (SCI) requires de novo protein synthesis. Calpain inhibitor E-64-d provides neuroprotection in SCI lesion and penumbra. Ann NY Acad Sci 939: 436–449.

Razon N, Soreq H, Roth E, Bartal A, Silman I (1984) Characterization of activities and forms of cholinesteraes in primary brain tumors. Exp Neurol 84: 681–695.

Renwick PJ, Renwick PJ, Birley AJ, Hulten MA (1997) Study of Alu sequences at the hypoxanthine phosphoribosyltranscferase (hprt) encoding region of man. Gene 184: 155–163.

Rhodin J, Thomas T, Bryant M, Clark L, Sutton ET (1999) Animal model of vascular inflammation. J Submicrosc Cytol Pathol 31: 305-311.

Robbins J, Dilworth SM, Laskey RA, Dingwall C (1991) Two independent basic domains in nucleoplasmin nuclear targetting sequence: Identification of a class of bipartite nuclear targeting sequence. Cell 64: 615–623.

Robinson JS, Moody RA (1980). Influence of respiratory stress and hypertension upon the blood-brain barrier. J Neurosurg 53: 666-673.

Roden LD, Myzka D (1996) Global analysis of a macromolecular interaction measured on BIAcore. Biochem Biophys Res Commu 225: 1073–1077.

Rodriguez MM, Ron D, Touhara K, Chen CH, Mochly-Rosen D (1999) RACK1, a protein kinase C anchoring protein, coordinates the binding of activated protein kinase C and select pleckstrin homology domains in vitro. Biochemistry 38: 13787-13794.

Roman-Goldstein S, Clunie DA, Stevens J, Hogan R, Monard J, Ramsey ., Neuwelt EA (1994) Osmotic blood-brain barrier disruption: CT and radionuclide imaging. AJNR. Am. J. Neuroradiol 15: 581-590.

Ron D, Jiang Z, Yao L, Vagts A, Diamond I, Gordon A (1999) Coordinated movement of RACK1 with activated betaIIPKC. J Biol Chem, 274: 27039-27046.

Ron D, Vagts AJ, Dohrman DP, Yaka R, Jiang Z, Yao L, Crabbe J, Grisel JE, Diamond I (2000) Uncoupling of betaIIPKC from its targeting protein RACK1 in response to ethanol in cultured cells and mouse brain. FASEB J 14: 2303-2314.

Rosen BP (1995) Resistance mechanism to arsenicals and antimonials. J Basic Clin Physiol Pharmacol 6: 251–263.

Rossi SG, Rotundo RL (1993) Localization of "non-extractable" acetylcholinesterase to the vertebrate neuromuscular junction. J Biol Chem 268: 19152-19159.

Rossman TG, Wang Z (1999) Expression cloning for arsenite-resistance resulted in isolation of tumor-suppressor fau cDNA: possible involvement of the ubiquitin system in arsenic carcinogenesis. Carcinogenesis 20: 311–316.

Rotundo RL (1990) Nucleus-specific translation and assembly of acetylcholinesterase in multinucleated muscle cells. J Cell Biol 110: 715-719.

Rubin LL, Staddon JM (1999) The cell biology of the blood-brain barrier. Annu Rev Neurosci 22: 11-28.

Ryabinin AE, Wang YM, Finn DA (1999) Different levels of Fos immunoreactivity after repeated handling and injection stress in two inbred strains of mice. Pharmacol Biochem Behav 63: 143-151.

Salpeter MM, Rogers AW, Kasprzak H, Mchenry FA (1978) Acetylcholinesterase in the fast extraocular muscle of the mouse by light and electron microscope autoradiography. J Cell Biol 78: 274-85.

Sanchez-Amate M, Flores P, Sanchez-Santed F (2001) Effects of chlorpyrifos in the plus-maze model of anxiety. Behav Pharmacol 12: 285-292.

Sapolsky RM (1996) Why stress is bad for your brain. Science 273: 749-750.

Sapolsky RM, Romero LM, Munck AU (2000) How do glucocorticoids influence stress responses? Endocr Rev 21: 55-89.

Scanziani M, Gahwiler BH, Thompson SM (1995) Presynaptic inhibition of excitatory synaptic transmission by muscarinic and metabotropic glutamate receptor activation in the hippocampus: are Ca2+ channels involved? Neuropharmacol 34: 1549-1557.

Schneider LS (2001) Treatment of Alzheimer's disease with cholinesterase inhibitors. Clin Geriatr Med 17: 337–358.

Schramm M, Eimerl S, Costa E (1990) Serum and depolarizing agents cause acute neurotoxicity in cultured cerebellar granule cells. Proc Natl Acad Sci USA 87: 1193-1197.

Schultze N, Burki Y, Lang Y, Certa U, Bluethmann H (1996) Efficient control of gene expression by single step integration of the tetracycline system in transgenic mice. Nature Biotech 14: 499-503.

Schwartzkroin PA, Baraban SC, Hochman DW (1998) Osmolarity, ionic flux, and changes in brain excitability. Epilepsy Res 32: 275-285.

Schwarz M, Loewenstein-Lichtenstein Y, Glick D, Liao J, Norgaard-Pedersen B, Soreq H (1995) Successive orgnophosphate inhibition and oxime reactivation reveals distinct responses of recombinant human cholinesterase variants. Mol Brain Res 31: 101-110.

Seeger T, Alzheimer C (2001) Muscarinic activation of inwardly rectifying K(+) conductance reduces EPSPs in rat hippocampal CA1 pyramidal cells. J Physiol 535: 383-396.

Segal M (1982). Multiple action of acetylcholine at a muscarinic receptor studied in the rat hippocampal slice. Brain Res 246: 77-87.

Seidman S, Sternfeld M, Ben Aziz Aloya R, Timberg R, Kaufer Nachum D, Soreq H (1995) Synaptic and epidermal accumulations of human acetylcholinesterase are encoded by alternative 3'-terminal exons. Mol Cell Biol 15: 2993-3002.

Sekiguchi R, Wolterink G. van Ree JM (1991) Short duration of retroactive facilitation of social recognition in rats. Physiol Behav 50: 1253-1256.

Senanayake N, Sanmuganathan PS (1995) Extrapyramidal manifestations complicating organophosphorus insecticide poisoning. Hum Exp Toxicol 14: 600-604.

Shannon HE, Peters SC (1990) A comparison of the effects of cholinergic and dopaminergic agents on scopolamine-induced hyperactivity in mice. J Pharmacol Exp Ther 255: 549-553.

Shapira M, Seidman S, Livni N, Soreq H (1998) In vivo and in vitro resistance to multiple anticholinesterases in Xenopus laevis tadpoles. Toxicol Lett 28: 205–209.

Shapira M, Tur-Kaspa I, Bosgraaf L, Livni N, Grant AD, Grisaru D, Korner M, Ebstein RP, Soreq H. (2000) A transcription-activating polymorphism in the ACHE promoter associated with acute sensitivity to anti-acetylcholinesterases. Hum Mol Genet 9:1273-1281.

Shapira M, Glick D, Gilbert JP, Soreq H (2001). Autism, stress and chromosome 7 genes. In: *The Research Basis of Autism Intervention*, Schloper E, Marcus L, Shulman C and Yirmiya N (eds). Kluwer Academic/Plenum Publishers, New York, pp. 103-113.

Sharabi Y, Danon YL, Berkenstadt H, Almog S, Mimouni-Bloch A, Zisman A, Dani S, Atsmon J (1991) Survey of symptoms following intake of pyridostigmine during the Persian Gulf war. Isr J Med Sci 27: 656-658.

Sharma HS, Kretzschmar R, Cervos-Navarro J, Ermisch,A, Ruhle HJ, Dey PK (1992) Age-related pathophysiology of the blood-brain barrier in heat stress. Prog Brain Res 91: 189-196.

Shohami E, Kaufer D, Chen Y, Seidman S, Cohen O, Ginzberg D, Melamed-Book N, Yirmiya R, Soreq H (2000) Antisense prevention of neuronal damages following head injury in mice. J Mol Med 78: 228-236.

Siegal T, Rubinstein R, Bokstein F, Schwartz A, Lossos A, Shalom E, Chisin R,Gomori JM (2000) In vivo assessment of the window of barrier opening after osmotic blood-brain barrier disruption in humans. J Neurosurg 92: 599-605.

Sinton CM, Fitch TE, Petty F, Haley RW (2000) Stressful manipulations that elevate corticosterone reduce blood-brain barrier permeability to pyridostigmine in the rat. Toxicol Appl Pharmacol 165: 99-105.

Sirevaag AM, Black JE, Greenough WT (1991) Astrocyte hypertrophy in the dentate gyrus of young male rats reflects variation of individual stress rather than group environmental complexity manipulations. Exp Neurol 111: 74-79.

Skoog I, Wallin A, Fredman ., Hesse C, Aevarsson O, Karlsson I, Gottfries CG, Blennow K (1998) A population study on blood-brain barrier function in 85-year-olds: relation to Alzheimer's disease and vascular dementia. Neurology 50: 966-971.

Slutsky I, Silman I, Parnas I, Parnas H (2001) Presynaptic M(2) muscarinic receptors are involved in controlling the kinetics of ACh release at the frog neuromuscular junction. J Physiol 536: 717-25.

Smith TF, Gaitatzes C, Saxena K, Neer EJ (1999) The WD repeat: a common architecture for diverse functions. Trends Biochem Sci 24: 181-185.

Sokolov MV, Kleschevnikov AM (1995) Atropine suppresses associative LTP in the CA1 region of rat hippocampal slices. Brain Res 672: 281-284.

Solberg Y, Belkin M (1997) The role of excitotoxicity in organophosphorous nerve agents central poisoning. Trends Pharmacol Sci 18: 183-185.

Soreq H, Glick D (2000) Novel roles for cholinesterases in stress and inhibitor responses. In: Giacobini E (ed) *Cholinesterases and Cholinesterase Inhibitors: Basic, Preclinical and Clinical Aspects*. Martin Dunitz, London, pp 47–61.

Soreq H, Seidman S (2001) Acetylcholinesterase - new roles for an old actor. Nat Rev Neurosci 2: 294-302.

Soreq H, Zakut H (1993)

Soreq H, Zevin-Sonkin D, Razon N (1984) Expression of cholinesterase gene(s) in human brain tissues. EMBO J 3: 1371-1375.

Soreq H, Kaufer D, Friedman A, Glick D (2001) Blood-brain barrier modulations and low-level exposure to xenobiotics. In Somani SM, Romano JA (eds.), *Chemical Warfare Agents: Low Level Toxicity*, CRC Press, Boca Raton, FL, pp. 121-144.

Starke K, Gothert M, Kilbinger H (1989) Modulation of neurotransmitter release by presynaptic autoreceptors. Physiol Rev 69: 864-989.

Steenbergen HL, Heinsbroek RP, Van Hest A, Van de Poll NE (1990) Sex-dependent effects of inescapable shock administration on shuttlebox- escape performance and elevated plus-maze behavior. Physiol Behav 48: 571-576.

Sternfeld M, Ming G, Song H, Sela K, Timberg R, Poo M, Soreq H (1998) Acetylcholinesterase enhances neurite growth and synapse development through alternative contributions of its hydrolytic capacity, core protein, and variable C termini. J Neurosci 18: 1240-1249.

Sternfeld M, Shoham S, Klein O, Flores-Flores C, Evron T, Idelson GH, Kitsberg D, Patrick JW, Soreq H (2000). Excess "readthrough" acetylcholinesterase attenuates but the "synaptic" variant intensifies neurodeterioration correlates. Proc Natl Acad Sci USA 97: 8647-8652.

Steward O, Schuman EM (2001) Protein synthesis at synaptic sites on dendrites Annu Rev Neurosci 24: 299-325.

Steward O, Wallace CS, Lyford GL, Worley PF (1998) Synaptic activation causes the mRNA for the IEG Arc to localize selectively near activated postsynaptic sites on dendrites. Neuron 21: 741-751.

Sudweeks SN, Yakel JL (2000) Functional and molecular characterization of neuronal nicotinic ACh receptors in rat CA1 hippocampal neurons. J Physiol 527: 515-528.

Suer C, Dolu N, Ozesmi C, Yilmaz A, Sahin O (1998) Effect of reversed light-dark cycle on skin conductance in male rats. Percept Mot Skills 87: 1267-1274.

Tainer JA, Getzoff ED, Alexander H, Houghten RA, Olson AJ, Lerner RA, Hendrickson WA (1984) The reactivity of anti-peptide antibodies is a function of the atomic mobility of sites in a protein. Nature 312: 127–134.

Takumi Y, Ramirez-Leon V, Laake P, Rinvik E, Ottersen OP (1999) Different modes of expression of AMPA and NMDA receptors in hippocampal synapses. Nat Neurosci 2: 618-624.

Tarrab-Hazdai R, Aharonov A, Silman I, Fuchs S, Abramsky O (1975) Experimental autoimmune myasthenia induced in monkeys by purified acetylcholine receptor. Nature 256: 128-130.

Tator CH, Schwartz ML (1971) Permeability in brain tumors. J Neurosurg 34: 460-462.

Tavitian B, Terrazzino S, Kuhnast B, Marzabal S, Stettler O, Dolle F, Deverre J, Jobert A, Hinnen F, Bendriem B, Crouzel C, Di Giamberardino L (1998) In vivo imaging of oligonucleotides with positron emission tomography. Nat Med 4: 467-471.

Taylor MC, Le Couteur DG, Mellick GD, Board PG. (2000) Paraoxonase polymorphisms, pesticide exposure and Parkinson's disease in a Caucasian population. J Neural Transm 107: 979-983.

Thomas MK, Devon ON, Lee JH, Peter A, Schlosser DA, Tenser MS, Habener J (2001) Development of diabetes mellitus in aging transgenic mice following suppression of pancreatic homeoprotein IDX-1. J Clin Invest 108: 319-329.

Thor DH, Holloway WR (1982) Social memory of the male laboratory rat. J Comp Psychol 96: 1000-1006.

Thornton JM, Edwards MS, Taylor WR, Barlow DJ (1986) Location of "continuous" antigenic determinants in the protruding regions of proteins. EMBO J 5: 409–413.

Thybusch-Bernhardt A, Aigner A, Beckmann S, Czubayko F, Juhl H (2001) Ribozyme targeting of HER-2 inhibits pancreatic cancer cell growth in vivo. Eur J Cancer 37: 1688-1694.

Tomlinson IM, Walter G, Marks JD, Llewelyn MB, Winter G (1992) The repertoire of human germline VH sequences reveals about fifty groups of V_H segments with different hypervariable loops. J Mol Biol 227: 776–798.

Traub RD, Borck C, Colling SB, Jefferys JG. (1996) On the structure of ictal events in vitro. Epilepsia 37: 879-891.

Triguero D, Lopez de Pablo AL, Gomez B, Estrada C (1988) Regional differences in cerebrovascular cholinergic innervation in goats. Stroke 19: 736-740.

Tronche F, Kellendonk C, Kretz O, Gass P, Anlag K, Orban P, Bock R, Klein R, Schutz G (1999) Disruption of the glucocorticoid receptor gene in the nervous system results in reduced anxiety. Nat Genet 23: 99-103.

Trullas R, Skolnick P (1993) Differences in fear motivated behaviors among inbred mouse strains. Psychopharmacol 111: 323-331.

Tsubokawa H, Ross WN (1997) Muscarinic modulation of spike backpropagation in the apical dendrites of hippocampal CA1 pyramidal neurons. J Neurosci 17: 5782-5791.

Van Amsterdam JG Opperhuizen A (1999) Nitric oxide and biopterin in depression and stress. Psychiatry Res 85: 33-38.

Van Lunteren E, Moyer M (1996) Effects of DAP on diaphragm force and fatigue, including fatigue due to neurotransmission failure. J Appl Physiol 81: 2214-2220.

Vaughan TJ, Williams AJ, Pritchard K, Osbourn JK, Pope AR, Earnshaw JC, McCafferty J, Hodits RA, Wilton J, Johnson KS (1996) Human antibodies with sub-nanomolar affinities isolated from a large non-immunized phage display library. Nat Biotechnol 14: 309–314.

Vays I, Heikkila RE, Nicklas WJ (1986) Studies on the neurotoxicity of 1-methyl-4-phenyl-1,2,3,6-tetrahydropyridine:inhibition of NAD-linked substrate oxidation by its metabolite,1-methyl-4-phenylpyridinium.J Neurochem 46: 1501-1507.

Victor M, Ropper AH (2001) *Adams and Victor's Principles of Neurology*. McGraw-Hill, New York.

Vincent A (1983). Acetylcholine receptors and myasthenia gravis. Clin Endocrinol Metab 12, 57-78.

Vincent A (1999). Immunology of the neuromuscular junction and presynaptic nerve terminal. Curr Opin Neurol 12: 545-551.

Vingerhoets FJG, Snow BJ, Tetrud JW, Langston JW, Schulzer M, Calne DB (1994) Positron emission tomographic evidence for progression of human MPTP-induced dopaminergic lesions. Ann Neurol 36: 765-770.

Wallace CS, Lyford GL, Worley PF, Steward O (1998) Differential intracellular sorting of immediate early gene mRNAs depends on signals in the mRNA sequence J Neurosci 18: 26-35.

Wang J, Liu Z (2000) No association between paraoxonase 1 (PON1) gene polymorphisms and susceptibility to Parkinson's disease in a Chinese population. Mov Disord 15: 1265-1267.

Wang Z, Rossman TG (1993) Stable and inducible arsenite resistance in Chinese hamster cells. Toxicol Appl Pharmacol 118: 80–86.

Weeber EJ, Atkins CM, Selcher JC, Varga AW, Mirnikjoo B, Paylor R, Leitges M, Sweatt, JD (2000) A role for the beta isoform of protein kinase C in fear conditioning. J Neurosci, 20: 5906-5914.

Weiner MF, Vobach S, Olsson K, Svetlik D, Risser RC (1997) Cortisol secretion and Alzheimer's disease progression. Biol Psychiatry 42: 1030-1038.

Wilson IB, Silman I (1977) Effects of quaternary ligands on the inhibition of acetylcholinesterase by arsenite. Biochemistry 16: 2701–2708.

Winslow JT, Camacho F (1995) Cholinergic modulation of a decrement in social investigation following repeated contacts between mice. Psychopharmacology (Berl) 121: 164-172.

Wirguin I, Brenner T, Sicsic C, Argov Z (1994) Variable effect of calcium channel blockers on the decremental response in experimental autoimmune myasthenia gravis. Muscle Nerve 17: 523-527.

Wirth T, Soeth E, Czubayko F, Juhl H. (2002) Inhibition of endogenous carcinoembryonic antigen (CEA) increases the apoptotic rate of colon cancer cells and inhibits metastatic tumor growth. Clin Exp Metastasis 19: 155-160.

Wright CI, Geula C, Mesulam MM (1993) Neurological cholinesterases in the normal brain and in Alzheimer's disease: relationship to plaques, tangles, and patterns of selective vulnerability. Ann Neurol 34: 373–384.

Xie J, McCobb DP (1998) Control of alternative splicing of potassium channels by stress hormones. Science 280: 443-446.

Yaka R, Thornton C, Vagts A, Phamluong K, Bonci A, Ron D (2002) NMDA receptor function is regulated by the inhibitory scaffolding protein, RACK1. Proc Natl Acad Sci USA 99: 5710-5715.

Yarwood SJ, Steele MR, Scotland G, Houslay MD Bolger GB (1999) The RACK1 signaling scaffold protein selectively interacts with the cAMP-specific phosphodiesterase PDE4D5 isoform. J Biol Chem 274: 14909-14917.

Ye Y, Meyer H, Rapoport T (2001) The AAA ATPase Cdc48/p97 and its partners transport proteins from the ER into the cytosol. Nature 414: 652-656.

Yirmiya R, Barak O, Avitsur R, Gallily R, Weidenfeld J (1997) Intracerebral administration of Mycoplasma fermentans produces sickness behavior: role of prostaglandins. Brain Res 749: 71-81.

Zakut H, Ehrlich G, Ayalon A, Prody CA, Malinger G, Seidman S, Kehlenbach R, Ginzberg D, Soreq H. (1990) Acetylcholinesterase and butyrylcholinesterase genes coamplify in primary ovarian carcinomas. J Clin Invest 86: 900–908.

Zhang GX, Xiao BG, Bai XF, van der Meide PH, Orn A, Link H (1999) Mice with IFN-gamma receptor deficiency are less susceptible to experimental autoimmune myasthenia gravis. J Immunol 162: 3775-3781.

4 Blood-Brain Barrier Modulations and Low-Level Exposure to Xenobiotics

Hermona Soreq, Daniela Kaufer, Alon Friedman, and David Glick

CONTENTS

I. Introduction 122
II. The Physical Basis of Blood-Brain Barrier Properties 122
A. Endothelial Cells in Brain Vasculature 123
B. Adherens and Tight Junctions 124
C. Potential Involvement of Acetylcholinesterase 124
D. Signal-Transducing Elements 126
E. Astrocyte Contributions to Blood-Brain Barrier Properties 128
III. Functional Characteristics of the Blood-Brain Barrier 128
A. Inward and Outward Movement across the Blood-Brain Barrier: Physiological Considerations 128
B. Cholinergic Involvement in Blood-Brain Barrier Functioning 129
C. Pericellular Passage across Blood-Brain Barrier Structures 129
D. Cell Culture, Organ Systems, and Imaging Approaches in Blood-Brain Barrier Research 130
E. Transgenic Engineering Models for Blood-Brain Barrier Studies 131
IV. Modulators of Blood-Brain Barrier Functions and Their Interrelationships 132
A. Nitric Oxide and Vasoactive Agents Involvement 133
B. Immunomodulators and Multi-Drug Transporters 133
V. Conditions Inducing Blood-Brain Barrier Distruption 134
A. Pathophysiological Induction of Blood-Brain Barrier Penetrance 134
B. Blood-Brain Barrier Disruption Following Acute Insults 135
C. Psychological and Physical Stressors Impair Blood-Brain Barrier Functioning 135

0-8493-0872-0/01/$0.00+$.50

D. Blood-Brain Barrier as a Complex Trait with Genetic and Physiological Components: Prospects 136
VI. Summary 137
Acknowledgments 138
References 138

I. INTRODUCTION

Separation of the brain from the peripheral blood is crucial for protecting this most delicate and important organ from various insidious agents that circulate in the blood. Conversely, the separation must allow for the nutrition of the brain and the removal from it of waste products. The existence of a physical barrier that separates the brain tissue from the general circulation was first proposed 100 years ago, by Ehrlich, who discovered that injection of a series of dyes into laboratory animals resulted in uncolored brains, as opposed to highly stained visceral organs.[1] The blood-brain barrier (BBB) is formed during the late embryonic and early postnatal period. It is an endothelial barrier present in the capillaries throughout the brain, contact-influenced by neighboring astrocytes.[2] Electron microscopic studies reveal two major factors that distinguish brain endothelial cells from their peripheral relatives: first, they contain lower amounts of endocytic vesicles, and second, the space between adjacent cells is sealed by tight junctions; both factors restrict intercellular flux. These features enable the formation of a barrier that hinders the entry of most xenobiotics into the brain, and is actively involved in exporting such substances from the brain when they do enter it. Small lipophilic molecules enter the brain fairly freely, but hydrophilic molecules enter via active transport, and specific transporters exist for required nutrients such as glucose, L-DOPA, and certain amino acids.[3]

The physical and functional complexity of the BBB has hampered research efforts to delineate its components and fully understand its mode of action. Numerous experimental approaches were developed for evaluating BBB integrity; these include *in vitro* and *in vivo* systems as well as transgenic engineering approaches. The use of these methods has revealed several modulators of BBB functioning and has demonstrated intricate relationships between these modulators in their effects on BBB integrity. Impairments of any element of these chains of factors can disrupt BBB functioning, but the extent and duration of such disruptions apparently depend on the genetics, health, and wellbeing of the involved organism. In the following, we discuss these considerations as they relate to the issue of low-level exposure to xenobiotics.

II. THE PHYSICAL BASIS OF BLOOD-BRAIN BARRIER PROPERTIES

Low-level exposure to xenobiotics would first affect the circulation; to affect the brain, the xenobiotic must traverse the BBB. In certain cases, e.g., under exposure to anticholinesterases, these agents interact with and inhibit the catalytic activity of their target enzymes, cholinesterases, in peripheral and brain systems alike. The cellular

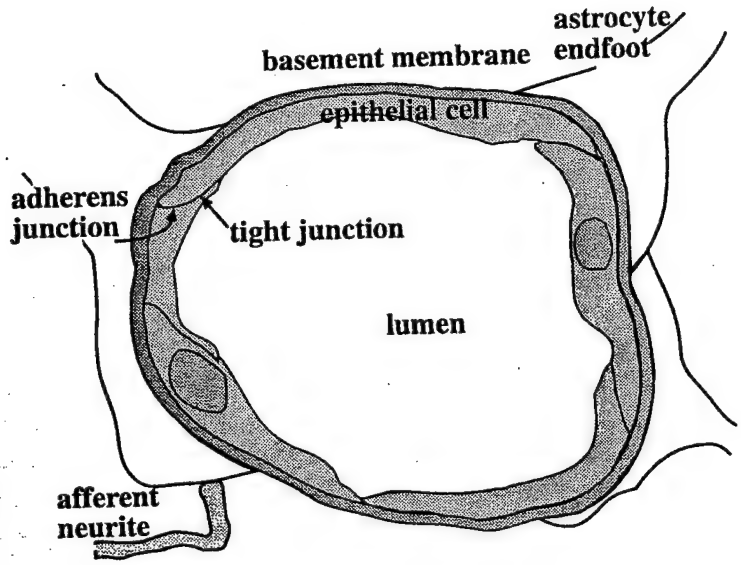

FIGURE 4.1 The physical components of the blood-brain barrier (BBB): Within the mammalian brain, blood vessels and microvessels transverse the brain tissue, bringing in essential compounds and removing metabolic end products. The three layers surrounding the microvessel lumen comprise the BBB, including endothelial cells lining the blood vessels, a basement membrane surrounding them, and astrocyte endfeet separating these structures from adjacent neurons, some of which interact with these astrocytes through contacting neurites. Two types of junctions connect endothelial cells to each other, tight and adherens junctions.

components of the BBB include the endothelial cells that line the inside of brain capillaries, the basement membrane surrounding them, and brain astrocytes, which constitute a third layer separating these blood vessels from the surrounding brain tissue. Intercellular BBB structures include adherens junctions, which attach endothelial cells to each other, as well as the tight junctions that seal them. Within these cells, surface membrane proteins transduce signals by activation of specific kinases, and the flow of information among the several cell types is affected by neuronal and astrocytic activities in the brain as well as by peripheral metabolic changes and external forces. Figure 4.1 presents a schematic view of these elements.

A. Endothelial Cells in Brain Vasculature

Many have reported the special properties of endothelial cells in brain vasculature.[4] Small hydrophobic molecules diffuse across the BBB; large and/or hydrophilic molecules may be transported only if a specific receptor or transporter exists. Thus, small hydrophobic molecules penetrate the brain by diffusion; nutrients such as glucose and certain amino acids are transported into the brain by specific transporters; and several large proteins like transferrin are transcytosed into the brain via specific receptors.

To enable these special properties, tight junctions connect brain endothelial cells, so that intercellular transport is extremely limited.[5] The expression of P glycoprotein

(the multi-drug resistance mdr protein) on their surface membrane controls both penetrance of small molecule drugs into the brain and their export from the brain. Genomic disruption of the mdrla (a.k.a. mdr3) gene causes extreme drug sensitivity, for example, to ivermectin.[6] This finding highlights the importance of active transport mechanisms for the integrity of BBB functioning and may imply that cumulative exposure can modulate BBB properties.

B. Adherens and Tight Junctions

A primary difference between endothelial cells of brain vasculature and the very similar cells that line peripheral blood cells relates to the composition and properties of the tight junctions between these cells.[7–10]

Adherens junctions are similar to the attachment structures of other cells in which their functions may be more easily studied on the molecular level. Yeast, for example, can express an analogue of the adherens junction, and its assembly was shown to depend upon the Ca^{++}-dependent protein kinase pathway.[11] Genetic studies in yeast are easy to perform, and since yeast has a well-described genome, the discovery of the genes that regulate junction formation is possible, and once the yeast gene is known, it is a relatively simple matter to discover its homologues in a mammalian genome.

Unlike adherens junctions, which form homophilic intercellular adhesion sites, tight junctions are complex structures recognized as being the molecular site of pericellular transport and its regulation.[12] In addition to adherens and tight junctions, brain capillary endothelial cells have transmembrane receptors for matrix proteins (e.g., integrins).[9] Impairment of either cell-cell or cell-matrix interactions can disrupt the BBB, in processes that parallel those of the peripheral endothelium. However, such impairments occur much less frequently in the brain.

Several proteins, including cingulin and occludin, were shown to be essential for the function of tight junctions.[13,14] More recently, junction-associated proteins such as Rho were reported to regulate tight junctions and perijunctional actin organization in polarized epithelia.[15] Junction proteins are physically linked to cytotskeletal elements such as actin or linking proteins like β-catenin in a manner subject to modulation by phosphorylation or dephosphorylation of specific kinases and phosphatases. This suggests a potential opening of tight junctions by kinase regulation, however, no experimental evidence is yet available to demonstrate such opening *in vivo*. Table 4.1 catalogs key proteins assumed to be associated with BBB junctions.

C. Potential Involvement of Acetylcholinesterase

Like yeast, for nearly a century the fruit fly *Drosophila melanogaster* has served as a model for genetics studies. With the introduction of genetic engineering and genomic databases, this has also become a powerful tool for the discovery of genes and gene products that participate in physiological functions. The identification of a physiological defect in the insect can be quickly traced to a specific gene, and the homologous sequence in the mammalian genome can then be identified, where it then serves as a candidate gene for the similar function in the mammal. For instance, a defect in

TABLE 4.1
Protein Components and Candidate Components of the Blood-Brain Barrier

Component	Intra/Extra Cellular[a]	Interaction Partners[b]	Reviewed in
7H6 antigen	Intra and extra	Tight junction	10
Acetylcholinesterase	Extra	Neurexin	16
Actin	Intra	Catenin	10
Band 4.1 protein	Intra	Cytoskeleton	16
Cadherin	Extra	Catenin, p120	10; 17
CASK[c]	Intra	Neurexin II β	16
β-catenin	Intra	Cadherin, actin	10
Cingulin	Intra	Tight junction	10
Gliotactin	Intra and extra	Neurexin IV	16
ICAM-1	Extra	ICAM	18
Neuoligin	Intra and extra	Neurexin II β	16
Neurexin	Intra and extra	Neuroligin 1, CASK	16
Nitzin	Intra	Cytoskeleton	16
Occludin	Extra	ZO-1/ZO-2/p130	10
p100	Intra	Cadhedrin	10; 19
p120	Intra	Cadherin/catenin	10; 17; 19
p130	Intra	Tight junction, ZO-1	10
PSD-95[d]	Intra	Neuroligin 1, NMDA receptor	20
RPTP[d]	Intra	Cadherin/catenin	10
Selectin	Extra		21
src	Intra	Adherens junction	10
Tyrosine kinase	Intra	ZO-1, β-catenin	10
ZO-1	Intra	Tight junction, p130, tyrosine kinase	10
ZO-2	Intra	Tight junction	10

[a]BBB components may function in extracellular locations (extra), convey signals within intracellular locations (intra), or do both.

[b]Independent factors to which attachment has been shown are separated by commas; aggregates of factors to which attachment has been shown are indicated by slashes.

[c]Post-synaptic density.

[d]Calmodulin-dependent protein kinase.

[d]Receptor-type protein tyrosine phosphatase.

the hemolymph-neuron barrier, which serves a function analogous to the BBB in mammals, was shown to depend on the structural and functional integrity of the special septate junctions, which seal this barrier in insect larva.[22,23] Disruption of these structures by genomic destruction of either of two different genes, neurexin IV and gliotactin, causes severe neuronal sensitivity to the high concentrations of K^+ in the hemolymph. This leads to paralysis and death of the developing insect larva. Such genomic disruption also impaired the subcellular targeting of coracle, a band 4.1 homologue that transduces signals from the cell membrane to the cytoskeleton.

Gliotactin is one of several structural homologues of the acetylcholine-hydrolyzing enzyme acetylcholinesterase (AChE) that were discovered in the past decade. Gliotactin, however, like the other AChE homologues, has no capacity for acetylcholine (ACh) hydrolysis. Intriguingly, AChE may compete with its structural homologues for their cell-cell interactions.[16,24] This potential involvement of AChE has raised the question of which of the three variants, formed by alternative splicing of the human AChE pre-mRNA, may be involved in these interactions. These variants are: AChE-S, the synaptic form, AChE-E, the erythrocyte form, and AChE-R, a soluble monomeric form which, perhaps significantly for BBB physiology, has been shown to be over-expressed under stress.[25]

Gliotactin, like several other AChE homologues, is equipped with an extracellular domain, a transmembrane peptide and C-terminal peptide that protrudes into the cytoplasm and can transduce signals into cells. In particular, it interacts with proteins, which modulate the cytoskeleton. Therefore, these discoveries present the entire series of AChE homologues and their yet unidentified binding partners as promising candidates to participate in control of the integrity of the BBB and transduction of signals that regulate its functioning. The impressive conservation of these inter- and intracellular factors, and the chain of interactions by which they may affect cytoskeletal properties, suggest at a mechanism by which AChE levels, and/or the specific chemical properties of its variants, affect the integrity of the BBB. Kaufer et al.[26] have recently discovered a feedback process that leads to AChE-R accumulation under exposure to anticholinesterases. This points to the AChE protein as a modulator that may be intimately involved in BBB disruption under exposure to such agents. That no embryonic impairment in BBB functioning is known in mammals most likely attests to the essential role played by the BBB in mammalian embryonic development, as early lethality of such a mutant would preclude its discovery. Figure 4.2 summarizes the evolutionary conservation of the structural properties of AChE as these may be involved in BBB integrity.

D. Signal-Transducing Elements

Appropriate functioning of the BBB and its capacity to respond to environmental insults evidently depend on fast, accurate, and sensitive transduction of appropriate signals from the periphery into the brain and vice versa. Over the past few years, several molecular components were discovered which ascertain such a flow of information and ensure its reliability. The role of guanine nucleotides in regulating BBB properties is of special interest. Endothelial capillary cells are polarized, being long and flat structures linked by tight junctions. GTP-Binding Rho proteins are responsible, in these cells, for the particular organization of the filamentous actin fibers that ensure their polarization.[15] Further, transduction of intracellular signals is based, in most polarized epithelial cells, primarily on PDZ domain proteins. Named for three members of this family, PDZ proteins include the post-synaptic density protein, PSD-95, the *Drosophila* tumor-suppressor protein, discs-large (DlgA), and the tight-junction protein, ZO-1; they are often found at the plasma membrane and transduce signals into the cell, affecting cytoskeletal organization.[27,28] That this is also the case

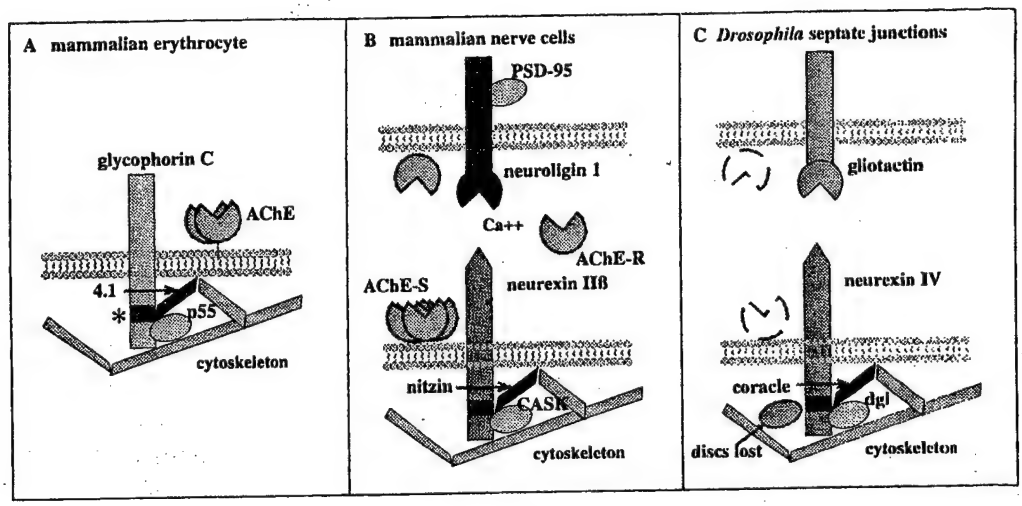

FIGURE 4.2 AChE and its structural homologues are potentially involved in BBB functioning. Shown are schematic drawings of membrane signaling and cytoskeletal components which involve AChE and its structural homologues. (A) In the mammalian erythrocyte, glycophorin C is located on the surface membrane, with one domain protruding into the cytoplasm. A conserved element within this domain (starred) interacts with the band 4.1 protein that serves as an anchor to the cytoskeleton. Another region in the cytoplasmic domain of glycophorin C binds p55, a PDZ protein. It is not yet known whether the AChE-E dimers, which are anchored by a glycophosphoinositol moiety to the outer surface of the erythrocyte membrane, are involved in glycophorin's role of modulating the erythrocyte structure. (B) In mammalian nerve cells, the major AChE isoform is AChE-S tetramers. The AChE-homologous neuronal membrane proteins, neuroligins, are expressed in the developing brain and in excitatory synapses. At least one of the neuroligins, neuroligin 1, interacts with at least one of the neurexins, neurexin II β, in a Ca^{++}-dependent manner. Both neuroligin and neurexin protrude into the cytoplasm, and both interact with PDZ proteins such as PSD-95 and CASK. Neurexins further associate with neuronal band 4.1 homologues, like nitzin,[16] creating a link with the cytoskeleton. Modulation of AChE properties under low-level exposure to an anticholinesterase (e.g., accumulation of AChE-R monomers) may therefore alter neuroligin-neurexin interactions, transducing signals to the neuronal cytoskeleton. (C) In *Drosophila* septate junctions, the AChE-homologous protein, gliotactin, protrudes into the cytoplasm. Another transmembrane protein, neurexin IV, shares with other neurexins an extracellular domain that may interact with the core domain module that is common to AChE and neuroligins. Neurexin IV also includes cytoplasmic glycophorin C elements; these regions intact with the insect band 4.1 homologue, coracle, as well as with the PDZ protein dg1 and the multi-PDZ domain protein, disc lost. Therefore, neurexin IV interactions with either gliotactin or the cytoskeleton are essential for maintaining septate junction integrity. It is not yet known whether AChE itself (broken-line structure) is expressed in these junctions.

for BBB components has recently been demonstrated in *Drosophila* embryos by Bellen and co-workers, who found a third protein that is essential for the integrity of septate junctions formation.[29] This protein, discs-lost, uses multiple PDZ domains to interact with intracellular components in a manner dependent on septate junction interactions. In general, PDZ domains interact with the carboxy terminal end of their

target proteins.[27] Therefore a multi-PDZ protein can aggregate a series of target proteins within the cell, simultaneously transducing multiple signals.[29] This enables an extremely sensitive biosensor activity, as is expected from a system designed to protect the brain from low-level exposures.

E. Astroycyte Contributions to Blood-Brain Barrier Properties

Janzer and Raff recognized the key function of astrocytes that surround brain capillaries in the dynamic properties of the BBB.[30] Specific interactions between astrocyte endfeet, which surround brain capillaries, are essential to ensure BBB integrity. The discovery of astrocytic responses to altered ion (e.g., Ca^{++}) concentrations in their environment sheds new light on the specificity of astrocyte interactions and their importance for ensuring BBB integrity.[31] In a tissue co-culture model, astrocytes were shown to affect the integrity of the tight junctions between adjacent endothelial cells.[32] More recently, astrocytes were demonstrated to enhance the defense of capillary endothelial cells against reactive oxygen species.[33] Thus, astrocytes both signal higher centers of the brain that the BBB has been disrupted and themselves receive signals from higher centers that cause them to modulate the BBB.

III. FUNCTIONAL CHARACTERISTICS OF THE BLOOD-BRAIN BARRIER

Designed to protect the brain from penetrance and accumulation of unwanted molecules and cells, the BBB has distinct properties at central and peripheral structures. To properly control the inward and outward flow of constituents to and from the brain, it must sense the needs of both the brain and the peripheral system. Therefore, both the electrophysiological activity in the brain and peripheral properties such as blood pressure must affect BBB properties. Similarly, changes in BBB integrity inevitably affect brain functioning; for example, BBB disruption will allow the passage into the brain of serum constituents, which are known to affect neuronal electric activity (e.g., amino acids). The relative contribution of such agents to brain function under BBB disruption awaits further investigation.

A. Inward and Outward Movement across the Blood-Brain Barrier: Physiological Considerations

Blood-brain barrier properties largely depend on the surrounding brain tissue. This is evident from a recent study that demonstrated the development of an intact BBB in brain tissue transplants in a manner dependent on the site of transplantation.[34] The integrity of BBB functioning is affected by cellular glutathione and is sensitive to oxidative stress.[35] Neuronal activity is another important factor in BBB functioning, perhaps through the activation of afferent axons innervating brain microvasculature. Indeed, both psychotropic drugs and nicotine impair dopamine transport across the BBB,[36] suggesting that BBB functioning is affected by the state of cholinergic or

dopaminergic neuronal activity, and that BBB integrity is imperative for preventing neurotoxicity under exposure to dopamine analogs (e.g., MPTP).[37] Thus, human cerebromicrovascular endothelium was shown to possess dopaminergic receptors linked to adenylyl cyclase, suggesting signal transduction activities. Adrenergic influences on BBB control were reported by Sarmento et al.,[38] who also demonstrated the influence of electrical stimulation of locus coeruleus on the rat BBB permeability to sodium fluorescein. Similar effects in a cell culture model were shown by Borges.[39]

B. Cholinergic Involvement in Blood-Brain Barrier Functioning

The importance of ACh innervation to cortical capillaries has been suggested on the basis of a body of biochemical and morphological data, and indicates the underlying mechanism. Purified capillaries are capable of releasing ACh in a Ca^{++}-dependent mechanism, in response to K^+ depolarization or electrical stimulation.[40] Moreover, specific cholinergic machinery was identified in isolated microvessels from goat cerebral cortex, as demonstrated by measuring AChE and choline acetyl transferase (ChAT) activities.[41] ChAT activity in bovine cerebral cortex capillaries does not originate from the endothelial cells, nor do they release ACh in response to electrical stimulation. Rather, cerebrovascular ACh apparently has a neuronal origin.[40] The origin of the perivascular cholinergic terminals was examined in rat brains in which the nucleus basalis of Mynert, accounting for 70% of cortical ChAT activity, was lesioned. No change was observed in the microvessel-associated ChAT activity in the lesioned animals, ruling out the basal forebrain as the origin of this pathway.[40] The existence of released ACh hints at the presence of receptors that respond to the signal, and, indeed, muscarinic ACh receptors were identified in rat brain cortical capillaries.[42,43] Taken together, all this points to the involvement of cholinergic innervation of cerebral microvessels in cerebral blood flow and BBB permeability, which is an essential requirement under various physiological and pathological insults. The cholinergic involvement in BBB functioning is particularly important under exposure to cholinesterase inhibitors such as organophosphates or carbamates, since these induce a feedback response of AChE accumulation, which would lead to cholinergic hypo-functioning.[26,44] Therefore, AChE may affect BBB disruption through two interrelated mechanisms, which involve its catalytic capacity for ACh hydrolysis or its structural resemblance to gliotactin, neuroligins, or related proteins.[20,29]

C. Pericellular Cell Passage across Blood-Brain Barrier Structures

One of the roles of the BBB likely involves protection of the brain from invasive bacteria, viruses, and fungi. However, when under BBB disruption any of these parasites invades the brain, the immune system must respond. This implies that under certain conditions, lymphocytes cross the BBB and reach those sites in the brain where their protective functions are needed. The existence of tight junctions between endothelial

cells in brain vasculature complicates this process and requires specific signaling to ensure the specificity of the pericellular transport. Also, the endothelial monolayer needs to be re-sealed once this transport has been completed. A recent study demonstrates that lymphocyte migration through brain endothelial cell monolayers involves signaling through endothelial I-CAM-1 via a Rho-dependent pathway, thus expanding the list of BBB-involved molecules.[18]

Mast cells represent another cell type that might penetrate the brain through BBB structures. This is of considerable importance because of the key role of mast cells in autoimmune demyelinating diseases.[45–47] When interacting with myelin basic protein, mast cells degranulate to induce by exocytosis immediate demyelination.[48,49] Under normal circumstances mast cells are located in leptomeninges and are concentrated along blood vessels, especially in dorsal thalamic nuclei.[50] Exposure to steroid hormones induces in mast cells massive secretion of, for example, histamine.[51] Several of the other neuromodulators, neurotransmitters, and growth factors secreted by mast cells can alter BBB properties.[52] Using confocal microscopy and vital dyes, Silverman et al.[53] very recently demonstrated rapid penetrance of mast cells through BBB structures into nests of glial processes. This transport may account for the rapid increases in mast cell populations after physiological manipulations.

D. Cell Culture, Organ Systems, and Imaging Approaches in Blood-Brain Barrier Research

The complexity and plasticity of BBB properties called for experimental dissection of the disruption process in both *in vitro* and *in vivo* conditions. Multiple cell and organ cultures, animal models, and measurement techniques have been developed, each of which addresses some of the issues involved. The development of research into BBB characteristics was initially approached in avian embryos, where transplanted endothelial quail cells invaded a developing chick chimera.[54] A simpler cell culture model of the BBB was developed by Rubin and co-workers.[55] More recently, an immortalized cell line created from vascular endothelial cells was used to develop another model of the BBB in co-cultures with glioma cells and was used to demonstrate nitric oxide-induced perturbations of these cells.[56] In another cell culture model, hypoxia was shown to increase the susceptibility to oxidative stress and intercellular permeability.[57]

Measurements of Evans blue penetrance proved useful in analyzing BBB properties in animal models.[58] Recent technological breakthroughs in brain imaging now offer a previously impossible view into the integrity of human BBB under various conditions. Imaging the human brain is widely used in the clinical and research settings by two major methods: (1) computerized tomography (CT) and (2) magnetic resonance imaging (MRI). In both methods, standard techniques use contrast agents to enhance signals and unmask brain pathologies. Both approaches are therefore aimed at delineation of the site, duration, and extent of potential BBB disruption in CNS pathologies.

Iodine is the only heavy atom that possesses the chemical properties suitable for intravascular use in CT analyses. The currently available iodinated contrast agents are

nonionic, are highly hydrophilic, and have low osmolarity and minimal toxicity. The paramagnetic atom gadolinium (Gd), with seven unpaired electrons, forms a stable complex with diethylenetriamine pentaacetic acid (DTPA) and is the contrast material used in MRI. The DTPA complex is well tolerated and even minimal concentrations lead to marked shortening of its observed relaxation times and increase in signal intensity.

Both contrast agents normally do not cross the BBB. When injected intravenously, neither Gd nor DTPA affects BBB integrity. In contrast, intra-arterial injection of iodinated contrast agents was shown to disrupt normal BBB functioning due to both osmotic and chemotoxic effects (reviewed by Sage et al.).[59] This study, performed to determine the safety of currently used contrast agents, is of considerable significance for predicting the risks involved in low-level exposure to xenobiotics, as it indicates that even minor arterial elevation of the concentration of potentially harmful agents may by itself disrupt BBB functions.

In healthy individuals with normally functioning BBB, CT and MRI contrast agents cannot accumulate in the extracellular fluid of the brain parenchyma. Therefore, brain structures are not enhanced and remain relatively transparent in the imaging scans. In cases when the permeability of the BBB is increased because of a pathological process, the passage of iodinated agents (in CT) or paramagnetic DTPA complex (in MRI) leads to enhancement of signals. This occurs through X-ray attenuation, creating enhanced brain images in CT scans, or shortening of relaxation times, which results in sharper images in MRI. Such alterations in BBB penetrance may be local or massive, reflecting brain tumors, infectious disease, or cerebrovascular impairments. Figure 4.3 demonstrates examples for such imaging analyses of human BBB disruption.

E. Transgenic Engineering Models for Blood-Brain Barrier Studies

Genetic manipulations of the molecular mechanisms controlling BBB functioning yield new insights into the corresponding physiological or pathological circumstances and the dissection of their effects on BBB integrity. Several transgenic and knockout models have unraveled key elements involved in BBB functioning. These included several intentional as well as serendipitous studies. Mice with a genetic disruption in the mdr1a gene (multiple drug resistance), encoding the drug-transporting P-glycoprotein, which resides in the BBB, display up to 10-fold increases in their dexamethasone uptake into the brain.[60] The effect of cytokine overproduction on BBB functioning was checked in transgenic mice that overexpress interleukin 3 (IL3) or interleukin 6 (IL6). The IL3 transgenics develop progressive demyelination and infiltrated CNS lesions associated with BBB defects.[61] The effects observed in IL6 transgenics were even more dramatic: extensive breakdown of the BBB was evident in the cerebellum of IL6-overproducing mice, followed by subsequent inflammation, reactive gliosis, axonal degeneration, and macrophage accumulation.[62] CuZn-superoxide dismutase (SOD) was discovered to have protective effects against trauma-induced BBB disruption, in a model of mice that overexpress human SOD.[63] These

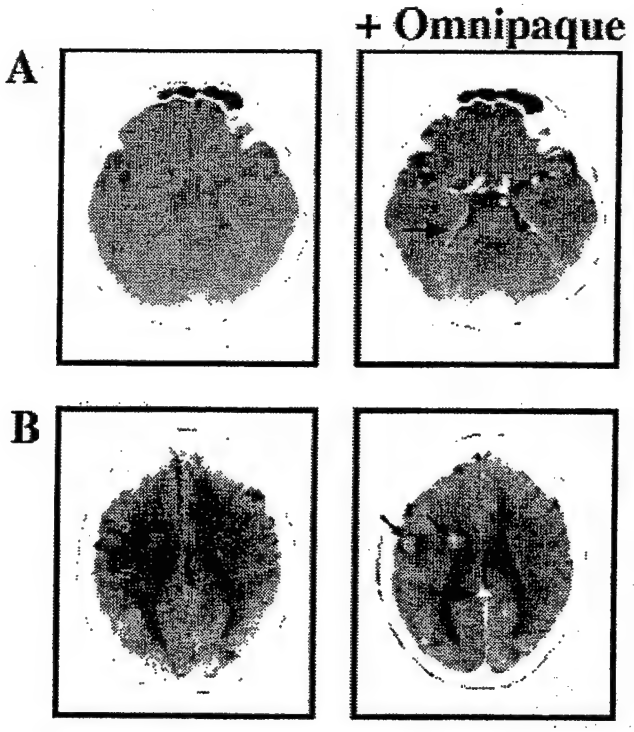

FIGURE 4.3 Blood-brain barrier disruption as revealed by computerized tomography: A. Normal CT scan, before and after injection of the enhancement material, Omnipaque™. Note the enhancement (hyperdense white) in brain arteries and vein sinuses (wide arrows) without penetration into the brain parenchyma. B. A case of multiple brain metastases in a 41-year-old female with a history of breast cancer. Following injection of Omnipaque™, several round white regions appear, reflecting focal BBB disruption in the regions harboring tumors (thin arrows).

mice were further found to display improved neurological recovery following traumatic brain injury,[64] which emphasizes the importance of oxidative stress in BBB disruption.

IV. MODULATORS OF BLOOD-BRAIN BARRIER FUNCTIONS AND THEIR INTERRELATIONSHIPS

Several considerations point to specific natural compounds and therapeutic agents as potential modulators of BBB functions. The rapid kinetics of BBB transport implicates post-translational control mechanisms in this process, simply because there is insufficient time to allow the slow transcription and translation processes to take place. The intimate relationship with vasculature properties points to vasoactive agents as potential modulators, and the necessity for penetrance of cells from the

immune system suggests the involvement of immunomodulators. These, and drug transporters, should all communicate with the complex array of molecules and cellular structures that together compose the BBB.

Kinase cascades, universal pathways for rapid signal transduction in numerous biological processes, were naturally investigated for their potential relevance to BBB functioning. To regulate BBB properties, such kinase cascades should be induced in the various cell types that comprise the BBB. This prediction is verified by the finding that a pituitary adenylyl cyclase-activating polypeptide is successfully transported across the BBB, preventing the ischemia-induced death of hippocampal neurons.[65] The next logical step in this kinase cascade is tyrosine phosphorylation, which may increase tight junction permeability.[66] That such phosphorylation is actively involved in regulating BBB transport processes is evident from findings of phosphorylation of endothelial Na-K-Cl co-transport protein under changes in tonicity and hormones.[67]

A. Nitric Oxide and Vasoactive Agents Involvement

A primary mediator that was demonstrated to participate in meningitis-induced BBB disruption is nitric oxide (NO). NO is produced in response to exposure to bacterial endotoxins by the host endothelial cells. In an animal model of lipopolysaccharide-induced meningitis, BBB disruption and NO production sites in the brain co-localized,[68] and NO-synthase inhibitors reduced the meningeal-associated alterations in BBB permeability.[69] NO is likely produced by astrocytes, and it decreases endothelin-1 secretion by brain microvessel endothelial cells.[70,71]

Agents that regulate vasoactive processes, such as bradykinin and angiotensin, were shown to effect biochemical opening of the BBB.[72] In tissue culture experiments, such agents were further demonstrated to modulate tight junction structures in BBB endothelial cells co-cultured with astrocytes.[32] In cultured A431 cells, the signaling cascade induced by these agents was shown to involve tyrosine phosphorylation and reorganization of the tight junction protein Z0–1, processes that are also mediated by epidermal growth factor-1 (EGF1).[73]

B. Immunomodulators and Multi-Drug Transporters

The passage of immunomodulators across the BBB has been the subject of much research activity, especially because of the known impairment in BBB functioning in autoimmune diseases such as multiple sclerosis (MS).[74] It is generally considered that basic mechanisms of brain inflammation involve massive, yet transient, disruption of BBB functioning that plays an important role in the acute episodes of several autoimmune diseases.[75] This may indicate that individuals with an inherited susceptibility to autoimmune responses are a high-risk group for low-level exposure to xenobiotics.

The mdra1 genomic disruption studies noted above have pointed to this multidrug transporter protein as a rate-limiting factor in the bidirectional transport of drugs across the BBB. This finding explained the drug-induced neurotoxicity under chemotherapy and opens interesting options for developing BBB-regulating drugs.

Interestingly, the mouse mdr1a gene is also the earliest known endothelial cell differentiation marker during BBB development.[76]

V. CONDITIONS INDUCING BLOOD-BRAIN BARRIER DISRUPTION

The pathophysiological origin of BBB impairments is of major clinical interest for several reasons. Impairment is dangerous, as it may cause extreme susceptibility to adverse drug responses, which would necessitate individualized drug dosage; however, breaching the barrier is sometimes useful to enable delivery of needed drugs to the brain (for example, under bacterial, fungal, or viral brain infection, or in cases of malignant brain tumors).

A. Pathophysiological Induction of Blood-Brain Barrier Penetrance

Several diseases are known which are associated with BBB disruption. These include brain tumor metastases; epilepsy and the more severe condition of status epilepticus; cerebrovascular disorders; autoimmune diseases such as multiple sclerosis; acute cerebral infarcts; meningeal carcinomatosis; and ischemic white matter lesions.[77–84] Several genetic polymorphisms are known which increase the susceptibility to BBB disruption. These include polymorphisms in glutathione transferase, important for protection against oxidative stress,[85] and malfunctioning variants of serum BChE (e.g., "atypical" *BCHE*).[86] In particular, such mutations increase the risk of BBB disruption that is involved with exposure to anticholinesterases or to lead sulfate batteries, with subsequent increased risk for Parkinson's disease.[87,88]

Disruption of the BBB was reported in MS patients examined by contrast-enhanced MRI.[89] Blood-brain barrier disruption in MS patients was suggested to be the initial event in the development of the brain lesions that are characteristic of the advanced stages of this disease.[90] It correlates with the severity of symptoms, and an earlier age of the disease onset.[91] Another pathological condition in which BBB breakdown was demonstrated is epilepsy. Disruption was demonstrated by computerized tomography (CT) in a patient following generalized seizure and by Evans blue penetration in a rat model of pentylentetrazol-induced seizures.[92,93]

Cerebrovascular pathologies are abundant in Alzheimer's disease (AD) and are demonstrated by changes in the endothelium, amyloid depositions in the cerebral blood vessels, and disruption of the BBB.[94] A possible mechanism that underlies this phenomenon may be drawn from *in vitro* studies using a BBB model of a monolayer of vascular endothelial cells. Amyloid β-peptide, which deposits in plaques of AD patients, induced in these cells permeability to albumin and apoptotic cell death.[95] The potential clinical relevance of this finding was emphasized by intracarotid infusion of amyloid β-peptide, which resulted in BBB damage.[96]

BBB disruption has also been reported for CNS infections, primarily in meningitis, where it is used as a differential diagnostic tool. In an acute cytokine-induced mouse model of meningitis, endothelial selectins (glycoproteins involved in cell adhesion) were demonstrated to contribute toward the disruption of the BBB.[21]

HIV-1 infection of the CNS was also suggested to involve a component of chronic brain tissue inflammation and BBB disruption, resulting in neuronal injury and death, which lead to cognitive, motor, and behavioral impairments.[97]

B. Blood-Brain Barrier Disruption Following Acute Insults

Blood-brain barrier disruption following ischemia is well documented. Carotid artery occlusion, followed by reperfusion resulted in transendothelial leakage of a marker horseradish peroxidase in the hippocampus.[98] Unilateral BBB permeabilization in the cortex and striatum subregions was demonstrated in a rabbit model of ischemic hemisphere using contrast-enhanced MRI.[99] Extreme temperature changes appear to be an additional factor influencing BBB integrity, as both cold and heat stress impair it. Cold injury in mice induced the penetrance of Evans blue, immediately following the injury, with reversal to the normal situation of intact BBB only 24 h post-injury.[100] In a milder model, infusion of hypothermic saline into the left carotid artery of rats resulted in disruption of the BBB in the left hemisphere, which did not occur with a normothermic solution.[93] The effects of hyperthermia, on the other hand, were checked in a model of local heating of a rat's head. BBB opening was observed from 6 h to 3 days post-injury.[101] Similar results were noted in rats that were exposed to general heat stress (38°C) for 4 hours.[102] The involvement of the NO pathway in this phenomenon[103] was indicated by the up-regulation of neuronal NO synthase activity, which coincided with BBB breakdown in distinct brain regions.[104]

Traumatic brain injury, simulated by a model of closed head injury to mice, had also been shown to result in disruption of the BBB.[105] The temporal resolution of this disruption was monitored by MRI in rats subjected to closed head injury. Blood-brain barrier disruption appeared immediately after the impact, and declined gradually, until full reversal to control levels 30 min post-injury.[106] Opening of the BBB was similarly demonstrated in response to acute anticholinesterase exposure, however, low-level exposure has not yet been tested. BBB disruption under anticholinesterase exposure was proven to be seizure-dependent, as it could be blocked by the use of anticonvulsant agents.[107] The anticholinesterase effect on BBB ultrastructure did not impair endothelial tight junctions. Yet, an increased number of endothelial vesicles were observed, suggesting increased transcytosis as the mechanism involved.[108]

C. Psychological and Physical Stressors Impair Blood-Brain Barrier Functioning

Friedman et al.[58] have demonstrated enhanced brain penetrance under psychological stress of relatively small molecules such as anticholinesterases, as well as larger dye-protein complexes and DNA plasmids. This stress-induced process putatively explains some of the nervous system-associated sequelae reported by Gulf War veterans, who were exposed to unknown doses and combinations of potentially harmful xenobiotics, particularly anticholinesterases. The anticipated chemical warfare agents would have irreversibly blocked AChE. For prophylactic protection from these agents, Gulf War soldiers were administered pyridostigmine, a reversible carbamate

cholinesterase inhibitor which has a quaternary ammonium group that under normal circumstances prevents its transport across the BBB. Pyridostigmine is routinely used to treat peripheral neuromuscular junction deficiencies in myasthenia gravis patients,[109] and was shown to cause mild, primarily peripheral side effects during peacetime clinical tests in healthy volunteers.[110] However, pyridostigmine use during the Gulf War caused a significant increase in reported CNS symptoms. Similarly, in animal experiments the dose of pyridostigmine required to block 50% of brain AChE in stressed mice was found to be 100-fold lower than that required in non-stressed mice, indicating a breakdown of the BBB.[58] More recently, heat stress, even extreme, reportedly failed to induce penetration of pyridostigmine into the brain of guinea pigs.[111] That BBB disruption depends on the status of neuronal activity in a brain-region specific manner was demonstrated in a study that compared stress-induced increase in BBB permeability in control and monosodium glutamate-treated rats, which reported increased BBB disruption in the hypothalamus and decreased in the brain stem, as compared with control animals.[112] Other reports demonstrate AChE overproduction in response to anticholinesterase exposure and to increases in interleukin 1.[26,113,114] Therefore, a long-term outcome of low-level exposure to an anticholinesterase may be a hypocholinergic state, due to entry of the agent into the brain, and the induction of AChE expression and excessive AChE-R accumulation.

D. Blood-Brain Barrier as a Complex Trait with Genetic and Physiological Components: Prospects

Blood-brain barrier properties are probably a complex genetic trait, in which the correlation of genotype to phenotype is difficult to dissect. Such a trait is termed complex or, if the phenotype is measured through a continuous variable, a quantitative trait. In certain cases, complex traits induce a susceptibility to a disease that depends upon environmental conditions. One example is the extreme adverse response to pyridostigmine treatment during the Gulf War that was found in a homozygous carrier of the "atypical" *BCHE* variant. The *BCHE,* with minor expression in the brain, gene encodes the butyrylcholinesterase (BChE, a.k.a. serum cholinesterase), that sequesters anticholinesterases such as pyridostigmine and prevents their reaction with AChE.[86] However, "atypical" BChE is incapable of binding pyridostigmine. Hence, homozygous carriers of this variant are at risk for extremely adverse responses, especially under the stress associated with war, to pyridostigmine doses in the circulation that would not affect individuals with normal *BCHE.* Therefore, the indirectly related *BCHE* gene becomes an important consideration for BBB disruption under the combination of stress and anticholinesterase exposure.

Loci in the genome that affect traits that may be quantified are called quantitative trait loci (QTL). Since many complex traits can be measured through a continuous variable (e.g., anxiety through cortisol measurements, Alzheimer's disease through cognition tests), QTL may serve as a general term for complex traits. Although the identification of QTL in humans and in model organisms is in its infancy, the QTL paradigm fits BBB properties from many points of view. Thanks to the human genome project and the development of related technologies, the detection of BBB genes will soon be aided by high-density single nucleotide polymorphism

(SNP) marker maps, which will allow population-based studies of greater significance than the current family-based studies. The human genome project, soon to be completed, will further provide important information on the sequence of all of the relevant genes and the homologies of their protein products. However, even with all the genome sequenced, significant additional work to assess functionality will be required. Expression analysis of endothelial cell genes through high-density microchip arrays will provide an independent dimension to increase the efficiency and efficacy of the QTL aspects of BBB research. Comparative genetics will also bring essential insights for functional determination. Finally bioinformatics and theoretical developments emerging from it will allow integration of all the various aspects of this multidisciplinary field to achieve the appropriate results. All of these efforts together will be needed to shed more light on the issue of BBB properties.

VI. SUMMARY

A comprehensive survey of the recent literature reveals an increasingly complex collection of BBB constituents and functions. For example, under low-level exposure to anticholinesterases, BBB integrity may be compromised because of four interrelated processes:

1. Anticholinesterase blockade of the ACh hydrolytic capacity of AChE induces a short-term hypercholinergic activation in the brain, leading by a rapid yet long-term feedback process to accumulation of an excess of AChE-R and modification of the cholinergic status in a manner affecting BBB properties at a later phase.
2. Anticholinesterase-AChE interactions may modify the flexible 3-dimensional structure of the AChE protein and change its capacity to compete in protein-protein interactions with its non-neuronal signal transducing homologues (e.g., gliotactin), or its neuronal homologues, like neuroligin. This could alter astrocyte or neuron properties that control BBB functioning.[115]
3. Anticholinesterase-induced AChE-R may differ from the normally present AChE-S in its ability to affect BBB integrity. Therefore, the combination of AChE's catalytic and structural properties with the anticholinesterase-induced feedback response would have a more dramatic effect on BBB properties than would any of these processes alone.
4. In individuals prone to adverse responses to stress stimuli, all of the above processes may be exacerbated in a complex manner, combining genetic and physiological mechanisms.

Blood-brain barrier disruption would affect brain functioning because of penetrance of the brain by peripheral compounds that may modulate the properties of glia and neurons. Therefore, the consequences of breaching the BBB, even for a short duration and in a limited area, may persist for long periods and involve larger brain areas. In an era when breakthroughs in molecular genetics that allow a previously unimagined dissection of biological processes, and with technological developments

that provide a dynamic real-time view of brain functions, the BBB represents a medical and scientific frontier awaiting exploration.

ACKNOWLEDGMENTS

The authors acknowledge with thanks Profs. E. Reichenthal (Beersheva), A. Miller (Haifa), and C. Minini (Paris) for reviewing a draft of this manuscript. Additionally, HS and AF thank the U.S. Army Medical Research and Materiel Command (DAMD 17-99-1975) and The Israel Science Foundation and Ester Neuroscience for research support.

REFERENCES

1. Pardridge, W.M., Connor, J.D., and Crawford, I.L., Permeability changes in the blood-brain barrier: Causes and consequences, *CRC Crit. Rev. Toxicol.*, 3(2), 159, 1975.
2. Rubin, L.L. and Staddon, J.M., The cell biology of the blood-brain barrier, *Ann. Rev. Neurosci.*, 22, 11, 1999.
3. Pardridge, W.M., CNS drug design based on principles of blood-brain barrier transport, *J. Neurochem.*, 70(5), 1781, 1998.
4. Gross, P.M., Circumventricular organ capillaries, *Prog. Brain. Res.*, 91, 219, 1992.
5. Risau, W., Differentiation of endothelium, *FASEB J.*, 9(10), 926, 1995.
6. Schinkel, A.H., Smit, J.J., van Tellingen, O., Beijnen, J.H., Wagenaar, E., van Deemter, L., Mol, C.A., van der Valk, M.A., Robanus-Maandag, E.C., te Riele, H.P., et al., Disruption of the mouse mdr1a P-glycoprotein gene leads to a deficiency in the blood-brain barrier and to increased sensitivity to drugs, *Cell*, 77(4), 491, 1994.
7. Dejana, E., Corada, M., and Lampugnani, M.G., Endothelial cell-to-cell junctions, *FASEB J.*, 9(10), 910, 1995.
8. Gumbiner, B.M., Cell adhesion: The molecular basis of tissue architecture and morphogenesis, *Cell*, 84(3), 345, 1996.
9. Lum, H. and Malik, A.B., Regulation of vascular endothelial barrier function, *Am. J. Physiol.*, 267(3 Pt 1), L223, 1994.
10. Staddon, J.M. and Rubin, L.L., Cell adhesion, cell junctions and the blood-brain barrier, *Curr. Opin. Neurobiol.*, 6(5), 622, 1996.
11. Balda, M.S., Gonzalez-Mariscal, L., Matter, K., Cereijido, M., and Anderson, J.M., Assembly of the tight junction: The role of diacylglycerol, *J. Cell Biol.*, 123(2), 293, 1993.
12. Anderson, J.M. and Van Itallie, C.M., Tight junctions and the molecular basis for regulation of paracellular permeability, *Am. J. Physiol.*, 269(4 Pt 1), G467, 1995.
13. Citi, S., Sabanay, H., Jakes, R., Geiger, B., and Kendrick-Jones, J., Cingulin, a new peripheral component of tight junctions, *Nature*, 333(6170), 272, 1988.
14. Furuse, M., Hirase, T., Itoh, M., Nagafuchi, A., Yonemura, S., and Tsukita, S., Occludin: A novel integral membrane protein localizing at tight junctions, *J. Cell Biol.*, 123(6 Pt 2), 1777, 1993.
15. Nusrat, A., Giry, M., Turner, J.R., Colgan, S.P., Parkos, C.A., Carnes, D., Lemichez, E., Boquet, P., and Madara, J.L., Rho protein regulates tight junctions and perijunctional actin organization in polarized epithelia, *Proc. Natl. Acad. Sci. U.S.A.*, 92(23), 10629, 1995.

16. Grifman, M., Galyam, N., Seidman, S., and Soreq, H., Functional redundancy of acetylcholinesterase and neuroligin in mammalian neuritogenesis, *Proc. Natl. Acad. Sci. U.S.A.*, 95(23), 13935, 1998.
17. Thoreson, M.A., Anastasiadis, P.Z., Daniel, J.M., Ireton, R.C., Whellock, M.J., Johnson, K.R., Hummingbird, D.K., and Reynolds, A.B., Selective uncoupling of p120ctn from E-cadhedrin disrupts strong adhesion, *J. Cell Biol.*, 148(1), 189, 2000.
18. Adamson, P., Etienne, S., Couraud, P.O., Calder, V., and Greenwood, J., Lymphocyte migration through brain endothelial cell monolayers involves signaling through endothelial ICAM-1 via a rho-dependent pathway, *J. Immunol.*, 162(5), 2964, 1999.
19. Ratcliffe, M.J., Rubin, L.L., and Staddon, J.M., Dephosphorylation of the cadherin-associated p100/p120 proteins in response to activation of protein kinase C in epithelial cells, *J. Biol. Chem.*, 272(50), 31894, 1997.
20. Irie, M., Hata, Y., Takeuchi, M., Ichtchenko, K., Toyoda, A., Hirao, K., Takai, Y., Rosahl, T.W., and Sudhof, T.C., Binding of neuroligins to PSD-95, *Science*, 277(5331), 1511, 1997.
21. Tang, T., Frenette, P.S., Hynes, R.O., Wagner, D.D., and Mayadas, T.N., Cytokine-induced meningitis is dramatically attenuated in mice deficient in endothelial selectins, *J. Clin. Invest.*, 97(11), 2485, 1996.
22. Auld, V.J., Fetter, R.D., Broadie, K., and Goodman, C.S., Gliotactin, a novel transmembrane protein on peripheral glia, is required to form the blood-nerve barrier in Drosophila, *Cell*, 81(5), 757, 1995.
23. Baumgartner, S., Littleton, J.T., Broadie, K., Bhat, M.A., Harbecke, R., Lengyel, J.A., Chiquet-Ehrismann, R., Prokop, A., and Bellen, H.J., A Drosophila neurexin is required for septate junction and blood-nerve barrier formation and function, *Cell*, 87(6), 1059, 1996.
24. Darboux, I., Barthalay, Y., Piovant, M., and Hipeau-Jacquotte, R., The structure-function relationships in Drosophila neurotactin show that cholinesterasic domains may have adhesive properties, *EMBO J.*, 15(18), 4835, 1996.
25. Grisaru, D., Sternfeld, M., Eldor, A., Glick, D., and Soreq, H., Structural roles of acetylcholinesterase variants in biology and pathology, *Eur. J. Biochem.*, 264(3), 672, 1999.
26. Kaufer, D., Friedman, A., Seidman, S., and Soreq, H., Acute stress facilitates long-lasting changes in cholinergic gene expression, *Nature*, 393(6683), 373, 1998.
27. Fanning, A.S. and Anderson, J.M., Protein-protein interactions: PDZ domain networks, *Curr. Biol.*, 6(11), 1385, 1996.
28. Saras, J. and Heldin, C.H., PDZ domains bind carboxy-terminal sequences of target proteins, *Trends Biochem. Sci.*, 21(12), 455, 1996.
29. Bhat, M.A., Izaddoost, S., Lu, Y., Cho, K.O., Choi, K.W., and Bellen, H.J., Discs lost, a novel multi-PDZ domain protein, establishes and maintains epithelial polarity, *Cell*, 96(6), 833, 1999.
30. Janzer, R.C. and Raff, M.C., Astrocytes induce blood-brain barrier properties in endothelial cells, *Nature*, 325(6101), 253, 1987.
31. Bellen, H.J., Lu, Y., Beckstead, R., and Bhat, M.A., Neurexin IV, caspr and paranodin—novel members of the neurexin family: Encounters of axons and glia, *Trends Neurosci*, 21(10), 444, 1998.
32. Wolburg, H., Neuhaus, J., Kniesel, U., Krauss, B., Schmid, E.M., Ocalan, M., Farrell, C., and Risau, W., Modulation of tight junction structure in blood-brain barrier endothelial cells. Effects of tissue culture, second messengers and cocultured astrocytes, *J. Cell Sci.*, 107(Pt 5), 1347, 1994.

33. Schroeter, M.L., Mertsch, K., Giese, H., Muller, S., Sporbert, A., Hickel, B., and Blasig, I.E., Astrocytes enhance radical defence in capillary endothelial cells constituting the blood-brain barrier, *FEBS Lett.*, 449(2–3), 241, 1999.
34. Granholm, A.C., Curtis, M., Diamond, D.M., Branch, B.J., Heman, K.L., and Rose, G.M., Development of an intact blood-brain barrier in brain tissue transplants is dependent on the site of transplantation, *Cell Transplant*, 5(2), 305, 1996.
35. Hurst, R.D., Heales, S.J., Dobbie, M.S., Barker, J.E., and Clark, J.B., Decreased endothelial cell glutathione and increased sensitivity to oxidative stress in an *in vitro* blood-brain barrier model system, *Brain Res.*, 802(1–2), 232, 1998.
36. Martel, C.L., Mackic, J.B., Adams, J.D., Jr., McComb, J.G., Weiss, M.H., and Zlokovic, B.V., Transport of dopamine at the blood-brain barrier of the guinea pig: Inhibition by psychotropic drugs and nicotine, *Pharm. Res.*, 13(2), 290, 1996.
37. Harik, S.I., MPTP toxicity and the "biochemical" blood-brain barrier, *NIDA Res. Monogr.*, 120, 43, 1992.
38. Sarmento, A., Borges, N., and Lima, D., Influence of electrical stimulation of locus coeruleus on the rat blood-brain barrier permeability to sodium fluorescein, *Acta Neurochir.*, 127(3–4), 215, 1994.
39. Borges, N., Shi, F., Azevedo, I., and Audus, K.L., Changes in brain microvessel endothelial cell monolayer permeability induced by adrenergic drugs, *Eur. J. Pharmacol.*, 269(2), 243, 1994.
40. Galea, E. and Estrada, C., Periendothelial acetylcholine synthesis and release in bovine cerebral cortex capillaries, *J. Cereb. Blood Flow Metab.*, 11(5), 868, 1991.
41. Estrada, C., Triguero, D., Munoz, J., and Sureda, A., Acetylcholinesterase-containing fibers and choline acetyltransferase activity in isolated cerebral microvessels from goats, *Brain Res.*, 453(1–2), 275, 1988.
42. Luiten, P.G., de Jong, G.I., Van der Zee, E.A., and van Dijken, H., Ultrastructural localization of cholinergic muscarinic receptors in rat brain cortical capillaries, *Brain Res.*, 720(1–2), 225, 1996.
43. Mohr, E., Subcellular RNA compartmentalization, *Prog. Neurobiol.*, 57(5), 507, 1999.
44. Kaufer, D., Friedman, A., Seidman, S., and Soreq, H., Anticholinesterases induce multigenic transcriptional feedback response suppressing cholinergic neurotransmission, *Chem. Biol. Interact.*, 119–120, 1999.
45. Powell, H.C., Braheny, S.L., Myers, R.R., Rodriguez, M., and Lampert, P.W., Early changes in experimental allergic neuritis, *Lab. Invest.*, 48(3), 332, 1983.
46. Seeldrayers, P.A., Yasui, D., Weiner, H.L., and Johnson, D., Treatment of experimental allergic neuritis with nedocromil sodium, *J. Neuroimmunol.*, 25(2–3), 221, 1989.
47. Brosnan, C.F., Claudio, L., Tansey, F.A., and Martiney, J., Mechanisms of autoimmune neuropathies, *Ann. Neurol.*, 27(Suppl), S75, 1990.
48. Theoharides, T.C., Spanos, C., Pang, X., Alferes, L., Ligris, K., Letourneau, R., Roznieckl, J.J., Webster, E., and Chrousos, G.P., Stress-induced intracranial mast cell degranulation: A corticotropin-releasing hormone-mediated effect, *Endocrinology*, 136(12), 5745, 1995.
49. Guo, Z., Turner, C., and Castle, D., Relocation of the t-SNARE SNAP-23 from lamellipodia-like cell surface projections regulates compound exocytosis in mast cells, *Cell*, 94(4), 537, 1998.
50. Goldschmidt, R.C., Hough, L.B., and Glick, S.D., Rat brain mast cells: Contribution to brain histamine levels, *J. Neurochem.*, 44(6), 1943, 1985.
51. Silver, R., Silverman, A.J., Vitkovic, L., and Lederhendler, I., Mast cells in the brain: Evidence and functional significance, *Trends Neurosci.*, 19(1), 25, 1996.

52. Zhuang, X., Silverman, A.J., and Silver, R., Distribution and local differentiation of mast cells in the parenchyma of the forebrain, *J. Comp. Neurol.*, 408(4), 477, 1999.
53. Silverman, A.-J., Sutherland, A.K., Wilhelm, M., and Silver, R., Mast cells migrate from blood to brain, *J. Neurosci.*, 20(1), 401, 2000.
54. Stewart, P.A. and Wiley, M.J., Developing nervous tissue induces formation of blood-brain barrier characteristics in invading endothelial cells: A study using quail—chick transplantation chimeras, *Dev. Biol.*, 84(1), 183, 1981.
55. Rubin, L.L., Hall, D.E., Porter, S., Barbu, K., Cannon, C., Horner, H.C., Janatpour, M., Liaw, C.W., Manning, K., Morales, J., et al., A cell culture model of the blood-brain barrier, *J. Cell. Biol.*, 115(6), 1725, 1991.
56. Hurst, R.D. and Fritz, I.B., Properties of an immortalised vascular endothelial/glioma cell co-culture model of the blood-brain barrier, *J. Cell Physiol.*, 167(1), 81, 1996.
57. Plateel, M., Dehouck, M.P., Torpier, G., Cecchelli, R., and Teissier, E., Hypoxia increases the susceptibility to oxidant stress and the permeability of the blood-brain barrier endothelial cell monolayer, *J. Neurochem.*, 65(5), 2138, 1995.
58. Friedman, A., Kaufer, D., Shemer, J., Hendler, I., Soreq, H., and Tur-Kaspa, I., Pyridostigmine brain penetration under stress enhances neuronal excitability and induces early immediate transcriptional response, *Nat. Med.*, 2(12), 1382, 1996.
59. Sage, M.R., Wilson, A.J., and Scroop, R., Contrast media and the brain. The basis of CT and MR imaging enhancement, *Neuroimaging Clin. N. Am.*, 8(3), 695, 1998.
60. Meijer, O.C., de Lange, E.C., Breimer, D.D., de Boer, A.G., Workel, J.O., and de Kloet, E.R., Penetration of dexamethasone into brain glucocorticoid targets is enhanced in mdr1A P-glycoprotein knockout mice, *Endocrinology*, 139(4), 1789, 1998.
61. Powell, H.C., Garrett, R.S., Brett, F.M., Chiang, C.S., Chen, E., Masliah, E., and Campbell, I.L., Response of glia, mast cells and the blood-brain barrier, in transgenic mice expressing interleukin-3 in astrocytes, an experimental model for CNS demyelination, *Brain Pathol.*, 9(2), 219, 1999.
62. Brett, F.M., Mizisin, A.P., Powell, H.C., and Campbell, I.L., Evolution of neuropathologic abnormalities associated with blood-brain barrier breakdown in transgenic mice expressing interleukin-6 in astrocytes, *J. Neuropathol. Exp. Neurol.*, 54(6), 766, 1995.
63. Chan, P.H., Epstein, C.J., Li, Y., Huang, T.T., Carlson, E., Kinouchi, H., Yang, G., Kamii, H., Mikawa, S., Kondo, T., et al., Transgenic mice and knockout mutants in the study of oxidative stress in brain injury, *J. Neurotrauma*, 12(5), 815, 1995.
64. Mikawa, S., Kinouchi, H., Kamii, H., Gobbel, G.T., Chen, S.F., Carlson, E., Epstein, C.J., and Chan, P. H., Attenuation of acute and chronic damage following traumatic brain injury in copper, zinc-superoxide dismutase transgenic mice, *J. Neurosurg.*, 85(5), 885, 1996.
65. Banks, W.A., Uchida, D., Arimura, A., Somogyvari-Vigh, A., and Shioda, S., Transport of pituitary adenylate cyclase-activating polypeptide across the blood-brain barrier and the prevention of ischemia-induced death of hippocampal neurons, *Ann. NY Acad. Sci.*, 805, 270, 1996.
66. Staddon, J.M., Smales, C., Schulze, C., Esch, F.S., and Rubin, L.L., p120, a p120-related protein (p100), and the cadherin/catenin complex, *J. Cell Biol.*, 130(2), 369, 1995.
67. O'Donnell, M.E., Martinez, A., and Sun, D., Endothelial Na-K-Cl cotransport regulation by tonicity and hormones: Phosphorylation of cotransport protein, *Am. J. Physiol.*, 269(6 Pt 1), C1513, 1995.
68. Jaworowicz, D.J., Jr., Korytko, P.J., Singh Lakhman, S., and Boje, K.M., Nitric oxide and prostaglandin E2 formation parallels blood-brain barrier disruption in an experimental rat model of bacterial meningitis, *Brain Res. Bull.*, 46(6), 541, 1998.

69. Boje, K.M., Inhibition of nitric oxide synthase attenuates blood-brain barrier disruption during experimental meningitis, *Brain Res.*, 720(1–2), 75, 1996.
70. Federici, C., Camoin, L., Creminon, C., Chaverot, N., Strosberg, A.D, and Couraud, P.O., Cultured astrocytes release a factor that decreases endothelin-1 secretion by brain microvessel endothelial cells, *J. Neurochem.*, 64(3), 1008, 1995.
71. O'Donnell, M.E., Martinez, A., and Sun, D., Cerebral microvascular endothelial cell Na-K-Cl cotransport: Regulation by astrocyte-conditioned medium, *Am. J. Physiol.*, 268(3 Pt 1), C747, 1995.
72. Black, K.L., Biochemical opening of the blood-brain barrier, *Adv. Drug Deliv. Rev.*, 15, 37, 1995.
73. Van Itallie, C.M., Balda, M.S., and Anderson, J.M., Epidermal growth factor induces tyrosine phosphorylation and reorganization of the tight junction protein ZO-1 in A431 cells, *J. Cell Sci.*, 108(Pt 4), 1735, 1995.
74. Stitt, J.T., Passage of immunomodulators across the blood-brain barrier, *Yale J. Biol. Med.*, 63(2), 121, 1990.
75. Lassmann, H., Basic mechanisms of brain inflammation, *J. Neural Transm. Suppl.*, 50, 183, 1997.
76. Qin, Y. and Sato, T.N., Mouse multidrug resistance 1a/3 gene is the earliest known endothelial cell differentiation marker during blood-brain barrier development, *Dev. Dyn.*, 202(2), 172, 1995.
77. Akeson, P., Larsson, E.M., Kristoffersen, D.T., Jonsson, E., and Holtas, S., Brain metastases—comparison of gadodiamide injection-enhanced MR imaging at standard and high dose, contrast-enhanced CT and non-contrast-enhanced MR imaging, *Acta Radiol.*, 36(3), 300, 1995.
78. Cornford, E.M. and Oldendorf, W.H., Epilepsy and the blood-brain barrier, *Adv. Neurol.*, 44, 787, 1986.
79. Correale, J., Rabinowicz, A.L., Heck, C.N., Smith, T.D., Loskota, W.J., and DeGiorgio, C.M., Status epilepticus increases CSF levels of neuron-specific enolase and alters the blood-brain barrier, *Neurology*, 50(5), 1388, 1998.
80. Klatzo, I., Disturbances of the blood-brain barrier in cerebrovascular disorders, *Acta Neuropathol. Suppl.*, 8, 81, 1983.
81. Larsson, H.B., Stubgaard, M., Frederiksen, J.L., Jensen, M., Henriksen, O., and Paulson, O.B., Quantitation of blood-brain barrier defect by magnetic resonance imaging and gadolinium-DTPA in patients with multiple sclerosis and brain tumors, *Magn. Reson. Med.*, 16(1), 117, 1990.
82. Merten, C.L., Knitelius, H.O., Assheuer, J., Bergmann-Kurz, B., Hedde, J.P., and Bewermeyer, H., MRI of acute cerebral infarcts, increased contrast enhancement with continuous infusion of gadolinium, *Neuroradiology*, 41(4), 242, 1999.
83. Siegal, T., Sandbank, U., Gabizon, A., Mizrachi, R., Ben-David, E., and Catane, R., Alteration of blood-brain-CSF barrier in experimental meningeal carcinomatosis. A morphologic and adriamycin-penetration study, *J. Neurooncol.*, 4(3), 233, 1987.
84. Skoog, I., A review on blood pressure and ischaemic white matter lesions, *Dement. Geriatr. Cogn. Disord.*, 9, Suppl 1, 13, 1998.
85. Menegon, A., Board, P.G., Blackburn, A.C., Mellick, G.D., and Le Couteur, D.G., Parkinson's disease, pesticides, and glutathione transferase polymorphisms [see Comments], *Lancet*, 352(9137), 1344, 1998.
86. Loewenstein-Lichtenstein, Y., Schwarz, M., Glick, D., Norgaard-Pedersen, B., Zakut, H., and Soreq, H., Genetic predisposition to adverse consequences of anti-cholinesterases in 'atypical' BCHE carriers, *Nat. Med.*, 1(10), 1082, 1995.

87. Soreq, H. and Glick, D., Novel roles for cholinesterases in stress and inhibitor responses, in *Cholinesterases and Cholinesterase Inhibitors: Basic, Preclinical and Clinical Aspects,* Giacobini, E., ed., Martin Dunitz, Ltd., London, 47–61, 2000.
88. Kuhn, W., Winkel, R., Woitalla, D., Meves, S., Przuntek, H., and Muller, T., High prevalence of Parkinsonism after occupational exposure to lead-sulfate batteries, *Neurology,* 50(6), 1885, 1998.
89. Rosenberg, G.A., Dencoff, J.E., Correa, N., Jr., Reiners, M., and Ford, C.C., Effect of steroids on CSF matrix metalloproteinases in multiple sclerosis: Relation to blood-brain barrier injury, *Neurology,* 46(6), 1626, 1996.
90. McFarland, H.F., The lesion in multiple sclerosis: Clinical, pathological, and magnetic resonance imaging considerations, *J. Neurol. Neurosurg. Psychiatry,* 64, Suppl 1, S26, 1998.
91. Stone, L.A., Smith, M.E., Albert, P.S., Bash, C.N., Maloni, H., Frank, J.A., and McFarland, H.F., Blood-brain barrier disruption on contrast-enhanced MRI in patients with mild relapsing-remitting multiple sclerosis: Relationship to course, gender, and age, *Neurology,* 45(6), 1122, 1995.
92. Clarke, H.B. and Gabrielsen, T.O., Seizure induced disruption of blood-brain barrier demonstrated by CT, *J. Comput. Assist. Tomogr.,* 13(5), 889, 1989.
93. Oztas, B. and Kucuk, M., Intracarotid hypothermic saline infusion: A new method for reversible blood-brain barrier disruption in anesthetized rats, *Neurosci. Lett.,* 190(3), 203, 1995.
94. Hachinski, V. and Munoz, D.G., Cerebrovascular pathology in Alzheimer's disease: Cause, effect or epiphenomenon?, *Ann. N.Y. Acad. Sci.,* 826, 1, 1997.
95. Blanc, E.M., Toborek, M., Mark, R.J., Hennig, B., and Mattson, M.P., Amyloid beta-peptide induces cell monolayer albumin permeability, impairs glucose transport, and induces apoptosis in vascular endothelial cells, *J. Neurochem.,* 68(5), 1870, 1997.
96. Jancso, G., Domoki, F., Santha, P., Varga, J., Fischer, J., Orosz, K., Penke, B., Becskei, A., Dux, M., and Toth, L., Beta-amyloid (1-42) peptide impairs blood-brain barrier function after intracarotid infusion in rats, *Neurosci. Lett.,* 253, 139, 1998.
97. Epstein, L.G. and Gelbard, H.A., HIV-1-induced neuronal injury in the developing brain, *J. Leukoc. Biol.,* 65(4), 453, 1999.
98. Shinnou, M., Ueno, M., Sakamoto, H., and Ide, M., Blood-brain barrier damage in reperfusion following ischemia in the hippocampus of the Mongolian gerbil brain, *Acta Neurol. Scand.,* 98(6), 406, 1998.
99. Lo, E.H., Pan, Y., Matsumoto, K., and Kowall, N.W., Blood-brain barrier disruption in experimental focal ischemia: Comparison between in vivo MRI and immunocytochemistry, *Magn. Reson. Imaging,* 12(3), 403, 1994.
100. Murakami, K., Kondo, T., Yang, G., Chen, S.F., Morita-Fujimura, Y., and Chan, P.H., Cold injury in mice: A model to study mechanisms of brain edema and neuronal apoptosis, *Prog. Neurobiol.,* 57(3), 289, 1999.
101. Urakawa, M., Yamaguchi, K., Tsuchida, E., Kashiwagi, S., Ito, H., and Matsuda, T., Blood-brain barrier disturbance following localized hyperthermia in rats, *Int. J. Hypertherm.,* 11(5), 709, 1995.
102. Sharma, H.S., Westman, J., Cervos-Navarro, J., and Nyberg, F., Role of neurochemicals in brain edema and cell changes following hyperthermic brain injury in the rat, *Acta Neurochir. Suppl.,* 70, 269, 1997.
103. Carpentier, P., Delamanche, I.S., Le Bert, M., Blanchet, G., and Bouchaud, C., Seizure-related opening of the blood-brain barrier induced by soman: possible correlation with the acute neuropathology observed in poisoned rats, *Neurotoxicology,* 11(3), 493, 1990.

104. Alm, P., Sharma, H.S., Hedlund, S., Sjoquist, P.O., and Westman, J., Nitric oxide in the pathophysiology of hyperthermic brain injury. Influence of a new anti-oxidant compound H-290/51. A pharmacological study using immunohistochemistry in the rat, *Amino Acids,* 14(1–3), 95, 1998.
105. Chen, Y., Constantini, S., Trembovler, V., Weinstock, M., and Shohami, E., An experimental model of closed head injury in mice: Pathophysiology, histopathology, and cognitive deficits, *J. Neurotrauma,* 13(10), 557, 1996.
106. Barzo, P., Marmarou, A., Fatouros, P., Corwin, F., and Dunbar, J., Magnetic resonance imaging-monitored acute blood-brain barrier changes in experimental traumatic brain injury, *J. Neurosurg.,* 85(6), 1113, 1996.
107. Petrali, J.P., Maxwell, D.M., Lenz, D.E., and Mills, K.R., Effect of an anticholinesterase compound on the ultrastructure and function of the rat blood-brain barrier: A review and experiment, *J. Submicrosc. Cytol. Pathol.,* 23(2), 331, 1991.
108. Grange-Messent, V., Bouchaud, C., Jamme, M., Lallement, G., Foquin, A., and Carpentier, P., Seizure-related opening of the blood-brain barrier produced by the anticholinesterase compound, soman: New ultrastructural observations, *Cell. Mol. Biol. (Noisy-le-grand),* 45(1), 1, 1999.
109. Soreq, H. and Zakut, H., *Human Cholinesterases and Anticholinesterases,* Academic Press, San Diego, 1993.
110. Glikson, M., Achiron, A., Ram, Z., Ayalon, A., Karni, A., Sarova-Pinchas, I., Glovinski, J., and Revah, M., The influence of pyridostigmine administration on human neuromuscular functions—studies in healthy human subjects, *Fundam. Appl. Toxicol.,* 16(2), 288, 1991.
111. Lallement, G., Foquin, A., Baubichon, D., Burckhart, M.F., Carpentier, P., and Canini, F., Heat stress, even extreme, does not induce penetration of pyridostigmine into the brain of guinea pigs, *Neurotoxicology,* 19(6), 759, 1998.
112. Skultetyova, I., Tokarev, D., and Jezova, D., Stress-induced increase in blood-brain barrier permeability in control and monosodium glutamate-treated rats, *Brain Res. Bull.,* 45(2), 175, 1998.
113. Kaufer, D., Friedman, A., and Soreq, H., The vicious circle: Long-lasting transcriptional modulation of cholinergic neurotransmission following stress and anticholinesterase exposure, *The Neuroscientist,* 5, 173, 1999.
114. Yuekui, L., Li, Y., Liu, L., Kang, J., Sheng, J.G., Barger, S.W., Mrak, R.E., and Griffin, W.S.T., Neuronal-glial interactions mediated by interleukin-1 enhance neuronal acetylcholinesterase activity and mRNA expression, *J. Neurosci.,* 20(1), 149, 2000.
115. Bourne, Y., Grassi, J., Bougis, P.E., and Marchot, P., Conformational flexibility of the acetylcholinesterase tetramer suggested by x-ray crystallography, *J. Biol. Chem.,* 274(43), 30370, 1999.

Cellular and Molecular Neurobiology, Vol. 21, No. 6, December 2001 (© 2002)

Frequent Blood–Brain Barrier Disruption in the Human Cerebral Cortex

Oren Tomkins,[1] Daniela Kaufer,[2,3] Akiva Korn,[1] Ilan Shelef,[4] Haim Golan,[5] Eli Reichenthal,[1] Hermona Soreq,[2] and Alon Friedman[1,6]

Received November 4, 2001; accepted November 11, 2001

SUMMARY

1. The blood–brain barrier (BBB) protects the brain from circulating xenobiotic agents. The pathophysiology, time span, spatial pattern, and pathophysiological consequences of BBB disruptions are not known.

2. Here, we report the quantification of BBB disruption by measuring enhancement levels in computerized tomography brain images.

3. Pathological diffuse enhancement associated with elevated albumin levels in the cerebrospinal fluid (CSF) was observed in the cerebral cortex of 28 out of 43 patients, but not in controls. Four patients displayed weeks-long focal BBB impairment. In 19 other patients, BBB disruption was significantly associated with elevated blood pressure, body temperature, serum cortisol, and stress-associated CSF "readthrough" acetylcholinesterase. Multielectrode electroencephalography revealed enhanced slow-wave activities in areas of focal BBB disruption. Thus, quantification of BBB disruption using minimally invasive procedures, demonstrated correlations with molecular, clinical, and physiological stress-associated indices.

4. These sequelae accompany a wide range of neurological disorders, suggesting that persistent, detrimental BBB disruption is considerably more frequent than previously assumed.

KEY WORDS: acetylcholinesterase; blood–brain barrier; cerebral cortex; computerized tomography.

[1] Department of Physiology and Neurosurgery, Soroka University Hospital, Zlotowski Center of Neuroscience, Ben-Gurion University, Beersheva, Israel.
[2] Department of Biological Chemistry, Institute of Life Sciences, Roland Center for Neurodegenerative Diseases, The Hebrew University, Jerusalem, Israel.
[3] Present address: Department of Biological Sciences, Stanford University, Stanford, California 94035.
[4] Department of Radiology, Soroka University Hospital, Zlotowski Center of Neuroscience, Ben-Gurion University, Beersheva, Israel.
[5] Department of Nuclear Medicine, Soroka University Hospital, Zlotowski Center of Neuroscience, Ben-Gurion University, Beersheva, Israel.
[6] To whom correspondence should be addressed at Department of Physiology, Soroka University Hospital, Zlotowski Center of Neuroscience, Ben-Gurion University, Beersheva 84105, Israel; e-mail: alonf@bgumail.bgu.ac.il.

0272-4340/01/1200-0675/0

INTRODUCTION

The blood–brain barrier (BBB) separates the brain's interstitial space from the blood and prevents the penetrance of circulating molecules and cells into the brain (Rubin *et al.*, 1999; Soreq *et al.*, 2000). Perturbations in the integrity of the BBB have been reported in both humans (Akeson *et al.*, 1995; Cornford and Oldendorf, 1986; Klatzo, 1983; Skoog *et al.*, 1998) and animal models (Abbruscato and Davis, 1999; Friedman *et al.*, 1996) under numerous pathological conditions. In animal studies, BBB permeability can be quantitatively evaluated by measuring the concentration in the brain of nonpermeable radioactive materials, traceable macromolecules, or dyes (Abbruscato and Davis, 1999; Friedman *et al.*, 1996). However, none of these approaches is applicable to humans because of their invasiveness and the potential risks involved. Therefore, in most human studies, BBB permeability has been estimated using brain imaging techniques (computerized tomography (CT) (Roman-Goldstein *et al.*, 1994), magnetic resonance imaging (MRI) (Akeson *et al.*, 1995), or single photon emission CT (SPECT) (Siegal *et al.*, 2000)). Alternatively, altered serum constituents were searched for in the cerebrospinal fluid (CSF) (Correale *et al.*, 1998). However, no quantitative, minimally invasive approach is as yet available for evaluating BBB integrity. Therefore, the extent of enhanced BBB permeability among different patients and to different molecules, as well as the clinical correlates that predict BBB disruption await definition. Likewise, the susceptibility of different brain subregions to BBB disruption and its time resolution are still unknown. Resolution of these issues would bear wide implications to many, as it may open the way both to rationalized drug delivery into the brain and to avoidance of such penetrance when undesired. To this end, we conducted a study to develop minimally invasive means for quantifying BBB integrity. Here, we report the use of brain CT image analysis for quantitative estimation of BBB integrity in patients with various central nervous system (CNS) disorders. Our search for clinical conditions associated with compromised BBB suggests stress responses as a possible common denominator, points to the cortex as particularly vulnerable to BBB disruption, and demonstrates that such disruption may persist for at least several weeks. Focal abnormal cortical activity in areas associated with BBB disruption suggests the functional implications of such conditions. This may assist in future studies BBB integrity in various diseases and its implications to brain functioning as well as to the susceptibility to the penetrance of serum constituents, including drugs.

METHODS

Brain CT was performed using the PICKER Helical CT-TWINS (Elscint, Haifa, Israel). Scans were taken at the standard axial slices (5-mm intervals) before and ca. 1 min after the injection of the contrast agent Omnipaque (1 cm^3/kg body weight). "Control" brain scans were from randomly selected ambulatory patients who were referred for investigation, and were interpreted as "normal" by two radiologists. "Patients" CTs included patients who by signs and/or symptoms were suspected to

suffer from CNS disorders and their brain CTs interpreted as abnormal. Eighteen patients from this group, as part of their clinical investigation, were subjected to blood analysis, lumbar tap for CSF analysis and brain CT, all within 12 h. Intensity was measured bilaterally in Hounsfield units (Brooks, 1977) in round, 5–8-mm diameter regions of interest (ROIs). ROIs included subcutaneous tissue of the neck, cerebellum (2 cm lateral from the fourth ventricle), pons (one ROI at midline), thalamus (1 cm lateral from the third ventricle), white matter (at the corona radiata, bilateral to the anterior horns of the lateral ventricles), and gray matter (bilateral frontal). Using an image analysis program (Adobe PhotoShop), images (pre and post contrast agent administration) were differentiated so as to reveal contrast agent enhancement. To compare between different patients, the differential image was rescaled using a colored spectrum (blue to red) between water and bone densities (0–1000 Hounsfield Units, respectively).

MRI was performed using a Philips "Gyroscan" T5-NT machine (power track 1000, 0.5 T). SPECT scans were performed using a dual headed "Varicam" gamma camera connected to an image processing "Expert" computer (acquisition mode, format 128 × 128 pixels 120 images—each image at 3°). BBB penetration was measured following the administration of the permeable compound ^{99m}Tc-diethylenetriaminepentaacetic acid (Tc-DTPA). To measure blood perfusion to brain regions, patients were administered (more than 48 h after the Tc-DTPA study) the freely permeable compound ^{99m}Tc-ethyl cysteinate dimer (Tc-ECD) as the radioactive material. Patient clinical indices were gathered from hospital records relating to the same day when scans had been performed. When more than a single value was available for a patient, an averaged value was deduced for up to 6 h before and after time of scanning.

To detect the stress-associated readthrough variant of acetylcholinesterase (AChE-R) and its C-terminal degradation products, CSF proteins (10 μL, diluted 1:10 in PBS) were separated on 4–20% polyacrylamide gels (Bio Rad laboratories, Hercules, CA). Albumin was detected on these gels by Ponceau staining and its migration compared to that of commercially available albumin (Sigma Chemical Co., St. Louis, MO). Resultant immunoblot filters were incubated with rabbit antibodies elicited against a recombinant fusion protein of glutathione S-transferase (GST) and a peptide with the sequence of the 26 C-terminal residues of AChE-R. Antibodies were preimmunoabsorbed using GST beads to ensure specificity and were proven to interact selectively with AChE-R and not with the alternative synaptic isoform AChE-S (Sternfeld *et al.*, 2000). To detect the core AChE protein, similar blots were incubated with Chemicon anti-AChE antibodies. Detection was with peroxidase-conjugated anti-rabbit immunoglobulins and ECLTM detection (Amersham, UK).

Electroencephalogram (EEG) recordings were collected using 23 standard scalp surface electrodes (Biologic Systems Corp. Mundelein, IL) according to the 10–20 standard system with additional bilateral mastoid recordings. Electrodes impedance was kept below 5 kΩ using abrasive skin prep-cream. EEG data were collected using a CEEGRAPH IV 128-channel EEG acquisition unit (Biologic Systems Corp. Mundelein, IL) while the patient was resting supine with eyes closed. Artifact-free data from all electrodes were segmented into 2-s epochs and a power spectrum for the entire time span was calculated for each electrode.

RESULTS

Under normal conditions, the enhancement agent Omnipaque accumulates in peripheral tissues but does not significantly penetrate most CNS regions because of the functioning of the BBB. In search for impairments in BBB integrity, radiopaqueness was measured (McCullough *et al.*, 1974) before and after the injection of Omnipaque. Figure 1 demonstrates these features in a cohort of 62 patients with normal neurological examination, who were subjected to brain CT in which pathology was excluded ("controls"). Mean percent enhancement of radiopaqueness in the soft-tissue of the neck was 25.0 ± 33.9 (mean $\pm$ SEM). The large intermeasured variance is likely due to technical (amount of the injected agent, scanning latency) and/or physiological (e.g., venous return, cardiac output, or cerebral blood flow) differences. Despite this variability, linear correlation was found between signal enhancement values in the two sides of the neck tissue (Fig. 1(A)). In contrast, brain signal enhancement measured in nine different ROIs was significantly lower ($(3.4 \pm 1.8)\%$, $p < 0.0001$, t test) and displayed a much smaller variability. No correlation was found between signal enhancement in any brain region to that of the neck tissue, demonstrating bilateral impermeability of the healthy brain to Omnipaque (Fig. 1(A)).

In 43 patients with neurological signs and symptoms suspected to be due to CNS abnormality ("neurological patients"), and no focal lesion was found on bCT, mean brain enhancement ranged at 5.9–110.2% ($(12.9 \pm 15.3)\%$, mean $\pm$ SEM). This enhancement, significantly higher than that in healthy controls ($p < 0.001$, t test), suggests that in neurological patients penetrance may occur often, reflecting a frequent impairment of the BBB. In 26 patients (60%) average brain enhancement was greater than two standard deviations from the mean enhancement in the control population, reflecting significant abnormal penetrance. No significant difference was found in soft-tissue enhancement between patients and controls, exclusing the possibility that differences could be attributed to the amount of injected contrast agent or variable blood flow. In most patients, the gray and white matter of the cerebral cortex were the only regions to show larger enhancement than the control population (gray matter enhancement was 8.5 ± 13.2 and 4.5 ± 3.2 in patients and controls, respectively, $p = 0.06$, t test). Interestingly, in neurological patients percent enhancement in the left cerebral cortex showed a tendency to be higher and more variable than in the right side (10.3 ± 20.2 vs. 6.8 ± 13.1), although this was without statistical significance.

The spatial distribution of Omnipaque penetration was also analyzed in CT scans from neurological patients with high enhancement values. Figure 2 shows pseudocolored differential images from four patients with various extents and patterns of Omnipaque penetration. In normal individuals (Fig. 2(A) and data not shown), contrast material was highly concentrated and limited to venous sinuses and to brain areas that are known to lack BBB characteristics (i.e., pineal gland and neurohypophysis) (Bakay, 1976). In patients suffering from brain tumors with vasculature having abnormal BBB properties (i.e., meningiomas) (Tator and Schwartz, 1971), or following severe brain trauma, we were able to detect focal accumulation of the contrast agent in the expected location (Fig. 2(B) and data not shown). However, in certain cases, contrast agent accumulation was detected in brain tissue which

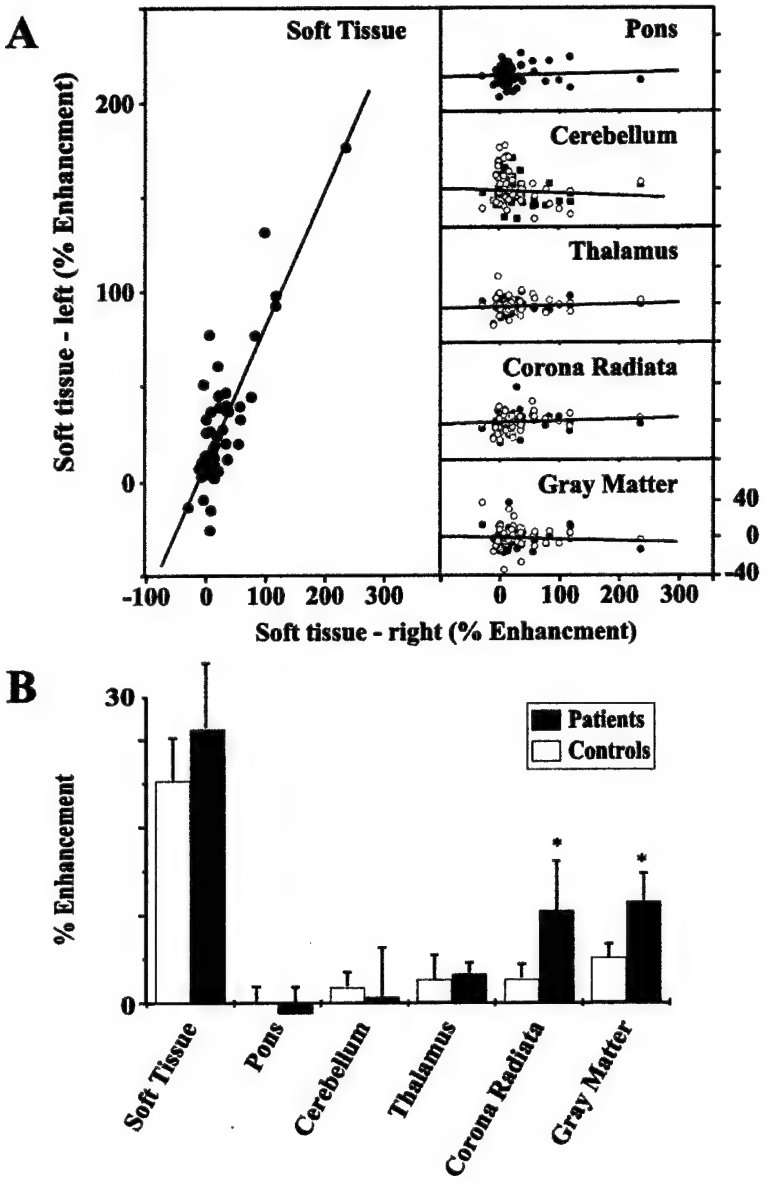

Fig. 1. CT enhancement in controls and neurological patients. (A) Control scans display impermeability to Omnipaque. All measurements were taken in Hounsfield units (HU) in 5–8-mm diameter ROIs (see Methods). Readings from the left side of the neck (soft tissue) were plotted as a function of those of the right side. Note that up to 300% bilateral enhancement was measured in neck (soft tissue, left), and no penetrance into brain regions (right). (B) Selective cortical susceptibility for BBB permeation in neurological patients. Shown are average enhancement values in controls ($n = 62$, open bars) and neurological patients ($n = 43$, filled bars). Stars note significantly higher ($p < 0.05$, t test) enhancement values in gray and white matter of the cerebral cortex (gray matter, corona radiata).

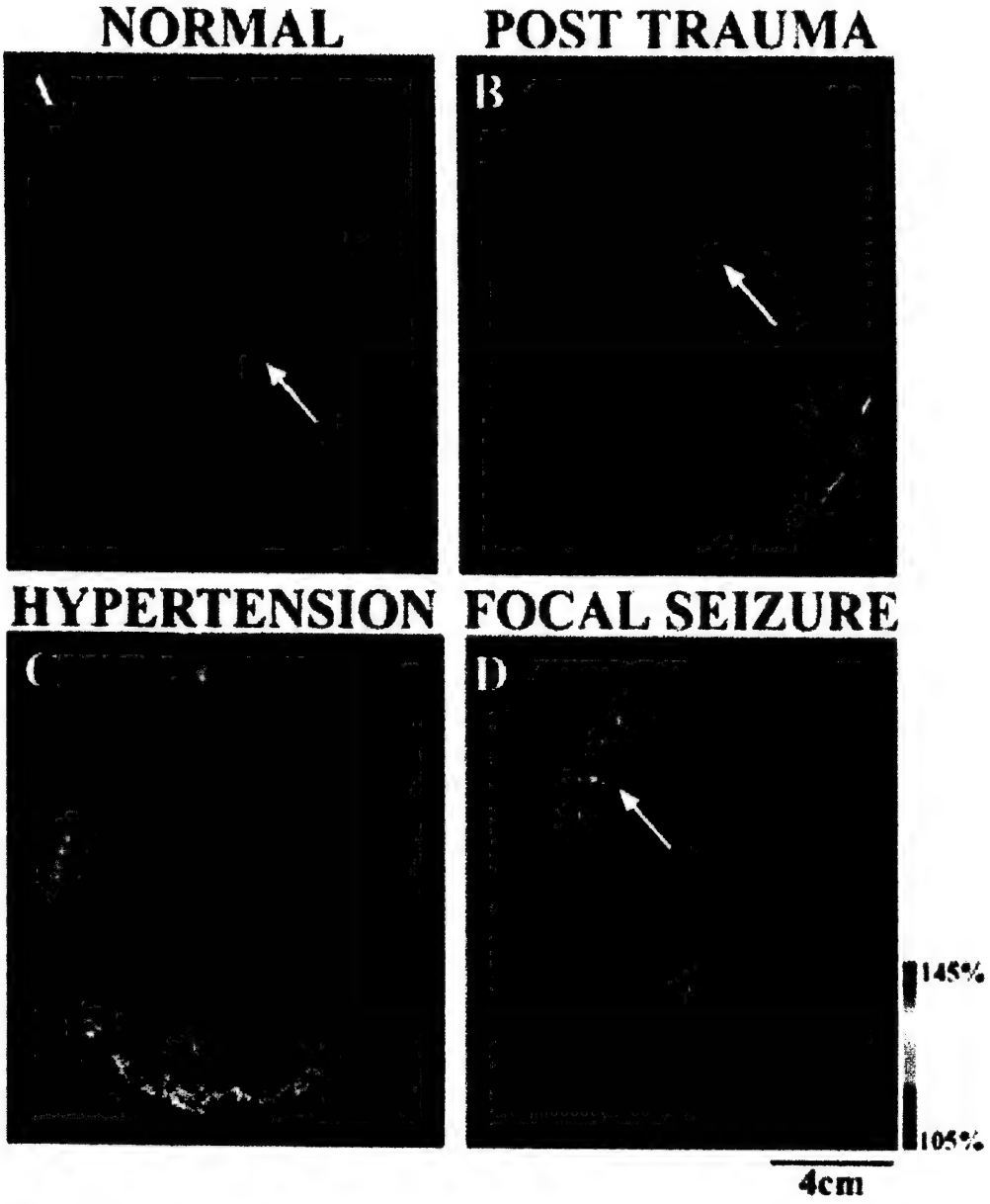

Fig. 2. Enhancement in variable brain regions in patients with CNS-related disorders. Shown are pseudocolored differential brain CT images in which signals before Omnipaque were subtracted from those following contrast agent injection. The color code refers to the range of radiopacity between water (no radiopacity, dark blue) and bone (full radiopacity, orange-red). Scale bars in all images represent 4 cm. (A) Ambulatory patient with a normal CT, with enhancement confined to choroid plexus (arrow). (B) Focal enhancement (arrow) in an 8-month-old infant 1 week following head trauma. (C) Diffuse enhancement in a 24-year-old pregnant woman presented with eclampsia. (D) Focal enhancement (arrow) in a 56-year-old man presented with a focal seizure in his left hand.

otherwise appeared normal. For example, diffuse penetration of Omnipaque into cortical gray matter was evident in a 24-year-old pregnant patient with decreased level of consciousness, who suffered from hypertensive encephalopathy (Fig. 2(C)). An abnormal focal enhancement to a cortical gyrus in the right fronto-parietal cortex was noted in another patient, presented to the emergency room with a focal seizure in his left hand (Fig. 2(D)).

Next, we wished to test the spatial distribution, persistence, and consistency of the disrupted BBB. We therefore compared brain accumulation of three different contrasting agents employed in various imaging approaches. In three patients who were subjected to several image analyses within 1 month, focal enhancement in precisely the same site was found for Omnipaque (in a CT scan), gadolinium (under MRI analysis) or Tc-DTPA (in SPECT analysis). Figure 3 shows a series of imaging studies demonstrating focal and persistently disrupted BBB in one of these patients 6 months following radiosurgery for arteriovenous malformation. One of the other two patients (images not shown) suffered from meningeal spread of tumor cells (primary CNS lymphoma) while the other from partial seizures. SPECT following administration of the brain nonpenetrating compound Tc-DTPA was then compared to perfusion analysis using the freely permeable Tc-ECD (Fig. 3(C)). In each of these three patients, focal BBB disruption was accompanied by decreased perfusion (Fig. 3(C) and data not shown). This rules out enhanced perfusion as the underlying cause for contrast agent accumulation.

The retrospective nature of our study offered an apportunity for nonbiased exploration of clinical correlates that accompany the enhancement in CT signals due to BBB disruption. To this end, we analyzed the general clinical profiles as well as the available data on serum and CSF constituents for 19 patients who were investigated within 12 h for various suspected neurological disorders but no focal abnormality was found in CT. These patients were classified by increasing order of signal enhancement and divided into three equal groups, displaying low, average, and high, diffuse gray matter enhancement of contrast agent signals (Table I). Average values of patients' blood pressure, heart rate, body temperature, white blood cell and platelet counts, CSF and serum glucose and albumin as well as serum cortisol was compared between the groups. In patients from the "low penetrance" group, the averaged postinjection signal generated by the contrast agent was not significantly different from that of preinjection ($(-1.8 \pm 3.8)\%$ enhancement, mean $\pm$ SEM), and was significantly lower than the >10% enhancement values calculated for the "high penetrance" group ($p = 0.001$). Statistically significant differences between these two groups ($p < 0.05$, Mann–Whitney test, see Table I) were also observed in body temperature, systolic and diastolic blood pressure, total CSF protein, and serum cortisol. The correlation ($r^2 = 0.85$) between enhancement values and CSF albumin concentration (Fig. 4(A)) further strengthens the notion that enhancement values indeed reflect quantitative estimations of the permeability of the BBB to large molecules. In all other clinical indices no significant difference was found between patients with low vs. high Omnipaque penetration (Table I). These findings suggest that inflammatory reactions in the peripheral or the CNS are not ultimate causes of BBB disruption (Abbott, 2000) (see Discussion).

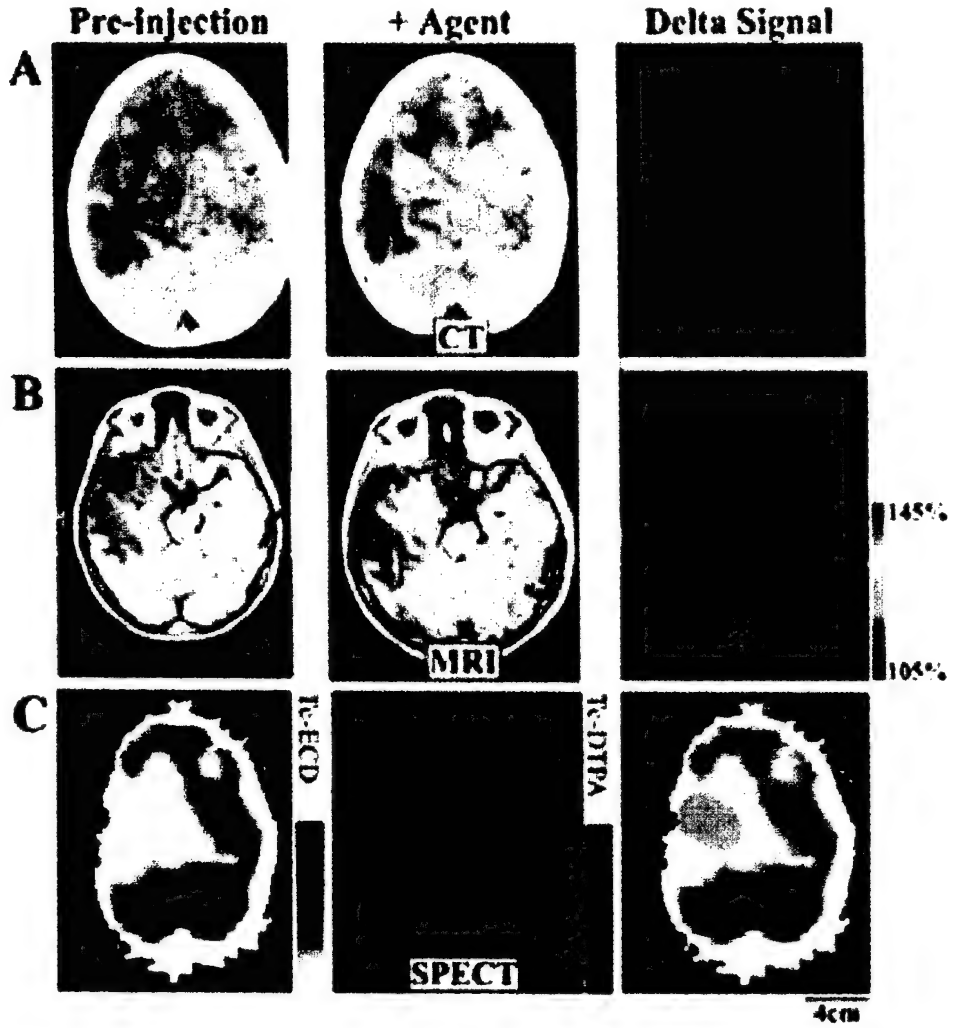

Fig. 3. BBB disruption as portrayed by CT, MRI, and SPECT. Shown are axial sections from a single patient, where BBB disruption was evident by brain signal enhancement in CT (A), MRI (B), and SPECT (C) following administration of Omnipaque, gadolinium, or Tc-DTPA, respectively, all within 1 month. Tc-ECD was used, 2 days after Tc-DTPA administration, for evaluating brain perfusion demonstrating that decreased perfusion (C, left) and increased brain penetrance (C, middle) overlapped (C, right).

BBB disruption could not be attributed to a single CNS pathology. In one patient (#16 in Table I), high CT signal enhancement was detected, yet no ovious CNS pathology found. In other patients, diagnosed for clinical conditions assumed to induce BBB disruption, no radiological or molecular evidence was found for increased BBB permeability. For example, in patients #1 and 7 who were presented with a generalized convulsion, CT displayed none or only mild cortical enhancement and no albumin was detected in their CSF. In contrast, patients #15 and 17, both of whom also presented with a generalized convulsion, displayed high penetration. Therefore, the cumulative average of our clinical and biochemical markers suggests general

Table I. Clinical Indices of "Neurological Patients"[a]

#	Age	Sex	Diagnosis	CT-% enhancement in gray matter	Hb (mg/dL)	Platelets (10^3 mm^{-3})	WBC (10^3 mm^{-3})	Serum glucose (mg/dL)	Serum cortisol (μg/dL)	CSF glucose (mg/dL)	CSF protein (mg/dL)	Heart rate (min^{-1})	B.p. systole (mbar)	B.p. diastole (mbar)	Core temp. (°C)
Low															
1	12	F	Fever, convulsions	−6.7	12.2	172	15.3	96	16.5	75	14	125	88	50	37.0
2	52	M	Coma, staphylococcal sepsis, S/P head trauma	−6.0	8.9	414	6.8	199	14.35	101	23	87	140	72	37.2
3	27	M	Headache, investigation	−2.0	15.8	340	14	132	41.7	93	27	—	—	—	—
4	1	M	Headache	0.7	13	501	15	85	16.4	66	42	118	94.5	43	37.1
5	93	M	Vomiting	1.4	11.7	215	11.7	124	26.4	81	45	89	133	64	38.2
6	19	F	Myelopathy	2.0	13.1	406	8.8	113	15.2	61	39	104	110	54	37.0
Average	**34**			**−1.8**	**12.5**	**341.3**	**11.9**	**124.8**	**21.8**	**79.5**	**21.7**	**104.6**	**113.1**	**56.6**	**37.3**
SDV	**33.6**			**3.8**	**2.2**	**126.2**	**3.5**	**40.3**	**10.7**	**15.4**	**12.2**	**16.9**	**22.9**	**11.5**	**0.5**
Medium															
7	36	F	Pneumococcal sepsis, convulsions	3.3	8.5	531	17.3	130	20.3	53	11	78	152	81	36.5
8	59	F	Fever for investigation, S/P head trauma	4.9	9.7	938	17.3	103	17.4	48	48	90	147	102	38.0
9	5/12	M	Meningitis proteus	5.4	13.7	88	8.2	70	—	3	95	140	—	—	34
10	40	F	S/P, pneumococcal meningitis	5.7	11.4	285	19.7	280	35	113	48	115	134	63	37.7
11	1	F	Febrile convulsions	5.8	12.6	288	25.9	125	—	90	14	147	113	59	37.4
12	31	M	Fever for investigation	8.2	16.8	313	10.0	111	14.8	69	41	72	120	73	37.5
13	10	M	Sagittal sinus vein thrombosis	10.1	9.6	309	10.0	103	21.1	85	16	108	120	77	37.8
Average	**25.3**			**6.2**	**11.8**	**393.1**	**15.5**	**131.7**	**21.7**	**65.9**	**39.0**	**107.1**	**131.0**	**75.8**	**36.9**
SDV	**22.1**			**2.3**	**2.9**	**272.4**	**6.4**	**68.2**	**7.3**	**35.6**	**29.5**	**29.2**	**15.9**	**15.3**	**1.4**
High															
14	68	M	Coma, investigation	11.0	11.9	193	12.3	137	28.5	97	41	114	166	92	37.7
15	1	M	Convulsive episode	12.6	11	449	10.4	70	25.6	85	26	137	115	57	37.4
16	1	M	Gastroenteritis—	15.3	7.9	669	16.1	105	27.5	—	126	148	112	55	38.3
17		M	Convulsive episode	16.7	17.3	241	10.2	393	76.2	213	64	120	143	89	37.5
18	55	F	Pneumococcal meningitis	26.4	12.3	296	20	200	92.9	62	99	103	150	72	39.2
19	69	M	Coma, investigation	33.9	10.6	497	11.4	335	20.7	184	72	112	184	88	37.6
Average	**38.8**			**19.3**	**11.8**	**390.8**	**13.4**	**206.7**	**45.2**	**128.2**	**71.3**	**122.3**	**145.0**	**75.5**	**38.0**
SDV	**34.9**			**8.9**	**3.1**	**180.3**	**3.9**	**130.5**	**31.0**	**66.2**	**36.8**	**16.9**	**28.2**	**16.6**	**0.7**
p (Mann–Whitney)	0.535			0.001	0.242	0.35	0.35	0.155	0.032	0.123	0.032	0.123	0.026	0.041	0.026

[a]Patients who were presented with "neurological signs and symptoms" but with no focal enhancing lesion in CT were evaluated. Presented in the table are the averages of available clinical data taken on several occasions within 6 h of the scan. Patients are sorted in ascending order by percent enhancement, for low, medium, and high enhancement values, averages and SDV are given in bold. In all cases the most specific available diagnosis is given. "Investigation" refers to patients who were admitted with a clinical picture indicating a neurological disorder which was not identified. "Meningitis" refers to bacterial infection (identified organism is noted). Patients #2 and 6 suffered from Head Trauma more than 1 month before the reported investigation. Patient #18 was more than 1 month following a brain surgery for total removal of meningioma. All convulsions were of the "general type." Percent enhancement in the cortical gray matter is given as the average of the two cerebral hemispheres. *p* values between low and high (using the nonparametric Mann–Whitney test) are presented in the last row (see text).

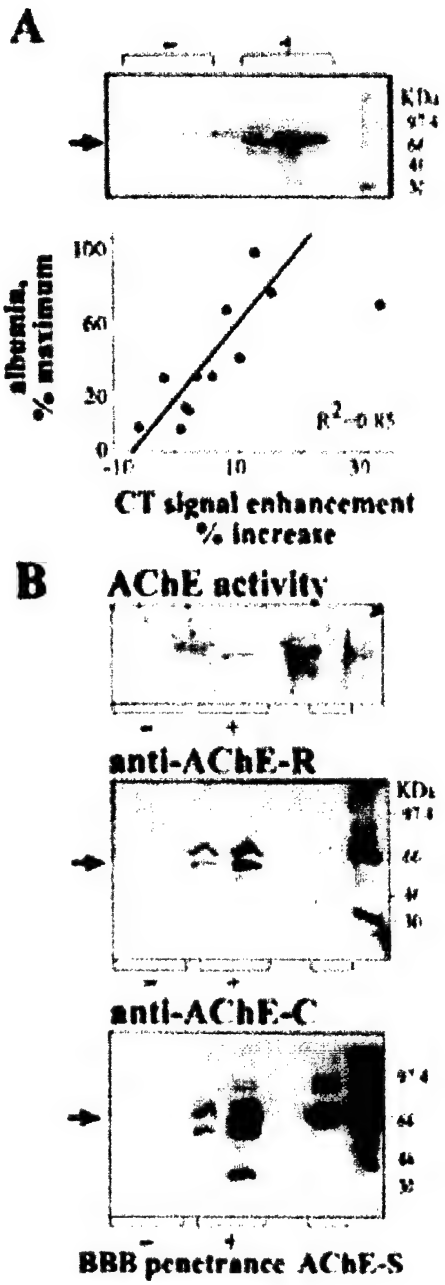

Fig. 4. BBB disruption is associated with CSF accumulation of albumin and AChE-R. (A) Albumin accumulation. Shown are albumin immunostaining following gel electrophoresis of CSF proteins (top) and correlation analysis (bottom) between CSF albumin concentrations (% of maximal level) and CT signal enhancement (% above preinjection signal intensity). Note that albumin concentrations are linearly correlated with CT signal enhancement. (B) AChE in CSF. Top: Shown is activity staining of CSF AChE following gel electrophoresis under nondenaturing conditions. Note that CSF samples with compromised (+) but not with intact (−) BBB display catalytically active AChE which co-migrates with recombinant (r) AChE-S or AChE-R produced in COS cells. Bottom: Immunoblot analyses following denaturing gel electrophoresis and incubation with antibodies selective for AChE-R (upper) or the C-terminally truncated AChE-core (lower). Note appearance of AChE-R in the same samples with AChE activity and the presence of proteolytic degradation products of the core AChE domain.

stress responses rather than a specific neurological condition as the phenotype common to patients with disrupted BBB.

Several groups have previously associated stress with focal or diffused BBB disruption (Belova and Jonsson, 1982; Ben-Nathan *et al.*, 1991; Esposito *et al.*, 2001, Friedman *et al.*, 1996; Sharma *et al.*, 1992), while others reported differently (Grauer *et al.*, 2000; Sinton *et al.*, 2000), possibly because of species, age, and experimental

manipulation differences, etc. Molecular biology approaches have associated such disruption with the rapid accumulation of the "readthrough" brain AChE-R isoform (Kaufer *et al.*, 1998a; Shohami *et al.*, 2000). To search for this AChE isoform in patients' CSF, we used antibodies selective for the C-terminal sequence unique to AChE-R. For comparison, we employed antibodies targeted to the core domain common to all AChE isoforms (Shohami *et al.*, 2000). Cytochemical staining of the electrophoretically separated CSF proteins was used to evaluate the capacity of CSF AChE to hydrolyze acetylthiocholine, a property common to all intact AChE isoforms (Soreq and Seidman, 2001). CSF samples from patients with compromised, but not with intact, BBB revealed conspicuous increases in catalytically active AChE (Fig. 4(B)). Comparative immunodetection with antibodies selective for the AChE-R variant indicated that these CSF samples included intact stress-associated AChE-R as well as degradation products from the C-terminus (Fig. 4(B)). Other AChE degradation products lacked the C-terminal peptide unique to AChE-R, as they reacted with antibodies targeted to the common core domain, but not to the C-terminus of AChE-R, and migrated faster than expected for the intact protein (Fig. 4(B)). Densitometric analysis of the immunopositive AChE-R bands displayed positive correlation with the signal enhancement levels, with an increase from an average of 29 ± 5 pixels for the low penetrance group to 58 ± 3 pixels for the high penetrance one. Further analysis will be required to test the significance of this increase in a larger group of patients.

To determine whether BBB disruption is associated with altered brain electrical activity, EEG recordings were performed on patients who showed a focal disruption in imaging studies. Figure 5 shows the results of such correlation in a 46-year-old female patient who suffered recurrent sensory disturbances in her right hand 12 months following the complete removal of a small meningioma. While MRI ruled out tumor recurrence, SPECT–DTPA showed abnormal BBB in cortical areas adjacent to the site of surgery (Fig. 5(A)). Power spectrum analyses of this patient's EEG showed clear increases in abnormal slow waves (3–6 Hz). This was associated with high alpha waves (10 Hz) activity in the records collected from the C3, but not from the C4 electrode in the contra lateral hemisphere (Fig. 5(B)). The location of these surface wave patterns matched that of a cortical area suffering from disrupted BBB (Fig. 5(B)).

DISCUSSION

In search for a minimally invasive approach for quantifying and characterizing BBB disruption in humans, we validated the use of CT brain imaging. Abnormal enhancement of brain CT signals was detected in over one half of neurological patients but not in ambulatory patients without neurological abnormalities. CSF albumin concentrations suggest that this abnormal enhancement reflects the extent of BBB disruption. Signal enhancement was also associated with significant increases in blood pressure, serum cortisol, and body temperature; in contrast, heart rate and WBC count appeared unrelated with BBB disruption. Focal BBB disruption correlated spatially with abnormal EEG, reflecting corresponding focal changes in neuronal

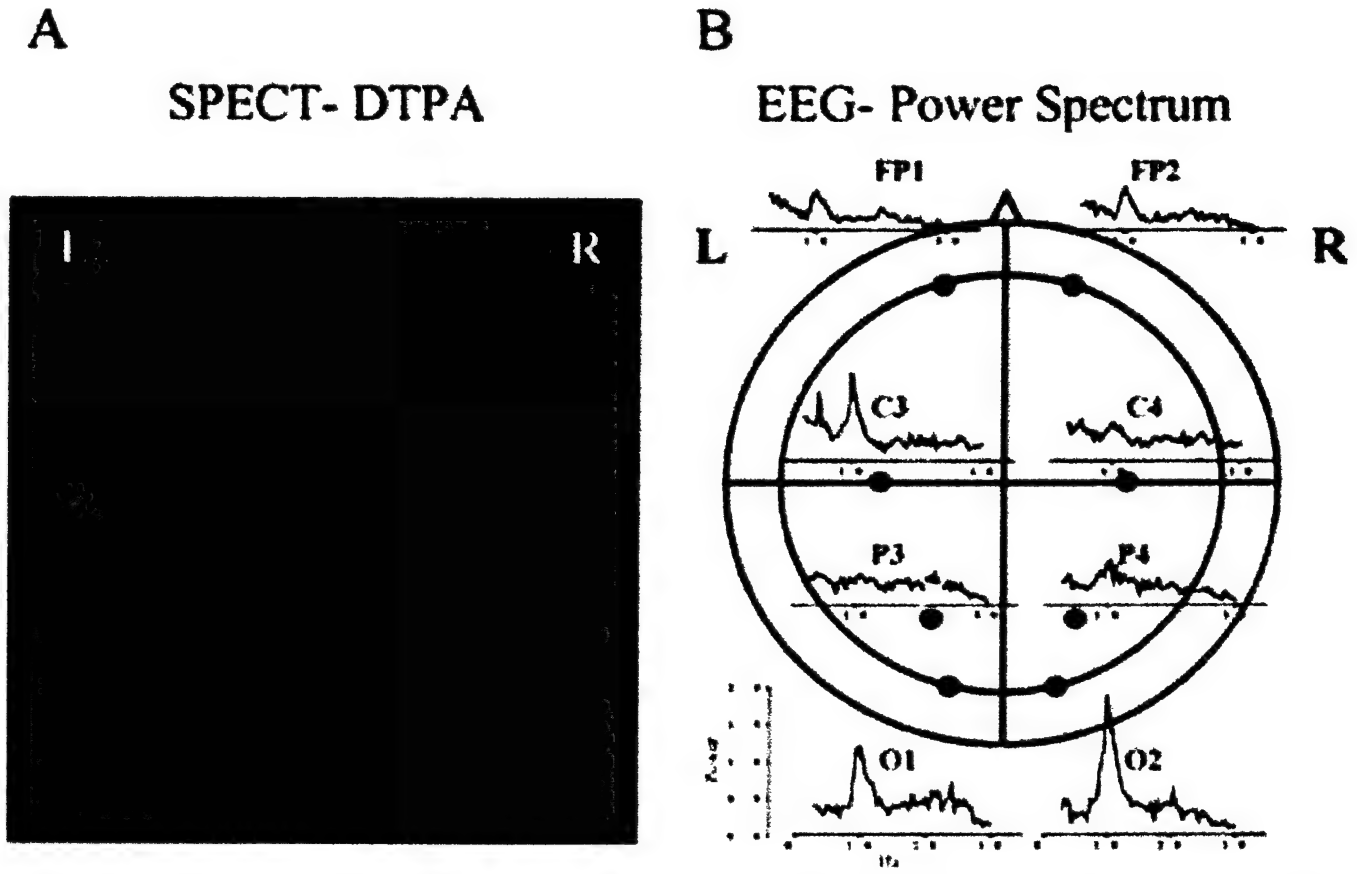

Fig. 5. EEG recordings match anatomic location of BBB disruption. (A) Axial SPECT image for the same patient performed following the administration of DTPA reveals increased signal in the left hemisphere (arrow). (B) Cortical mapping of power spectra based on 20 two-second epochs of spontaneous EEG activity (eyes closed), collected from a patient with a focal BBB disruption 12 months following surgery for the removal of a meningioma. Brain CT did not show any evidence for tumor. Spectral analyses is shown from three bilaterally matching scalp electrodes of the international 10–20 system. Left and right paired spectra are symmetrical in all electrodes, with exception of the centrally located C3 and C4 electrodes, where increased slow delta and alpha frequency are shown over the left hemisphere. This area corresponds to the area of abnormal SPECT shown in part A.

activity, as found by EEG recordings. These colonized changes indicate the importance of an intact BBB for the maintenance of normal brain function. The significant increase in CSF AChE-R accumulation in the CSF of patients with BBB disruption further emphasizes the linkage between the cholinergic system, stress, and the control over BBB permeability. Rather unexpectedly, in several patients, stable penetration patterns were observed during several weeks of clinical investigation. This suggests that BBB breakdown may persist for a long period, emphasizing the importance of the use of brain imaging for diagnosis. Recognition of BBB disruption may, in turn, call for adjustment of the treatment protocol for these patients.

The observed high incidence and persistence of BBB disruption bears both clinical and basic research implications at several levels. Regardless of the contrast agent employed, each of the brain imaging approaches yielded similar locations and apparent extent of BBB disruption. This reinforces the concept that BBB disruption may be confined to specific brain areas. The more intense general enhancement in the cerebral cortex most likely reflects a particular vulnerability of this region to BBB disruption.

The cerebral cortex microvasculature differs from other brain regions in the mechanisms controlling its blood flow (Inanami *et al.*, 1992) as well as in its cholinergic receptors' distribution (Elhusseiny *et al.*, 1999), and afferent innervation (Triguero *et al.*, 1988). This further raises the possibility that the barrier function at the level of the cerebral cortex can be modulated by neuronal activity. For example, BBB permeability has been known to increase following activation of the noreadrenergic locus coeruleus (Raichle *et al.*, 1975). Our imaging analysis supports previous reports showing BBB breakdown in epileptic patients (Cornford and Oldendorf, 1986); however, in our patients, persistent BBB disruption was observed in the absence of any evidence for active epileptic foci. Although it is generally assumed that seizures induce BBB disruption, it is not known how increased BBB permeability effects the physiological response of neurons. However, cortical neurons are known for their vulnerability to small changes in their extracellular environment (Lux, 1980; Schwartzkroin *et al.*, 1998) and for their tendency to develop synchronous epileptic activity (Jefferys, 1988). This raises the possibility of consequent neuronal toxicity (Charriaut-Marlangue *et al.*, 1996; Meldrum, 1993) in areas of persistent BBB disruption. Indeed, Kadota *et al.* (1997) reported that hippocampal neurons display excitotoxic damage following local serum infusion. Moreover, stress-induced cytokines, hormones, or small molecules such as nitric oxide (van Amsterdam and Opperhuizen, 1999) may be expected by preferentially affect cortical neurons and glial cells (Sapolsky, 1996).

At the molecular level, this study adds AChE-R to albumin as a CSF-accumulated marker of BBB disruption. Persistent stress-induced accumulation of the AChE-R protein therefore emerges as a stress response that is common to rodents and humans. The immediate source of AChE-R in human CSF can be the circulation, like albumin. Alternatively, or in addition, this secretory soluble protein may reach the CSF from stress-responding brain neurons (Shohami *et al.*, 2000) and/or endothelial cells lining vascular brain capillaries (Flumerfelt *et al.*, 1973). AChE-R degradation products may reflect the stress-induced increase in proteases (Chan and Mattson, 1999).

Apart from convulsions, with the highest predicted value for BBB disruption, our findings could only correlate this phenomenon with the intensity of stress responses. However, the mechanisms underlying stress-associated BBB disruption are yet to be found. Inflammatory responses (Rhodin *et al.*, 1999), hemodynamic changes (i.e. blood pressure) (Robinson and Moody, 1980), and brain-derived modulators are all possible candidates. Individual variations in BBB disruption may also be due to its being a complex genetic trait. For example, recent findings of signal transduction in brain endothelial cells attribute rapid and long-lasting changes in their functioning to the NO-synthase cascade (Calingasan *et al.*, 1998). Administration of NO-synthase inhibitors was indeed shown to reduce meningitis-associated BBB disruption in rodents (Boje, 1996). This calls for seeking potential correlations(s) between compromised BBB in patients and the NO pathway. Another example refers to the multiple drug resistance (*mdr1a*) gene, which encodes the drug transporting P-glycoprotein that resides in the BBB. Genomic disruption of *mdr1a* induces up to 10-fold increases in the uptake of dexamethasone into the mouse brain (Meijer *et al.*, 1998). This raises the general question whether patients under massive drug treatments, in whom the mdr1a protein is fully saturated, develop transiently modulated susceptibility for BBB disruption. A yet more specific example is that of the "atypical" allele of butyrylcholinesterase (BChE) (Loewenstein-Lichtenstein *et al.*, 1995), which increases the brain permeation of cholinesterase inhibitors due to reduced scavenging of such poisons in the circulation. Homozygous carriers of this allele may present genetic predisposition to hypersensitivity for BBB disruption under anticholinesterase exposure. Also relevant is polymorphism in a specific isoform of glutathione transferase (GSTp), which resides in endothelial cells of brain vasculature and protects the brain tissue from penetration of xenobiotics. One of the GSTp variants, with impaired substrate specificity, was found with much higher incidence in patients with Parkinson's disease, as compared to controls (Menegon *et al.*, 1998). The common denominator to all of the genes with apparent linkage to BBB disruption (mdr1a, GSTp, BCHE, and NO synthase) is that they are all involved in scavenging processes. Acquired hypersensitivity because of previous drug or chemical exposure may hence provide a major cause of BBB disruption (Kaufer *et al.*, 1998b). Increases in the risk for developing Parkinson's disease were indeed reported following exposure to brain-penetrable chemicals (e.g., lead from batteries (Kuhn *et al.*, 1998) and organophosphorous insecticides (Senanayake and Sanmuganathan, 1995)). These acquired and inherited risks may point to the intriguing possibility that BBB disruption is causally involved with neurodegenerative diseases, so that its impaired maintenance may be relevant to both acute and delayed syndromes. While our study points to stress as an important cause underlying prolonged BBB disruption in humans, future research will elucidate the association between such disruption and stress-related excitotoxic brain damage (Haley *et al.*, 2000; Sapolsky, 1996).

ACKNOWLEDGMENTS

This work was supported by grants from the U.S. Army Medical Research and Development Command (DAMD17-99-1-9547 to H. Soreq and A. Friedman), The

Israeli Health Ministry (to A. Friedman), The Israel Science Foundation and Ester Neurosciences, Ltd. (to H. Soreq).

REFERENCES

Abbott, N. J. (2000). Inflammatory mediators and modulation of blood-brain barrier permeability. *Cell Mol. Neurobiol.* **20:**131–147.

Abbruscato, T. J., and Davis, T. P. (1999). Protein expression of brain endothelial cell E-cadherin after hypoxia/aglycemia: Influence of astrocyte contact. *Brain Res.* **842:**277–286.

Akeson, P., Larsson, E. M., Kristoffersen, D. T., Jonsson, E., and Holtas, S. (1995). Brain metastases-comparison of gadodiamide injection-enhanced MR imaging at standard and high dose, contrast-enhanced CT and non-contrast-enhanced MR imaging. *Acta Radiol.* **36:**300–306.

Bakay, L. (1976). Blood-brain barrier and its alteration in pathological states. In Vinken, P. J., and Bruyn, G. W. (eds.), *Handbook of Clinical Neurology, Vol. 28*, Elsevier/North-Holland Biomedical Press, Amsterdam, p. 370.

Belova, I., and Jonsson, G. (1982). Blood-brain barrier permeability and immobilization stress. *Acta Physiol. Scand.* **116:**21–29.

Ben-Nathan, D., Lustig, S., and Danenberg, H. D. (1991). Stress-induced neuroinvasiveness of a neurovirulent noninvasive Sindbis virus in cold or isolation subjected mice. *Life Sci.* **48:**1493–1500.

Boje, K. M. (1996). Inhibition of nitric oxide synthase attenuates blood-brain barrier disruption during experimental meningitis. *Brain Res.* **720:**75–83.

Brooks, R. A. (1977). A quantitative theory of the Hounsfield unit and its application to dual energy scanning. *J. Comput. Assist. Tomogr.* **1:**487–493.

Calingasan, N. Y., Park, L. C., Calo, L. L., Trifiletti, R. R., Gandy, S. E., and Gibson, G. E. (1998). Induction of nitric oxide synthase and microglial responses precede selective cell death induced by chronic impairment of oxidative metabolism. *Am. J. Pathol.* **153:**599–610.

Chan, S. L., and Mattson, M. P. (1999). Caspase and calpain substrates: Roles in synaptic plasticity and cell death. *J. Neurosci. Res.* **58:**167–190.

Charriaut-Marlangue, C., Aggoun-Zouaoui, D., Represa, A., and Ben-Ari, Y. (1996). Apoptotic features of selective neuronal death in ischemia, epilepsy and gp 120 toxicity. *Trends Neurosci.* **19:**109–114.

Cornford, E. M., and Oldendorf, W. H. (1986). Epilepsy and the blood-brain barrier. *Adv. Neurol.* **44:**787–812.

Correale, J., Rabinowicz, A. L., Heck, C. N., Smith, T. D., Loskota, W. J., and DeGiorgio, C. M. (1998). Status epilepticus increases CSF levels of neuron-specific enolase and alters the blood-brain barrier. *Neurology* **50:**1388–1391.

Elhusseiny, A., Cohen, Z., Olivier, A., Stanimirovic, D. B., and Hamel, E. (1999). Functional acetylcholine muscarinic receptor subtypes in human brain microcirculation: Identification and cellular localization. *J. Cereb. Blood Flow Metab.* **19:**794–802.

Esposito, P., Gheorghe, D., Kandere, K., Pang, X., Connolly, R., Jacobson, S., and Theoharides, T. C. (2001). Acute stress increases permeability of the blood-brain barrier through activation of brain mast cells. *Brain Res.* **888:**117–127.

Flumerfelt, B. A., Lewis, P. R., and Gwyn, D. G. (1973). Cholinesterase activity of capillaries in the rat brain. A light and electron microscopic study. *Histochem. J.* **5:**67–77.

Friedman, A., Kaufer, D., Shemer, J., Hendler, I., Soreq, H., and Tur-Kaspa, I. (1996). Pyridostigmine brain penetration under stress enhances neuronal excitability and induces early immediate transcriptional response. *Nat. Med.* **2:**1382–1385.

Grauer, E., Alkalai, D., Kapon, J., Cohen, G., and Raveh, L. (2000). Stress does not enable pyridostigmine to inhibit brain cholinesterase after parenteral administration. *Toxicol. Appl. Pharmacol.* **164:**301–304.

Haley, R. W., Marshall, W. W., McDonald, G. G., Daugherty, M. A., Petty, F., and Fleckenstein, J. L. (2000). Brain abnormalities in Gulf War syndrome: Evaluation with 1H MR spectroscopy. *Radiology* **215:**807–817.

Inanami, O., Ohno, K., and Sato, A. (1992). Responses of regional cerebral blood flow to intravenous administration of thyrotropin releasing hormone in aged rats. *Neurosci. Lett.* **143:**151–154.

Jefferys, J. G. (1998). Mechanisms and experimental models of seizure generation. *Curr. Opin. Neurol.* **11:**123–127.

Kadota, E., Nonaka, K., Karasuno, M., Nishi, K., Teramura, K., and Hashimoto, S. (1997). Neurotoxicity of serum components, comparison between CA1 and striatum. *Acta Neurochir. Suppl. (Wien)* **70:**141–143.

Kaufer, D., Friedman, A., Seidman, S., and Soreq, H. (1998a). Acute stress facilitates long-lasting changes in cholinergic gene expression. *Nature* **393:**373–377.

Kaufer, D., Friedman, A. Seidman, S., and Soreq, H. (1998b). Anticholinesterases induce multigenic transcriptional feedback response suppressing cholinergic neurotransmission. *Chem. Biol. Interact.* **119:**349–360.

Klatzo, I. (1983). Disturbance of the blood-brain barrier in cerebrovascular disorders. *Acta Neuropathol. Suppl. (Berl)* **8:**81–8.

Kuhn, W., Winkel, R., Woitalla, D., Meves, S., Przuntek, H., and Muller, T. (1998). High prevalence of parkinsonism after occupational exposure to lead-sulfate batteries. *Neurology* **50:**1885–1886.

Loewenstein-Lichtenstein, Y., Schwarz, M., Glick, D., Norgaard-Pedersen, B., Zakut, H., and Soreq, H. (1995). Genetic predisposition to adverse consequences of anti-cholinesterases in 'atypical' BCHE carriers. *Nat. Med.* **1:**1082–1085.

Lux, H. D. (1980). Ionic conditions and membrane behavior. *Adv. Neurol.* **27:**63–83.

McCullough, E. C., Baker, H. L., Jr., Houser, O. W., and Reese, D. F. (1974). An evaluation of the quantitative and radiation features of a scanning x-ray transverse axial tomograph: The EMI scanner. *Radiology* **111:**709–715.

Meijer, O. C., de Lange, E. C., Breimer, D. D., de Boer, A. G., Workel, J. O., and de Kloet, E. R. (1998). Penetration of dexamethasone into brain glucocorticoid targets is enhanced in mdr1A P-glycoprotein knockout mice. *Endocrinology* **139:**1789–1793.

Meldrum, B. S. (1993). Excitotoxicity and selective neuronal loss in epilepsy. *Brain Pathol.* **3:**405–412.

Menegon, A., Board, P. G., Blackburn, A. C., Mellick, G. D., and Le Couteur, D. G. (1998). Parkinson's disease, pesticides, and glutathione transferase polymorphisms. *Lancet* **352:**1344–1346.

Raichle, M. E., Hartman, B. K., Eichling, J. O., and Sharpe, L. G. (1975). Central noradrenergic regulation of cerebral blood flow and vascular permeability. *Proc. Natl. Acad. Sci. U.S.A.* **72:**3726–3730.

Rhodin, J., Thomas, T., Bryant, M., Clark, L., and Sutton, E. T. (1999). Animal model of vascular inflammation. *J. Submicrosc. Cytol. Pathol.* **31:**305–311.

Robinson, J. S., and Moody, R. A. (1980). Influence of respiratory stress and hypertension upon the blood-brain barrier. *J. Neurosurg.* **53:**666–673.

Roman-Goldstein, S., Clunie, D. A., Stevens, J., Hogan, R., Monard, J., Ramsey, F., and Neuwelt, E. A. (1994). Osmotic blood-brain barrier disruption: CT and radionuclide imaging. *AJNR Am. J. Neuroradiol.* **15:**581–590.

Rubin, L. L., and Staddon, J. M. (1999). The cell biology of the blood-brain barrier. *Annu. Rev. Neurosci.* **22:**11–28.

Sapolsky, R. M. (1996). Why stress is bad for your brain. *Science* **273:**749–750.

Schwartzkroin, P. A., Baraban, S. C., and Hochman, D. W. (1998). Osmolarity, ionic flux, and changes in brain excitability. *Epilepsy Res.* **32:**275–285.

Senanayake, N., and Sanmuganathan, P. S. (1995). Extrapyramidal manifestations complicating organophosphorus insecticide poisoning. *Hum. Exp. Toxicol.* **14:**600–604.

Sharma, H. S., Kretzschmar, R., Cervos-Navarro, J., Ermisch, A., Ruhle, H. J., and Dey, P. K. (1992). Age-related pathophysiology of the blood-brain barrier in heat stress. *Prog. Brain Res.* **91:** 189–196.

Shohami, E., Kaufer, D., Chen, Y., Seidman, S., Cohen, O., Ginzberg, D., Melamed-Book, N., Yirmiya, R., and Soreq, H. (2000). Antisense prevention of neuronal damages following head injury in mice. *J. Mol. Med.* **78:**228–236.

Siegal, T., Rubinstein, R., Bokstein, F., Schwartz, A., Lossos, A., Shalom, E., Chisin, R., and Gomori, J. M. (2000). In vivo assessment of the window of barrier opening after osmotic blood-brain barrier disruption in humans. *J. Neurosurg.* **92:**599–605.

Sinton, C. M., Fitch, T. E., Petty, F., and Haley, R. W. (2000). Stressful manipulations that elevate corticosterone reduce blood-brain barrier permeability to pyridostigmine in the rat. *Toxicol. Appl. Pharmacol.* **165:**99–105.

Skoog, I., Wallin A., Fredman, P., Hesse, C., Aevarsson, O., Karlsson, I., Gottfries, C. G., and Blennow, K. (1998). A population study on blood-brain barrier function in 85-year-olds: Relation to Alzheimer's disease and vascular dementia. *Neurology* **50:**966–971.

Soreq, H., Kaufer, D., Friedman, A., and Glick, D. (2000). Blood-brain barrier modulations and low-level exposure to xenobiotics. In Somani S. M., and Romano J. A. (eds.), *Chemical Warefare Agents: Low Level Toxicity*, CRC Press, Boca, Raton, FL, pp. 121–144.

Soreq, H., and Seidman, S. (2001). Acetylcholinesterase—new roles for an old actor. Nature *Neurosci. Rev.* **2:**294–302.

Sternfeld, M., Shoham, S., Klein, O., Flores-Flores, C., Evron, T., Idelson, G. H., Kitsberg, D., Patrick, J. W., and Soreq, H. (2000). Excess "read-through" acetylcholinesterase attenuates but the "synaptic" variant intensifies neurodeterioration correlates. *Proc. Natl. Acad. Sci. U.S.A.* **97:**8647–8652.

Tator, C. H., and Schwartz, M. L. (1971). Permeability in brain tumors. *J. Neurosurg.* **34:**460–462.

Triguero, D., Lopez de Pablo, A. L., Gomez, B., and Estrada, C. (1988). Regional differences in cerebrovascular cholinergic innervation in goats. *Stroke* **19:**736–740.

van Amsterdam, J. G., and Opperhuizen, A. (1999). Nitric oxide and biopterin in depression and stress. *Psychiatry Res.* **85:**33–38.

Cellular and Molecular Neurobiology, Vol. 21, No. 6, December 2001 (© 2002)

Genomic Dissection Reveals Locus Response to Stress for Mammalian Acetylcholinesterase

Alastair D. Grant,[1] Michael Shapira,[1,2] and Hermona Soreq[1,3]

Received October 15, 2001; accepted October 30, 2001

SUMMARY

The mammalian acetylcholinesterase (*ACHE*) locus was investigated using computational predictive methods and experiments of reverse transcription polymerase chain reaction (RT-PCR). Computational analysis identified two genes downstream to *ACHE*, an inversely oriented arsenite resistance gene homologue (*ARS*), and a novel previously unidentified gene (*PIX*), co-oriented with *ACHE*. Experimental evidence shows coregulation of murine *ACHE* and *ARS* following confined swim, indicating coordinated locus response to stress, that is possibly mediated by altered cholinergic neurotransmission.

KEY WORDS: acetylcholinesterase; ARS; PIX; stress response; locus response.

INTRODUCTION

Chromosomal abnormalities involving the *ACHE* locus harboring the gene that codes for the acetylcholine hydrolyzing enzyme, acetylcholinesterase (AChE), are associated with much human pathology. Some of these abnormalities are attributed to chromosomal aberrations involving band 7q22, harboring the human (h)*ACHE* locus (e.g., h*ACHE* gene amplification in ovarian carcinoma (Zakut *et al.*, 1990)) and to frequent breakage in various types of leukemias (Johnson and Cotter, 1997). Others appear to involve changes in AChE expression. Increased AChE levels were reported in glioma tumors, as compared with benign astrocytes (Razon *et al.*, 1984), whereas reduced AChE levels were observed in lymphomas (Lampert and Van Noorden, 1996). While it is possible that the noncatalytic proliferative capacities of AChE (reviewed by Soreq and Seidman, 2001) are causally involved in these pathologies, the molecular mechanism(s) underlying such processes are not yet known.

[1] Department of Biological Chemistry, The Alexander Silberman Institute of Life Sciences, Hebrew University of Jerusalem, Jerusalem, Israel.
[2] Present address: Department of Genetics, Stanford University School of Medicine, Stanford, California.
[3] To whom correspondence should be addressed at Department of Biological Chemistry, The Alexander Silberman Institute of Life Sciences, Hebrew University of Jerusalem, Givat Ram, 91904 Jerusalem, Israel; e-mail: soreq@shum.huji.ac.il.

0272-4340/01/1200-0783/0

In the central nervous system, abnormally high AChE expression was shown in transgenic mouse models to be associated with long-term structural and functional impairments (Andres *et al.*, 1997; Beeri *et al.*, 1995; Erb *et al.*, 2001; Sternfeld *et al.*, 2000). This suggests long lasting, delayed consequences of AChE accumulation that are most likely associated both with its catalytic and noncatalytic activities. Both psychological stress and exposure to anti-AChEs, such as Alzheimer's disease drugs (reviewed by Soreq and Glick, 1999), induce similarly efficient AChE overproduction (Friedman *et al.*, 1996; Kaufer *et al.*, 1998; Shapira *et al.*, 2000), demonstrating that this long-lasting impairment is physiologically relevant. Moreover, long-term exposure to organophosphate anti-AChE insecticides increases the risk for non-Hodgkin's lymphomas (Brown *et al.*, 1990), possibly hinting at locus involvement under such environmental exposure as well.

The intricate regulation of the *ACHE* gene in conjunction with the apparent instability of the *ACHE* locus raise interesting questions with regard to the general control over transcription from this locus. Several loci are known where transcriptional activation spans more than one gene, for example, the β-globin locus, which contains a developmentally regulated "switch" in the form of locus control regions (LCRs). These are cis-acting DNA segments that are needed for activation of an entire locus or gene cluster (Hardison *et al.*, 1997). Another such locus, with yet uncharacterized regulation but probably with some degree of coordination in its transcription, is the cholinergic locus. This locus comprises two genes, encoding the vesicular acetylcholine transporter (vAChT) and the choline acetyltransferase gene (ChAT), the former located within an intron of the latter (Eiden, 1998; Mallet *et al.*, 1998). A coordinately regulated locus implies that conditions that activate one gene would also induce expression of adjacent genes in the locus. In the context of the *ACHE* locus, one would expect such candidate genes to be activated during embryonic development (Grisaru *et al.*, 1999; Layer, 1996; Massoulie *et al.*, 1998), under psychological stress in cholinergic neurons (Kaufer *et al.*, 1999) and hematopoietic cells alike (Grisaru *et al.*, 2001), and in both brain and intestinal epithelium under exposure to anti-AChEs (Shapira *et al.*, 2000). Because neighboring gene(s) may have other biological roles, such activation can have far-reaching implications on additional, yet undefined physiological processes.

To investigate the *ACHE* locus, one should: (a) identify neighboring genes on this locus; (b) characterize the tissue expression profiles of such genes as compared to that of the *ACHE* gene; and (c) test for selective changes in their expression levels under conditions where *ACHE* gene expression is modulated. A later phase, dependent on knowledge of the biological role(s) of the neighboring genes, would enable prediction of the physiological outcome of changes in their expression levels.

On the basis of these arguments, we initiated a search for structural features in the *ACHE* locus that may be responsible for genomic instability. We further tested the expression from this locus; for evaluating the possible consequences of such expression, we combined molecular genetic approaches with searches of genomic databases to explore genes residing on the h*ACHE* locus. These analyses identified h*ARS*, a gene overexpressed in Chinese hamster cells when those become resistant to the toxin arsenite, and h*PIX*, a cysteine protease homologous gene located between

ARS and *ACHE*. Here, we report both h*ARS* and h*PIX* exon/intron structure and tissue-specific expression patterns, and demonstrate *ARS* coinduction with *ACHE* in the mouse brain under psychological stress. We further discuss these results in relation to arsenite resistance as well as to AChE responses to anti-AChEs.

METHODS

Sequence Analyses

Searches for open reading frames (ORFs) in the h*ACHE* locus, percentage GC content, repetitive sequences in the *ACHE* upstream sequence, and expression sequence tags (ESTs) derived from this locus were performed using the programs RepeatMasker2 and BLAST. Analysis of putative protein products was performed using the following programs: PSORT (cellular localization prediction), PSSM (protein folding prediction), and Expasy ProtScale (hydrophobicity plots).

cDNA Clones

Deposited cDNA clones were obtained from Genetic Research (Huntsville, AL, U.S.A.), distributors for the IMAGE Consortium and the National Human Genome Research Institute/NIH.

Sequencing of cDNA Clones

DNA sequencing was performed by chromosome walking using an ABI377 automated sequencer (Applied Biosystems Pharmacia, Foster City, CA).

Reverse Transcription PCR (RT-PCR)

Primers were designed using the OLIGO primer design program. Primers for PCR amplification were as follows: for homologous murine m*ARS* 5′-CAGGTCCC-GATATTCCACAAT-3′(+) and 5′-CTCTGCCTGAGATCAAGCCA-3′(−); for homologous murine m*PIX* 5′-GTTGCGATGGACTGGATGAC-3′(+) and 5′-CCT-CTACACAGCCGATCCAG-3′(−); for homologous murine actin m*ACT* 5′-TGAAACAACATACAATTCCATCATGAAGTGTGAC-3′(+) and 5′-AGGAGCGATAATCTTGATCTTCATGGTGCT-3′(−); primers complementary to exon 2 of murine (m)*ACHE* which is common to all AChE isoforms, as well as kinetic follow-up of PCR products accumulation were as described (Friedman *et al.*, 1996).

Animal Experiments

Animal experiments were performed as described elsewhere (Kaufer *et al.*, 1998; Shapira *et al.*, 2000). All experiments were approved by the committee for Animal Experimentation at the Institute of Life Sciences.

RESULTS

Potential Molecular Basis for Genomic Instability at the hACHE Locus

RepeatMasker2 analysis of the h*ACHE* locus indicates an extremely high prevalence of Alu repeats, nonviral retrotransposons which are part of the family of short interspersed elements (SINEs; Fig. 1(A)).

Thirty-nine of these repeats were identified along 22 kb of *ACHE* upstream sequence. This is a higher density of SINEs than that reported for the hypoxanthine phosphoribosyl transferase gene locus (*HPRT*), considered to be rich in Alu repeats, which contains 49 such repeats in 57 kb (Renwick *et al.*, 1997).

The presence of so many Alu repeats in a relatively small region is compatible with both a long history of transposition events and unequal crossing-over in this region. In accordance with this hypothesis, the upstream region was found to be

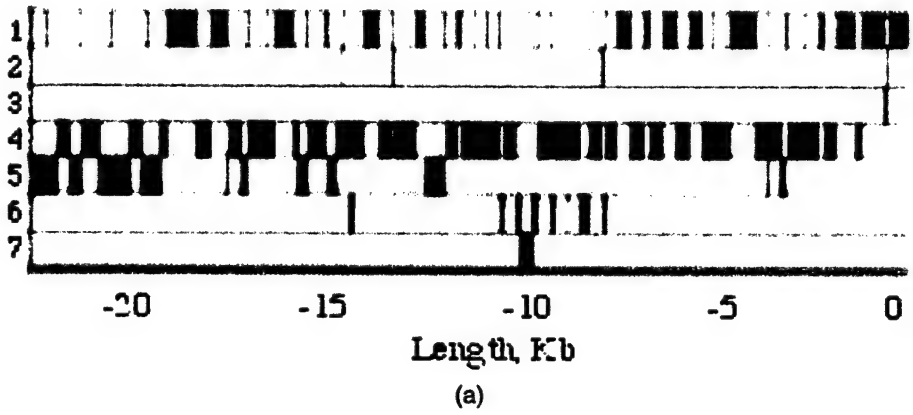

(a)

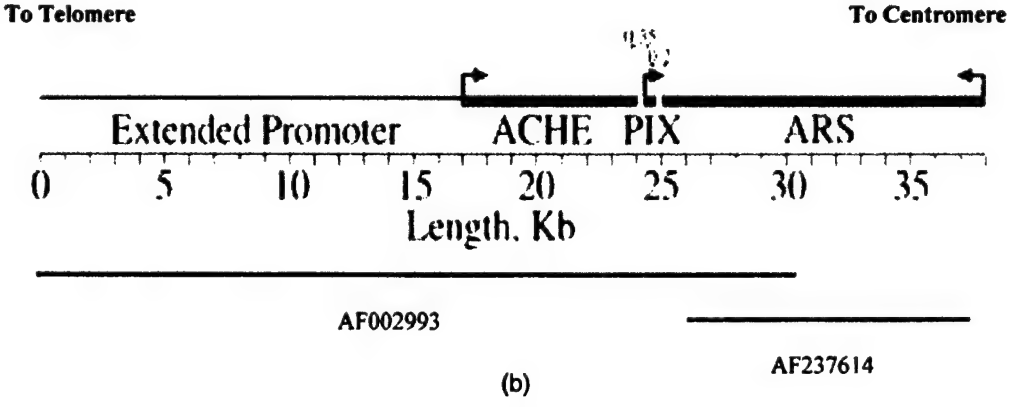

(b)

Fig. 1. The Mammalian ACHE Locus. (A) Sequence characteristics in the *ACHE* extended promoter. Presented is a down-to-scale analysis of the h*ACHE* extended promoter (22.5 kb), with the transcription start site being at position 0. 1: Repeatless regions, variable repeat elements; 2: Simple sequence DNA; 3: Low complexity sequence; 4: Short interspersed nucleotide elements (SINEs), most of which are Alu repeats; 5: LTRs; 6: Retroviral long interspersed nucleotide elements (LINES); 7: SRP classed SINEs. (B). Map of the Human ACHE Locus. Shown is a drawn to scale physical map of the human acetylcholinesterase locus containing the extended promoter, ACHE, PIX, and ARS. Note the close proximity of the three genes at this locus.

markedly lower in its GC content than the *ACHE* gene itself. Taken together, these data provide a possible basis for the instability of the *ACHE* locus.

ARS and PIX Identified Downstream to ACHE

One kilobase downstream from *ACHE* we identified a gene that showed conspicuous homology to the Chinese hamster (ch)*ARS2* cDNA, the expression of which is induced in cell cultures resistant to arsenite poisoning (Wang and Rossman, 1993). Briefly, the chARS gene was isolated from a subtraction cDNA library prepared from a cell line of lung origin that was treated with subtoxic concentrations of arsenite and then selected by exposure to very high, normally toxic concentrations of this poison (Wang and Rossman, 1993). ch*ARS2* was shown to confer arsenite resistance on cultured cells, demonstrating its functional relevance (Rossman and Wang, 1999). The human gene was named, accordingly, h*ARS*.

Further analysis of expressed sequence tag (EST) alignments to the *ACHE* region identified another gene called Potentially Induced eXon or h*PIX*, completely contained within the kilobase of sequence between h*ACHE* and h*ARS*. The 7 kb long h*ACHE* gene is hence followed by the much shorter 800 bp h*PIX* gene, located only 350 bp downstream in the same orientation as h*ACHE*. One hundred base pairs downstream from h*PIX* lies the 13 kb long h*ARS* gene, inversely orientated to both h*PIX* and h*ACHE* (Fig. 1(B)). Genomic PCR amplification of mouse DNA, using primers from the 3′ domains of *ARS* and the inversely oriented *ACHE* genes, resulted in the production of a 1.6 kb fragment, confirming similar proximity for these genes in the mouse and human genomes.

To discover which tissues express h*ACHE*, h*ARS*, and h*PIX*, we searched the dbEST. ESTs originating from both h*ACHE* and h*ARS* mRNA transcripts were found in many different tissues, including both adult (brain, intestine, skeletal muscle, colon, and kidney) and fetal tissues (liver and spleen, lung and heart) (Table I). h*ARS* mRNA was considerably more abundant than the other two transcripts; in addition, a variety of alternatively spliced h*ARS* mRNA sequences were found in all of the above tissues as well as in B cells, breast tissue, placenta, pituitary gland, fetal lung, cervix, thymus, T cells, and fibroblasts. In contrast, dbEST data reflecting h*PIX* expression were limited to very few tissue types, mostly tumors (brain glioblastoma, skin melanoma, and ovarian carcinoma). RT-PCR of total RNA extracts showed a wider mouse tissue distribution than that indicated by the dbEST. The m*PIX* transcripts were detected in cortex and kidney, with lower level expression in lung, and no transcripts were detected in pancreas (Table I).

In silico comparison of h*ARS* ESTs from cDNA libraries of various tissue origins was used to outline its alternative splicing patterns in various tissues (Fig. 2). On the basis of a dbEST Blast search, three brain cDNA clones were ordered (accession numbers R87621, AA077557, and R90838; Genetic Research, Huntsville, AL, U.S.A.) and were fully sequenced to derive the human brain mRNA sequence. Comparison to the cosmid sequence revealed that the 5'-end of the cDNA extended beyond AF002993. Therefore, an adjacent cosmid clone (AF237614, gratefully received from Lap-Chee Tsui, Toronto) containing a partially overlapping insert was sequenced by primer walking. This extended the gene sequence by adding ca. 3 kb

Table I. Expression From the 7q22 Locus as Reflected in the EST Database

Tissue origin of EST	Expressed gene h*ARS*	Expressed gene h*PIX*	Expressed gene h*ACHE*
Brain	++[a]	++[a]	++
B cells	++		(+)[b,c]
Breast	++		
Retina	++		++
Heart	++		+
Colon	++		++
Kidney	++	(+)[b]	++
Skeletal muscle			++
Skin–melanotic melanoma		+	
Placenta	++		
Germ cell tumors			++
Fetal liver and spleen	++		++
Pituitary gland	+		
Fetal lung	+	(+)[b]	++
Cervix	+		
Ovary	+	+	
Uterus	+		
Testis	+		(+)[b]
Prostate	+		
Bone marrow	+		(+)[b]
Bone	+		(+)[b]
Thymus	+		(+)[b]
T cells	+		
Pineal gland			+
Omentum			+
Fibroblasts	+		

Note. Shown is a summary of Blasts output obtained by a search against the dbEST, with the AF002993 cosmid as a query sequence and restricting the search to human sequences. Designated are the tissue origins of the different ESTs.
[a]Highly-represented tissues (with >3 ESTs of the respective tissue origins).
[b]In parentheses are tissues where RT-PCR experiments from our group present *ACHE* or *PIX* expression.
[c]Very low expression.

to its 5′-end (data not shown). The resultant brain h*ARS* gene-product shows a 76% identity to the rodent *ARS* gene-product (U41500) as well as 46% homology to a recently deposited *Drosophila* genomic sequence (AAF57281). A comparison of the brain cDNA sequence with the sequence of a cloned human brain cDNA recently deposited in GenBank (AL096723) identified several differences between the two sequences.

h*ARS*

The AL096723 sequence contained a longer 5′-end, and therefore a more upstream translation start site for the putative protein product. It also included an insert at its 3′-end, resulting in an alternative C-terminus for its putative protein product (Fig. 3). These differences may point to the existence of more than one brain mRNA variant for the h*ARS* gene. However, the absolute majority of ESTs including the 3′ insert in both brain and other tissues points at the sequence lacking it as an exception.

The putative translation product of the composite brain h*ARS* cDNA sequence is a hydrophilic 791 amino acid protein, which contains a bipartite nuclear localization

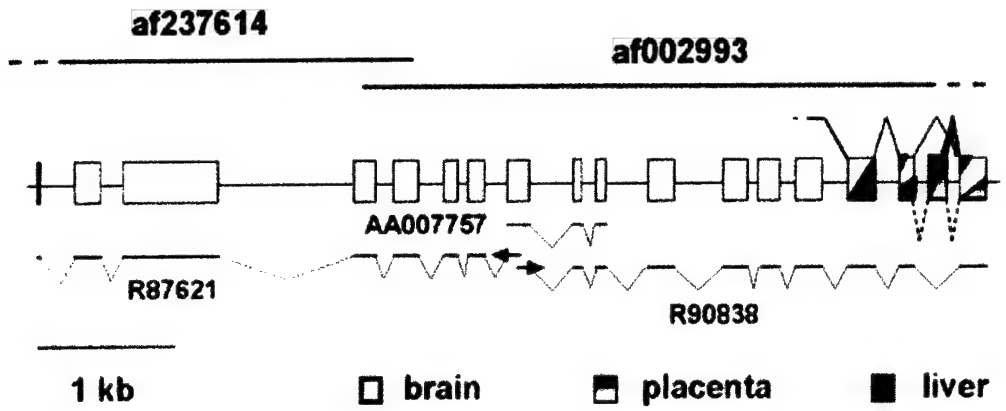

Fig. 2. Alternative splicing in hARS mRNA. Depicted is the drawn-to-scale exon–intron structure of brain hARS cDNA, as derived from the sequenced brain clones. Intronic sequences are shown as thin lines, brain exons as open boxes, and 3-alternative splicing patterns as dashed or full connecting lines, with the alternative exons shaded according to the tissue sources of dbEST clones from which they were derived. The 3′ liver alternative splicing pattern is shown as a thick line and a dashed line represents yet missing information referring to the liver splicing pattern in upstream exons. Below this scheme are depicted the brain cDNA clones used to derive this information with the corresponding accession numbers of the original ESTs. As above, thin connecting lines represent spliced sequences that are not found in these cDNA sequences. Note that the 5′-3′ orientation in this figure is opposite to that of Figs. 1 and 2.

signal (NLS), KKEDSEKEAKKSSKKRN. This type of NLS was first identified in *Xenopus* nucleoplasmin (Robbins *et al.*, 1991), and has the signature pattern of 2 basic residues, a 10 residue spacer, and another basic region consisting of at least 3 basic residues out of 5 residues (Fig. 3). On the basis of this, the prediction made by the PSORT program, is a 56% chance of this protein being nuclear. Arsenite extrusion by various transporters, or modification by methylases or by glutathione S-transferase (reviewed in Rosen, 1995), predicts the existence of transmembrane domains or homologies to the already known arsenite resistance proteins, respectively. However, the PSORT program could not identify in h*ARS* putative transmembrane domains; a hydropathy plot supported the absence of such domains (Fig. 4(A)). h*ARS* further lacks resemblance to any known protein or common protein motif, including other arsenite resistance proteins.

h*PIX*

The identification of h*PIX* from ESTs showed that h*PIX* contains a short TATA-less promoter region, a 5′ untranslated region (UTR), and a 3′ UTR. The open reading frame for h*PIX* shows a predicted peptide of 227 amino acids encoded by a single exon.

Predicted h*PIX* is a soluble, hydrophilic protein of 24.2 kD in weight (Fig. 4(B)). The nucleotide and peptide sequences share homologous sequences in mouse and rat. Murine (m)*PIX*, like h*PIX* is located directly downstream to m*ACHE* and encodes a generally neutral (Fig. 4(B)) polypeptide of similar size and composition (m*PIX* is 217aa). Protein homology searches reveal homologous protein sequences

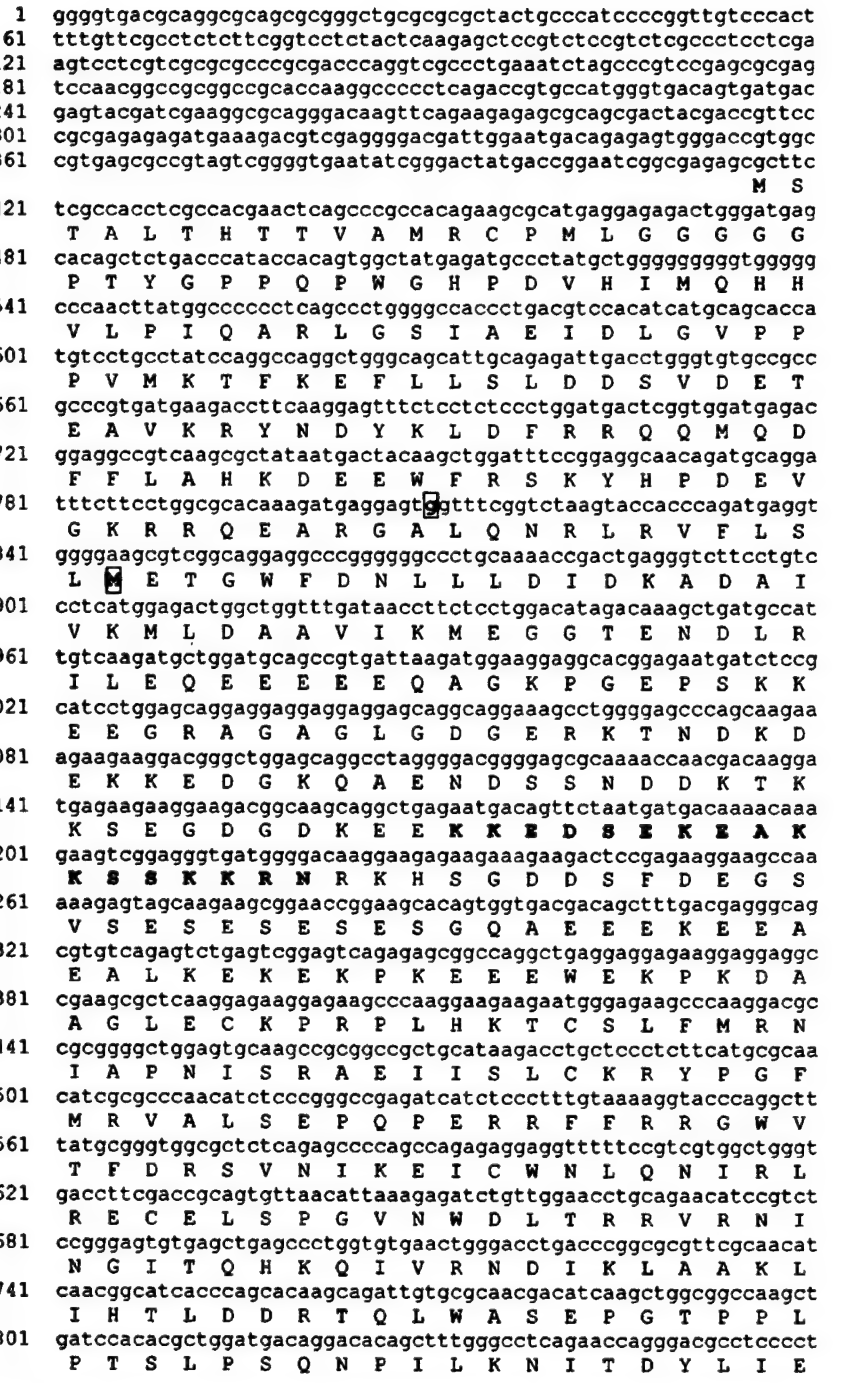

Fig. 3. Brain hARS cDNA sequence and its translation product. Shown is the sequence of the brain cDNA clone (accession number AL096723) and its translation product aligned with the respective codons. Boxed letters indicate the first nucleotide and first methionine of the sequence we obtained from the 3 assembled brain cDNA clones and its translation product, respectively. Bold nucleotides represent an insert existing in AL096723 and most other ESTs compared with our sequence, causing a putative alternative C-terminus. Bold amino acids designate a bipartite nuclear localization signal existing in both predicted proteins. Underlined sequences designate the location of the PCR primers used for quantitative RT-PCR.

```
1861  gcccacgagcctgccctcgcaaaacccgatcttgaagaatatcaccgactacctgatcga
       E  V  S  A  E  E  E  E  L  L  G  S  S  G  G  A  P  P  E  E
1921  ggaagtaagcgccgaggaggaggagctgctggggagcagcgggggcgctcctcctgagga
       P  P  K  E  G  N  P  A  E  I  N  V  E  R  D  E  K  L  I  K
1981  gcctcctaaggaagggaacccggcagagatcaacgtggagcgggatgagaagttgattaa
       V  L  D  K  L  L  L  Y  L  R  I  V  H  S  L  D  Y  Y  N  T
2041  ggtcttggacaagctcctcctttacctgcgcatcgtgcattccttggattattacaacac
       C  E  Y  P  N  E  D  E  M  P  N  R  C  G  I  I  H  V  R  G
2101  ctgtgagtaccccaacgaggacgagatgcccaatcgctgtgggatcatccacgttcgggg
       P  M  P  P  N  R  I  S  H  G  E  V  L  E  W  Q  K  T  F  E
2161  gcccatgccacccaaccgcatcagtcacggggaagtgctggagtggcagaagacttttga
       E  K  L  T  P  L  L  S  V  R  E  S  L  S  E  E  E  A  Q  K
2221  ggagaagctcacgccgttgctgagtgtgcgggagtcactctcagaggaagaggcccagaa
       M  G  R  K  D  P  E  Q  E  V  E  K  F  V  T  S  N  T  Q  E
2281  gatggggcgcaaagacccagagcaggaagtggagaagttcgtcacctccaacacgcagga
       L  G  K  D  K  W  L  C  P  L  S  G  K  K  F  K  G  P  E  F
2341  actgggcaaggataagtggctgtgtcctctcagtggcaagaaattcaagggtcctgagtt
       A  R  K  H  I  F  N  K  H  A  E  K  I  E  E  V  R  K  E  V
2401  tgcgcgcaaacatatcttcaacaagcatgcagagaaaattgaggaagtgagaaaggaagt
       A  F  F  N  N  F  L  T  D  A  K  R  P  A  L  P  E  I  K  P
2461  cgcgtttttttaacaacttcctcactgatgctaagcgcccagctctgcctgagatcaagcc
       A  Q  P  P  G  P  A  Q  I  L  P  P  G  L  T  P  G  L  P  Y
2521  agcccagccacctggccccgcccagatactccccccaggtttgaccccaggactccccta
       P  H  Q  T  P  Q  G  L  M  P  Y  G  Q  P  R  P  P  I  L  G
2581  cccacaccagactccccagggcctgatgccctatggtcagccccggcccccgatcttggg
       Y  G  A  G  A  V  R  P  A  V  P  T  G  G  P  P  Y  P  H  A
2641  ctatggagctggtgctgtccgccctgcagtccccacaggaggccctccataccccccatgc
       P  Y  G  A  G  R  G  N  Y  D  A  F  R  G  Q  G  G  Y  P  G
2701  cccgtatggtgctggtcgagggaactatgatgccttccgaggccagggaggctatcctgg
       K  P  R  N  R  M  V  R  G  D  P  R  A  I  V  E  Y  R  D  L
2761  gaaacctcgcaacaggatggttcgtggagacccaagggccattgtggaatatcgggacct
       D  A  P  D  D  V  D  F  F  *
2821  ggatgccccagacgatgttgatttcttttgagccgtcccccgttcctcagtcctgtatca
2881  tccatacttgtactaccttgtcctatgaagctctgagaatttttgtacgatcagccttа
2941  ctgctaataaaagcacttccacagggaaaaaaaaaaaaaaaaaa
```

Fig. 3. (*Continued*).

in a multitude of organisms (*Drosophila melanogaster*, *Caenorhabditis elegans*, *Arabidopsis thalania*, *Staphylococcus xylosus*, and *Schizosaccharomyces pombe*) including an additional human peptide sequence, raising the possibility of a conserved family of PIX-like proteins in humans and other organisms. In several organisms (e.g., *Caenorhabditis elegans*), the *PIX* homologous region is linked to an additional protein domain, creating a much longer polypeptide, possibly indicating domain integration producing novel functional members in the *PIX*-like family.

Protein sequence analysis indicates that the PIX family of peptides share a low level of sequence homology (36%) with cysteine protease-like enzymes. However, h*PIX* includes within the h*PIX* family homologous regions only two of the three amino acid residues that are required to compose the Cys-His-Asn catalytic triad, and lacks several other highly conserved residues characteristic of cysteine proteases. Homology between *PIX* family members is confined to several small regions, encompassing the cysteine protease catalytic domain and supporting secondary structures. In those PIX family members that are much longer than others, the h*PIX*-like domain, with homology to other family members, is restricted to the last 200 residues. These are preceded by 400 residues which appear to fold into a separate domain, and have an as yet unknown role.

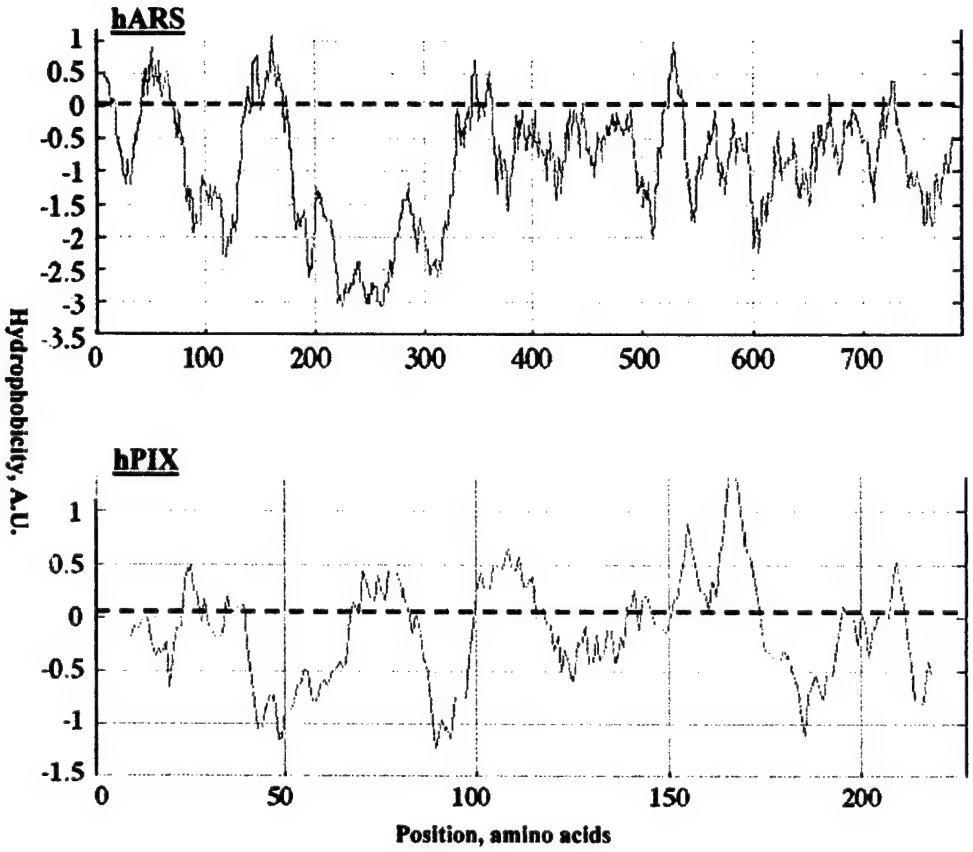

Fig. 4. Hydropathy plot of the hARS (upper) and hPIX (lower) brain gene-products prepared in the Expasy ProtScale web site according to the Kyte and Doolittle algorithm; window size used for analysis was 19 residues. Hydrophobic segments have values above zero in the *Y*-axis; Areas of the protein with values that are greater than or equal to +1.8 are possibly in a transmembrane domain. Note that most of the hARS protein is highly hydrophilic, except its N-terminus which is slightly hydrophobic, while hPIX is also mostly hydrophilic.

Analysis of the folding properties (PSSM fold recognition server) and composition of the h*PIX* peptide is, at this phase, only indicative. h*PIX* can fold, with a PSSM fold accuracy value of 83%, into a papain-like cysteine protease fold family. Cysteine proteases are notably involved in many normal cellular processes, as well as several pathological phenomenae, for example, neuronal apoptosis following spinal cord injury (Ray *et al.*, 2001). This family of papain-like cysteine proteases is extensive and includes members with low overt homology to one another, but with two putative residues in distinct conserved sequences separated by a substantial nonconserved region (Fig. 5).

Coregulation of m*ACHE* and m*ARS*

ACHE is known to be transcriptionally activated under exposure to anti-AChEs, and arsentie is known to be a quasi-irreversible AChE inhibitor (Shapira *et al.*, 1998; Wilson and Silman, 1977), thought to bind to AChE in the vicinity of the active site.

```
   1 ccggggagcgcgtccccagtctgcgcgccggtcctgcggcagctggcccaagacccggag
  61 ccgaaaggaagtgttggagcctgaggtcgctccgcgccgctaggaggacgctgtgcctgg
       M  G  H  P  F  P  P  T  A  L  E  P  L  R  D  V  H  V  G  L
 121 catgggacatccgttcccgcccaccgccctggagccgctcagggacgtccacgtgggcct
       S  P  P  S  R  G  P  V  R  L  A  L  L  S  G  H  Y  L  Y  Y
 181 gtccccgccgagccgcggccctgtccgcctggcgctgctctcgggccactacctctacta
       H  Y  G  C  D  G  L  D  D  R  G  W  G  C  G  Y  R  T  L  Q
 241 ccactacggctgcgacggcctggacgaccgcggctggggctgcggctaccgcactctgca
       T  L  C  S  W  P  E  G  Q  P  A  G  V  P  G  L  A  A  V  Q
 301 gacgctgtgctcgtggccagagggccagcccgcgggcgtacctggactggccgccgtaca
       A  A  L  E  D  M  G  D  K  P  P  G  F  R  G  S  R  D  W  I
 361 ggcggccctggaggacatgggcgacaagccccccggcttccggggctcccgggactggat
       G  C  V  E  A  S  L  C  L  A  H  F  G  G  P  Q  G  R  L  C
 421 cggctgcgtggaggccagcctctgcctcgctcacttcggagggccccagggacgcctctg
       H  V  P  R  G  V  G  L  H  G  E  L  E  R  L  Y  S  H  F  A
 481 ccacgtaccccggggagtggggctgcacggggagctggagcggctttactcgcacttcgc
       G  G  G  G  P  V  M  V  G  G  D  A  D  A  R  S  K  A  L  L
 541 agggggtgggggcccagtcatggttgggggggacgcagatgccaggtccaaggccttgct
       G  V  C  V  G  S  G  T  E  A  Y  V  L  V  L  D  P  H  Y  W
 601 gggagtctgcgtagggtcaggcacggaagcctatgtcctggtattggcccctcactactg
       G  T  P  K  S  P  S  E  L  Q  A  A  G  W  V  G  W  Q  E  V
 661 gggcactccaaaaagccccagtgaactacaggctgctgggtgggtgggctggcaagaggt
       S  A  A  F  D  P  N  S  F  Y  N  L  C  L  T  S  L  S  S  Q
 721 gagtgcagcctttgaccccaactccttctacaacctgtgcttgaccagccttagctccca
       Q  Q  Q  R  T  L  D  *
 781 acagcagcagcgcaccttggactgaggacgaagttacagaactgagattctcgggtccca
 841 gacacgcacctatgtacctcccactggtgtccctgcaaagcctggcgcttttgacatcaa
 901 taataaaagtggcagggctgagcaacacctcaggagttactctggaaggatggagagtta
 961 tgtaacacacgagagtcaggagccctgtggaagtgcttttattagcagtaaggctgat
```

Fig. 5. Human PIX mRNA sequence and its translation product. Shown is the sequence of a brain EST and its translation product aligned with the respective codons. Boxed letters indicate the first codon and first methionine of the brain EST and its translation product, respectively. Underlined residues represent conserved PIX-family motifs. The cysteine and histidine residues at the predicted positions of the conserved Pix-family motifs that are possible members of the Cys-His-Asn cysteine protease catalytic triad are boxed.

A novel possibility therefore emerged which postulated a general locus control, with AChE serving as a sensor for different stressors, including arsenite. To be subject to joint regulation, the mammalian *ARS* and *ACHE* genes should display coexpression patterns in different tissues and experimental conditions. Their colocalization in the human genome could facilitate such regulation through locus control.

The partial overlap in tissue distribution of mRNA transcripts of h*ARS* and h*ACHE* (Table I), together with their close genomic proximity in both man and mouse, supported the possibility of coordinated transcriptional regulation of this entire chromosomal domain. To test whether this is also the case under experimental modulations of transcription, we compared the levels of mAChE and mARS mRNA in the brain of control mice to those in mice subjected to the forced-swim protocol causing psychological stress (Friedman *et al.*, 1996). ARS specific primers that were employed for RT-PCR were complementary to sequences flanking the region differing between the two inferred brain cDNAs (Fig. 2(B)). The size of the PCR product (ca. 320 bp) demonstrated that the transcript containing this amplified sequence is, at least in the mouse brain, the major variant obtained from the *ARS* gene. Stressed mice displayed, as expected, increased AChE mRNA levels in their brain (Kaufer *et al.*, 1998; Shapira *et al.*, 2000).

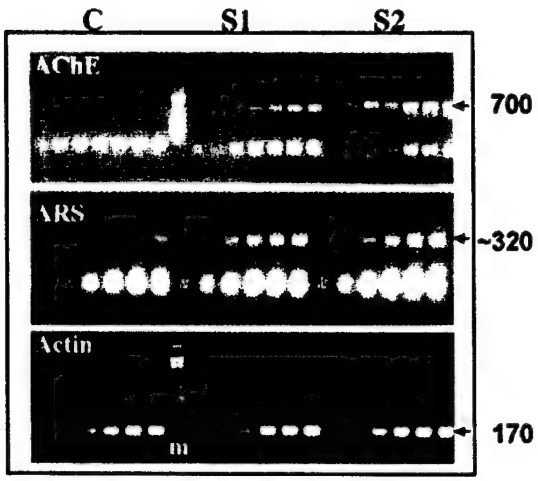

Fig. 6. Psychological stress increases both AChE and ARS mRNA levels in the mouse medulla. Shown is one out of three reproducible experiments presenting a semiquantitative kinetic follow-up of RT-PCR evaluation, with amplified DNA samples removed at every cycle. Arrow-labeled are AChE, ARS, and actin cDNA products in extracts prepared from the brain stem (medulla) region of either a control mouse (C) or two different mice subjected to psychological stress (S) (Kaufer *et al.*, 1998). Densitometry of the fluorescent signals presented 8-fold stress-related increases for the AChE transcripts. Fourfold increases were detected for ARS products in brains of stressed as compared to control mice. Actin products showed no difference associated with stress, demonstrating specificity of the AChE and ARS increases.

The medulla region from these mice displayed massive coinduction in the brain of *ARS* and AChE mRNA 2 h poststress, while maintaining unchanged actin mRNA levels (Fig. 6). This supported the notion of a stress-associated regulation of gene expression in the *ACHE* locus.

DISCUSSION

The human *ACHE* gene, located on the long arm of chromosome seven, extends into a long upstream region void of genes. This sequence contains a very high number of repetitive elements, which may contribute to the inherent instability of this genomic region. Together, these repetitive upstream sequences constitute a region rich in highly complex and diverse regulatory sequence motifs. These can potentially modulate the expression, not only of the *ACHE* gene, but also of the wider *ACHE* locus. Our current analysis shows that the human *ACHE* gene is less isolated at its downstream end, where two newly characterized genes, h*ARS* and h*PIX*, are situated extremely close to h*ACHE*. The *ACHE* and *ARS* genes have potentially

related functional characteristics that permit consideration of several complex interregulatory mechanisms for the entire region, especially with regards to chemical exposure and stress. Likewise, the evolutionary conservation of *PIX* homologues is likely indicative of a common basic function of this gene. Cysteine proteases are known to be induced under various stressful insults, for example, under exposure to the dopaminergic neurotoxin, MPP(+), which induces cell death in substantia nigra neurons (Choi *et al.*, 2001). While the *PIX* protein product may not be catalytically active, its conserved folding pattern suggests that it may interact with the protein targets of cysteine proteases. The very short distance, and same orientation of h*ACHE* and h*PIX*, and their murine counterparts, suggest concerted regulation of this gene as well.

It is not clear yet whether *PIX* may be independently regulated by its own very short promoter, or if its induction exclusively depends on ACHE being transcribed. Also, the absence of existing sequences of previously characterized proteins with significant homology to h*PIX* is of considerable disadvantage in the process of deducing a role for this gene through reliable comparative homology. In contrast, h*ARS* shares homology with several proteins with a previously characterized role in arsenite resistance.

Overexpression of the Chinese hamster *ARS* protein appears to be not merely coincidental with arsenite resistance, but is rather able to confer such a resistance in transfected cells (Rossman and Wang, 1999). However, ARS contains no known protein domains or motifs; therefore, it is very unlikely that the h*ARS* protein confers arsenite resistance through any of the known mechanisms. Moreover, arsenite extrusion by various transporters, or modification by methylases or by glutathione S-transferase (reviewed in Rosen, 1995), predicts the existence of transmembrane domains, even in cases where there are no homologies to the already known arsenite resistance proteins. That no such domains were found in h*ARS* suggests that it is actively involved in conferring arsenite resistance through a new, yet unknown mechanism(s).

The notion of *ARS* being coregulated with *ACHE* is supported by our experimental results. *AChE* inhibitors would cause an increase in acetylcholine levels, enhancing cholinergic gene expression in a manner similar to that occurring under psychological stress. That both arsenite and better known anti-AChEs induce transcriptional activation of the *ACHE* locus, together with arsenite being an AChE inhibitor, suggests a role for AChE as a sensor of arsenite, which can cause a protective multigenic transcriptional response. That brain m*ARS* expression also increases under stress suggests that acetylcholine is the cause, as it is for *ACHE* gene expression, and raises the question whether the ARS protein product also exerts function(s) associated with mammalian stress responses. While it is still unclear whether h*ARS* function requires and/or induces alterations in *ACHE* gene expression, an interesting link is that arsenite exposure, like anti-AChEs exposure, increases the risk for tumorogenesis (Lee *et al.*, 1988). It thus appears that transcriptional overactivation of the *ACHE* locus often leads to changes in cell proliferation, albeit not necessarily in the same tissues. A general locus response to stress, where *ACHE*, *PIX*, and *ARS* are regulated as a single unit is an intriguing possibility.

ACKNOWLEDGMENTS

The authors are grateful to Dr. Lap-Chee Tsui, Toronto, for the Chr.7q22 Cosmids. This work was supported by the U.S. Army Medical Research and Materiel Command (Grant no. DAMD 17-99-1-9547) and by Ester Neuroscience Ltd. (to H.S.). A.D.G. was the incumbent of a fellowship from the British Friends of the Hebrew University.

REFERENCES

Andres, C., Beeri, R., Friedman, A., Lev-Lehman, E., Henis, S., Timberg, R., Shani, M., and Soreq, H. (1997). Acetylcholinesterase-transgenic mice display embryonic modulations in spinal cord choline acetyltransferase and neurexin Ibeta gene expression followed by late-onset neuromotor deterioration. *Proc. Natl. Acad. Sci. USA* **94**(15):8173–8178.

Beeri, R., Andres, C., Lev-Lehman, E., Timberg, R., Huberman, T., Shani, M., and Soreq, H. (1995). Transgenic expression of human acetylcholinesterase induces progressive cognitive deterioration in mice. *Curr. Biol.* **5**(9):1063–1071.

Brown, L. M., Blair, A., Gibson, R., Everett. G. D., Cantor, K. P., Schuman, L. M., Burmeister, L. F., Van Lier, S. F., and Dick, F. (1990). Pesticide exposure and other agricultural risk factors for leukemia among man in Iowa and Minnesota. *Cancer Res.* **50**(20):6585–6591.

Choi, W. S., Lee, E. H., Chung, C. W., Jung, Y. K., Jin, B. K., Kim, S. U., Oh, T. H., Saido, T. C., and Oh, Y. J. (2001). Cleavage of Bax is mediated by caspase-dependent or -independent calpain activation in dopaminergic neuronal cells: Protective role of Bcl-2. *J. Neurochem.* **77**(6):1531–1541.

Eiden, L. E. (1998). The cholinergic gene locus. *J. Neurochem.* **70**(6):2227–2240.

Erb, C., Troost, J., Kopf, S., Schmitt, U., Löffelholz, K., Soreq, H., and Klein, J. (2001). Compensatory mechanisms enhance hippocampal acetylcholine release in transgenic mice expressing human acetylcholinesterase. *J. Neurochem.* **77**(2):638–646.

Friedman, A., Kaufer-Nachum, D., Shemer, J., Hendler, I., Soreq, H., and Tur-Kaspa, I. (1996). Pyridostigmine brain penetration under stress enhances neuronal excitability and induces early immediate transcriptional response. *Nat. Med.* **2**:1382–1385.

Grisaru, D., Sternfeld, M., Eldor, A., Glick, D., and Soreq, H. (1999). Structural roles of acetylcholinesterase variants in biology and pathology. *Eur. J. Biochem.* **264**:672–686.

Grisaru, D., Deutsch, V., Shapira, M., Pick, M., Sternfeld, M., Melamed-Book, N., Kaufer, D., Galyam, N., Lessing, B., Gait, M., Owen, D., Eldor, A., and Soreq, H. (2001). Arp, a peptide derived from the stress-associated acetylcholinesterase variant has hematopoetic growth promoting activities. *Mol. Med.* **7**(2):93–105.

Hardison, R., Slightom, J. L., Gumucio, D. L., Goodman, M., Stojanovic, N., and Miller, W. (1997). Locus control regions of mammalian beta-globin gene clusters: Combining phylogenetic analyses and experimental results to gain functional insights. *Gene* **205**(1/2):73–94.

Johnson, E., and Cotter, F. E. (1997). Monosomy 7 and 7q—associated with myeloid malignancy. *Blood Rev.* **11**(1):46–55.

Kaufer, D., Friedman, A., Seidman, S., and Soreq, H. (1998). Acute stress facilitates long-lasting changes in cholinergic gene expression. *Nature* **393**:373–377.

Kaufer, D., Friedman, A., and Soreq, H. (1999). Anticholinesterases induce multigenic transcriptional feedback response suppressing cholinergic neurotransmission. *Chem. Biol. Interact.* **14**:119–120, 349–360.

Lampert, I. A., and Van Noorden, S. (1996). Acetylcholinesterase is expressed in the follicular dendritic cells of germinal centres: Differences between normal and neoplastic follicles. *J. Pathol.* **180**:169–174.

Layer, P. G. (1996). Non-classical actions of cholinesterases: Role in cellular differentiation, tumorigenesis and Alzheimer's disease. *Neurochem. Int.* **28**(5/6):491–495. Review.

Lee, T. C., Tanaka, N., Lamb, P. W., Gilmer, T. M., and Barrett, J. C. (1988). Induction of gene amplification by arsenic. *Science* **241**:79–81.

Mallet, J., Houhou, L., Pajak, F., Oda, Y., Cervini, R., Bejanin, S., and Berrard, S. (1998). The cholinergic locus: ChAT and VAChT genes. *J. Physiol. Paris* **92**:145–147.

Massoulie, J., Anselmet, A., Bon, S., Krejci, E., Legay, C., Morel, N., and Simon, S. (1998). Acetylcholinesterase: C-terminal domains, molecular froms and functional localization. *J. Physiol. Paris* **92**:183–190.

Ray, S. K., Matzelle, D. D., Wilford, G. G., Hogan, E. L., and Banik, N. L. (2001). Cell death in spinal cord injury (SCI) requires de novo protein synthesis. Calpain inhibitor E-64-d provides neuroprotection in SCI lesion and penumbra. *Ann. NY Acad. Sci.* **939:**436–449.

Razon, N., Soreq, H., Roth, E., Bartal, A., and Silman, I. (1984). Characterization of activities and forms of cholinesteraes in primary brain tumors. *Exp. Neurol.* **84:**681–695.

Renwick, P. J., Renwick, P. J., Birley, A. J., and Hulten, M. A. (1997). Study of Alu sequences at the hypoxanthine phosphoribosyltranscferase (hprt) encoding region of man. *Gene* **184:**155–163.

Robbins, J., Dilworth, S. M., Laskey, R. A., and Dingwall, C. (1991). Two independent basic domains in nucleoplasmin nuclear targetting sequence: Identification of a class of bipartite nuclear targetting sequence. *Cell* **64:**615–623.

Rosen, B. P. (1995). Resistance mechanism to arsenicals and antimonials. *J. Basic Clin. Physiol. Pharmacol.* **6**(3/4):251–263.

Rossman, T. G., and Wang, Z. (1999). Expression cloning for arsenite-resistance resulted in isolation of tumor-suppressor fau cDNA: Possible involvement of the ubiquitin system in arsenic carcinogenesis. *Carcinogenesis* **20**(2):311–316.

Shapira, M., Seidman, S., Livni, N., and Soreq, H. (1998). In vivo and in vitro resistance to multiple anticholinesterases in Xenopus laevis tadpoles. *Toxicol. Lett.* **28:**102–103, 205–209.

Shapira, M., Tur-Kaspa, I., Bosgraaf, L., Livni, N., Grant, A. D., Grisaru, D., Korner, M., Ebstein, R. P., and Soreq, H. (2000). A trasncription-activating polymorphism in the ACHE promoter associated with accute sensitivity to anti-acetylcholinesterases. *Hum. Mol. Genet.* **9:**1273–1281.

Soreq, H., and Glick, D. (1999). Novel roles for cholinesterases in stress and inhibitor responses. In Giacobini, E. (ed.), *Cholinesterases and Cholinesterase Inhibitors: Basic, Preclinical and Clinical Aspects, Vol. 4*, Martin Dunitz Ltd., pp. 47–62, London.

Soreq, H., and Seidman, S. (2001). Acetylcholinesterase—new roles for an old actor. *Nat. Rev. Neurosci.* **2**(4):294–302.

Sternfeld, M., Shoham, S., Klein, O., Flores-Flores, C., Evron, T., Idelson, G. H., Kitsberg, D., Patrick, J. W., and Soreq, H. (2000). Excess "read-through" acetylcholinesterase attenuates but the "synaptic" variant intensifies neurodeterioration correlates. *Proc. Natl. Acad. Sci. USA* **97:**8647–8652.

Wang, Z., and Rossman, T. G. (1993). Stable and inducible arsenite resistance in Chinese hamster cells. *Toxicol. Appl. Pharmacol.* **118:**80–86.

Wilson, I. B., and Silman, I. (1977). Effects of quaternary ligands on the inhibition of acetylcholinesterase by arsenite. *Biochemistry* **16**(12):2701–2708.

Zakut, H., Ehrlich, G., Ayalon, A., Prody, C. A., Malinger, G., Seidman, S., Kehlenbach, R., Ginzberg, D., and Soreq, H. (1990). Acetylcholinesterase and butyrylcholinesterase genes coamplify in primary ovarian carcinomas. *J. Clin. Invest.* **86**(3):900–908.

Alternative Splicing and Neuritic mRNA Translocation Under Long-Term Neuronal Hypersensitivity

Eran Meshorer,[1] Christina Erb,[1] Roi Gazit,[2] Lev Pavlovsky,[3] Daniela Kaufer,[1]* Alon Friedman,[3] David Glick,[1] Nissim Ben-Arie,[2] Hermona Soreq[1]†

To explore neuronal mechanisms underlying long-term consequences of stress, we studied stress-induced changes in the neuritic translocation of acetylcholinesterase (AChE) splice variants. Under normal conditions, we found the synaptic AChE-S mRNA and protein in neurites. Corticosterone, anticholinesterases, and forced swim, each facilitated a rapid (minutes), yet long-lasting (weeks), shift from AChE-S to the normally rare AChE-R mRNA, promoted AChE-R mRNA translocation into neurites, and induced enzyme secretion. Weeks after stress, electrophysiological measurements in hippocampus slices displayed apparently normal evoked synaptic responses but extreme hypersensitivity to both anticholinesterases and atropine. Our findings suggest that neuronal hypersensitivity under stress involves neuritic replacement of AChE-S with AChE-R.

Traumatic stress is often followed by long-term pathological changes (*1, 2*). In humans, extreme cases of such changes are clinically recognized as posttraumatic stress disorder (PTSD) (*3*). Although the immediate response to acute stressful insults has been extensively studied, the molecular mechanisms leading to the long-term neuronal hypersensitivity that is characteristic of PTSD are yet unknown. Stimulus-induced changes in alternative splicing have recently emerged as a major mechanism of neuronal adaptation to stress, contributing to the versatility and complexity of the expression patterns of the human genome (*4–6*). Another stimulus-induced post-transcriptional process is dendritic mRNA translocation, which has been described for several transcripts (*7–12*). Because psychological, physical, and chemical stressors all cause neuronal activation and hyperexcitation, dendritic translocation of specific target mRNAs may follow.

Acetylcholinesterase (AChE) modulations provide an appropriate case study for exploring long-term stress effects. Chemical, psychological, and physical stresses all shift splicing from the primary mRNA product that encodes the synaptic membrane AChE-S multimeric protein to the normally rare "readthrough" AChE-R transcript, which yields soluble monomers (*13*). We thus examined neuronal distributions of the two splice variants, which have characteristic 3′ regions (Fig. 1A). A comprehensive search of the NCBI GenBank and EST databases revealed several AChE-S mRNAs but only a single AChE-R mRNA of rodent brain origin (GenBank accession number X70141), attesting to the scarcity and/or instability of neuronal AChE-R mRNA under normal conditions. To study changes in gene expression at the subcellular level, we used double-label fluorescence in situ hybridization (FISH) of specific AChE mRNA splice variants (*14*) and confocal microscope image analysis.

FISH detection efficiencies likely depend on probe sequences, but subcellular distributions can be reliably compared for single transcripts in different cells and conditions. Cultured PC12 cells (*15*), primary cultures of mouse cerebellar neurons (*16*), and pyramidal neurons in paraffin-embedded sections of the prefrontal cortex (*17*) all displayed a larger fraction of AChE-S mRNA transcripts in neuronal processes than of AChE-R mRNA (Fig. 1, B through D). Also, both cell types displayed nuclear localization of AChE-R but not of AChE-S mRNA (Fig. 1, B and C) (*18*). To test whether labeling properties prejudiced this conclusion, we reversed the fluorophores on the two probes (Fig. 1, B and C). In paraffin-embedded brain sections from naïve mice, cortical pyramidal neurons presented dispersed AChE-S mRNA through-

Departments of [1]Biological Chemistry and [2]Cell and Animal Biology, The Institute of Life Sciences and The Eric Roland Center for Neurodegenerative Diseases, The Hebrew University of Jerusalem, Israel 91904. [3]Departments of Physiology and Neurosurgery, Zlotowsky Center of Neuroscience, Ben Gurion University and Soroka Medical Center, Beersheva, Israel 84105.

*Present address: Department of Biological Sciences, Stanford University, Stanford, CA 94305, USA.
†To whom correspondence should be addressed. E-mail: soreq@shum.huji.ac.il

out the processes, while AChE-R mRNA was localized to the cell body. In addition, the perikaryal cytoplasm exhibited punctated concentrations of AChE-R mRNA alternating with double-labeled regions, whereas neurites had AChE-S mRNA with foci of both transcripts (Fig. 1D). The neurite contents of cultured PC12 cells and developing cerebellar neurons, also known to express ample AChE (*19*), and of prefrontal cortex neurons in vivo were 22 ± 3, 28 ± 4 and 28 ± 7%, respectively, for AChE-S mRNA but only 10 ± 2, 7 ± 2 and 11 ± 6% for AChE-R mRNA ($P < 0.05$, two-tailed Student's *t*-test). AChE-S mRNA, thus, preferentially localized in neurites (except under stress, see Fig. 1E, below).

The human *ACHE* gene includes a glucocorticoid response element (GRE) about 17 kb upstream from the transcription initiation site (Fig. 1A). In humans, a deletion adjacent to the GRE causes constitutive overexpression and anti-AChE hypersensitivity (*20*), which suggests a physiologically significant role for glucocorticoids in regulating both neuronal *ACHE* gene expression and anticholinesterase hypersensitivity. We therefore compared PC12 cells treated for 6 hours with corticosterone (10 μM, 0.1% ethanol) to control cells (0.1% ethanol). Twenty-four hours after treatment, catalytic activity against acetylthiocholine rose by 25 ± 14% ($P < 0.05$) in PC12 cells. Corticosterone, further, increased by 30 to 50% the levels of both splice variants within 24 hours ($P < 0.05$) (Fig. 2, A through H). However, the AChE-S mRNA-labeled area remained essentially unchanged under control conditions (distance from nuclear border to limit of mRNA labeling = 37 ± 13 μm) or corticosterone (34 ± 13 μm). In contrast, AChE-R mRNA labeling extended a smaller distance from the nucleus, 25 ± 9 μm under control conditions, increasing to 33 ± 17 μm under corticosterone ($P < 0.05$).

Three-hour incubation of PC12 cells with 1.5 nM EN101, an antisense oligonucleotide that induces preferential degradation of AChE-R mRNA (*15*), affected the selective, yet limited, suppression of AChE-R mRNA (30 ± 8%, $P < 0.05$), but left unchanged AChE-S mRNA levels (Fig. 2, E through H). An inversely oriented sequence, INV101, affected neither the AChE-R mRNA level nor its distribution in PC12 cells (*21*), attesting to the sequence specificity of the antisense effect. The labeled area remained unchanged either with AChE-S or AChE-R cRNA probes, following EN101 treatment, suggesting full EN101 accessibility to the cell body (Fig. 2, I and J).

To test whether EN101 is effective similarly in neurites and perikaryal subcellular sites, we employed cerebellar neurons in primary culture. DIG labeling of AChE-S mRNA was not affected differently by EN101 and INV101, in either cell body or neurites. In contrast, EN101 reduced AChE-R mRNA labeling in the cell body of cerebellar neurons in culture, down to almost 50% of its level in INV101-treated controls (*22*). This suppression was completely restricted to the perikaryon, with no difference observed for neuritic AChE-R mRNA in antisense-treated cerebellar neurons.

Cytochemical staining of catalytically active AChE (*17*) revealed intensified AChE activity in the cell bodies of corticosterone-treated cultured cerebellar neurons (Fig. 3, A and C). This suggested that the overexpressed AChE mRNA transcripts were translated to yield active enzyme. Immunocytochemical staining with an antibody targeted against recombinant AChE-S (*23*) presented apparently similar staining patterns in neurites of control and corticosterone-treated cultured cerebellar neurons (Fig. 3, B and D). This indicated that neurites under stress secrete the hormone-induced soluble AChE-R, with no increase in the synaptic membrane-associated AChE-S.

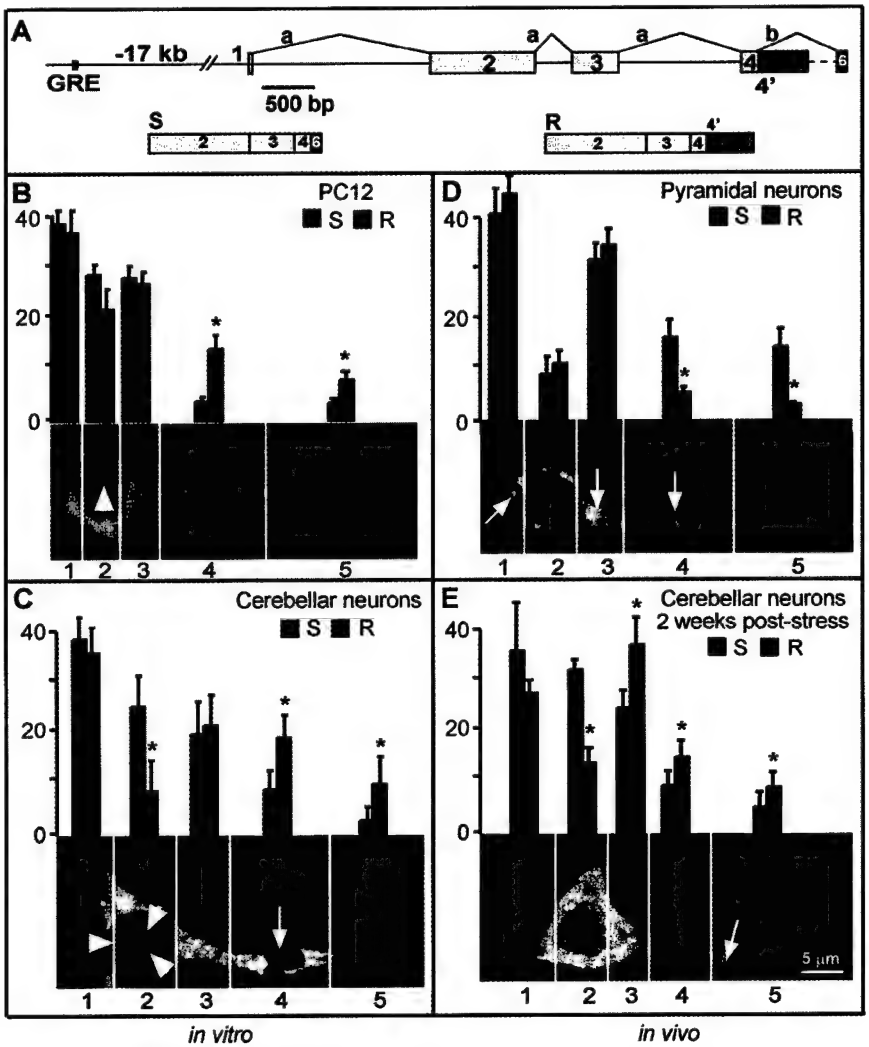

Fig. 1. Variant-specific subcellular distribution of AChE mRNAs. (**A**) Alternative splicing. Shown are the distal enhancer glucocorticoid response element (GRE) and the mouse *ACHE* gene (top), as well as AChE-S mRNA (S) and AChE-R mRNA (R). Linkage of exons 2, 3, and 4 is common to both variants (a). The R transcript includes at its 3′ terminus pseudointron 4 (green) and exon 5; option b yields the S transcript by connecting exon 4 to 6 (red). (**B** through **E**) Localization of the S and R transcripts in vitro and in vivo. Shown are percentages ± SD of FISH signals for the S and R transcripts (each totaling 100%) in three parts of the perikaryon and two neurite areas of 10 PC12 cells (B), cultured primary cerebellar neurons (C), pyramidal neurons from a paraffin-embedded slice of the prefrontal cortex (D), and cerebellar neurons from an embedded brain slice of a mouse that had been stressed for four consecutive days (2× 4 min forced swim), and sacrificed 2 weeks later (E). In control mice (D), the fraction of AChE-R mRNA in segments 4+5 was 9 ± 2% in both cortical and cerebellar neurons; for poststress mice, it was 24 ± 7% (E) ($P < 0.05$). Note nuclear labeling of the R transcript in cultured cerebellar neurons (arrowheads) and the punctated pattern of transcript accumulation in vivo [arrows in (D) and (E)]. Asterisks indicate columns with significant differences between AChE-S and AChE-R mRNAs ($P < 0.05$).

We used FISH detection of the intracellular AChE-R mRNA transcript to assess the expression levels of this variant in vivo. Dorsal hippocampus neurons of naïve FVB/N mice express extremely low levels of AChE-R mRNA under normal conditions (Fig. 3E). Two days following the stress of surgical implantation of a microdialysis cannula (*24*), the range of neurite labeling increased from 2.0 ± 0.3 to 5.1 ± 1.0 μm from the nucleus (Fig. 3G, $P < 0.0005$). Injection through the cannula of the AChE inhibitor neostigmine (125 nmol) resulted in a more extensive translocation of AChE-R mRNA within 25 min (to 8.5 ± 1.2 μm from the nucleus, Fig. 3I). In neurites of untreated hypersensitive AChE-S transgenic mice, AChE-R mRNA reached greater distances from the nucleus (9 ± 1 μm) than those of their strain-matched controls (Fig. 3F, $P < 0.0005$). Sham injection failed to further increase transport (10 ± 1 μm, Fig. 3H), but AChE-R mRNA reached dendrite distances of 15 ± 2 μm under neostigmine (Fig. 3J), significantly longer than either similarly treated nontransgenic animals, or sham injected transgenics (in both cases $P < 0.0005$; Fig. 3, K and L).

Reported rates of mRNA dendrite transport range from 10 to 20 μm·hour^{-1} (*25*) to 300 to 360 μm·hour^{-1} (*26*). In our study, assuming a constant rate, AChE-R mRNA traveled a minimum of 8 ± 5 μm·hour^{-1} in anticholinesterase-treated FVB/N mice, which increased to 14 ± 7 μm·hour^{-1} in similarly treated hAChE-S transgenic mice ($P < 0.0005$). This rate is consistent with the lower range estimate. The stability of AChE-R mRNA in the face of an antisense agent predicted long-lasting poststress neuritic presence of this transcript in vivo. To test this, we subjected FVB/N mice to 4 consecutive days of forced swim (two 4-min sessions per day). In naïve mice, cerebellar granule neuron processes were loaded with 28 ± 12% of the cellular AChE-S mRNA but only 9 ± 2% of the AChE-R mRNA content (Fig. 1C). Two weeks post-stress, a considerably larger fraction (24 ± 7%) of the stress-increased amount of AChE-R mRNA translocated into neurites and displayed patches of concentrated AChE-R mRNA in both the cell bodies and processes (Fig. 1E). Thus, both the absolute levels and the neurite fraction of AChE-R mRNA increased considerably.

In nontransgenic mice, hippocampal AChE-R mRNA is generally limited to the granular layer (*17*). AChE-R mRNA levels remained considerably higher than baseline 4 weeks after 4 consecutive days of forced swim or 3-day exposure to very low diisopropylfluorophosphonate (DFP) levels (0.1 mg·kg^{-1}·day^{-1}, i.p., LD_{50} = 2.5 mg·kg^{-1}). Prestressed or preexposed animals presented high-intensity labeling in the hippocampus CA1 region, dentate gyrus, and dendrite layer (Fig. 4, A through F), predicting modified composition of neuritic AChE variants either after stress or low-level exposure to an anticholinesterase.

Released neuronal acetylcholine binds to both pre- and postsynaptic receptors and is assumed to serve as a modulatory neurotransmitter and set the response level of the neuronal network to incoming stimuli (*27*). This involves electrophysiological mechanisms that are only partly understood, but depend on synaptic hydrolysis of acetylcholine by AChE-S. To test whether the supplementation of neuritic AChE-S with AChE-R compromises the capacity to confront intensified cholinergic stimuli, we stimulated the CA2/CA3 region of the stratum oriens, a region rich in cholinergic fibers, and recorded population field potentials (pfps), which sum the responses of a large number of neurons, in the cell body layer of the CA1 region (*17*). Recording in hippocampus slices (*28*) was performed 1 month after exposure to stress or in slices from naïve animals. The anticholinesterase physostigmine induced an increase (42 ± 15%, $P < 0.05$) in the amplitude of the evoked population spike response of naïve mice (Fig. 4, G and I). This response was 70% reversible following the addition of atropine to the bathing solution, indicating major action through muscarinic receptors. In

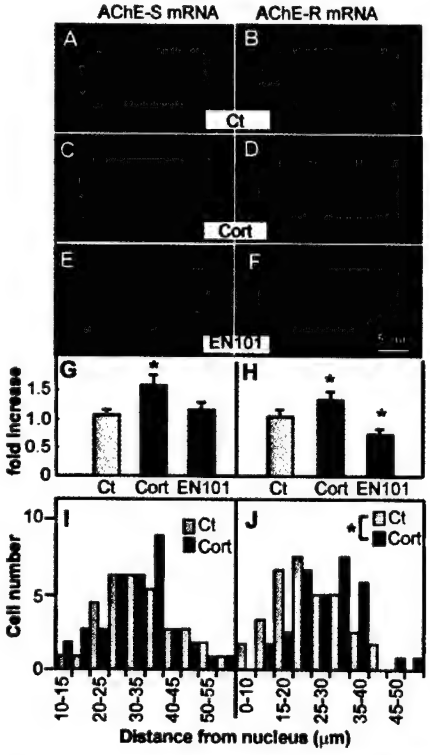

Fig. 2. Corticosterone induction and antisense suppression of AChE mRNA in PC12 cells. Shown are confocal micrographs (**A** through **F**), average labeling intensities (**G** and **H**) and distributions of distances from the nucleus to the cell border (**I** and **J**) of the S (red) and R (green) transcripts in PC12 cells ($n = 40$) under control conditions [(A) and (B)], or after 3 hours in 10 μM corticosterone [(C) and (D)] or 1.5 nM EN101 [(E) and (F)]. Asterisks indicate columns with significant differences from controls ($P < 0.05$). Panels (I) and (J) present the numbers of cells that contain AChE-S or AChE-R mRNA versus their maximum distance from the nucleus.

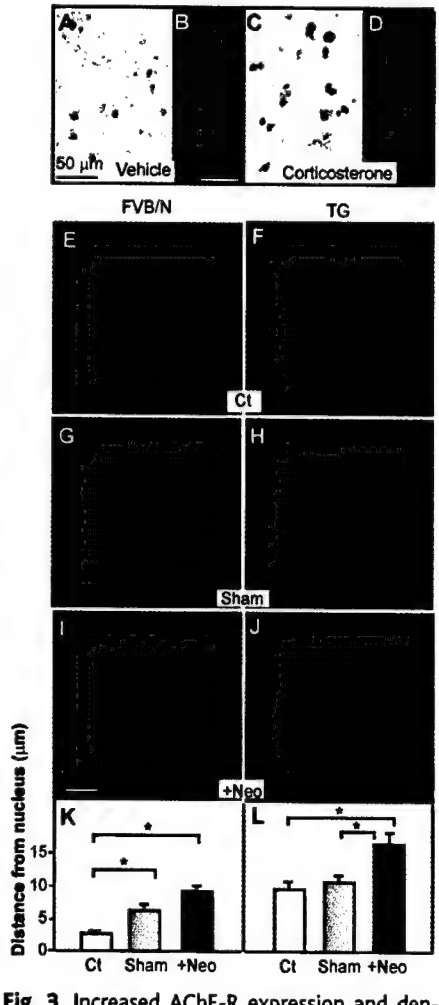

Fig. 3. Increased AChE-R expression and dendritic translocation under hormone, genetic background, sham injection, and chemical stressors. (**A** through **D**) Shown are primary cerebellar neurons stained for AChE activity under vehicle treatment [(A), 0.1% ethanol] or corticosterone [(C), 10 μM, 6 hours]. (B) and (D) Higher magnification immunocytochemical AChE-S labeling. (**E** through **J**) Confocal field images of hippocampal CA1 neurons from normal FVB/N mice [(E), (G), and (I)] and transgenic animals overexpressing human AChE [(F), (H), and (J)], under control conditions [(E) and (F)], 2 days following cannula implantation and perfusion with artificial cerebrospinal fluid [(G) and (H)], or following injection through this probe of 125 nmol neostigmine [(I) and (J)]. (**K** and **L**) Neuritic translocation of detectable AChE-R mRNA labeling (in μm from nucleus) for 30 neurons from at least two animals in each group. Significant differences from noted values are starred ($P < 0.0005$).

nonstimulated slices from animals tested 1 month following 4 days of repeated stress, the mean pfp amplitude was similar to that of nonstimulated controls. However, exposure of slices from stressed mice to physostigmine resulted in a 12-fold larger increase over baseline in stimulation-evoked population spike amplitudes than that observed in nonstressed animals. Atropine administration reversibly blocked this response by more than 90%, much more effectively than its capacity to block field potentials in the control brain (Fig. 4H versus 4G). The stronger responses to both stimulators and antagonists following stress spanned the entire range of stimulus intensity (Fig. 4, I and J), similar to the hypersensitivity patterns seen in humans as PTSD. As in control mice, the evoked pfp was blocked by the NMDA and AMPA antagonists, aminophosphonopentanoic acid (APV) and dinitroquinoxalinedione (DNQX), respectively, attesting to the glutamatergic, i.e., excitatory, nature of the hypersensitized synapses. Neuronal hypersensitivity has long been known to follow stressful experiences (*29*), but the mechanisms leading to it remained unknown. Our current findings suggest a role for stimulus-induced AChE-R overexpression and neuritic translocation in this phenomenon.

Translocation into neuronal processes presumably depends on *cis*-acting elements and/or secondary structures, primarily within the 3′ untranslated region (*26, 30*). AChE-R mRNA includes no known neurite-targeting motif; its transport into dendrites may thus be associated with its unique 3′ sequence, or with the stress-induced accumulation of many more nascent AChE-R mRNA transcripts. The normally short half-life of AChE-R mRNA, ~4 hours (*31*), also appears to be modified following stress. AChE-R mRNA includes a long U-rich element in the 3′-UTR (positions 13,020 through 13,007 in GenBank accession number AF312033), which may contribute to mRNA destabilization through the binding of *trans*-acting proteins (*32*). Although the importance of this element to the stability of AChE-R mRNA remains to be tested, the differential resistance of neurite AChE-R mRNA to antisense oligonucleotide-mediated degradation may reflect low nuclease levels in neurites, especially of ribonuclease H, which targets DNA-RNA hybrids. AChE mRNA had been shown to be stabilized during neuronal differentiation (*33*); our observations suggest that this may be due, at least partially, to AChE-R transcripts being sequestered in neurites.

The weeks-long hypersensitivity of prestressed hippocampus to anticholinesterases attributes a role to the hippocampus in the cholinergic component of post-stress sensitization. The recorded field potentials were sensitive to both cholinergic and glutamatergic antagonists, suggesting a long-term change in the interactions between these two transmitter systems. Cholinergic-glutamatergic interactions have been associated with higher brain functions such as long-term potentiation, memory, and behavior (*34*), all of which are affected by stress. The hypersensitization may also reflect an involvement of neuritic AChE-R in plasticity, due to its capacity to affect cell-cell and cell-matrix interactions (*13*).

In conclusion, we find that the stress-induced increases in cholinergic neurotransmission (*35*) promote a long-term replacement of synaptic membrane AChE-S protein by its soluble AChE-R counterpart. The long-

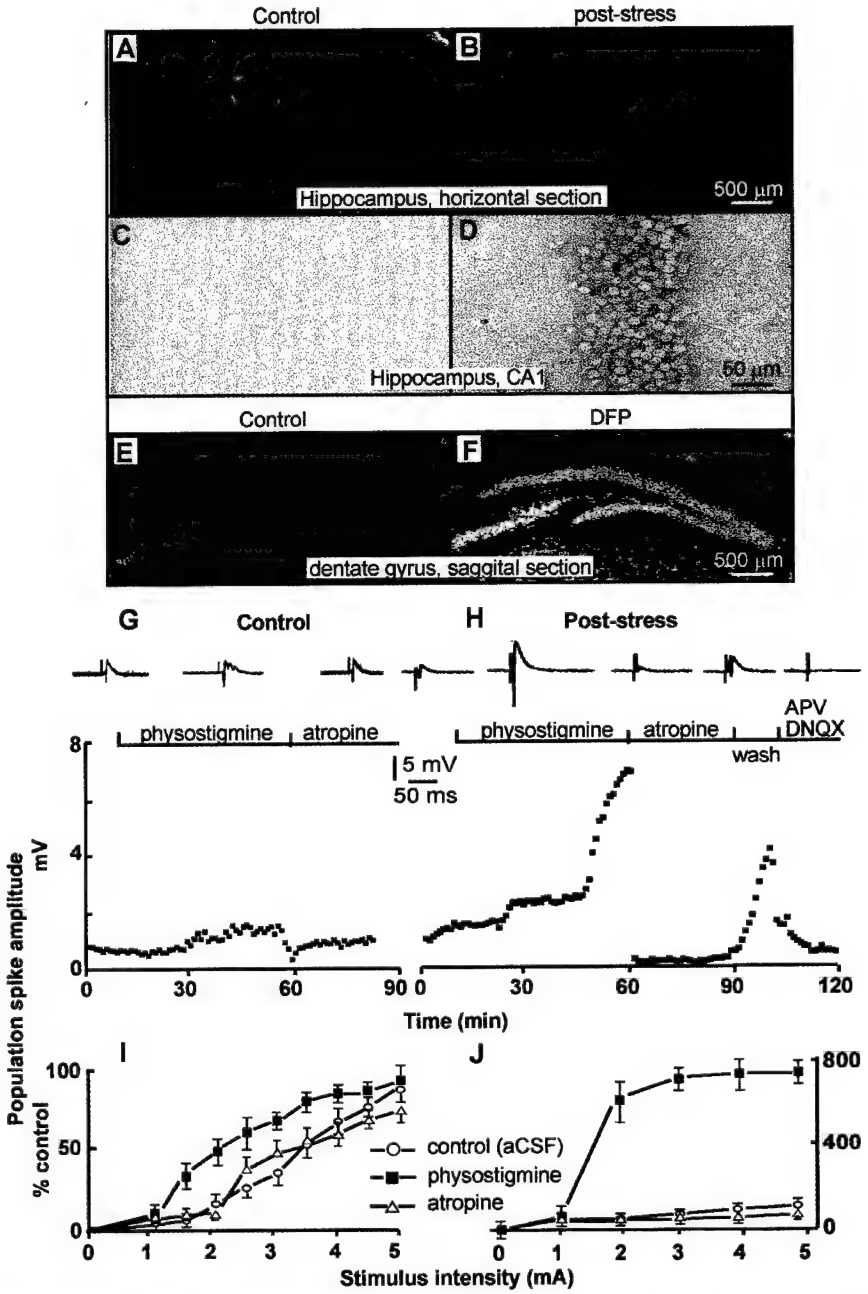

Fig. 4. Hypersensitivity in hippocampal slices under long-lasting overexpression of AChE-R mRNA. (**A** through **F**) Neuronal overexpression. Shown is a comparison of hippocampal slices from control mice to those stressed 1 month earlier by forced swim [(A) to (D), Fast Red colorimetry] or exposure to DFP [0.1 mg kg^{-1}, three consecutive daily injections, (E) and (F), ELF fluorimetry]. (**G** through **J**) Cholinergic hypersensitivity. Shown are extracellular recordings (average ± SD) on the CA1 areas of two to four hippocampus slices from each of three mice, in response to stratum oriens stimulation of slices from controls [(G) and (I)] or 1 month following consecutive daily stress sessions [(H) and (J)]. Above treatment descriptions are shown representative voltage traces. Stimulations (20 s each) were delivered using a bipolar electrode (10 μm insulated tungsten wires, 200 μm apart) placed in the Schaffer collaterals. Applied drug concentrations were: physostigmine, 10 μM; atropine, 10 μM; APV, 50 μM; DNQX, 20 μM.

term hypersensitization to repeated stimuli shown by cholinergic brain tracts may be due to this substitution.

References and Notes

1. B. S. McEwen, *Annu. Rev. Neurosci.* **22**, 105 (1999).
2. R. M. Sapolsky, L. M. Romero, A. U. Munck, *Endocr. Rev.* **21**, 55 (2000).
3. G. Mezey, I. Robbins, *Brit. Med. J.* **323**, 56 (2001).
4. J. A. McCormick *et al.*, *Mol. Endocrinol.* **14**, 506 (2000).
5. J. Xie, D. P. McCobb, *Science* **280**, 443 (1998).
6. R. Daoud, M. Da Penha Berzaghi, F. Siedler, M. Hubener, S. Stamm, *Eur. J. Neurosci.* **11**, 788 (1999).
7. L. Davis, G. A. Banker, O. Steward, *Nature* **330**, 477 (1987).
8. J. A. Foster, I. R. Brown, *J. Neurosci. Res.* **46**, 652 (1996).
9. O. Steward, C. S. Wallace, G. L. Lyford, P. F. Worley, *Neuron* **21**, 741 (1998).
10. H. Kang, E. M. Schuman, *Science* **273**, 1402 (1996).
11. C. H. Bailey, D. Bartsch, E. R. Kandel, *Proc. Natl. Acad. Sci. U.S.A.* **93**, 13445 (1996).
12. O. Steward, E. M. Schuman, *Annu. Rev. Neurosci.* **24**, 299 (2001).
13. H. Soreq, S. Seidman, *Nature Rev. Neurosci.* **2**, 294 (2001).
14. Poly-L-ornithine–coated cover slips [0.5 mg ml^{-1}, 10 min at room temperature (RT)] were sterilized by ultraviolet irradiation (TUV/c 8 W, 3 hours at RT). Cover slip–grown cells were fixed in 3% paraformaldehyde (20 min), dried (1 hour at 37°C), washed 2× 5 min in phosphate-buffered saline (PBS) and 2× 5 min in 0.2% Tween-20 PBS (PBT), incubated with 10 mg/ml proteinase K (5 min at RT), and rewashed (PBT, 2× 5 min). Streptavidin (1 mg ml^{-1}, 30 min at RT) served to block nonspecific labeling. Hybridization was in a humidified chamber with 10 μg ml^{-1} probe in 50% formamide, 5× SSC, 10 mg ml^{-1} tRNA, 10 mg ml^{-1} heparin (90 min at 52°C). Washes were in 50% formamide, 5× SSC, and 0.5% sodium dodecyl sulfate, and in 50% formamide, 2× SSC at 60°C, then at RT in tris-buffered saline (pH 7.5), with 0.1% Tween-20 (TBST) including 2 mM levamisole. Following blockade in 1% skim milk (30 min), digoxigenin-labeled probes were detected with fluorescein- or rhodamine-labeled anti-DIG antibodies (1 hour at RT, three washes in TBST). Biotin-labeled probes were detected (a) fluorometrically by conjugation with streptavidin-Cy2 or -Cy3 (Figs. 1 and 2) or (b) the ELF method (Molecular Probes, Eugene, OR) (Fig. 4, E and F), or (c) colorimetrically with streptavidin-alkaline phosphatase conjugates using Fast Red (Roche Diagnostics, Mannheim, Germany) (Fig. 3, E to J, and Fig. 4, A to D). Mounting was with Immu-Mount (Shandon, Pittsburgh, PA).
15. N. Galyam *et al.*, *Antisense Nucleic Acid Drug Dev.* **11**, 51 (2001).
16. M. Schramm, S. Eimerl, E. Costa, *Proc. Natl. Acad. Sci. U.S.A.* **87**, 1193 (1990).
17. D. Kaufer, A. Friedman, S. Seidman, H. Soreq, *Nature* **393**, 373 (1998).
18. Following hybridization with an AChE-R cRNA probe, 43 of 50 PC12 cells and 45 of 50 cultured primary cerebellar neurons displayed nuclear as well as cytoplasmic labeling. In contrast, only 9 of 50 PC12 cells and 5 of 50 primary neurons labeled for AChE-S mRNA showed nuclear labeling, reflecting different ratios of nuclear pre-mRNA to mature variant transcripts.
19. H. Soreq, D. Zevin-Sonkin, N. Razon, *EMBO J.* **3**, 1371 (1984).
20. M. Shapira *et al.*, *Hum. Mol. Genet.* **9**, 1273 (2000).
21. When treated with 1.5 nM INV101, an oligonucleotide of sequence inverse to EN101, both PC12 cells and cultured primary cerebellar neurons were labeled as extensively as untreated cells with both AChE-S and AChE-R cRNAs (n = 20 cells; SD < 17 and 12%, respectively, and $P > 0.5$ for the two probes).
22. Supplementary material is available at www.sciencemag.org/cgi/content/full/295/5554/508/DC1
23. Samples were incubated with monoclonal anti-AChE-S antibodies (Transduction Laboratories, San Diego, CA), dilution 1:200, 1 hour at RT overnight 4°C, then similar incubations with HRP-tagged goat anti-mouse secondary antibodies (1:500). Detection was with Tyramide Signal Amplification system and Cy5 fluorophore (NEN Life Science Products, Boston, MA).
24. C. Erb *et al.*, *J. Neurochem.* **77**, 638 (2001).
25. L. Davis, B. Burger, G. A. Banker, O. Steward, *J. Neurosci.* **10**, 3056 (1990).
26. C. S. Wallace, G. L. Lyford, P. F. Worley, O. Steward, *J. Neurosci.* **18**, 26 (1998).
27. R. Gray, A. S. Rajan, K. A. Radcliffe, M. Yakehiro, J. A. Dani, *Nature* **383**, 713 (1996).
28. A. Friedman, D. Kaufer, L. Pavlovsky, H. Soreq, *J. Physiol. Paris* **92**, 329 (1998).
29. S. M. Antelman, A. J. Eichler, C. A. Black, D. Kocan, *Science* **207**, 329 (1980).
30. A. Blichenberg *et al.*, *J. Neurosci.* **19**, 8818 (1999).
31. R. Y. Chan, F. A. Adatia, A. M. Krupa, B. J. Jasmin, *J. Biol. Chem.* **273**, 9727 (1998).
32. J. Guhaniyogi, G. Brewer, *Gene* **265**, 11 (2001).
33. Z. D. Luo *et al.*, *Mol. Pharmacol.* **56**, 886 (1999).
34. T. G. Aigner, *Curr. Opin. Neurobiol.* **5**, 155 (1995).
35. A. Imperato, S. Puglisi-Allegra, P. Casolini, L. Angelucci, *Brain Res.* **538**, 111 (1991).

36. We thank K. Löffleholz and J. Klein (Mainz) for fruitful discussions and N. Melamed-Book (Jerusalem) for assistance. Supported by the U.S. Army Medical Research and Materiel Command (DAMD 17-99-1-9547 to H.S. and A.F.), U.S.-Israel Binational Science Foundation (1999/115 to H.S., 1998/066 to N.B.-A., 1997/00174 to A.F.), European Community (QLG3-CT-2000-00072 to N.B.-A), and Ester Neuroscience, Ltd. (to H.S.). C.E. was a Minerva Foundation postdoctoral fellow.

2 October 2001; accepted 30 November 2001

This is the presentation by Prof. Soreq at the Bioscience 2002 Medical Defense Review, Hunt Valley MD (June 2002)

Anti-cholinesterase intensification and antisense suppression of molecular genetic impairments in cholinergic homeostasis

Osnat Cohen[1,2], Eran Meshorer[1], Alon Friedman[3], Liat Ben-Moyal[1],Dalia Ginzberg[1], David Glick[1], Raz Yirmiya[2] and Hermona Soreq[1]. Departments of [1]Biological Chemistry and [2]Psychology, The Hebrew University of Jerusalem, Israel; [3]Departments of Physiology and Neurosurgery; Soroka Medical Center, Ben-Gurion University, Beersheva, Israel

Abstract

Using molecular genetics, we have found that over 5% of the Israeli population carry a dominant activating polymorphism in the *ACHE* promoter that is associated with AChE over-expression and with anti-AChE hypersensitivity. In experimental animals, a variety of stresses induce some of the physiological changes reported in humans for post-exposure. The *ACHE* gene is activated under exposure to anti-AChEs to over-express the normally rare AChE-R mRNA variant and its AChE-R protein product. Within 45 min of the injection of physostigmine through a brain cannula or following the stress of forced swim, AChE-R mRNA mRNA travels to the dendritic neurites, where it remains for weeks, a surprising result that was confirmed in several types of nerve cells. A more dramatic effect on brain neurons was evoked by these stresses under chronic transgenic over-expression of human AChE. Transgenic mice that constitutively over-express both human AChE-S and human AChE-R, present behavioral impairments, including stress-induced bursts of irregular locomotor activity and failure of memory . In these animals, AChE-R mRNA levels in the hyper-producing primary neurons and in mouse brain may be selectively suppressed by nanomolar levels of the antisense agent, EN101; intracerebroventricular injection of EN101 also reverses the behavioral and cognitive deficits of the mice (effect apparent for >24 hr, vs. <45 min for the anti-cholinesterase tacrine). The advantages of antisense agents are specificity, low dosage and the prevention of production of a potentially harmful protein. The possibility arises of addressing these atypical responses to stress and anti-AChE exposure by development of an antisense oligonucleotide-based therapy.

Introduction

The neurotransmitter, acetylcholine, is released into cholinergic synapses and neuromuscular junctions in small quanta from the pre-synaptic membrane and diffuses across the synapse to the post-synaptic neuronal or muscle acetylcholine receptor where it initiates a post-synaptic action potential (Taylor, 1996). The normal discrimination between milliseconds-long nerve impulses is assured by hydrolysis of acetylcholine by acetylcholinesterase (AChE), in preparation for the next release of acetylcholine. The normal train of nerve impulses depends on the balance of acetylcholine release (itself dependent upon acetylcholine synthesis and storage), access of acetylcholine to the post-synaptic site and its hydrolysis by AChE. Several pathological conditions disrupt this balance. In neurodegenerative diseases, such as Alzheimer's disease, the level of cholinergic activity is generally depressed, and a strategy to therapeutically compensate for this uses AChE inhibitors to raise the basal level of acetylcholine (Winkler et al., 1998). Similarly, in myasthenia gravis, in which post-synaptic acetylcholine receptors are largely absent, anti-AChE agents are also used to raise the basal level of acetylcholine (Berrouschot et al., 1997). Furthermore, the cholinergic system is the target of anti-AChE chemical warfare agents and insecticides that are intended to disrupt normal cholinergic neurotransmission by preventing the

clearance of acetylcholine from the synapses. The strategy used during the Gulf War to anticipate this, employed pyridostigmine to temporarily and reversibly block AChE prior to and during the acute phase of exposure to the essentially irreversible anti-AChE chemical warfare agents (Millard and Broomfield, 1995). As the acute danger passes, the blocked AChE spontaneously regenerates and normal cholinergic function resumes. Among what was unknown then, and is still only partially grasped, are the longer-term effects of exposure to an anti-AChE agent and the biological role of butyrylcholinesterase (BChE) and its many natural variations (Soreq and Glick, 2000).

The role of BChE, has recently been raised when knockout mice which lack AChE were shown to survive. It seems that in the absence of any unusual stress, their BChE allows a minimum level of cholinergic neurotransmission (Mesulam et al., 2002). Humans with mutations that partially or completely inactivate BChE are likewise not normally adversely affected, but respond disasterously under exposure to anti-cholinesterases (Loewenstein-Lichtenstein et al., 1995; Prody et al., 1989). Thus, BChE seems to complement the action of AChE: selective inhibition of BChE leads to rise in intracortical acetylcholine (Giacobini, 2000), indicating that BChE does function physiologically, even if in its absence AChE may compensate. One of the most dramatic instances is seen following treatment with succinylcholine, an acetylcholine analog that blocks the receptor and that is used as a muscle relaxant before surgery. Normally, it is slowly hydrolyzed by BChE, but individuals homozygous for the widespread 'atypical' BChE mutation are incapable of reversing the effect (Neville et al., 1990). More recent is the report that Alzheimer's disease patients with the K variant of BChE do not respond to treatment with the AChE inhibitor, rivastigmine (Lehmann et al., 1997). Diet also, may be a factor: glycoalkaloids of potato and other solanacea are inhibitors of AChE and BChE and can initiate cholinergic syndromes (Krasowski et al., 1997). Clearly, BChE modulates the biological response to anti-AChEs. While the basic principles involved are probably not that complex, the relevant genetic, biochemical and clinical data have not yet been assembled to adequately address anomalies in AChE-based therapies.

Zebrafish, in which the *ACHE* gene has been knocked out, can be rescued from lethality by a compensatory mutation in the α-subunit of the nicotinic acetylcholine receptor (Behra et al., 2002). As these animals have no BChE, cholinergic neurotransmission in them apparently depends on spontaneous (non-enzymatic) hydrolysis of acetylcholine, and/or its diffusion from the synapse or extrasynaptic sites of neurotransmission.

An additional issue concerns the ever-accumulating evidence that demonstrates "non-classical" functions of AChE, i.e. biologically significant functions that are apart from its well-documented function in terminating cholinergic neurotransmission (Soreq and Seidman, 2001). For several years now, we have been intrigued by the similarities between the symptoms of post-traumatic stress disorder (PTSD) and those of individuals who are recovering from accidental exposure to AChE inhibitors, mainly agricultural insecticides. This suggested direct involvement of the AChE protein, and possibly the events leading to its production, in long-term stress responses. Our studies addresses the molecular, cellular and physiological mechanisms that may explain this involvement by exploring the effects of AChE overexpression in cultured neurons and transgenic mouse pedigrees that carry natural variants of human AChE.

Materials and Methods

For animal experiments, we employed *ACHE*-transgenic mice derived from the FVB/N strain. This human transgenic mouse line was originally reported by Beeri et al. (1995), and their stress-related phenotype was described in subsequent publications (Andres et al., 1997; Beeri et al., 1997; Erb et al., 2001; Sternfeld et al., 2000). The preparation of primary cerebellar neurons was according to Schramm et al. (1990); tissue preparation, fluorescent in situ hybridization and image analysis was described in Meshorer et al. (2002). Briefly, fluorescent in situ hybridization involved the use of Cy3- or Cy5-labeled 2'-O-methylated cRNA probes targeted at exons in the AChE mRNA transcript. Behavioral studies following intracerebroventricular (*i.c.v.*) injection of antisense agents are reported in Cohen et al. (in press).

The sequence of mouse EN101 is 5'-CTGCAATATTTTCTTGCACC-3'.

Results

Using molecular genetics, we have studied the population incidence of anti-AChE-hypersensitizing mutations at the human *ACHE* locus (Shapira et al., 2000). In our screen, we found that over 5% of the Israeli population carry a dominant activating polymorphism in the *ACHE* promoter (Fig. 1). This is associated with both overexpression of AChE in the serum and with hypersensitivity to anti-AChEs, suggesting that such sensitivity is inherited, but its expression may be latent under most circumstances. To these should be added the many individuals who carry BChE polymorphisms, many of which cause unexpected reactions to anti-AChE agents. The finding that a significant fraction of humans may react very atypically to anti-AChE agents, combined with the unfortunate fact of widespread accidental exposure to anti-AChE insecticides, raises a question of how best to treat these exposures.

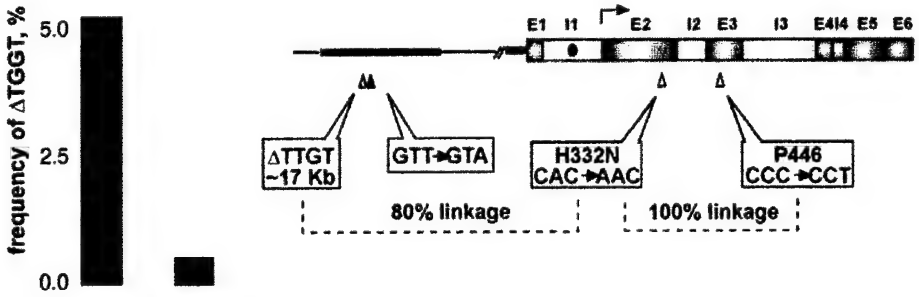

Fig. 1. *ACHE* polymorphisms associated with anti-cholinesterase hypersensitivity are common in a Middle East population.

The deletion in the *ACHE* promoter was found much more frequently in the Israeli population than in an American population. It abolishes one of two HNF transcription factor binding sites and results in an up-regulation of AChE and a hypersensitivity to anti-AChEs. The deletion is closely linked to the Yt^b blood group marker in exon 2, which is itself fully linked to a redundant coding substitution in exon 3.

Alternative splicing of the pre-mRNA from the single *ACHE* gene usually produces synaptic AChE-S or and erythrocytic AChE-E. However, several lines of experimentation converge on the relatively rare AChE variant, AChE-R ("readthrough", because of the translation of pseudo-intron I4), as a key player in long-term neurodeterioration. Table 1 presents the different molecular and functional features of AChE-R. Overproduction of AChE-R may be induced in mouse brain and in cultured cerebellar neurons by exposure to either cholinesterase inhibitors or to cortisol, the stress hormone. Cortisol binds a nuclear receptor which then attaches to specific DNA sequences and enhances the expression of the adjacent genes. One such sequence is located

up-stream from the *ACHE* gene, and we have demonstrated that cortisol enhances AChE production in nerve cells. While cortisol elevates AChE mRNA by 30-50%, other stresses, e.g. exposure to the organophosphate, diisopropylfluorophosphonate (Kaufer et al., 1999), elevate AChE several-fold. Certainly, the human *ACHE* promoter region contains binding motifs for many potential regulators (Grisaru et al., 2001). Within an hour, stress induces both a transcriptional activation and a shift in alternative splicing, which leads to production of the variant AChE-R mRNA. Furthermore, under stress, this variant travels to the dendritic neurites, where it remains for weeks (Fig. 2). This surprising result was confirmed in different types of cultured nerve cells as well as in the mouse brain, demonstrating for the first time that dendritic translocation of mRNA may be a consequence of stress to the nervous system (Meshorer et al., 2002). Under normal conditions, AChE-S mRNA is neuritic and AChE-R mRNA is perinuclear, while the stress of forced swim provokes transport specifically of AChE-R mRNA. Furthermore, the same effect on neurons was evoked within several minutes by the *i.c.v.* injection of an anti-cholinesterase. Thus, AChE-R mRNA is one of a select group of mRNAs for signaling molecules that travel along the dendrites, where these mRNAs may be translated to yield their protein products when those are required for rapid response by that nerve cell or synapse (Steward and Schuman, 2001). In several of these transcripts specific regions in the 3' non-translated sequence were shown to facilitate such transport, however, since they shared no common sequence motif, it is largely assumed that a common topography signals their transport. It is the dendrites that create the network of brain cells. They project a considerable distance from the neuronal cell body and interact with many other neurons. As AChE-R mRNA moves further along dendrites, it can affect the interactions of its neuron with a geometrically expanding number of other neurons. This rapid (minutes) yet long-lasting (weeks) translocation of AChE-R mRNA into neurites accompanies an extreme neuronal hypersensitivity to both anti-AChEs and the acetylcholine antagonist, atropine (Meshorer et al., 2002).

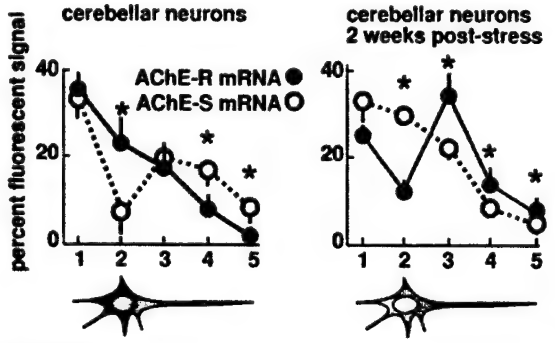

Fig. 2. Stress-induced migration of AChE-R mRNA into neurites.

The two variant AChE mRNAs were detected by fluorescent *in situ* hybridization in 10 cerebellar neurons from paraffin-embedded brains of forced-swim stressed and unstressed FVB/N mice. The fluorescent output of each variant, each totaling 100%, was tabulated for 5 separate regions of the neuron, as indicated. Two weeks following a forced swim, AChE-R mRNA migrated up to 15 μm into the neurites and persisted there for weeks. Asterisks indicate statistical significance ($P < 0.05$).

Table 1. Features of AChE-R expression

	Experimental approach	Reference
Soluble monomers, secretory	*Xenopus* oocyte microinjection	(Seidman et al., 1994)˜
AChE hydrolytic activity	Enzyme activity measurement	(Seidman et al., 1995)
Post-stress hippocampal activity	Electrophysiology	(Kaufer et al., 1998)
Vulnerability to head injury	Survival and recovery	(Shohami et al., 2000)
Muscle pathology	Organophosphate injection	(Lev-Lehman et al., 2000)
Proliferation of myeloid cells	Hematopoietic cell culture	(Grisaru et al., 2001)˜
Male infertility	*In situ* analysis of gene products	(Mor et al., 2001)˜
Neuronal hypersensitivity	Exposure to anti-cholinesterase	(Meshorer et al., 2002)
Sort-term memory	Social exploration tests	(Cohen et al., in press)˜

AChE-R appears to be a molecule well suited to some of the "non-classical" morphogenic roles that have been attributed to AChE, among them neuritogenesis, synaptogenesis, hematopoiesis, amyloid fiber assembly and cell adhesion (Behra et al., 2002; Soreq and Seidman, 2001). A molecular basis of this action may lie in AChE being homologous with a family of intrinsic membrane proteins, the neuroligins, with which it shares the ability to bind another class of membrane proteins, the neurexins (Darboux et al., 1996). As neuroligin is able to replace AChE in its neuritogenic function, and as AChE-R is secretory and soluble, it may disrupt the cell-cell adhesion effected by the neuroligin-neurexin bridge (Fig. 3). Because neurexin and neuroligin have been shown to co-reside specifically in excitatory synapses (Song et al., 1999), they appear to be associated with glutamatergic pathways, such as those shown in our reported electrophysiological analyses (Meshorer et al., 2002) to be altered under stress.

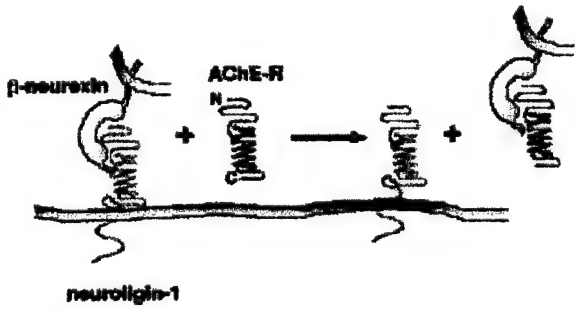

Fig. 3. Putative disruption of cell-cell interactions by soluble AChE-R.
AChE-R displaces neuroligin from neurexin and thus may disrupt the synaptic bridge between the neuroligin-expressing and the neurexin-expressing cell. This may have profound effects on synaptic neurotransmission, especially on glutamatergic synapse, which express these genes.

Among the long-term effects of stress that have aroused the most interest are the effects on behavior. In experimental mice, a well-studied model of learning and memory is social recognition (Carlson, 1994). In this test, an experimental mouse it confronted with a younger mouse. His first reaction is to make the acquaintance of the new mouse, largely by sniffing. The time spent in this "social exploration" is significantly shortened if the exploring mouse has already met, and remembered, the newcomer. As this recognition normally holds no more than 30 min, social exploration time is an inverse measure of the short-term ability to learn and remember. As there are intrinsic differences among mice in their behavior, 30 FVB/N mice were divided into 3 equal groups according to their basal exploration times: short-, long- and medium-explorers, i.e. good, poor and fair learners (Cohen et al., in press). The group that had the longest exploration time, those with the poorest performance in the social exploration paradigm, had lower levels of AChE in the hippocampus and cortex, areas of the brain associated with learning and memory, than did the mice that performed better. As lower levels of AChE, which under normal conditions is chiefly AChE-S, allow higher levels of acetylcholine and therefore of cholinergic neurotransmission, learning and memory correlate inversely with intensified cholinergic neurotransmission. This is consistent with reported memory impairments under stress, which involves elevated acetylcholine release, e.g. (Roberto and Brunelli, 2000).

An increase in acetylcholine release may be useful as an immediate response to stress, if it is a mild response and not of long duration; it allows the animal to be more alert, and, when appropriate, more neurons to be activated. The feedback overproduction of AChE-R is also useful, as it terminates this stress effect and prevents epileptic seizures. However, our findings indicate that prolonged AChE-R accumulation under stress -- forced swim, head injury, exposure to anti-AChE agents -- can have deleterious long-lasting detrimental effects. Furthermore, transgenic mice that constitutively overexpress both human AChE-S and human AChE-R present behavioral impairments, including bursts of irregular locomotor activity induced by the mildly stressful shift of the light-dark circadian cycle, and failure of short-term memory (Cohen et al., in press). The use of anti-AChEs would be inefficient for correcting this problem, as it induces more AChE-R production. These observations led us to develop the antisense approach to limiting the accumulation of AChE-R mRNA. (Cohen et al., in press). EN101 is a novel 20-mer antisense drug that has been demonstrated to induce the preferential destruction of the stress-induced AChE-R mRNA variant (Galyam et al., 2001). Unlike conventional drugs, which are targeted at proteins, EN101, like other antisense agents are short synthetic nucleic acids that target mRNAs. Because they are sequence-based, they can be extremely selective. EN101 is effective at low dosage (nanomolar levels, orders of magnitude lower than conventional drugs) and prevents the production of the potentially harmful AChE-R protein, rather than merely its chemical blockade. AChE-R mRNA levels may be selectively suppressed by nanomolar levels of EN101 in the hyperproducing cultured neurons and mouse brain (Meshorer et al., 2002). The behavioral effects of EN101 are most apparent on the hypersensitized mice that carry the human AChE transgene. *I.c.v.* injection of EN101 reverses the cognitive deficits of the transgenic mice (effect apparent for >24 hr, vs. <45 min for tacrine) (Table 2). To study another kind of behavior, the activity of mice was observed before and after the mild stress of a change in the diurnal light-dark cycle. The mice were implanted with a transmitter that signaled their movements. Control mice accommodated themselves to the change in diurnal cycle by presenting slightly depressed activities; but the transgenic mice showed irregular bursts of activity after the change in cycle. This hyperactivity could be suppressed effectively by intraperitoneal injection of EN101 (effect apparent for several hours) (Fig. 4).

Table 2. Antisense suppression of AChE-R levels correlates with reduced exploration behavior time in AChE-transgenic mice.

Genotype	Treatment	Social exploration[a]	AChE-R[b]	EN101 effect
FVB/N parent strain	AS-BCHE[c]	102 ± 10	242 ± 1	20% reduced basal AChE-R levels, no behavioral effect
	+ EN101[d]	102 ± 9	200 ± 6	
ACHE-transgenic	AS-BCHE[c]	125 ± 15	380 ± 22	25% reduced AChE-R levels, suppressed excessive behavior
	+ EN101[d]	80 ± 4	298 ± 21	

[a]Post-treatment social exploration of long-explorer mice, percent of baseline.
[b]Evaluated by immunodetection in cortical extracts, percent of staining intensity (pixels/100 μm^2) of uncannulated control animals.
[c]Irrelevant antisense agent targeted against the butyrylcholinestease gene.
[d]25 ng/mouse, injected *i.c.v.* on 2 consecutive days (Cohen et al., in press).

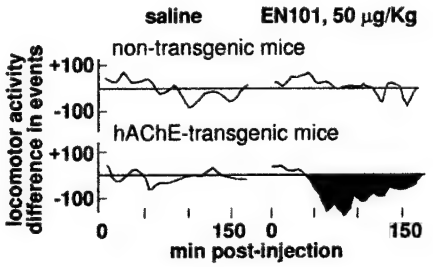

Fig. 4. Locomotor activity of control and transgenic mice.
Three days after a light-to-dark shift of the diurnal cycle, saline or EN101 was injected intraperitoneally and locomotion (events per 10 min) was followed with the aid of implanted transmitters, with each mouse's values self-compared to their movements 24 h earlier. Transgenic, but not control, mice responded with reduced locomotion after treatment

Conclusion

The efficacy of our antisense experiments raises the possibility of using antisense agents to achieve AChE variant specificity, long-lasting effect, and, presumably, fewer side effects than is offered by conventional therapy. In a wider context is the question of atypical, and therefore unexpected, reactions to usually effective therapy for exposure to anti-cholinesterases on the battlefield and, subsequently, of these casualties during recovery. Because stress induces long-lasting accumulation of the AChE-R variant, our findings may lead to improved diagnosis, treatment and prevention of long-term stress illnesses, notably in the case of PTSD.

Acknowledgements

This research was supported by the US Army Medical Research and Materiel Command grant DAMD17-99-1-9547 to H.S. and A.F.), the US-Israel Binational Science Foundation and Ester Neurosciences Ltd. (Tel-Aviv).

References

Andres, C., Beeri, R., Friedman, A., Lev-Lehman, E., Henis, S., Timberg, R., Shani, M., and Soreq, H. (1997). Acetylcholinesterase-transgenic mice display embryonic modulations in spinal cord choline acetyltransferase and neurexin Iß gene expression followed by late-onset neuromotor deterioration. *Proc Natl Acad Sci USA* 94, 8173-8178.

Beeri, R., Andres, C., Lev-Lehman, E., Timberg, R., Huberman, T., Shani, M., and Soreq, H. (1995). Transgenic expression of human acetylcholinesterase induces progressive cognitive deterioration in mice. *Curr Biol* 5, 1063-1071.

Beeri, R., Le Novere, N., Mervis, R., Huberman, T., Grauer, E., Changeux, J. P., and Soreq, H. (1997). Enhanced hemicholinium binding and attenuated dendrite branching in cognitively impaired acetylcholinesterase-transgenic mice. *J Neurochem* 69, 2441-2451.

Behra, M., Cousin, X., Bertrand, C., Vonesch, J. L., Biellmann, D., Chatonnet, A., and Strahle, U. (2002). Acetylcholinesterase is required for neuronal and muscular development in the zebrafish embryo. *Nat Neurosci* 5, 111-118.

Berrouschot, J., Baumann, I., Kalischewski, P., Sterker, M., and Schneider, D. (1997). Therapy of myasthenic crisis. *Crit Care Med* 25, 1228-1235.

Carlson, N. R. (1994). *Physiology of Behavior* (Needham Heights, MA: Allyn and Bacon).

Cohen, O., Erb, C., Ginzberg, D., Pollak, Y., Seidman, S., Shoham, S., Yirmiya, R., and Soreq, H. (in press). Neuronal overexpression of "readthrough" acetylcholinesterase is associated with antisense-suppressible behavioral impairments. *Mol Psych.*

Darboux, I., Barthalay, Y., Piovant, M., and Hipeau Jacquotte, R. (1996). The structure-function relationships in Drosophila neurotactin show that cholinesterasic domains may have adhesive properties. *EMBO J* 15, 4835-4843.

Erb, C., Troost, J., Kopf, S., Schmitt, U., Loffelholz, K., Soreq, H., and Klein, J. (2001). Compensatory mechanisms enhance hippocampal acetylcholine release in transgenic mice expressing human acetylcholinesterase. *J Neurochem* 77, 638-646.

Galyam, N., Grisaru, D., Grifman, M., Melamed-Book, N., Eckstein, F., Seidman, S., Eldor, A., and Soreq, H. (2001). Complex host cell responses to antisense suppression of ACHE gene expression. *Antisense Nucl Acid Drug Dev* 11, 51-57.

Giacobini, E. (2000). Cholinesterase inhibitors: from the Calabar bean to Alzheimer therapy. In *Cholinesterases and Cholinesterase Inhibitors*, E. Giacobini, ed. (London: Martin Dunitz), pp. 181-226.

Grisaru, D., Deutch, V., Shapira, M., Galyam, N., Lessing, B., Eldor, A., and Soreq, H. (2001). ARP, a peptide derived from the stress-associated acetylcholinesterase variant, has hematopoietic growth promoting activities. *Mol Med* 7, 93-105.

Kaufer, D., Friedman, A., Seidman, S., and Soreq, H. (1998). Acute stress facilitates long-lasting changes in cholinergic gene expression. *Nature* 393, 373-377.

Kaufer, D., Friedman, A., Seidman, S., and Soreq, H. (1999). Anticholinesterases induce multigenic transcriptional feedback response suppressing cholinergic neurotransmission. *Chem Biol Interact* 119-120, 349-360.

Krasowski, M. D., McGehee, D. S., and Moss, J. (1997). Natural inhibitors of cholinesterases: implications for adverse drug reactions. *Can J Anaesth* 44, 525-534.

Lehmann, D. J., Johnston, C., and Smith, A. D. (1997). Synergy between the genes for butyrylcholinesterase K variant and apolipoprotein E4 in late-onset confirmed Alzheimer's disease. *Hum Mol Genet* 6, 1933-1936.

Lev-Lehman, E., Evron, T., Broide, E. S., Meshorer, E., Ariel, I., Seidman, S., and Soreq, H. (2000). Synaptogenesis and myopathy under acetylcholinestrase overexpression. *J Mol Neurosci* 14, 93-105.

Loewenstein-Lichtenstein, Y., Schwarz, M., Glick, D., Norgaard Pedersen, B., Zakut, H., and Soreq, H. (1995). Genetic predisposition to adverse consequences of anti-cholinesterases in 'atypical' BCHE carriers. *Nature Med* 1, 1082-1085.

Meshorer, E., Erb, C., Gazit, R., Pavlovsky, L., Kaufer, D., Friedman, A., Glick, D., Ben-Arie, N., and Soreq, H. (2002). Alternative splicing and neuritic mRNA translocation under long-term neuronal hypersensitivity. *Science* 295, 508-512.

Mesulam, M. M., Guillozet, A., Shaw, P., Levey, A., Duysen, E. G., and Lockridge, O. (2002). Acetylcholinesterase knockouts establish central cholinergic pathways and can use butyrylcholinesterase to hydrolyze acetylcholine. *Neuroscience* 110, 627-639.

Millard, C. B., and Broomfield, C. A. (1995). Anticholinesterases: medical applications of neurochemical principles. *J Neurochem* 64, 1909-1918.

Mor, I., Grisaru, D., Titelbaum, L., Evron, T., Richler, C., Wahrman, J., Sternfeld, M., Yogev, L., Meiri, N., Seidman, S., and Soreq, H. (2001). Modified testicular expression of stress-associated "readthrough" acetylcholiensterase predicts male infertility. *FASEB J* 15, 2039-2041.

Neville, L. F., Gnatt, A., Padan, R., Seidman, S., and Soreq, H. (1990). Anionic site interactions in human butyrylcholinesterase disrupted by two single point mutations. *J Biol Chem* 265, 20735-20738.

Prody, C. A., Dreyfus, P., Zamir, R., Zakut, H., and Soreq, H. (1989). De novo amplification within a "silent" human cholinesterase gene in a family subjected to prolonged exposure to organophosphorous insecticides. *Proc Natl Acad Sci USA* 86, 690-694.

Roberto, M., and Brunelli, M. (2000). PACAP-38 enhances excitatory synaptic transmission in the rat hippocampal CA1 region. *Learn Mem* 7, 303-311.

Seidman, S., Aziz Aloya, R. B., Timberg, R., Loewenstein, Y., Velan, B., Shafferman, A., Liao, J., Norgaard Pedersen, B., Brodbeck, U., and Soreq, H. (1994). Overexpressed monomeric human acetylcholinesterase induces subtle ultrastructural modifications in developing neuromuscular junctions of Xenopus laevis embryos. *J Neurochem* 62, 1670-1681.

Seidman, S., Sternfeld, M., Ben Aziz Aloya, R., Timberg, R., Kaufer Nachum, D., and Soreq, H. (1995). Synaptic and epidermal accumulations of human acetylcholinesterase are encoded by alternative 3'-terminal exons. *Mol Cell Biol* 15, 2993-3002.

Shapira, M., Tur-Kaspa, I., Bosgraaf, L., Livni, N., Grant, A. D., Grisaru, D., Korner, M., Ebstein, R. P., and Soreq, H. (2000). A transcription-activating polymorphism in the ACHE promoter associated with acute sensitivity to anti-acetylcholinesterases. *Hum Mol Genet* 9, 1273-1281.

Shohami, E., Kaufer, D., Chen, Y., Seidman, S., Cohen, O., Ginzberg, D., Melamed-Book, N., Yirmiya, R., and Soreq, H. (2000). Antisense prevention of neuronal damages following head injury in mice. *J Mol Med* 78, 228-236.

Song, J. Y., Ichtchenko, K., Sudhof, T. C., and Brose, N. (1999). Neuroligin 1 is a postsynaptic cell-adhesion molecule of excitatory synapses. *Proc Natl Acad Sci USA* 96, 1100-1105.

Soreq, H., and Glick, D. (2000). Novel roles for cholinesterases in stress and inhibitor responses. In *Cholinesterases and Cholinesterase Inhibitors: Basic, Preclinical and Clinical Aspects*, E. Giacobini, ed. (London: Martin Dunitz), pp. 47-61.

Soreq, H., and Seidman, S. (2001). Acetylcholinesterase - new roles for an old actor. *Nature Rev Neurosci* 2, 294-302.

Sternfeld, M., Shoham, S., Klein, O., Flores-Flores, C., Evron, T., Idelson, G. H., Kitsberg, D., Patrick, J. W., and Soreq, H. (2000). Excess "readthrough" acetylcholinesterase attenuates but the "synaptic" variant intensifies neurodeterioration correlates. *Proc Natl Acad Sci USA* 97, 8647-8652.

Steward, O., and Schuman, E. M. (2001). Protein synthesis at synaptic sites on dendrites. *Annu Rev Neurosci* 24, 299-325.

Taylor, P. (1996). Agents acting at the neuromuscular junction and autonomic ganglia. In *Goodman & Gilman's The Pharmacological Basis of Therapeutics*, J. G. Hardman and L. E. Limbird, eds. (New York: McGraw-Hill), pp. 177-197.

Winkler, J., Thal, L. J., Gage, F. H., and Fisher, L. J. (1998). Cholinergic strategies for Alzheimer's disease. *J Mol Med* 76, 555-567.

ANTISENSE INTERVENTION WITH CHOLINERGIC IMPAIRMENTS ASSOCIATED WITH NEURODEGENERATIVE DISEASE

Eran Meshorer and Hermona Soreq*

1. INTRODUCTION

Current therapies for Alzheimer's disease are based on suppression of acetylcholine hydrolysis with inhibitors of acetylcholinesterase (AChE) (Figure 1). However, recent data demonstrated that various stressors, including cholinesterase inhibition, promote long-lasting up-regulation of a rare AChE isoform, AChE-R, having isoform-specific non-catalytic morphogenic activities[1,2]. The role of this protein in the etiology of neurodegenerative disease therefore deserves a fresh examination.

2. METHODS

The regulation and biological functions of AChE were studied in patients hypersensitive to anticholinesterases, transfected cells, transgenic mice, and normal mice subjected to psychological stress, anticholinesterase treatment, or closed head injury[3]. AChE gene expression was manipulated in cells and *in vivo*, using partially 2'-*O*-methyl-protected antisense oligonucleotides (ASON)[4].

3. RESULTS AND INTERPRETATION

Several inherited causes are known which confer hypersensitivity to cholinesterase inhibitors[5]. All vertebrates possess two cholinesterase proteins, AChE and

* Eran Meshorer and Hermona Soreq, The Hebrew University of Jerusalem, Jerusalem, Israel 91904

Mapping the Progress of Alzheimer's and Parkinson's Disease
Edited by Mizuno *et al.*, Kluwer Academic/Plenum Publishers, 2002

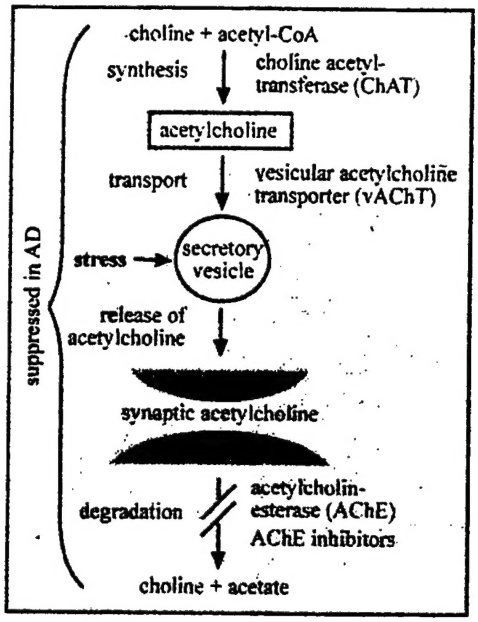

Figure 1. The cholinergic consequences of anti-cholinesterase therapy. Inhibitors of acetylcholinesterase (AChE) are common therapeutic agents employed to treat diseases that involve impaired acetylcholine-mediated neurotransmission. In such diseases (i.e. Alzheimer's Disease or Myasthenia Gravis), the cascade leading from choline and acetyl-CoA to acetylcholine and its subsequent degradation via AChE, is suppressed, leading to a state of hypocholinergic neurotransmission. AChE hydrolyses acetylcholine (ACh) in the synaptic cleft to release choline and acetate. Therefore, its inhibition increases ACh levels in cholinergic synapses, retrieving closer to normal levels of cholinergic communication.

Table 1. Inherited causes for anticholinesterase hypersensitivity

anti-AChE used	Gene (Chr.)	Mutation	Allele frequency	Adverse responses	Reference
Pyridostigmine	BCHE (3q26)	D70G (atypical) *recessive*	1:1000[a]	depression weight loss anxiety	Loewenstein-Lichtenstein et al., 1995
Parathion	BCHE (3q26)	Silent *recessive*	1:100,000[a]	muscle fasciculation leading to asphyxia	Whittaker, 1986 Prody et al., 1989
Pyridostigmine	ACHE (7q22)	Distal enhancer deletion *dominant*	1:50[a]	muscle fasciculations intense headache rhinnorea lacrimation	Shapira et al., 2000
Diazoxon	PON1 (7q21)	Q192R M55L	0.25-0.32[b]	excessive sweating chest tightness nausea muscle twitching	Davies et al., 1996 Haley et al., 1999

[a] Average in the Israeli population
[b] Average in the American population

Table 2. Conditions inducing AChE-R overproduction

Stressor	Overexpressing cell type	Reference
Confined swim	cortical neurons bone marrow cells	Kaufer et al., 1998 Grisaru et al., 2001
DFP	brain muscle retinal neurons	Shapira et al., 2000 Lev-Lehman et al., 2000 Broide et al., 1999
Closed head injury	cortical neurons	Shohami et al., 2000
Glucocorticoids	hematopoietic cells	Grisaru et al., 2001

butyrylcholinesterase (BuChE). While AChE has long been recognized for its catalytic function of hydrolyzing acetylcholine, the function of BuChE, which is non-essential for normal life, has long been a mystery. A suggestion was that BuChE operates as a scavenger, acting to protect the nervous system from anti-cholinesterases (anti-ChEs), thus preventing excessive blockade of the essential AChE. Adverse symptoms were reported for anticholinesterase-exposed carriers of 'atypical' BuChE[6], which is far less sensitive than normal BuChE to inhibition by pyridostigmine and several other carbamate anti-ChEs. Moreover, atypical BuChE demonstrated 1/200th the affinity for tacrine of normal BuChE or AChE. Inherited BuChE mutations may thus explain at least some of the adverse responses to anti-ChE therapies. Another metabolic enzyme that operates as an organophosphate scavenger is paraoxonase (PON1)[7,8]. PON1 mutations, as well as promoter polymorphisms in an upstream enhancer domain of the human ACHE locus, also cause extreme hypersensitivity to anti-ChEs (Table 1). At the post-transcriptional level, alternative splicing associated with overexpression of AChE-R mRNA and its AChE-R protein product were shown following psychological stress, exposure to anti-ChEs or head trauma (Table 2). In addition, unique, non-catalytic, morphogenic properties were attributed to each of the AChE splice variants[3]. Therefore, anticholinesterases used for treating Alzheimer's disease induce AChE-R overproduction and may lead to undesired morphogenic effects.

In principle, most of the currently used drugs are targeted towards proteins with adverse effects. However, thanks to the human genome project, we now know the sequence of many of the mRNA transcripts encoding these proteins. This enables the development of antisense oligonucleotides (ASON) preventing the production of undesired proteins rather than blocking their active sites (Figure 2). Nanomolar doses of ASON mediating selective destruction of stress-induced AChE-R mRNA prevented AChE-R accumulation, as was shown using AChE-R selective hybridization probes[4]. Furthermore, anti-AChE ONs improved memory and behavior in transgenic mice (Cohen et al., unpublished results), protected hippocampal neurons, minimized mortality, and facilitated recovery of transgenic mice following head injury, the highest known risk for non-familial Alzheimer's disease[9].

4. CONCLUSIONS

Inherited promoter polymorphisms, state-of-mind-, drug-, and injury-induced feedback processes all induce accumulation of a previously unknown AChE variant. These

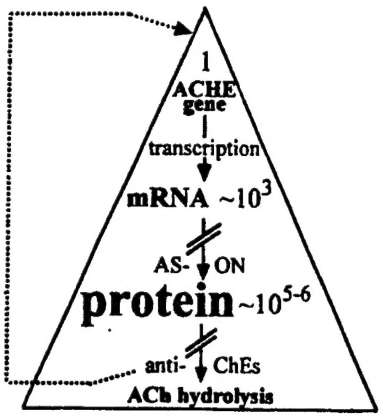

Figure 2. Amplification process from one gene to many protein products. The concentration of AChE mRN/ molecules per cell was estimated by Karpel et al. (1994). Given the life span of an AChE mRNA transcrip (ca. 4-8 hrs (Chan et al., 1998; Luo et al., 1999 respectively)), and that of the AChE protein (ca. 3.5 day (Wenthold et al., 1974)), together with the amplification at the translation phase, an amplification facto from mRNA to protein of 100-1000 can be estimated. Therefore, ASON drugs can be used in much lowe doses than their counterpart enzyme inhibitors, especially since such inhibitors enhance AChE-R mRN/ production (dashed arrow; Soreq and Seidman, 2001).

and the neglected morphogenic properties of AChE should all be considered when contemplating the etiology of cholinergic impairments in neurodegenerative diseases. Antisense technology has emerged as a valuable research tool and a promising direction of novel therapies.

ACKNOWLEDGEMENTS

Supported by the US Army Medical Research and Development Command (DAMD 17-99-1-9547) and by Esther Neuroscience, Ltd. (to H.S.).

REFERENCES

1. D. Kaufer, A. Friedman, S. Seidman, and H. Soreq. Acute stress facilitates long-lasting changes in cholinergic gene expression. *Nature* **393**,373-377(1998).
2. M. Shapira, I. Tur-Kaspa, L. Bosgraaf, N. Livni, A. D. Grant, D. Grisaru, M. Korner, R. P. Ebstein, and H. Soreq. A transcription-activating polymorphism in the ACHE promoter associated with acute sensitivity to anti-acetylcholinesterases. *Hum Mol Genet* **9**, 1273-1281(2000).
3. H. Soreq, and S. Seidman, S. Acetylcholinesterase - new roles for an old actor. *Nat Rev Neurosci* **2**,294-302(2001).
4. N. Galyam, D. Grisaru, M. Grifman, N. Melamed-Book, F. Eckstein, S. Seidman, A. Eldor, and H. Soreq. Complex host cell responses to antisense suppression of ACHE gene expression. *Antisense Nucleic Acid Drug Dev* **11**,51-57(2001).
5. H. Soreq, and D. Glick. Novel roles for cholinesterases in stress and inhibitor responses. In Cholinesterases and Cholinesterase Inhibitors, E. Giacobini, ed. (London: Martin Dunitz), pp. 47-61(2000).
6. Y. Loewenstein-Lichtenstein, M. Schwarz, D. Glick, B. Norgaard Pedersen, H. Zakut, and H. Soreq. Genetic predisposition to adverse consequences of anti-cholinesterases in 'atypical' BCHE carriers. *Nat Med* **1**,1082-1085(1995).
7. H. Davies, R.J. Richter, M. Keifer, C. A. Broomfield, J. Sowalla, C. E. and Furlong. The effect of the human serum paraoxonase polymorphism is reversed with diazoxon, soman and sarin. *Nat Genet* **14**,334-336(1996).
8. R. Haley, S. Billecke, B. N. and La Du, B. N.. Association of low PON1 type Q (type A) arylesterase activity with neurologic symptom complexes in Gulf War veterans. *Toxicol Appl Pharmacol* **157**,227-233(1999).
9. E. Shohami, D. Kaufer, Y. Chen, S. Seidman, O.Cohen, D. Ginzberg, N. Melamed-Book, R. Yirmiya, R., and H. Soreq, Antisense prevention of neuronal damages following head injury in mice. *J. Mol. Med*. **78**,228-236(2000).